



**HAL**  
open science

# Evaluation of the performance of a spray scrubber for the removal of nanoparticles contained in incineration fumes

Emmanuel Adah

► **To cite this version:**

Emmanuel Adah. Evaluation of the performance of a spray scrubber for the removal of nanoparticles contained in incineration fumes. Chemical and Process Engineering. Ecole nationale supérieure Mines-Télécom Atlantique, 2023. English. NNT : 2023IMTA0346 . tel-04247309

**HAL Id: tel-04247309**

**<https://theses.hal.science/tel-04247309>**

Submitted on 18 Oct 2023

**HAL** is a multi-disciplinary open access archive for the deposit and dissemination of scientific research documents, whether they are published or not. The documents may come from teaching and research institutions in France or abroad, or from public or private research centers.

L'archive ouverte pluridisciplinaire **HAL**, est destinée au dépôt et à la diffusion de documents scientifiques de niveau recherche, publiés ou non, émanant des établissements d'enseignement et de recherche français ou étrangers, des laboratoires publics ou privés.

# THESE DE DOCTORAT DE

l'École Nationale Supérieure

Mines-Télécom Atlantique Bretagne Pays de la Loire –  
IMT Atlantique

Ecole Doctorale n° 648

*Sciences pour l'Ingénieur et le Numérique*

Spécialité : Génie des procédés et des Bioprocédés

Par

**Emmanuel ADAH**

## **Evaluation of the Performance of a Spray Scrubber for the Removal of Nanoparticles Contained in Incineration Fumes**

Thèse présentée et soutenue à IMT Atlantique Campus de Nantes, le 06 Mars 2023

Unité de recherche : GEPEA UMR CNRS 6144

Thèse N° : 2023IMTA0346

### **Rapporteurs avant soutenance :**

Eberhard SCHMIDT                      Professeur, Bergische Universität Wuppertal  
Cornelius SCHÖNNENBECK        Maître de conférences HDR Université de Haute Alsace

### **Composition du Jury :**

Président:	Jean-Pascal BORRA	Directeur de Recherche CNRS Université Paris Saclay
Examineur:	Emmanuel PORCHERON	Chercheur HDR - Directeur adjoint de laboratoire à IRSN
	Eberhard SCHMIDT	Professeur, Bergische Universität Wuppertal
	Cornelius SCHÖNNENBEC	Maître de conférences HDR Université de Haute Alsace

Dir. de thèse :	Laurence LE COQ	Professeure IMT Atlantique Nantes
Co-dir. de thèse :	Aurélien JOUBERT	Maître de conférences HDR IMT Atlantique Nantes

### **Invité(s)**

Sylvain DURECU	Directeur de la recherche et développement, Séché Environnement
Marc HENRY	Directeur de la recherche, Séché Environnement

## Acknowledgments

I am deeply grateful to my Ph.D. supervisor, Professor Laurence LE COQ, for her unwavering support and guidance throughout my doctoral studies. Her expertise and insights were invaluable in helping me overcome the numerous challenges I encountered. In addition, Professor Laurence LE COQ's experience and work ethic have greatly contributed to my growth and development in this field. I would also like to express my sincere appreciation to Dr. Aurélie JOUBERT for her invaluable support, advice, and technical guidance during my Ph.D. Both Professor Laurence LE COQ and Dr. Aurélie JOUBERT were always there for me, providing help and support for both the professional and personal challenges I faced. I am truly grateful for their guidance.

I would like to extend my sincere thanks to Dr. Sylvain DURECU and Marc HENRY from Séché Environnement for their financial support and for keeping my research relevant to the industry. I am also grateful for their willingness to welcome me to their industrial sites and for their valuable insights on my research papers. I am particularly thankful to both Dr. Eric DUMONT and Dr. Emmanuel PORCHERON, who served on my Comité de suivi individuel (CSI) and provided valuable guidance and direction during my Ph.D.

I am also thankful to members of the jury Professor Eberhard SCHMIDT, Dr. Cornelius SCHÖNNENBECK, Dr. Jean-Pascal BORRA and Dr. Emmanuel PORCHERON for taking the time to review my manuscript and for sharing insights on ways to improve this doctoral dissertation.

I would like to express my sincere gratitude to Dr. Ala BOUHANGUEL, Angela HOYOS, and Savari KOGNOLE for their guidance and support during my thesis journey. I also want to thank Sabine VANDEPEUTTE for coordinating meetings with Professor Laurence LE COQ. A special thank you goes to the technical team at the GEPEA Lab, particularly Yvan GOURIOU who built the pilot-scale test bench used in my experiments and was always available to modify it when needed. I also want to thank the rest of the technical team: Jérôme MARTIN, François-Xavier BLANCHET, Eric CHEVREL, Katell CHAILLOU, and Patrick BRION for their assistance during my laboratory experiments and for helping with the relevant software. I am grateful to the faculty at the Energy Systems and Environment Department (DSEE) at IMT Atlantique, including Professor Yves Andres, Dr. Sary AWAD, Dr. Audrey VILLOT, Dr. Khaled LOUBAR, and Dr. Felicie THERON. I also want to thank

Dominique BRIAND and Ludivine SAHRAOUI for their administrative assistance. I am thankful to current and former Ph.D. students, including Sylvester, Nouha ZINE-FILALI, Mayumi METE, Christelle RABBAT, Millicent IGWEBUIKE, Ali HAJJ, Siavoche GHODS, Sarah FAKIH, Moeen EL BAST, Henrietta, ABDELAAL Ali, Dr. Walid MRAD and ABI HANNA Rita for making my time at IMT Atlantique enjoyable. I also want to thank my office colleagues and dearest friends, Morgane POSER and Gaëtan PAVARD, I am really lucky to have you both. I am grateful to the entire research team at Athena incubator. Finally, I want to thank my sweet mother Elizabeth Adah, my amazing siblings Andrew, Agatha, James, Lawrence, Paul, Isaiah, and Raphael, and my beautiful wife Martha Ogwuche and lovely children Ariel and Kairo for their love, support, and prayers. Without their support, I would not have come this far. Thank you very much.

## **Dedication**

I dedicate my Ph.D. studies to my father, *Sylvester Adah*, who passed away in 2012. My dad was a constant source of support and encouragement throughout my life, and I am deeply grateful for all the wisdom and guidance he provided me. Although he is no longer with us, his influence will always be a part of me and my work forever. I miss him deeply.

## Résumé

Les nanotechnologies sont considérées comme une technologie clé du XXI<sup>e</sup> siècle [1] et ont permis de réaliser des progrès considérables dans divers secteurs importants, notamment l'agriculture, l'énergie, les soins de santé, l'électronique, les soins personnels et la protection de l'environnement. L'utilisation généralisée des nanotechnologies dans ces secteurs devrait faire grimper le marché mondial des nanotechnologies à plus de 62,8 milliards d'USD d'ici 2031 [2].

Avec l'augmentation de l'utilisation des nanomatériaux manufacturés (ENM) dans les produits industriels et de consommation, une plus grande quantité d'ENM se retrouvera probablement dans les flux de déchets à la fin de leur vie et sera potentiellement rejetée dans l'environnement. Actuellement, on estime que plus de 300 000 tonnes métriques d'ENM sont rejetées chaque année dans les décharges, le sol, l'eau et l'air [3].

Malgré les risques potentiels connus pour la santé et l'environnement de l'exposition aux nanomatériaux manufacturés (ENM) [4–7], il n'existe actuellement aucune réglementation concernant l'élimination sûre des ENM à la fin de leur cycle de vie. Cette absence de réglementation est d'autant plus préoccupante que le volume des nanodéchets (NW), ou déchets contenant des ENM, devrait augmenter. Il existe un besoin croissant de cadres réglementaires sur la gestion des NW [8, 9], et il est important de comprendre comment les NW sont affectés par les systèmes actuels de gestion des déchets. Bien que des quantités croissantes de déchets non dangereux soient recyclées [10], les risques potentiels et les incertitudes associés aux déchets non dangereux ont conduit à une préférence pour la gestion des déchets non dangereux par le biais d'installations centralisées de valorisation énergétique des déchets, telles que l'incinération.

Des recherches récentes ont montré que les nanomatériaux manufacturés peuvent survivre au processus de combustion dans l'incinération des déchets et se retrouver dans les gaz de combustion [10–13]. Cependant, on connaît mal l'efficacité des technologies actuelles d'épuration des gaz de combustion pour éliminer les ENM dans les usines d'incinération des déchets. Un type de technologie d'épuration des gaz de combustion couramment utilisé dans les UIOM est le laveur humide, qui est principalement conçu pour traiter les polluants acides.

Les laveurs sont connus pour leur faible efficacité à collecter les particules inférieures à 5,0  $\mu\text{m}$ . Cependant, une étude de Kim et al. [14] a montré que, dans certaines conditions, un épurateur peut collecter efficacement des particules inférieures à 1,0  $\mu\text{m}$ . Les laveurs offrent

une certaine flexibilité dans le traitement des gaz de combustion, notamment la capacité de traiter les polluants acides et de traiter les PM inflammables/explosives dans les gaz de combustion à haute température. C'est pourquoi les laveurs sont souvent présents dans les usines d'incinération de déchets dangereux [15]. Les laveurs sont également employés dans d'autres applications industrielles telles que la production de semi-conducteurs et de ciment, où l'on sait que des particules de taille nanométrique sont émises pendant les processus de fabrication [16, 17]. Plusieurs études ont examiné l'influence des paramètres de fonctionnement d'un épurateur sur la collecte de  $PM > 1,0 \mu m$  [18–22], et quelques-unes se sont concentrées sur l'optimisation des paramètres de fonctionnement des épurateurs [23–26]. Cependant, à notre connaissance, aucune étude n'a été réalisée pour évaluer les performances d'un épurateur par aspersion concernant la collecte de nanoparticules dans des conditions d'incinération de déchets.

La présente thèse vise à évaluer les performances d'un laveur à échelle pilote concernant la collecte de nanoparticules contenues dans un gaz de combustion représentant les conditions d'un laveur à pulvérisation d'une usine d'incinération de déchets dangereux en termes de rapport hauteur/diamètre, de rapport liquide/gaz, de températures d'entrée/sortie du gaz, d'humidité du gaz, de temps de résidence du gaz, et de régime d'écoulement du gaz, de diamètre des gouttelettes et de concentrations des particules. De plus, l'influence de trois facteurs opérationnels indépendants - le débit de gaz, le débit de liquide et le diamètre des gouttelettes - sur la collecte des nanoparticules de carbone par un épurateur à l'échelle pilote a été étudiée en utilisant la méthodologie de conception Box-Behnken.

Les travaux de recherche décrits dans cette thèse ont été soutenus par l'Agence pour la Transition Ecologique - ADEME - (Subvention No. TEZ19-002) et la Région Pays de la Loire en collaboration avec le Groupe Séché Environnement en tant que partenaire industriel. La thèse a été réalisée au laboratoire GEPEA du Département systèmes énergétiques et environnement (DSEE) d'IMT Atlantique - Campus de Nantes entre le 1er novembre 2019 et le 28 février 2023. Le manuscrit est organisé comme suit :

**Le chapitre I** propose une revue bibliographique qui vise à résumer la définition, les types et la production des nanomatériaux sur la base des travaux publiés. Il examine également les impacts potentiels des nanomatériaux sur la santé et l'environnement. Compte tenu de l'absence actuelle de réglementation sur l'élimination sûre des nanomatériaux en fin de vie, cette revue examine les différentes méthodes actuellement utilisées pour traiter les nanodéchets. Un accent est ensuite mis sur le devenir des nanomatériaux dans les usines

d'incinération des déchets. Le deuxième objectif de ce chapitre est d'examiner la technologie d'épuration par voie humide, notamment son principe de fonctionnement, les différents types de laveur, les applications industrielles et les différents mécanismes de collecte des particules. Enfin, ce chapitre examine l'influence du débit de gaz, de la température du gaz, du taux d'humidité du gaz, du débit de liquide et du diamètre des gouttelettes sur l'efficacité de collecte des particules d'un épurateur humide.

Dans **le chapitre II**, les matériels et méthodes utilisés dans cette thèse sont présentés. Le dispositif expérimental est décrit, y compris sa conception pour imiter un épurateur à pulvérisation à grande échelle rencontré dans la ligne de traitement des gaz de combustion d'une usine d'incinération de déchets dangereux en termes de rapport hauteur/diamètre, de rapport liquide/gaz, de températures d'entrée et de sortie du gaz, d'humidité du gaz, de temps de résidence du gaz, de régime d'écoulement du gaz, de diamètre des gouttelettes et de concentration des particules. L'aérosol étudié est également décrit, ainsi que les appareils utilisés pour générer et compter l'aérosol. Les pulvérisateurs de gouttelettes utilisés sont décrits, ainsi que la méthode de calcul des particules collectées dans l'eau de rejet. La méthodologie expérimentale générale et le plan d'expériences Box-Behnken sont également décrits. Les résultats du transfert des nanoparticules vers l'eau de rejet sont également présentés dans ce chapitre, ainsi qu'une discussion sur la collecte des nanoparticules par les parois de l'épurateur et l'appareil à buses. Enfin, étant donné la technologie de pulvérisation utilisée dans ce travail, l'effet secondaire possible de la modification de la configuration de la buse est discuté.

**Le chapitre III** présente les résultats expérimentaux obtenus en utilisant la méthodologie de conception Box-Behnken. Pour les modèles BBD qui se sont avérés statistiquement significatifs, les équations de régression sont utilisées pour prédire les réponses et les résultats sont comparés aux données expérimentales. Des graphiques de surface montrant l'influence combinée de deux facteurs indépendants (tout en maintenant le troisième constant) sont également tracés. À l'aide du logiciel Design Expert V13, les conditions de fonctionnement optimales qui maximisent les réponses de l'épurateur à l'échelle pilote sont déterminées, et des essais expérimentaux de confirmation sont effectués.

**Le chapitre IV** présente un modèle de collecte des particules qui tient compte des contributions individuelles des mécanismes d'impaction inertielle, de diffusion brownienne, d'interception et de thermophorèse. Les paramètres clés du modèle, tels que la vitesse de sédimentation des gouttelettes, la vitesse relative gouttelette-particule, la compacité des

gouttelettes dans le laveur et la densité effective des particules, sont estimés. Un ajustement du modèle est ensuite effectué pour sélectionner, parmi les différents auteurs examinés dans le chapitre I, un modèle mécanistique qui s'adapte le mieux aux résultats expérimentaux dans des conditions nominales. Une analyse de sensibilité est menée pour examiner l'influence de la densité effective des particules, de la densité de tassement (compacité) des gouttelettes et de la vitesse relative gouttelettes-particules sur l'efficacité de collecte de l'épurateur. L'influence du débit de gaz, du débit de liquide et du diamètre des gouttelettes est également étudiée à l'aide du modèle mécanistique sélectionné. Enfin, la robustesse du modèle mécanistique est testée en comparant les résultats à ceux de trois séries expérimentales DOE (série 6, série 13 et série 15).

**Mots clés :** Incinération, épurateur par pulvérisation, nanoparticules, efficacité de la collecte, conception de Box-Behnken

## Abstract

As the use of engineered nanomaterials (ENM) in industrial and consumer products increases, a larger amount of ENM will likely end up in waste streams at the end of their life and potentially be released into the environment. Currently, it is estimated that more than 300,000 metric tons of ENM are released into landfills, soil, water, and air each year [3].

Despite the known potential health and environmental risks of exposure to engineered nanomaterials (ENM) [4–7], there are currently no regulations addressing the safe disposal of ENM at the end of their life cycle. This lack of regulation is particularly concerning as the volume of nanowaste (NW – waste containing ENM) is expected to increase. There is a growing need for regulatory frameworks on NW management [8, 9], and it is important to understand how NW is affected by current waste management systems.

Recent research has shown that engineered nanomaterials (ENM) can survive the combustion process in waste incineration and end up in flue gas [10–13]. However, there is a limited understanding of how effective current flue gas cleaning technologies (FGCT) are at removing ENM in waste incineration plants (WIP). One type of FGCT commonly used in WIP is a scrubber, which is primarily designed to treat acid pollutants. Scrubbers are known to have low efficiency for collecting particulate matter (PM) smaller than 5.0  $\mu\text{m}$ . However, a study by Kim et al. [14] found that under certain conditions, a scrubber can effectively collect PM smaller than 1.0  $\mu\text{m}$ . Several studies have investigated the influence of the operating parameters of a scrubber on the collection of PM > 1.0  $\mu\text{m}$  [18–22], and a few were focused on optimizing the operating parameters of the scrubbers [23–26]. However, to our knowledge, no study has been carried out to evaluate the performance of a spray scrubber concerning nanoparticle collection under waste incineration conditions. The present thesis aims to evaluate the performance of a pilot-scale scrubber concerning nanoparticle collection contained in a flue gas representing the conditions of a hazardous waste incineration plant spray scrubber in terms of height-to-diameter ratio, liquid-to-gas ratio, gas inlet/outlet temperatures, gas humidity, gas residence time, and gas flow regime, droplet diameter and particle concentrations. Also, the influence of three independent operating factors - gas flowrate, liquid flowrate and droplet diameter on the collection of carbon nanoparticles by a pilot-scale scrubber was investigated using the Box-Behnken design methodology.

**Keywords:** Incineration, Spray scrubber, Nanoparticle, Collection efficiency, Box-Behnken design

# Contents

THESE DE DOCTORAT DE .....	1
L'ÉCOLE NATIONALE SUPERIEURE .....	1
MINES-TELECOM ATLANTIQUE BRETAGNE PAYS DE LA LOIRE – IMT ATLANTIQUE.....	1
ECOLE DOCTORALE N° 648 <i>Sciences pour l'Ingénieur et le Numérique</i> Spécialité : Génie des procédés et des Bioprocédés.....	1
List of Figures.....	13
List of Tables .....	16
Nomenclature .....	17
General introduction .....	23
Chapter 1: State of the Art .....	27
1.1 Introduction .....	28
1.2 Nanomaterials.....	28
1.2.1 Engineered nanomaterial market .....	30
1.2.2 Health and Environmental effect of engineered nanomaterials.....	31
1.2.3 End-of-life management of engineered nanomaterials .....	31
1.2.4 Incineration of engineered nanomaterials.....	32
1.3 Particle size distribution in a waste incineration plant .....	34
1.4 Wet scrubbing technology .....	34
1.4.1 Operating principles.....	36
1.4.2 Types of scrubbers .....	36
1.4.3 Applications of scrubbers .....	38
1.5 Particle collection mechanisms in a wet scrubber.....	39
1.5.1 Inertial impaction mechanism, $\eta_{imp}$ .....	40
1.5.2 Brownian Diffusion mechanism, $\eta_{diff}$ .....	43
1.5.3 Interception mechanism, $\eta_{int}$ .....	45
1.5.4 Other collection mechanisms .....	46
1.5.5 Single droplet collection efficiency, $\eta_{SD}$ .....	48
1.5.6 Role of scrubber walls on overall particle collection efficiency .....	49
1.6 Influence of operating parameters on wet scrubbing .....	50
1.6.1 Gas flowrate .....	50
1.6.2 Gas temperature .....	51
1.6.3 Gas humidity rate.....	51
1.6.4 Liquid flowrate .....	52
1.6.5 Droplet diameter .....	53
1.6.6 Particle diameter .....	54

1.7 Overview of experimental and theoretical studies about particle removal by wet Scrubber.....	55
1.8 Conclusions of the chapter .....	60
<b>Chapter 2: Materials and methods .....</b>	<b>61</b>
2.1 Introduction .....	62
2.2 Description of the experimental setup .....	62
2.2.1 Incineration plant – Full-scale spray scrubber .....	62
2.2.2 Pilot-scale spray scrubber .....	63
2.2.3 Collection efficiency measurement.....	68
2.2.4 Measurement of uncertainty .....	69
2.3 Aerosol Investigated.....	69
2.3.1 Carbon particle generator and measurement equipment.....	70
2.3.2 Dilution before counting/sampling .....	71
2.3.3 Carbon particle size distribution and concentration.....	72
2.4 Liquid collectors .....	73
2.4.1 Droplet characterization.....	73
2.4.2 Range of droplet diameter.....	76
2.5 Methodology.....	77
2.5.1 Overall methodology .....	77
2.5.2 Design of Experiment .....	78
2.5.3 Operating conditions for experimental campaigns .....	79
2.5.4 Statistical analysis of BBD results.....	80
2.6 Qualification of experimental setup .....	81
2.6.1 Particle removal efficiency of the pilot-scale scrubber with no liquid injection ...	81
2.6.2 Influence of nozzle configurations on the particle collection efficiency.....	84
2.6.3 Quantification of transfer of nanoparticles to liquid-phase .....	88
2.7 Conclusions of the chapter .....	89
<b>Chapter 3: Optimization of nanoparticle collection by spray scrubber using Box-Behnken Design .....</b>	<b>91</b>
3.1 Introduction .....	92
3.2 Box-Behnken Design (BBD) responses .....	92
3.3 Box–Behnken statistical analysis .....	94
3.3.1 Analysis of Variance (ANOVA).....	94
3.3.2 Examination of residuals .....	102
3.4 Box–Behnken Design experimental results.....	104
3.5 Interactions of independent parameters.....	107
3.5.1 Responses $Y_2$ @ 20 nm.....	108
3.5.2 Responses $Y_5$ @ 35 nm.....	113
3.5.3 Responses $Y_8$ @ 62 nm.....	117
3.6 Box–Behnken design model optimization.....	121
3.6.1 Individual response surfaces and desirability approach.....	121
3.6.2 Optimal operating factors and confirmatory experiment.....	122
3.7 Conclusion of the chapter .....	123
<b>Chapter 4: Mechanistic modeling of particle collection efficiency .....</b>	<b>125</b>

4.1 Introduction .....	126
4.2 Calculation of model parameters .....	126
4.2.1 Particle effective density ( $\rho_e$ ) .....	126
4.2.2 Droplet settling velocity ( $V_t$ ) .....	127
4.2.3 Relative velocity between droplets and particles ( $U$ ) .....	129
4.2.4 Droplet packing density ( $\alpha$ ) .....	131
4.3 Model selection .....	132
4.4 Adjusted experimental data .....	136
4.5 Sensitivity analysis at nominal conditions .....	137
4.5.1 Particle effective density .....	137
4.5.2 Droplet packing density .....	137
4.5.3 Relative velocity .....	138
4.6 Mechanistic modeling of the influence of operating parameters .....	139
4.6.1 Influence of Gas flowrate .....	139
4.6.2 Influence of Liquid flowrate .....	140
4.6.3 Influence of Droplet diameter and Droplet velocity .....	140
4.7 Mechanistic model robustness verification .....	141
4.8 Conclusion of the chapter .....	144
<b>General conclusions and perspectives.....</b>	<b>145</b>
<b>Annexes .....</b>	<b>153</b>
<b>References.....</b>	<b>183</b>

# List of Figures

Figure 1 Sources of nanomaterials .....	29
Figure 2 Types of Engineered nanomaterials.....	30
Figure 3 Effects and potential release pathways of ENM .....	31
Figure 4 Published studies on the incineration of ENM-containing wastes .....	32
Figure 5 Schematic of co-current and counter-current wet scrubber .....	35
Figure 6 Types of scrubbers .....	37
Figure 7 Application of scrubbers .....	39
Figure 8 Impaction collection mechanism .....	40
Figure 9 Brownian diffusion mechanism .....	43
Figure 10 Interception mechanism.....	45
Figure 11 Overall collection efficiency and individual contribution of each mechanism (adapted from Ardon-Dryer et al.[124]).....	49
Figure 12 Full-scale Industrial unit TREDI Salaise-2 © Groupe Séché Environnement .....	63
Figure 13 Scheme of the experimental setup .....	66
Figure 14 Photograph of the experimental setup .....	67
Figure 15 Image of nozzles at four different spray headers .....	67
Figure 16 Breakdown of the experimental test procedure (not drawn to scale).....	68
Figure 17 SEM observation of carbon nanoparticle agglomerates generated by the DNP 2000 generator (Palas).....	70
Figure 18 Principle of the spark generator .....	71
Figure 19 VKL 100 dilution system © Palas .....	72
Figure 20 Particle size distribution of carbon nanoparticles upstream of setup at nominal conditions (average for N:4; standard deviation).....	72
Figure 21 single orifice hollow cone nozzle 220.185.1Y.AC nozzle .....	73
Figure 22 Cumulated droplet number/surface.....	75
Figure 23 Droplet velocity intensity vs (a) Droplet size number distribution and (b) Droplet size surface distribution.....	75
Figure 24 Linear extrapolation of droplet parameters at 20 mm from the nozzle.....	76
Figure 25 Overall research methodology .....	77
Figure 26 Graphical representation of three-factor Box–Behnken design.....	78
Figure 27 BBD cube matrix of 17 runs for 3 independent factors and 8 responses.....	80
Figure 28 Nanoparticle collection efficiency by the scrubber with no liquid injection at varying gas flowrates at 70°C - 1% RH (average for N: 4; standard deviation).....	82
Figure 29 Particle size distribution upstream and downstream of the scrubber operating with no liquid injection at varying gas flowrates (average for N:4; standard deviation).....	84
Figure 30 Collection efficiency at Test A conditions for varying nozzle configurations (average N=4; standard deviation) .....	87
Figure 31 Collection efficiency at Test B conditions for varying nozzle configurations (average N=4; standard deviation) .....	87
Figure 32 Collection efficiency at Test C conditions for varying nozzle configurations (average N=4; standard deviation) .....	88
Figure 33 Particle/liquid vacuum filtration apparatus.....	88
Figure 34 Mass balance of carbon nanoparticles at nominal conditions.....	89

Figure 35 Range of BBD responses .....	93
Figure 36 Depiction of chosen responses at average nominal conditions.....	93
Figure 37 Diagnostic plots for $Y_2$ .....	103
Figure 38 Diagnostic plots for $Y_5$ .....	103
Figure 39 Diagnostic plots for $Y_8$ .....	104
Figure 40 Experimental (actual) particle removal efficiency versus predicted particle removal efficiency for $Y_2$ , $Y_5$ and $Y_8$ .....	107
Figure 41 Counter and response surface plots showing the influence of factors A and B on $Y_2$ at constant C (a:60 and b:80 $\mu\text{m}$ ) .....	110
Figure 42 Counter and response surface plots showing the influence of factors A and C on $Y_2$ at constant B (a:4.8 and b:1.6 $\text{L}\cdot\text{min}^{-1}$ ).....	111
Figure 43 Counter and response surface plots showing the influence of factors B and C on $Y_2$ at constant A (a:55 and b:35 $\text{Nm}^3\cdot\text{h}^{-1}$ ).....	112
Figure 44 Counter and response surface plots showing the influence of factors A and B on $Y_5$ at constant C (a:60 and b:80 $\mu\text{m}$ ) .....	114
Figure 45 Counter and response surface plots showing the influence of factors A and C on $Y_5$ at constant B (a:4.8 and b:1.6 $\text{L}\cdot\text{min}^{-1}$ ).....	116
Figure 46 Counter and response surface plots showing the influence of factors B and C on $Y_5$ at constant A (a:55 and b:35 $\text{Nm}^3\cdot\text{h}^{-1}$ ).....	117
Figure 47 Counter and response surface plots showing the influence of factors A and B on $Y_8$ at constant C (a:60 and b:80 $\mu\text{m}$ ) .....	118
Figure 48 Counter and response surface plots showing the influence of factors A and C on $Y_8$ at constant B (a:4.8 and b:1.6 $\text{L}\cdot\text{min}^{-1}$ ).....	119
Figure 49 Counter and response surface plots showing the influence of factors B and C on $Y_8$ at constant A (a:55 and b:35 $\text{Nm}^3\cdot\text{h}^{-1}$ ) .....	120
Figure 50 Individual response surfaces showing predicted collection efficiencies .....	121
Figure 51 Parity plot showing the distribution of experimental vs. predicted responses.....	123
Figure 52 Cumulative particle size distribution of the carbon nanoparticles measured upstream of the scrubber with SMPS and ELPI particle counters (average for N:2; standard deviation) .....	127
Figure 53 Principal forces acting on a droplet flowing in a fluid .....	128
Figure 54 Cross-sectional view of the pilot-scale scrubber .....	130
Figure 55 Comparison of overall collection efficiency considering selected impaction and diffusion models with experimental results at nominal conditions (average for N:4; standard deviation).....	134
Figure 56 Comparison of overall collection efficiency considering selected impaction, diffusion and Interception models with experimental results at nominal conditions (average for N:4; standard deviation) .....	134
Figure 57 Comparison of overall collection efficiency considering selected impaction, diffusion, interception and thermophoresis models with experimental results at nominal conditions (average for N: 4; standard deviation).....	135
Figure 58 Comparison of experimental, adjusted experimental and mechanistic results at nominal conditions (average for N: 4; standard deviation).....	136
Figure 59 Comparison of mechanistic and experimental collection efficiencies at varying particle densities at nominal conditions (average for N: 4; standard deviation).....	137
Figure 60 Comparison of mechanistic and experimental collection efficiencies at varying droplet packing density at nominal conditions (average for N: 4; standard deviation) .....	138

Figure 61 Comparison of mechanistic and experimental collection efficiency at varying droplet-particle relative velocity at nominal conditions (average for N: 4; standard deviation) .....	139
Figure 62 Mechanistic model results of the influence of gas flowrate on collection efficiency at a constant liquid flowrate of 3.2 L.min <sup>-1</sup> and droplet diameter of 70 μm (average for N: 4; standard deviation) .....	139
Figure 63 Mechanistic model results of the influence of liquid flowrate on collection efficiency at a constant gas flow rate of 45 Nm <sup>3</sup> .h <sup>-1</sup> and droplet diameter of 70 μm (average for N: 4; standard deviation) .....	140
Figure 64 Mechanistic model results of the (a) droplet diameter and (b) combined influence of droplet diameter and velocity on collection efficiency at a constant gas flow rate of 45 Nm <sup>3</sup> .h <sup>-1</sup> and liquid flowrate of 3.2 L.min <sup>-1</sup> (average for N: 4; standard deviation) .....	141
Figure 65 Comparison of experimental, BBD model and mechanistic model results at Run 15 – A: 35 Nm <sup>3</sup> .h <sup>-1</sup> , B: 1.6 L.min <sup>-1</sup> and C: 70 μm (average for N: 4; standard deviation).....	142
Figure 66 Comparison of experimental, BBD model and mechanistic model results at Run 6 – A: 55 Nm <sup>3</sup> .h <sup>-1</sup> , B: 3.2 L.min <sup>-1</sup> and C: 60 μm (average for N: 4; standard deviation).....	143
Figure 67 Comparison of experimental, BBD model and mechanistic model results at Run 13 – A: 45 Nm <sup>3</sup> .h <sup>-1</sup> , B: 4.8 L.min <sup>-1</sup> and C: 60 μm (average for N: 4; standard deviation).....	143

# List of Tables

Table 1 Particle collection based on impaction mechanisms .....	42
Table 2 Particle collection models based on diffusion mechanisms .....	44
Table 3 Particle collection models based on interception mechanisms .....	46
Table 4 Summary of studies on particle removal in wet scrubber .....	55
Table 5 Full-scale and pilot-scale spray scrubbers parameters at nominal conditions .....	64
Table 6 Summary of droplet characterization measurement.....	74
Table 7 Range of droplet parameters for a single spray nozzle .....	76
Table 8 Box–Behnken design responses .....	79
Table 9 Box–Behnken design experimental variables .....	79
Table 10 Carbon nanoparticle relaxation time .....	84
Table 11 Nozzle configurations for test A, B and C .....	86
Table 12 Full ANOVA data for $Y_2$ .....	95
Table 13 Reduced ANOVA data for $Y_2$ .....	96
Table 14 Full ANOVA data for $Y_5$ .....	97
Table 15 Reduced model for response $Y_5$ .....	99
Table 16 Full ANOVA data for $Y_8$ .....	100
Table 17 Reduced model for response $Y_8$ @ 62 nm .....	101
Table 18 Summary of ANOVA of reduced BBD models.....	102
Table 19 Box–Behnken design matrix for the three independent factors and corresponding responses .....	106
Table 20 Optimal values for the collection of nanoparticles .....	122
Table 21 Summary of the influence independent factors.....	124
Table 22 Relative velocities for sensitivity analysis at nominal conditions .....	131
Table 23 Droplet residence times for droplet packing density sensitivity analysis .....	132
Table 24 Summary of mechanistic model parameters .....	132
Table 25: Final model composition.....	135

# Nomenclature

$b_0$ ,	Regression constant term	[-]
$b_1$ , $b_2$ , and $b_3$	Regression coefficients of linear terms	[-]
$b_{11}$ $b_{22}$ $b_{33}$	Regression coefficients of quadratic terms	[-]
$b_{12}$ $b_{13}$ $b_{23}$	Regression coefficients of interaction terms	[-]
$C_c$	Cunningham coefficient	[-]
$C_{down,api}$	Downstream concentration at characteristic diameter of the $i$ th particle size range	[#.cm <sup>-3</sup> ]
$C_o$	Number of center points	[-]
$C_{up,api}$	Upstream concentration at characteristic diameter of the $i$ th particle size range	[#.cm <sup>-3</sup> ]
$d$	Diameter of scrubber	[m]
$d_a$	Aerodynamic equivalent diameter	[ $\mu$ m]
$d_m$	Electrical mobility diameter	[ $\mu$ m]
$d_p$	Particle diameter	[m]
$D$ or Factor C	Droplet diameter	[m]
$D_{diff}$	Particle diffusion coefficient	[-]
$D_{32}$	Sauter mean diameter	[ $\mu$ m]
$DV_{10}$	Droplet diameter below which 10% of the total volume of droplets fall	[ $\mu$ m]
$DV_{50}$	Droplet diameter below which 50% of the total volume of droplets fall	[ $\mu$ m]
$DV_{90}$	Droplet diameter below which 90% of the total volume of droplets fall	[ $\mu$ m]

<i>Eff</i>	Fractional Efficiency	[-]
F	Mathematical desirability function	[-]
F <sub>B</sub>	Buoyant forces	[N]
F <sub>D</sub>	Upward drag	[N]
F <sub>G</sub>	Force of gravity	[N]
g	Gravitational acceleration	[m.s <sup>-2</sup> ]
h	Height of the scrubber	[m]
k	Number of independent variables	[-]
K <sub>a</sub>	Thermal conductivity of gas	[Kg.m.s <sup>-3</sup> .K <sup>-1</sup> ]
k <sub>B</sub>	Boltzmann constant	[m <sup>2</sup> .kg.s <sup>-2</sup> .K <sup>-1</sup> ]
K <sub>p</sub>	Thermal conductivity of particle	[Kg.m.s <sup>-3</sup> .K <sup>-1</sup> ]
J	Hydrodynamic factor	[-]
K	Hydrodynamic factor	[-]
N	Total number of measurements	[-]
n	Number of particle size	[-]
U	Droplet-Particle Relative Velocity	[m.s <sup>-1</sup> ]
U <sub>G</sub>	Gas velocity in the tower	[m.s <sup>-1</sup> ]
P <sub>c</sub>	Particle concentration	[#.cm <sup>-3</sup> ]
<i>P<sub>e</sub></i>	Peclet number	[-]
<i>Pr</i>	Prandtl number of gas	[-]
Q <sub>G</sub> or Factor A	Gas flowrate	[Nm <sup>3</sup> .h <sup>-1</sup> ]
Q <sub>L</sub> or Factor B	Liquid flowrate	[m <sup>3</sup> .s <sup>-1</sup> ]
R	Interception number	[-]
R <sub>D</sub>	Droplet radius	[m]
Re	Reynolds number	[-]

$S_c$	Schmidt number	[-]
SD	Standard deviation	[-]
SE	Standard error	[-]
SMD	Sauter Mean diameter	[ $\mu\text{m}$ ]
Stk	Stokes number	[-]
Stk*	Stokes number defined by Slinn et al. [27]	[-]
T	Gas temperature inside scrubber	[K]
$T_a$	Gas inlet temperature	[K]
$T_d$	Droplet surface temperature	[K]
$T_D$	Residence time of a droplet	[s]
$U_D$	Droplet velocity	[ $\text{m}\cdot\text{s}^{-1}$ ]
$X_i$	Individual measurement	[-]
$\bar{X}$	Mean of the measurements	[-]
$\text{Vol}_D$	Total volume of droplets in the scrubber	[ $\text{m}^3$ ]
$\text{Vol}_p$	Volume of particle	[ $\text{m}^3$ ]
$V_t$	Terminal Settling Velocity of Droplet	[ $\text{m}\cdot\text{s}^{-1}$ ]
Y	Predicted response	[-]
$Y_1$	Predicted response at a particle diameter of 17 nm	[ $\text{m}^2\cdot\text{s}^{-1}\cdot\text{V}^{-1}$ ]
$Y_2$	Predicted response at a particle diameter of 20 nm	[-]
$Y_3$	Predicted response at a particle diameter of 24 nm	[-]
$Y_4$	Predicted response at a particle diameter of 29 nm	[-]
$Y_5$	Predicted response at a particle diameter of 35 nm	[-]
$Y_6$	Predicted response at a particle diameter of 42 nm	[-]
$Y_7$	Predicted response at a particle diameter of 51 nm	[-]

$Y_8$	Predicted response at a particle diameter of 62 nm	[-]
-------	--	-----

**Greek letters**

$\alpha$	Packing density	[-]
$\tau_p^+$	Relaxation time of particle	[-]
$\phi_1$	Outbound gas phase particle flux	[-]
$\phi_2$	Particle flow transferred to the liquid phase	[-]
$\phi_e$	Inbound gas phase particle flux	[-]
$\mu$	Dynamic gas viscosity	[Pa.s]
$\epsilon$	Wall/surface losses	[-]
$\mu$	Gas dynamic viscosity	[-]
$\sigma$	Viscosity ratio of water to air	[-]
$\lambda$	Mean free path of gas molecules	[m]
$\rho_D$	Droplet density	[kg.m <sup>-3</sup> ]
$\rho_e$	Particle effective density	[kg.m <sup>-3</sup> ]
$\rho_0$	Reference density	[kg.m <sup>-3</sup> ]
$\rho_p$	Particle density	[kg.m <sup>-3</sup> ]
$\rho_{eff}$	Particle Effective density	[kg.m <sup>-3</sup> ]
$\eta_{diff}$	Single droplet collection efficiency due to Brownian diffusion Mechanism	[-]
$\eta_{imp}$	Single droplet collection efficiency due to Inertial Impaction Mechanism	[-]
$\eta_{int}$	Single droplet collection efficiency due to Interception Mechanism	[-]
$\eta_{Ef}$	Single droplet collection efficiency due to electrostatic attraction	[-]

$\eta_{thph}$	Single droplet collection efficiency due to thermophoresis	[-]
$\eta_{diph}$	Single droplet collection efficiency due to diffusiophoresis	[-]
$\eta_G$	Single droplet collection efficiency due to gravitational settling	[-]
$\eta_{SD}$	Single Droplet Collection Efficiency	[-]

### Abbreviations

ADEME	French Agency for Ecological Transition
AICc	Corrected version of Akaike Information Criterion
ANOVA	Analysis of variance
BBD	Box-Behnken Design
BCWS	Bubble Column Wet Scrubber
CAGR	Compound Annual Growth Rate
CDS	Charged-Droplet Scrubber
CFD	Computational Fluid Dynamic
CPC	Condensation Particle Counter
CPWS	Composite Wet Scrubber
CWS	Cyclone Wet Scrubber
DF	Degrees of freedom
DMA	Differential Mobility Analyzer
DOE	Design of Experiment
DSEE	Energy Systems and Environment Department
EC	European Commission
ENM	Engineered Nanomaterial
ELPI	Electrical Low-Pressure Impactor
EPA	Environmental Protection Agency
ESP	Electrostatic Precipitator

EWS	Electrostatic Wet Scrubber
FGCT	Flue Gas Cleaning Technology
FST	Flow Pattern Control Device Scrubbing Tower
HAS	Heat Absorbing Scrubber
ISO	International Organization for Standardization
IWS	Innovative Wet Scrubber
MPPS	Most Penetrating Particle Size
MSWI	Municipal Solid Waste Incineration
NP	Nanoparticle
NW	Nanowaste
OST	Open Scrubbing Tower
OWS	Orifice Wet Scrubber
PCDD/F	Polychlorinated Dibenzo-P-Dioxins and Furans
PSD	Particle Size Distribution
PM	Particulate Matter
USD	United States Dollars
U-TS	U-Type Scrubber
RSM	Response Surface Methodology
SCR	Selective Catalytic Reduction
SPWS	Sieve Plate Wet Scrubber
SNCR	Selective non-Catalytic Reduction
SMPS	Scanning Mobility Particle Sizer
SWS	Spray Wet Scrubber
TST	Tray Scrubbing Tower
TWS	Turbulent Wet Scrubber
VWS	Venturi Wet Scrubber
WFGDSS	Wet Flue Gas Desulfurization Scrubber
WIP	Waste Incineration Plant

# **General introduction**

Nanotechnology is considered a key technology of the 21st century [1] and has led to significant progress in various important industries, including agriculture, energy, healthcare, electronics, personal care, packaging, and environmental remediation. The widespread use of nanotechnology in these sectors is expected to increase the global nanotechnology market to over 62.8 billion USD by 2031 [2].

As the use of engineered nanomaterials (ENM) in industrial and consumer products increases, a larger amount of ENM will likely end up in waste streams at the end of their life and potentially be released into the environment. Currently, it is estimated that more than 300,000 metric tons of ENM are released into landfills, soil, water, and air each year [3].

Despite the known potential health and environmental risks of exposure to ENM [4–7], there are currently no regulations addressing the safe disposal of ENM at the end of their life cycle. This lack of regulation is particularly concerning as the volume of nanowaste (NW – waste containing ENM) is expected to increase. There is a growing need for regulatory frameworks on safe NW management [8, 9], and it is important to understand how NW is affected by current waste management systems. While increasing amounts of NW are recycled [28], the potential risks and uncertainties associated with NW have resulted in a preference for NW management via centralized waste-to-energy facilities such as incineration.

Recent research has shown that engineered nanomaterials (ENM) can survive the combustion process encountered during waste incineration and end up in flue gas [10–13]. However, there is a limited understanding of how effective current flue gas cleaning technologies (FGCT) are at removing ENM in waste incineration plants (WIP). One type of FGCT commonly used in WIP is a scrubber, which is primarily designed to treat acid pollutants.

Scrubbers offer flexibility in flue gas treatment including the ability to treat acid pollutants and handle flammable/explosive PM in high-temperature flue gases. This makes scrubbers often present in hazardous waste incineration plants [15]. Scrubbers are known to have low efficiency for collecting particulate matter (PM) smaller than 5.0  $\mu\text{m}$ . However, a study by Kim et al. [14] found that under certain conditions, a scrubber can effectively collect PM smaller than 1.0  $\mu\text{m}$ .

Scrubbers have also been reported to be used in other industrial applications such as semiconductor and cement production, where nano-sized particles are known to be emitted during manufacturing processes [16, 17]. Several studies have investigated the influence of

the operating parameters of a scrubber on the collection of  $PM > 1.0 \mu m$  [18–22], and a few were focused on optimizing the operating parameters of the scrubbers [23–26]. However, to our knowledge, no study has been carried out to evaluate the performance of a spray scrubber concerning nanoparticle collection under waste incineration conditions.

The present thesis aims to evaluate the performance of a pilot-scale scrubber concerning nanoparticle collection contained in an incineration flue gas representative of the conditions of a hazardous waste incineration plant spray scrubber in terms of height-to-diameter ratio, liquid-to-gas ratio, gas inlet/outlet temperatures, gas humidity, gas residence time, and gas flow regime, droplet diameter and particle concentrations. Carbon nanoparticles are the aerosols investigated in this thesis. Also, the influence of three independent operating factors - gas flowrate, liquid flowrate and droplet diameter on the collection of carbon nanoparticles by a pilot-scale scrubber was investigated using the Design of Experiment (DOE) - Box-Behnken design methodology.

The research work described in this dissertation was supported by The Agency for Ecological Transition – ADEME – (Grant No. TEZ19-002) and Région Pays de la Loire in collaboration with Séché Environnement Group as an industrial partner. The thesis was been carried out at the Département systèmes énergétiques et environnement (DSEE) GEPEA laboratory of the IMT Atlantique – Campus de Nantes and is scheduled from 1st November, 2019 to 28th February, 2023. The manuscript is organized as follows:

**Chapter I** proposes a bibliographic review that aims to summarize the definition, types, and production of engineered nanomaterials (ENM) based on published works. It also examines the potential health and environmental impacts of ENM. Given the current lack of regulations on the safe disposal of ENM at the end of its life, this review looks at the various methods currently used for treating waste containing ENM. A focus is then placed on the fate of ENM in waste incineration plants. The second objective of this chapter is to examine wet scrubbing technology, including its operating principles, types, industrial applications, and the various particle collection mechanisms involved in a scrubber. Finally, this chapter reviews the influence of key operating conditions such as the gas flow rate, gas temperature, gas humidity rate, liquid flow rate, and droplet diameter on the particle collection efficiency of a wet scrubber.

In **chapter II**, the materials and methods used in this thesis are presented. The experimental setup is described, including its design to mimic a full-scale spray scrubber present in the

flue-gas cleaning line of a hazardous waste incineration plant. The aerosol being studied is also described, along with the apparatus used for generating and counting the aerosol. The droplet collectors used are described, as well as the method for calculating the collected particles in the discharge water. The general experimental methodology, the Box-Behnken design, is also described. The results of the transfer of nanoparticles to the discharge water are also presented in this chapter, along with a discussion of the nanoparticle collection by both the walls of the scrubber and the nozzle apparatus. Finally, given the spraying technology used in this work, the possible secondary effect of modifying the nozzle configuration is discussed.

**Chapter III** presents the experimental results obtained from the Box-Behnken design (BBD) methodology. The Design Expert V13 software is used for the experimental data analysis and interpretation of the proposed BBD models (regression equations). For the BBD models that were found to be statistically significant, the regression equations are used to predict the responses and the results are compared to the experimental data. Surface plots showing the combined influence of two independent factors (while keeping the third constant) are plotted. Using the Design Expert V13 software, the optimal operating conditions that maximize the responses by the pilot-scale scrubber are determined, and confirmatory experimental runs are conducted.

In **Chapter IV**, a particle collection model that considers the individual contributions of inertial impaction, Brownian diffusion, interception, and thermophoresis mechanisms is presented. The key model parameters, such as the droplet settling velocity, the droplet-particle relative velocity, the droplet packing density, and the particle effective density, are estimated. A model fitting is then carried out to select a final mechanistic model from the various authors reviewed in chapter I that "best fits" the experimental results at nominal conditions. A sensitivity analysis is conducted to examine the influence of the particle effective density, droplet packing density, and droplet-particle relative velocity on the collection efficiency of the scrubber. The influence of the gas flow rate, liquid flow rate, and droplet diameter is also investigated using the selected mechanistic model. Finally, the mechanistic model is tested for robustness by comparing its results to those of three DOE experimental runs (Run 6, Run 13, and Run 15).

# **Chapter 1: State of the Art**

## 1.1 Introduction

In this chapter, efforts have been made to establish the definition, the types and the production of engineered nanomaterials (ENM) from published works. A literature review has also been carried out on the potential health and environmental effects of ENM. Given the current lack of regulations on the safe disposal of ENM at end-of-life, an attempt has been made to report the various methods by which nanowaste (i.e., waste containing ENM) are treated today. A focus is then made on the fate of ENM in waste incineration plants.

The second objective of this chapter is targeted at wet scrubbing technology. Specifically, the operating principles, the types, the industrial application and various particle collection mechanisms involved in a wet scrubber.

Lastly, this chapter ends with a review of the influence of key operating parameters such as gas flowrate, gas temperature, gas humidity rate, liquid flowrate and droplet diameter on particle collection efficiency by a wet scrubber.

## 1.2 Nanomaterials

There is currently no global consensus on the definition of a nanomaterial (NM). Saner et al. [29] reported that over 27 definitions of NM are given by various national and transnational bodies. The International Organization for Standardization (ISO) defines a “nanomaterial as a material with at least one external dimension or an internal structure or surface structure in the nanoscale (1 to 100 nm)” [30].

In the United States, the Environmental Protection Agency (EPA) defines a nanomaterial as a “chemical substance that is solid at 25 °C and standard atmospheric pressure, that is manufactured or processed in a form where the primary particles, including aggregates and agglomerates, are in the size range of 1–100 nm in at least one dimension, and that is intentionally manufactured or processed to exhibit unique and novel characteristics or properties because of their size” [31].

Recently, the European Commission (EC) [32] revised its definition of a nanomaterial to be a natural, incidental, or manufactured material consisting of solid particles present, either on their own or as identifiable constituent particles in aggregates or agglomerates where 50% or more of these particles in the number-based size distribution fulfills at least one of the following conditions:

- ❖ one or more external dimensions of the particle are in the size range of 1 nm to 100 nm;
- ❖ the particle has an elongated shape, such as a rod, fiber or tube, where two external dimensions are smaller than 1 nm and the other dimension is larger than 100 nm;
- ❖ the particle has a plate-like shape, where one external dimension is smaller than 1 nm and the other dimensions are larger than 100 nm

The ISO, EPA and EC definitions of nanomaterials do refer to the size or structure of the materials. The EPA definition goes further to emphasize the novel properties (like catalytic activity, chemical reactivity, or electrical conductivity) of the material. Source emphasis is further placed by the EC definition to include manufactured, natural and incidental nanomaterials. Broadly speaking, nanomaterials can be produced from two origins; Natural and synthetic sources (Figure 1). Natural nanomaterials are formed via different biogeochemical processes and include sources such as chemical weathering processes, volcanic eruptions, lightning and flash-pyrolysis [33, 34]. It is estimated that about 342 megatons of natural nanomaterials are present in the Earth's atmosphere annually [35]. Examples of both organic and inorganic sources of natural nanomaterials are shown in Figure 1 below.

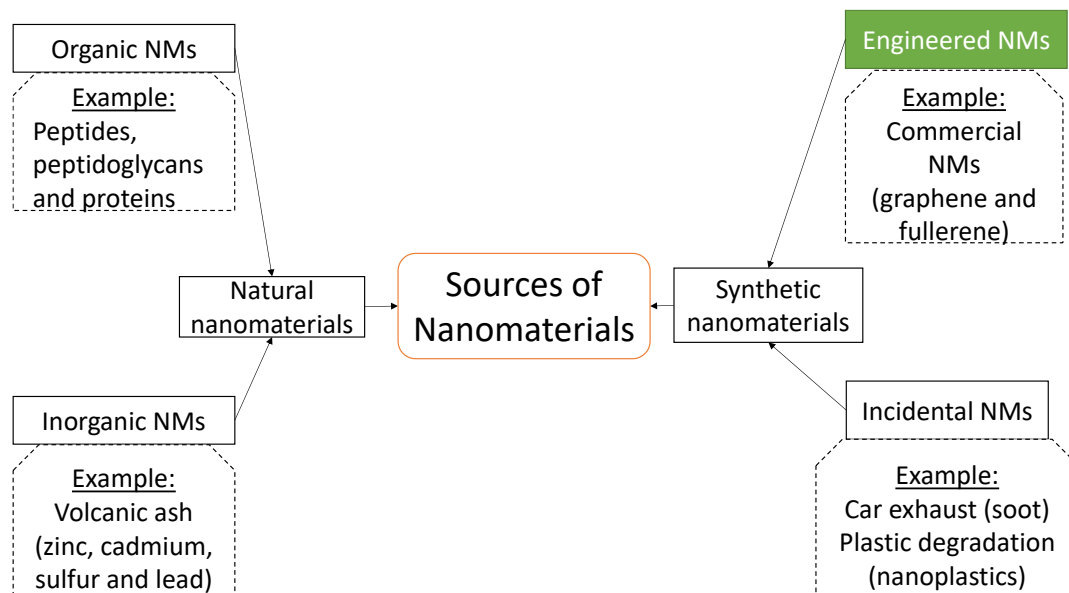


Figure 1 Sources of nanomaterials

Synthetic nanomaterials are formed from human (anthropogenic) activities and are classified into engineered (intentional) and unintentional nanomaterials. Hochella et al. [35] estimate that 10.3 megatons of synthetic nanomaterials are released into the atmosphere yearly. Although synthetic NM have a smaller volume in the environment compared to natural NM,

they are considered potentially hazardous to both humans and the environment and thus, are labeled as pollutants. Indeed, the unique physical (e.g., size, shape, surface area, and number concentrations), chemical (e.g., surface reactivity, stability, and solubility), optical, thermal and electrical properties that make engineered NM desirable in numerous industrial and consumer applications could also lead to their increase toxicity. The present study emphasizes intentionally produced synthetic *engineered nanomaterials (ENM)*.

### 1.2.1 Engineered nanomaterial market

The wide adoption of nanotechnology in vital sectors of the economy such as semiconductors, agriculture, health care, packing and personal care products has led to rapid growth in the production of ENM for commercial usage. Classifications of ENM either based on their synthesis or their structure exist in the literature [6, 36–38]. Engineered nanomaterials are generally classified into four groups; Organic-based, inorganic-based, carbon-based, and composite-based nanomaterials (Figure 2) [38].

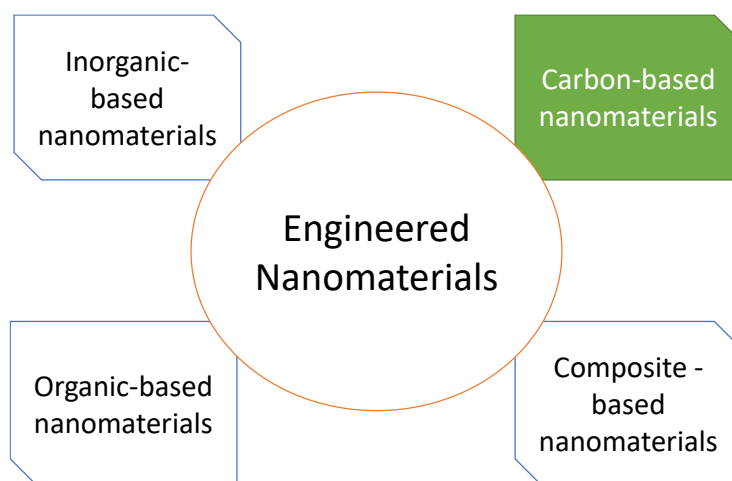


Figure 2 Types of Engineered nanomaterials

Inorganic-based nanomaterials comprise metal (e.g., copper, iron and zinc.) and metal oxide nanomaterials (e.g., titanium dioxide (TiO<sub>2</sub>) and copper oxide (CuO)). While organic-based nanomaterials exclude carbon materials and include dendrimers, cyclodextrin, liposomes, and micelle. Carbon-based nanomaterials comprise graphene, carbon fiber, fullerene, carbon black (soot) and carbon nanotubes. The combination of two or the three types of ENM mentioned above give a composite-based nanomaterial.

According to market experts [2], the global ENM market will grow at a 14.6% compound annual growth rate (CAGR) from its 2021 value of \$16.3 to \$62.8 billion by 2031. The global carbon ENM market is expected to reach \$31.6 billion by 2031 from a value of \$2.9 billion in

2021[39]. This shows that the carbon ENM market is growing at a higher CAGR (27.7%) than the overall ENM market. *The present work focuses on carbon nanoparticles i.e., a carbon-based ENM with all its external dimensions in the size range of 1 – 100 nm.*

### 1.2.2 Health and Environmental effect of engineered nanomaterials

To determine the potential effects of ENM on humans and the environment, it is relevant to understand their likely exposure pathways. The human body comes in contact with released NM either through the skin, the lungs, or the gastrointestinal tract. Figure 3 shows a representative possible pathway by which released ENM could end up in the human body. Exposure to nanoparticles has been associated with neurological (Alzheimer's and Parkinson's) diseases [40], and respiratory and cardiovascular diseases [7, 41]. In the environment, the formation of dust-cloud and light absorption by certain nanoparticles is linked to the depletion of the ozone layer [42, 43]. In aquatic organisms and lower plants, studies have reported that the presence of nanoparticles in a medium leads to bioaccumulation, physical abnormalities, and an increased death rate [44–46].

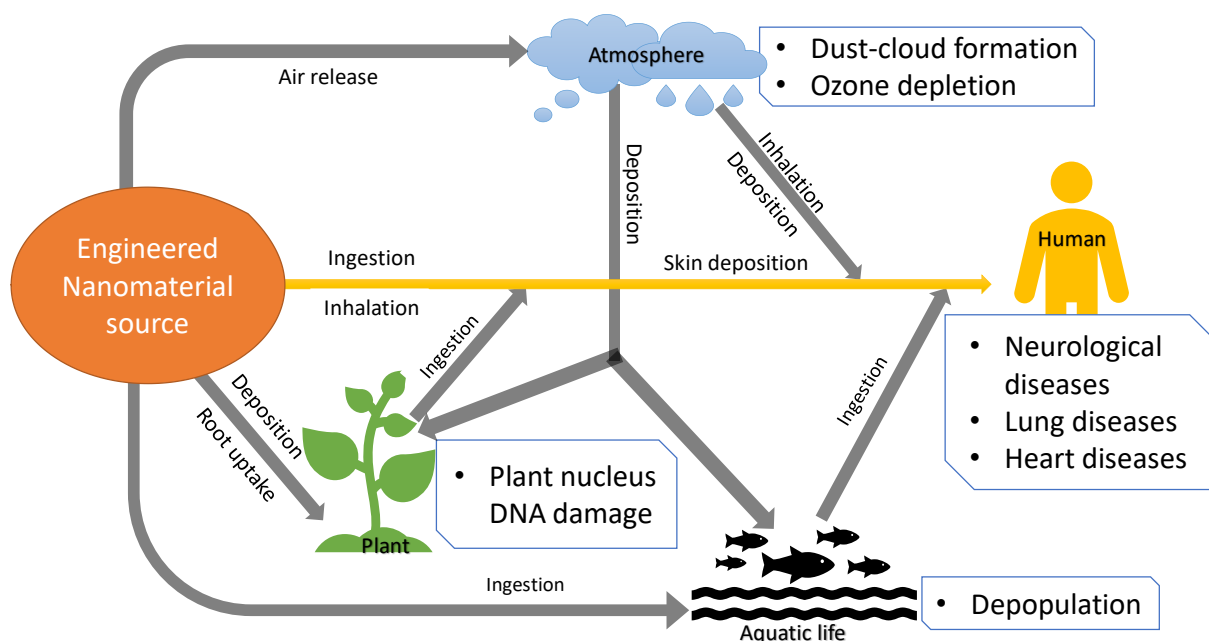


Figure 3 Effects and potential release pathways of ENM

### 1.2.3 End-of-life management of engineered nanomaterials

To date, there are no national or global regulations targeted at the safe disposal of ENM at their end-of-life. As such, nanowaste (NW - waste containing ENM) follows conventional

waste management pathways such as recycling, composting, incineration and landfilling. Several investigations have been carried out to model the possible destination of ENM at their end of life [47–52]. Insight into where existing and future NW end up could help establish their fate in these facilities and thus proper NW management guidelines. An increasing amount of NW are recycled typically in the construction industry for the production of high-strength concrete aggregates [53] or to increase the corrosion protection steel [28]. Biodegradable NW are treated via composting [54–57], however, the majority of NW today ends up in either waste incineration or landfills [52, 53, 58]. Gottschalk et al. [51] reported that the incineration of products containing ENM (in addition to sewage sludge and wastewater sources) is the major source of environmental release of ENM.

#### 1.2.4 Incineration of engineered nanomaterials

As stated above, the majority of ENM at end-of-life end up undergoing thermal incineration and/or being landfilled. In incineration, bulk or product-containing ENM are thermally treated at a temperature of 850 – 1100 °C, with high oxygen/fuel contact for at least 2 seconds residence time in the post-combustion zone of the incineration furnace. There are however limited studies on the fate of ENM during waste incineration. As such significant knowledge gap on the overall fate of nanoparticles during incineration still exist. Three (3) numerical studies were identified in the literature on the incineration of ENM [52, 59, 60]. Eighteen (18) experimental studies can be reported from the literature review of which five (5) are full-scale studies [10, 12, 61–63] and thirteen (13) are lab or pilot-scale studies [11, 64–75] (Figure 4).

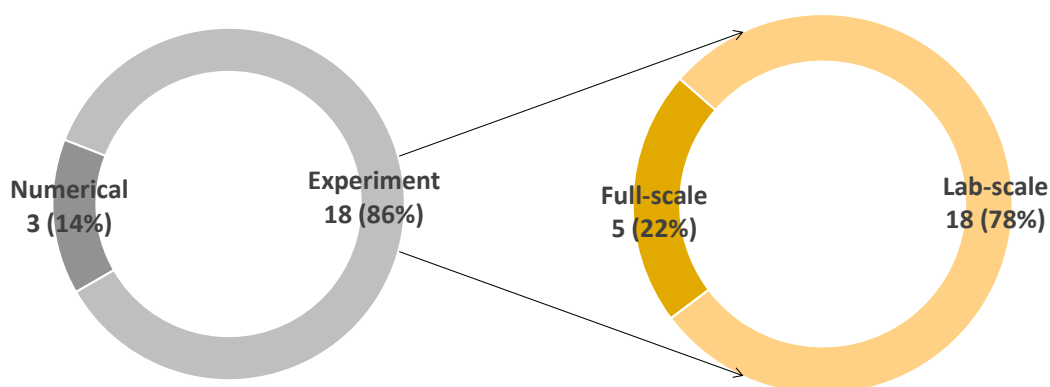


Figure 4 Published studies on the incineration of ENM-containing wastes

##### 1.2.4.1 The fate of engineered nanomaterials in the combustion chamber

Several factors play a vital role in determining the fate and behavior of ENM during incineration. Mueller et al. [52] reported that if the ENM are free or loosely bonded to a

substrate, they can be easily released during incineration, thus, joining the flue gas. If the ENM is however tightly bonded to another material, they are more likely to be accumulated in the bottom ash during incineration. The second factor to consider is the melting or boiling temperature of the ENM. If the boiling point of an ENM is lower or equal to the combustion temperature, the ENM will likely evaporate and re-condensate during incineration and hence join the flue gas stream. Thus, the ENM is unlikely to return to its nanoscale. On the other hand, if the combustion temperature is lower than the boiling point of the considered ENM, the ENM is more likely to retain its form during incineration [52, 76]. Also, Froggett et al. [77] reported that the thermochemical stability of ENM should be considered in determining the fate of ENM during incineration. Actually, for the ENM currently investigated, the majority of the ENM ended in the bottom ash during incineration [10, 12, 63, 78] except for the incineration of C<sub>60</sub> fullerenes as reported by Vejerano et al. [11]. A fraction of the ENM does however join the flue gas as was the case in the study by Walser et al. [10] where up to mass efficiency 45% (in mass concentration) of the 1 Kg of cerium oxide nanoparticles (nano-CeO<sub>2</sub>) introduced into the incineration furnace ended up in the flue gas. Some authors observed the morphological or chemical transformation of the ENM after incineration [64, 78] others did not [10, 11, 13]. It should be noted that the conclusions concerning morphological and chemical transformation, from the different authors cited above, are derived from the properties of the bulk ENM materials investigated by those authors and as such may not be extended to all ENM or even to the same ENM under different conditions. Existing knowledge gaps on the incineration of ENM need to be bridged as the presence of ENM in waste streams has been reported to result in increased emissions of some polycyclic aromatic hydrocarbons (PAHs) and polychlorinated-dibenzo-p-dioxins dibenzofurans (PCDD/Fs) species during incineration [79, 80].

#### **1.2.4.2 The fate of engineered nanomaterials in flue-gas cleaning technology**

To account for the ENM that joined the flue gas during waste incineration, Walser et al. [10] investigated the nano-CeO<sub>2</sub> removal efficiency by the flue gas cleaning technology (FGCT) units consisting of an electrostatic precipitator, a selective non-catalytic reduction (SNCR) and a wet scrubber present in a full-scale municipal waste incineration (MSWI) plant with a grate firing furnace. The authors reported a nano-CeO<sub>2</sub> mass collection efficiency greater than 99.9% in mass concentration. Lang et al. [62] obtained similar results (>99.9%) when they investigated the collection efficiency of nano-CeO<sub>2</sub> in a pilot-scale incineration plant with a rotary furnace and a spray absorber, a fabric filter, 2-stage wet scrubber and a SCR as the

FGCT units. Baran and Quicker [12] reported a nano-BaSO<sub>4</sub> removal efficiency of over 99.85% by the combined treatment of an evaporating cooler, a fabric filter, and a SCR in a MSWI plant with a grate firing furnace. Oischinger et al. [61] found a collection efficiency of 99.6% – 99.99% for nano titanium dioxide (nTiO<sub>2</sub>) incinerated in a MSWI plant with a cyclone, a spray dryer, a bag filter and a 2-stage scrubber as the FGCT units. Whether these high collection efficiencies can be generalized for other types of ENM is left to be investigated. The authors above did not mention the specific ENM collection efficiency by each of the FGCT units but reported only the combined ENM removal efficiency by all the units composing the FGCT. As the various FGCTs in a WIP are not the final destination of the collected or treated pollutants, it is essential to investigate the individual FGCT unit ENM collection efficiency. In the case of a wet scrubber, the discharged pollutant-containing water is could be sent to water treatment facilities not capable of handling ENM.

### **1.3 Particle size distribution in a waste incineration plant**

Several authors have characterize the particle size distribution in an incineration flue gas at various location along the flue gas cleaning units [81–83]. In a MSWI plant with a fuel rate of 9-10 Mg.h<sup>-1</sup>, a fabric filter and a wet SCR, Buonanno et al. [83] reported a particle size range in number of 5.5 – 800 nm with a mode in number distribution shifting between 60 and 100 nm at peak emission. Similarly, in a MSWI plant with a fuel rate of 23 MW, a moving grater furnace, a wet scrubber, a wet ESP and a fabric filter, Maguhn et al. [81] observed a PSD in number of 17 – 30000 nm with a modal range of 70 – 167. For Cernuschi et al. [84] in a moving grater furnace and an ESP, a SCR and a fabric filter as the FGCT units with a fuel rate of 900 – 1200 Mg.d<sup>-1</sup>, the particle size ranged from 7 – 2500 nm in number concentration with a modal number distribution of 32 nm. Similarly, Zeuthen et al. [85] reported a PSD in number of 14 – 800 nm with a model value of 167 nm from the incineration of waste in a grate furnace and a fabric filter and a wet scrubber as the FGCT units.

### **1.4 Wet scrubbing technology**

A wet scrubber is FGCT unit designed primarily to treat inorganic pollutants (i.e., sulfur dioxide, chromic acid, hydrogen sulfide, ammonia and chloride fluorides) contained in industrial exhaust gas streams. Scrubbers are also reported to treat particulate matter (> 1.0 μm), heavy metals, trace organics, and odors [20, 86]. Employing spray nozzles or orifices, liquid collectors (e.g., water droplets but also a continuum of liquid such as forms or bubbles)

are atomized and dispersed into the gas stream to simultaneously absorb and neutralize gaseous pollutants. Particle capture consists of a physical absorption process by which droplets trap particles through agglomeration, adherence, or encapsulation. A mist collector is used to recover suspended liquid droplets from the gas stream. The liquid containing the pollutant is collected at the bottom of the scrubber and treated before disposal. Often, a wet scrubber is composed of two or more scrubbers in a series or multiple stages of spraying liquids. This is done so that an individual scrubber or stage can use an absorbent specific to a pollutant. An example of this is commonly found in waste incineration, where a stage of the scrubber or the first scrubber uses a basic-based absorbent solution (e.g., a lime-based slurry of  $\text{CaCl}_2$ ) to remove acid pollutants followed by a second stage or second scrubber of an acid-based absorbent solution to neutralize basic-based pollutants. Higher removal efficiencies are possible in a multistage scrubber system than would otherwise be possible with a single-stage scrubber. Wet scrubbers are broadly oriented as cross-flow, countercurrent flow, or co-current flow. In a co-current wet scrubber (Figure 5a), the flue-gas and the spraying liquid droplets travel in the same direction. In a countercurrent wet scrubber, the flue-gas enters the scrubber at the bottom before coming in contact with the liquid droplets traveling in the opposite (gravity) direction (Figure 5b).

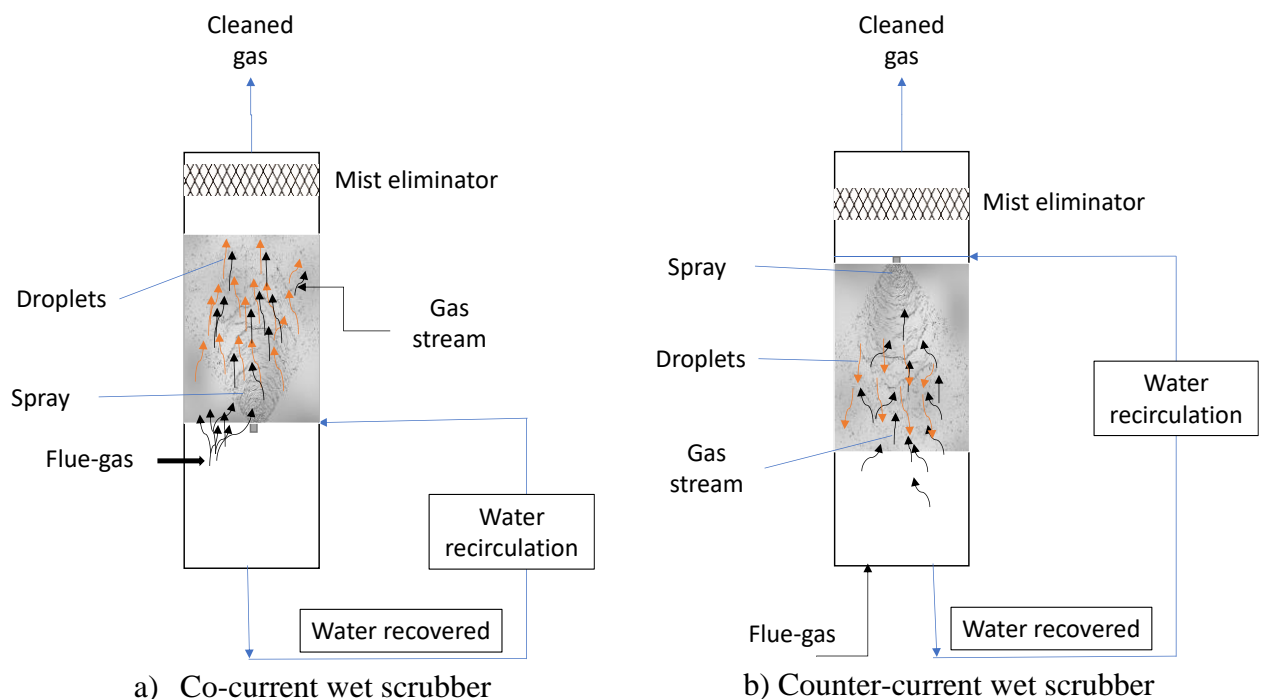


Figure 5 Schematic of co-current and counter-current wet scrubber

Wet scrubbers have certain advantages compared with other operation units of FGCT such as electrostatic precipitators (ESP) and bag filters. For the same volume of flue-gas treated, wet

scrubbers are more compact and occupy smaller spaces than bag filters or ESP. Scrubbers also have a lower investment cost and similar operation and maintenance costs than ESPs and bag filters [87]. Although ESP and bag filters are primarily designed for particle removal due to their high collection efficiencies, wet scrubbers are preferred when the particles are hygroscopic, flammable, corrosive, or in a gas stream with high temperature (for exhaust waste heat reduction purposes) or moisture content. In waste incineration plants, wet scrubbers are used in various configurations with other operation units of FGCT such as ESP, bag filter, and cyclones to treat (particle) pollutants contained in the flue-gas before stack release. A drawback of wet scrubbers is that they generate waste in the form of discharge sludge which requires treatment before disposal. Also, downstream corrosion could occur except if the added moisture is adequately removed from the gas downstream of the scrubber.

#### **1.4.1 Operating principles**

The principle of operation of a typical wet scrubber consists of the generation of droplets in a moving gas stream to create a medium of high particle-droplet interaction (or gas absorption i.e., transfer of gaseous pollutant from the gas stream to the liquid phase) with the ultimate collection of the particles by impingement upon contact with the droplets or droplets films on the scrubber walls [88]. To achieve this, a scrubber consists of six (6) components; a fan-powered flue-gas control system, an inlet, a series of spray nozzles, a water source, a mist eliminator and an outlet. Depending on the scrubber type, the operations or the components of the scrubber could be somewhat different.

#### **1.4.2 Types of scrubbers**

Several types of wet scrubbers (Figure 6) exist to treat specific pollutant(s) released from industrial processes. This section discusses the major types of wet scrubbers encountered in industrial applications.

*Spray scrubbers* are one of the commonest types of scrubbers in use. In a spray scrubber, flue-gas enters the scrubber where it contacts liquid droplets produced by spray nozzles. The droplets can be directed perpendicular, counter, or in the same direction as the gas stream. In a counter-current scrubber, the flue gas stream enters at the bottom of the scrubber and flows upward while the spray droplets travel downward from nozzles placed on the walls of the scrubber or mounted on nozzle heads at the radial center of the scrubber, several nozzle stages possibly placed along the height of the scrubber. Water droplets capture particles in the gas

stream through impaction, Brownian diffusion and interception mechanisms [14, 20]. Large droplets settle under gravity to the bottom of the scrubber and impaction forming liquid films on the internal walls of the scrubber. Several authors have investigated the removal of particles by a spray scrubber [22, 89–91].

**Packed bed scrubbers** contain layers of packing material such as Raschig rings, woodchips, spiral rings, or Berl saddles to increase the gas-liquid contact. Packed scrubbers are primarily designed to treat acid gases as the collection of particles by these scrubbers leads to a progressive clogging of the packing which requires additional maintenance costs. Packing materials come in different types and sizes. Pollutant removal efficiency and liquid distribution improve with a decrease in the sizes of the packing materials but this lead to an increase in pressure drop [92]. Other parameters to consider when designing a packed bed scrubber include the packing-to-scrubber diameter to limit wall effects, the pressure drop, the height of the packed-bed scrubber, the packing method and the liquid distribution [92].

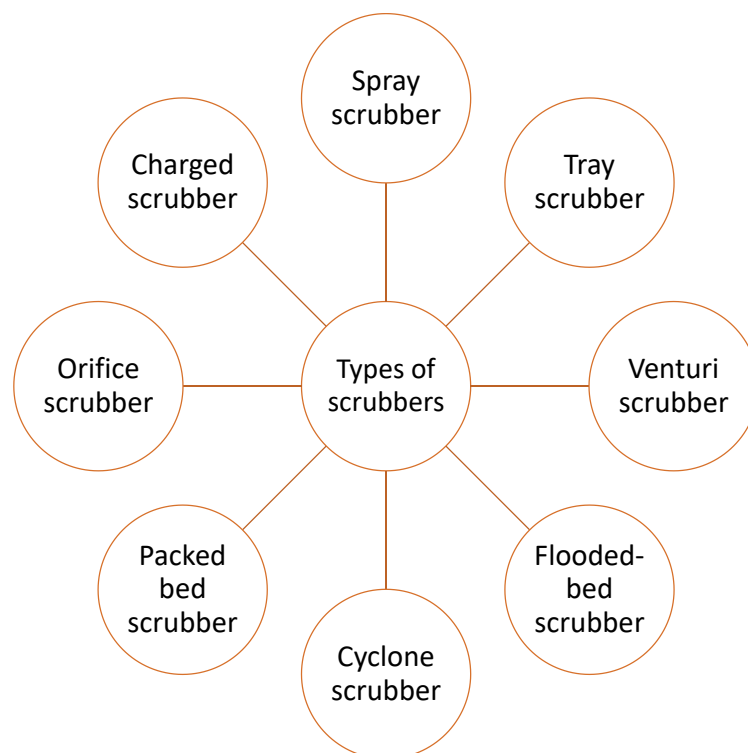


*Figure 6 Types of scrubbers*

**Tray scrubbers** comprise a column with punctured, perforated, or woven trays placed horizontally in the scrubber. The trays are continuously washed by the collecting liquid which is flowing from the top and across the trays to the bottom of the scrubber so that the clogging

of the tray is minimized. Tray towers are ineffective for the removal of particles with diameters less than 1.0  $\mu\text{m}$  but have up to 97% removal efficiency for  $\text{PM} > 5 \mu\text{m}$  [93].

By far, *venturi scrubbers* are the most common types of scrubbers employed in industrial flue-gas treatment. This is partly due to their higher collection efficiency of particles less than 1.0  $\mu\text{m}$  when compared to other types of wet scrubbers. A venturi consists of three sections; a converging duct section, a straight section (throat) and a diverging section. The scrubbing liquid is introduced upstream of the throat before being atomized by the turbulence in the throat section, resulting in to increase in the gas-liquid contact. To separate the entrained droplets in the gas stream, a centrifugal separator is used. Several researchers have studied the capture of particles by a venturi scrubber [94–97]. Jones et al. [98] described the operation of a venturi scrubber where the collecting liquid enters the scrubber at the throat before being evenly dispersed. The flue-gas enters the venturi scrubber upstream using an induced-draft fan typically located after the cyclonic separator. A gas-liquid collision occurs at the venturi throat, where the liquid then accelerates and gets interrupted. The gas then decelerates in the diverging section; where further particle-droplet interactions occur but also significant droplet coalescence before droplet removal by centrifugal force. Various authors have reported the working principles of a gravitational scrubber [14], a flooded bed scrubber [99] and a spray scrubber [100]. Other types of wet scrubbers include charged scrubbers, orifice scrubbers, flooded-bed scrubbers and cyclone scrubbers. While these scrubbers represent an innovative attempt to improve the collection efficiency of the conventional scrubbers previously discussed. They are not discussed here as they are not widely used in industrial applications such as waste incineration.

### **1.4.3 Applications of scrubbers**

Wet scrubbers may be employed in a range of industrial processes to minimize the environmental release of pollutants. Scrubbers are widely used in industries such as cement, fertilizer, mining activities, chemicals, paper, incineration, steel and metal finishing. Figure 7 shows some of the industrial applications of a scrubber [101].

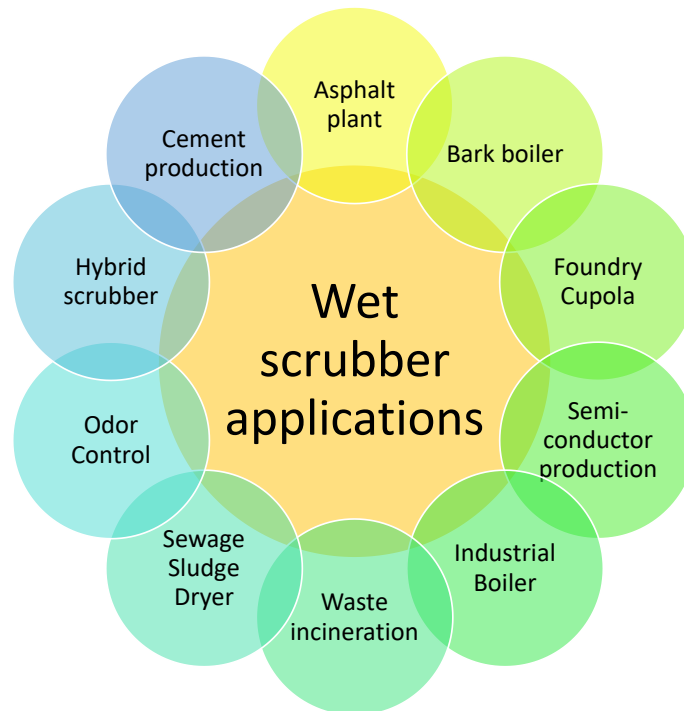


*Figure 7 Application of scrubbers*

Scrubbers have also been reported to be employed in treating pollutants from the production of ferrous metals (foundry cupolas), boilers that run on wood shavings (bark boilers scrubbers) and in asphalt production [101].

### **1.5 Particle collection mechanisms in a wet scrubber**

Particle collection by a droplet in a wet scrubber is governed by several mechanisms. These mechanisms include impaction, Brownian diffusion, interception, phoretic forces, condensation, electrostatic attraction and gravitational settling. Depending on the particle size and the operating conditions of the scrubber, a droplet can collide with a particle in several ways. To determine the collection efficiency, usually, both the droplet and the particle are assumed to be spherical. The scrubber's overall collection efficiency is calculated as a function of the various mechanisms and this collection efficiency is defined as the fraction of particles in the scrubber that are swept-out by the droplets i.e., that collide with the droplets and stay retained. Generally, it is assumed that particle collection occurs if there is a droplet-particle collision. A discussion of the main collection mechanisms involved with particle collection in a wet scrubber is as follows.

### 1.5.1 Inertial impaction mechanism, $\eta_{imp}$

Inertial impaction is the dominant particle collection mechanism in a wet scrubber for particles with diameters larger than 1.0  $\mu\text{m}$  or a flue gas stream with a velocity greater than 0.3  $\text{m}\cdot\text{s}^{-1}$  [102–104]. However, Kim et al. [105] reported that the impaction mechanism could begin to act on particles of diameters as low as 0.05  $\mu\text{m}$ . Impaction acts primarily on the particle inertia and the flow field around a droplet [106]. Impaction occurs when a particle has sufficient inertia to maintain its trajectory in a moving gas streamline until it strikes a droplet (Figure 8). Stokes number (Stk) is the dimensionless parameter that represents the inertial impaction mechanism and is defined as the ratio of particle response time to the gas characteristic time scale [107]. Particles with large Stk numbers are easily captured by droplets due to the impaction mechanism [108]. Reynolds number (Re) characterizes the flow field around a droplet. It is another important parameter that determines particle capture due to impaction mechanism [109]. As Re increase, particle collection due to impaction have been reported to improve [109].

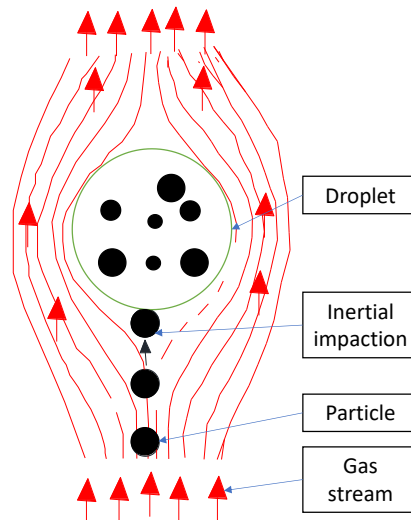


Figure 8 Impaction collection mechanism

Mathematically, the Stokes number is given by the following equation:

$$Stk = \frac{\rho_p d_p^2 U}{18\mu D} \quad (1)$$

Where  $\rho_p$  is the particle density  $\text{kg}\cdot\text{m}^{-3}$ ,  $d_p$  is the particle diameter (m),  $D$  is the droplet diameter (m),  $\mu$  is the gas viscosity (Pa.s) and  $U$  is the relative velocity between particles and liquid droplets ( $\text{m}\cdot\text{s}^{-1}$ ).

Several authors have investigated the single droplet particle collection efficiency considering impaction. Table 1 below presents the main models encountered in the literature. Licht et al. [104] proposed an analytical model for wet scrubbers by assuming a proportionality to the Stokes number (Stk). However, Kim et al. [14] found the model by Licht et al. [104] not suitable for the moment equation used for a lognormal distribution and proposed the semi-empirical impaction model for the range of Stokes number shown in Table 1 below. Kim et al. [14] derived their model in a gravitational wet scrubber with a liquid-to-gas ratio of 0.025 to 0.05, a relative velocity of 10 to 150 cm.s<sup>-1</sup> and a particle diameter of 0.01 to 5.0 μm.

Slinn et al. [110] used dimensional analysis coupled with experimental results to find the mathematical expression for single rain droplet particle collect efficiency due to the impaction mechanism. Bae et al. [111] modified the model by Slinn et al. [110] (Table 1) to a form suitable for the moment method in their study of below-cloud particle scavenging. Bae et al. [111] investigated their model for an air temperature of 0 to 30 °C, RH of 0.5 to 1.0, rain intensity of 1.0 mm.h<sup>-1</sup> and particle diameter of 0.1 to 10 μm.

Calvert et al. [112] derived a mechanistic model due to the impaction collection mechanism in a venturi scrubber. The authors made the following assumptions:

- Particles are captured only by atomized liquid
- The mechanism for particles to collect on single droplets is determined by the relative velocity of the droplet and the air
- The acceleration of droplets is calculated using a linear approximation of the drag coefficient for accelerating droplets

In deriving the impaction model in a reverse jet scrubber, Lim et al. [20] made three assumptions:

- In the complex reverse jet scrubber, it is assumed that the diameter (D) and concentration of the spray droplets remain constant and unchanging and that there is no interaction between the droplets.
- The spray droplets immediately and completely cover the spray chamber upon injection.
- There is no pressure or force applied to the spray droplets, and particles adhere to the droplets' surface upon contact

Lim et al. [20] argued that the model could be used in reverse jet (counter-current) scrubber where large gas-liquid interfacial area, long residence time and high relative velocities exist.

The authors tested their model for a liquid flowrate of 31 to 57 cm<sup>3</sup>.s<sup>-1</sup>, droplet velocity of 1000 to 5000 cm.s<sup>-1</sup>, droplet diameter of 440 to 600 μm and gas flowrate of 50 to 200 cm.s<sup>-1</sup>.

Table 1 Particle collection based on impaction mechanisms

Authors	Year	Model	Condition	Remark
Walton and Woolcock [113] as cited by Davenport et al. [114]	1960	$\eta_{imp} = \frac{1}{\left(1 + \frac{0.7}{Stk}\right)^2}$	-	A theoretical model for atmospheric PM scavenging
Licht et al. [104]	1988	$\eta_{imp} = \left(\frac{Stk}{Stk + 0.35}\right)^2$	-	Analytical model for wet scrubber
Kim et al. [14]	2001	$\eta_{imp} = 3.4 (Stk)^{\frac{9}{5}},$ $\eta_{imp} = 1$	For $Stk \leq 0.5$ For $Stk > 0.5$	A semi-empirical model for Gravitational wet scrubber
Calvert et al. [112]	1970	$\eta_{imp} = \left(\frac{Stk}{Stk + 0.7}\right)^2$	-	mechanistic model in a venturi scrubber
Lim et al. [20]	2006	$\eta_{imp} = 0.6 \cdot Stk$ $\eta_{imp} = 0.1 \cdot Stk + 0.49$ $\eta_{imp} = 0.02 \cdot Stk + 0.79$	for $Stk \leq 1.0$ for $1.0 < Stk \leq 3.0$ for $Stk \geq 10.0$	A semi-empirical model for reverse-jet scrubber
Bae et al. [111]	2009	$\eta_{imp} = 1 - 0.9 \cdot Stk^{-0.5}$	-	A theoretical model for atmospheric PM scavenging
Slinn et al. [110]	1983	$\eta_{imp} = \left(\frac{\frac{2}{3}}{Stk - Stk^*} + 1\right)^{-\frac{2}{3}}$	$Stk = \frac{2\tau (V_t(D) - v_t(d_p))}{D}$ $Stk^* = \frac{1.2 + \frac{1}{12 \ln(1 + Re)}}{1 + \ln(1 + Re)}$	-

Where  $Re$  is the droplet Reynolds number and  $V_t$  is the droplet terminal velocity

### 1.5.2 Brownian Diffusion mechanism, $\eta_{diff}$

The collection of fine particles is governed by Brownian diffusion. In diffusion, the random motion of a particle in the flue gas as a result of the particle's constant collision with the gaseous molecules leads a particle to be collected by a droplet (Figure 9) as the particles move from regions of high concentration to regions of low concentration. Thus, particle removal due to the Brownian mechanism increases as the particle size is decreasing. Particles smaller than  $0.1 \mu\text{m}$  are reported to be effectively collected as a result of Brownian diffusion [106]. Kim et al. [14] revealed that the diffusion-dominant region starts at a particle diameter lower than  $0.05 \mu\text{m}$ .

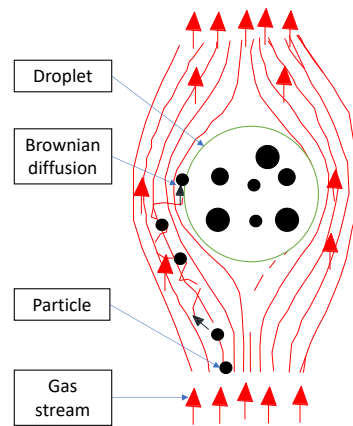


Figure 9 Brownian diffusion mechanism

$Pe$ , Peclet number is the dimensionless parameter that describes the Brownian diffusion mechanism and is defined as:

$$Pe = \frac{DU}{D_{diff}} \quad (2)$$

$D_{diff}$  is the particle diffusion coefficient:

$$D_{diff} = \frac{k_B T C_c}{3\pi\mu d_p} \quad (3)$$

Where  $T$  is the gas absolute temperature,  $k_B$  is the Boltzmann constant and  $C_c$  the Cunningham slip correction factor.

Several authors have proposed particle collection efficiency of a single droplet sphere based on the diffusion mechanism as presented in Table 2 below. Fuchs [115] proposed a theoretical

model for the diffusion mechanism using dimensional analysis based on mass transfer. Bae et al. [111] proposed a diffusion model in their study of below-cloud particle scavenging. Bae et al. [111] investigated their model for an air temperature of 0 to 30 °C, RH of 0.5 to 1.0, rain intensity of 1.0 mm.h<sup>-1</sup> and particle diameter of 0.1 to 10 µm. Carotenuto et al. [116] reported a theoretical diffusion model based on atmospheric aerosol scavenging. The authors validated their model in a wet electrostatic scrubber of gas flow of 170 L.s<sup>-1</sup>, liquid flow of 120 ml.min<sup>-1</sup>, droplets with diameters between 225 and 950 µm and particles with sizes from 0.68 to 6 µm. Fan et al. [117] developed a single droplet collection efficiency based on diffusion (Table 2) in a conventional spray scrubber using a condensation growth dynamic model for particle sizes 0.01 to 10 µm. Jung and Lee [118] developed an analytical particle collection model due to the diffusion mechanism by considering the collection of particles in a system comprising multiple fluid spheres such as water droplets. The authors developed a model that describes the efficiency of particle collection due to diffusion, which takes into account the packing density ( $\alpha$ ) and the Peclet number (Pe) for both solid spheres and bubbles (Table 2).

Table 2 Particle collection models based on diffusion mechanisms

Authors	Year	Model	Condition	Remark
Fuchs [115] cited by Davenport et al. [114]	1978	$\eta_{diff} = \frac{3.8}{Re^{\frac{1}{2}} Sc^{\frac{2}{3}}}$	-	A theoretical model involving mass transfer
Jung and Lee [118]	1988	$\eta_{diff} = 0.7 \left\{ \frac{4}{\sqrt{3}} \left( \frac{1-\alpha}{J+\sigma K} \right)^{1/2} Pe^{-\frac{1}{2}} + 2 \left( \frac{\sqrt{3}\pi}{4Pe} \right)^{\frac{2}{3}} \left[ \frac{(1-\alpha)(3\sigma+4)}{J+\sigma K} \right]^{\frac{1}{3}} \right\}$	-	Semi-empirical model
Bae et al. [111]	2009	$\eta_{diff} = \frac{4}{ReSc} \left( 1 + 0.4Re^{\frac{1}{2}} Sc^{\frac{1}{3}} + 0.16Re^{\frac{1}{2}} Sc^{\frac{1}{2}} \right)$	-	Theoretical model for atmospheric PM scavenging
Carotenuto et al. [116]	2010	$\eta_{diff} = 4.18Re^{1/6} Pe^{-2/3}$	-	Theoretical model based on atmospheric aerosol scavenging
Fan et al. [117]	2010	$\eta_{diff} = 2 \sqrt{\frac{2}{PeD}}$	-	Analytical model for a spray scrubber

Where  $Sc$  is the particle Schmidt number,  $Re$  is Reynolds number,  $Pe$  is Peclet number,  $\alpha$  is packing density,  $\sigma$  is viscosity ratio of water to air,  $K$  and  $J$  are hydrodynamic factors

### 1.5.3 Interception mechanism, $\eta_{int}$

Particles traveling in a gas stream may not always depart from the flow stream of the gas. In such a case, a particle may still be collected when the particle passes within one particle radius from the droplet surface. This collection mechanism called interception holds for intermediate-sized particles with negligible inertia, gravitational settling and Brownian motion and hence can follow the gas stream at angles far less than  $90^\circ$  until they are engulfed by a droplet [119]. Particle capture by interception mechanism increases when the density of droplets increases.

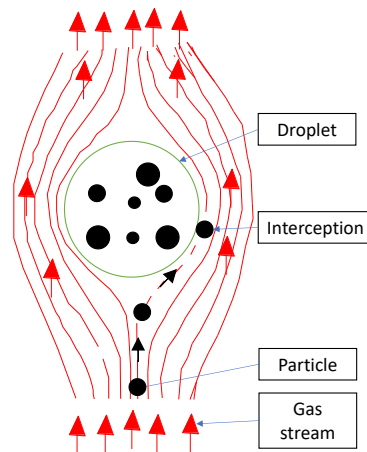


*Figure 10 Interception mechanism*

The interception parameter  $R$ , defined as the ratio of particle diameter to the liquid droplet diameter, represents the dimensionless parameter describing the interception mechanism:

$$R = \frac{d_p}{D} \quad (4)$$

Table 3 is a summary of the mathematical expressions from various authors for the particle collection due to interception mechanisms. Similar conditions were reported for the model derivation as was for impaction (Table 1) and interception mechanism (Table 2).

Table 3 Particle collection models based on interception mechanisms

Author s	Year	Model	Conditio n	Remark
Fuchs [115]	1964	$\eta_{int} = (1 + R)^2 - \frac{1}{1 + R}$	-	A theoretical model involving mass transfer
Jung and Lee [118]	1988	$\eta_{int} = \frac{1 - \alpha}{J + \sigma K} \left[ \frac{R}{1 + R} + \frac{1}{2} \left( \frac{R}{1 + R} \right) + \frac{1}{2} \left( \frac{R}{1 + R} \right)^2 (3\sigma + 4) \right]$	-	Semi-empirical model
Bae et al. [111]	2009	$\eta_{int} = 4R \left( \frac{1}{\sigma} + \left( 1 + Re^{\frac{1}{2}} \right) R \right)$	-	-
Fan et al. [117]	2010	$\eta_{int} = (1 + R)^2 - \frac{3}{2(1 + R)} + \frac{1}{2(1 + R)}$	-	Analytical model for spray scrubber

#### 1.5.4 Other collection mechanisms

When temperature differences and water vapor concentration exist in a scrubber, thermophoresis and diffusiophoresis may be exerted on the particles [120]. **Diffusiophoresis** ( $\eta_{diph}$ ) is the motion of particles suspended in a gas stream due to the concentration gradient in a multi-component gas. In a wet scrubber, the particles will tend to move toward the air molecules which are heavier than the water vapor molecules. In literature, many authors have reported the effect of diffusiophoresis on the particle collection efficiency scrubbers [121, 122]. Sparks and Pilat [121] proved that negative diffusiophoresis (droplet evaporation) could cause poor scrubber performance, especially for fine particles, while positive diffusiophoresis (condensation) could result in improved particulate collection.

A related phenomenon is **thermophoresis** ( $\eta_{thph}$ ). In this area, the temperature gradient across or between molecules in a gas stream tends to transport the particles from a higher to a lower temperature region or droplet [123]. Gas molecules have a kinetic energy that fluctuates depending on temperature gradient and can alter the motion of particles in the gas. Gas molecules exert greater forces on the hot side of particles than on the cold side which causes the particles to move towards the colder side i.e., a droplet. Several authors reported that the

intermediate region (Figure 11) also known as the Greenfield gap where neither of the three principal particle collection efficiency in a scrubber is dominant, is dominated by thermophoresis and diffusiophoresis [123–125]. The mathematical expression for the contribution of the thermophoresis mechanism was reported Waldman and Schimdt [126], and Skelland [127] as cited in Davenport et al.[114] as shown in equation (5) below.

$$\eta_{thph} = \frac{4 \left( \frac{2C_c \left( K_a + 5 \frac{\lambda}{D_p} K_p \right) K_a}{5P \left( 1 + 6 \frac{\lambda}{D_p} \right) \left( 2K_a + K_p + 10 \frac{\lambda}{D_p} K_p \right)} \right) \left( 2 + 0.6Re^{\frac{1}{2}}Pr^{\frac{1}{3}} \right) (T_a - T_d)}{D_d V_t} \quad (5)$$

Where  $\lambda$  is the mean free path length of gas molecules (m),  $Pr$  is the Prandtl number of gas,  $V_t$  is the terminal settling velocity of a droplet ( $m.s^{-1}$ ),  $T_a$  is gas inlet temperature (K),  $T_d$  is droplet surface temperature (K),  $K_a$  and  $K_p$  are thermal conductivity of gas and particle ( $Kg.m.s^{-3}.K^{-1}$ ) respectively.

If significant evaporation or condensation takes place, **Stefan flow** can impose a supplementary aerodynamic impact on particle motion. Stefan flow is the movement of particles resulting from gas molecule motion which exerts a force in the direction of the flow. Stefan flow is sometimes considered a type of diffusiophoresis [128]. Stefan flow occurs near a surface that is either evaporating or condensing. The vapor causes the particles to move with the gas molecules toward the droplet where the capture of the particles [129]. For condensation, Stefan flow is occurring in the direction of the liquid surface, however, the evaporating vapor leads to the revers and hinders the collection of particles in the scrubber.

Lastly, the application of **electrostatic forces** ( $\eta_{Ef}$ ) in conventional scrubbers to enhance their submicronic particle capture has attracted the interest of many researchers [116, 130–132]. Electrostatic charges are the introduction to the droplets, the particles or both. The electrostatic force is an important mechanism responsible for fine particle collection when the collector has an opposite electric charge to the particle. According to Jaworek et al. [133] five (5) forms of electrostatic scrubbers considering different methods of charging the particles and the droplets are found in the literature [130]:

- ❖ Both droplets and particles are oppositely charged and particle capture by droplets occurs as a result of Coulomb forces
- ❖ Droplets and particles are charged to the same polarity. The arising repulsive force drives the particles onto the chamber walls, where they are washed out.

- ❖ Equal number of positively and negatively droplets are charged while the particles are negatively charged. In this case, the positively charged droplets capture negatively charged particles due to attractive Coulomb forces, and finally, they coagulate with negatively charged droplets.
- ❖ Particles are charged to either polarity and the droplets are uncharged, so that electrostatic capture mainly occurs due to an image charge on the droplet.
- ❖ Droplets are charged to a polarity while the particles are left uncharged, thus, particle capture occurs due to image charge induced on the particle electrostatic charges.

### 1.5.5 Single droplet collection efficiency, $\eta_{SD}$

As previously discussed in this chapter, although primarily designed to treat acid pollutants, a wet scrubber could be efficient for the removal of particles from industrial flue gas. The basis of the performance of a wet scrubber lies in understanding the particle capture by a single droplet. Kim et al. [14] reported that the collection efficiency of a single droplet in a scrubber is the sum of the impaction efficiency, diffusion efficiency and interception efficiency. Other authors such as Wu et al. [22] have proposed the addition of other particle collection mechanisms such as gravitational settling. Yet, it is not uncommon to find single droplet collection efficiency involving phoretic and electrostatic forces [116]. The simplest way of approximating single droplet collection efficiency is to sum the contributions from different mechanisms assuming the interdependence between mechanisms [134]:

$$\eta_{SD} = \eta_{imp} + \eta_{diff} + \eta_{int} + \eta_{thph} + \eta_{Ef} + \eta_G + \eta_{diph} \quad (6)$$

Where  $\eta_G$  is the particle collection due to gravitational settling.

An alternate approach that considers the interdependence of the contributions of the collection mechanisms is to assume that the particle removal by a single droplet is the product of the different mechanisms [22, 135] i.e., that the mechanisms act in series [136]:

$$\eta_{SD} = 1 - (1 - \eta_{imp})(1 - \eta_{diff})(1 - \eta_{int})(1 - \eta_{thph})(1 - \eta_{Ef})(1 - \eta_G)(1 - \eta_{diph}) \quad (7)$$

Calculations gotten this way have revealed that there is a coupling effect between Brownian diffusion and inertial impaction for particles in the intermediate-sizes [135].

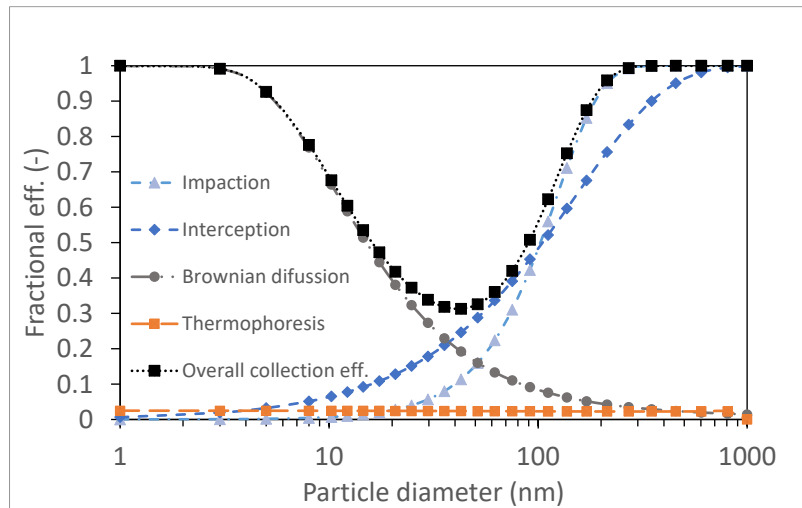


Figure 11 Overall collection efficiency and individual contribution of each mechanism (adapted from Ardon-Dryer et al. [124])

The overall collection efficiency is obtained based on the total dispersed droplets in the entire volume of the scrubber. This is calculated from the single droplet model (7) and involves a discrete material balance equation for the particles in a cell volume [22]. The overall collection efficiency as shown in Figure 11 above is expressed as [103]:

$$\eta_{\text{Overall}} = 1 - e^{\left[ \frac{-3 Q_L h}{2 Q_G D (v_t - U_G)} \eta_{SD} \right]} \quad (8)$$

Where  $Q_L$  is the liquid flow rate ( $\text{m}^3 \cdot \text{s}^{-1}$ ),  $Q_G$  is the gas flow rate ( $\text{m}^3 \cdot \text{s}^{-1}$ ),  $v_t$  the terminal settling velocity of droplets ( $\text{m} \cdot \text{s}^{-1}$ ),  $U_G$  the gas velocity in the tower ( $\text{m} \cdot \text{s}^{-1}$ ),  $h$  the height of the tower (m).

### 1.5.6 Role of scrubber walls on overall particle collection efficiency

In a wet scrubber, it is unavoidable that droplets will collide with the walls of the scrubber and either spread, break, rebound, stick or splash. Thus, the scrubber walls play an important role in the overall particle collection efficiency. Indeed, water droplets deposited on the scrubber wall form a thin liquid layer (film) flowing down along the wall. This could in theory provide additional deposition surface for particles. Ali et al. [137] confirms this when they reported that particle collection does take place by the liquid film on the walls of a centrifugal wet scrubber. However, in a venturi scrubber, Viswanathan et al. [138] reported that the scrubber wall liquid layer does not participate in the particle collection. Whether this is true for a spray scrubber involved in the collection of nanoparticles is yet to be established. The Lagrangian approach can be used to predict if a particle will strike a wall liquid film but

the succeeding motion of the particle within the liquid film depends on the surface tension of the collecting liquid surface [137]. According to Pemberton et al. [139] if the motion energy of a particle is greater than the surface tension of the collecting liquid, the particle will be collected. Experimentally, it remains challenging to ascertain the collection of particles only by direct contact with droplets while ignoring the wall liquid film. But an attempt is made in the present work to estimate the fraction of the nanoparticles that are collected by the scrubber walls.

## **1.6 Influence of operating parameters on wet scrubbing**

From the literature review, wet scrubbers are reported to be inefficient or very poorly efficient for the collection of a particle with diameters smaller than 1.0  $\mu\text{m}$  [104, 140], however, Kim et al. [14] revealed that suitable operating conditions, particles much smaller than 0.1  $\mu\text{m}$  in diameters can be effectively collected using scrubbers. Thus, the following section discusses the effect of certain key operating parameters on the particle collection by a wet scrubber by exploring published works. Although not an operating parameter, the influence of the particle diameter is also presented.

### **1.6.1 Gas flowrate**

The gas flowrate in a scrubber could (dis)favor the collection of particles by a given mechanism, thus affecting the overall performance of the wet scrubber [22, 141]. In their work on the modeling of PM (1–3  $\mu\text{m}$ ) collection efficiency by a spray scrubber with twin-fluid air-assist atomizers, Mohan et al. [103] revealed that at a constant liquid flowrate of  $16.67 \cdot 10^{-6} \text{ m}^3 \cdot \text{s}^{-1}$ , an increase in the gas flowrate (from  $1 \cdot 10^{-6} \text{ m}^3 \cdot \text{s}^{-1}$  to  $5 \cdot 10^{-6} \text{ m}^3 \cdot \text{s}^{-1}$ ) led to an improvement in the particle collection efficiency of the scrubber. Similar conclusions were reached by Lim et al. [20] in their study to predict the particle collection efficiency of a reverse jet scrubber. Lim et al. [20] argued that the increase in the collection efficiency as the gas flowrate increased as a result of an increase in the relative velocities between the droplets and the gas (particles). In a spray scrubber, Wu et al. [22] obtained an increment of the dust (20  $\mu\text{m}$  in diameter) removal efficiency from 90.7% to 95.6% when they studied the impact of varying the gas flowrate from 79 to 129  $\text{m}^3 \cdot \text{h}^{-1}$ . Wu et al. [22] also reported an increase in the dust removal efficiency from 80.9% to 94.8% when the gas flowrate of a sieve-tray spray scrubber was increased from 83 to 136  $\text{m}^3 \cdot \text{h}^{-1}$ . Wu et al. [22] associated this improvement to improve inertia collision with higher gas flowrate. In their research on the study of the

removal efficiency of dust in a self-priming venturi scrubber, Ali et al [142] also concluded that a higher gas flow led to a higher removal efficiency due to improved relative velocity between gas and droplets in the throat section. Generally, as the gas flowrate in a scrubber increases, the particle collection is improved [95, 143]. This is not always the case. Meikap et al. [144] conducted experimental studies on the scrubbing of fly ash (2–15  $\mu\text{m}$ ) in a novel wet scrubber using water as the scrubbing medium. Beyond a gas flow rate of  $4.2 \cdot 10^{-3} \text{ Nm}^3 \cdot \text{s}^{-1}$ , the collection efficiency did not improve with an increase in the gas flowrate but was instead limited due to coalescence which led to reduced bubble reformation. Lee et al [145] reported that higher gas flowrates do indeed favored the collection of sub-micrometer particles smaller than 1  $\mu\text{m}$ . Lee et al [145] argues that the gas-liquid contact for effective particle collection is well established for larger particles even at low gas flow rates.

### 1.6.2 Gas temperature

A change in the flue gas temperature in a wet scrubber could play a significant role in the collection of particles by the scrubber. The gas temperature could also modify other influent parameters such as the droplet diameter, droplet evaporation rate and gas flowrate. Darbandi et al. [146] conducted CFD modeling to investigate the forces responsible for the collection of nanoparticles in a wet scrubber. The authors varied the flue gas temperature from  $100^{\circ}\text{C}$  to  $300^{\circ}\text{C}$  increasing the collection efficiency. The temperature gradient positively impacted the collection of particles due to the diffusiophoresis mechanism. Fan et al. [147] presented in their paper the experimental collection of coal-fired particles ( $\text{PM}_{2.5}$ ) by a condensation scrubber. For the particle size 1.0  $\mu\text{m}$  to 3.0  $\mu\text{m}$ , the removal efficiency was higher (15% to 35%) when the inlet gas temperature was set at  $95^{\circ}\text{C}$  than it was when the gas temperature was at  $35^{\circ}\text{C}$  (8% to 35%). The authors attributed this to heterogeneous nucleation and particle collection due to the diffusiophoresis mechanism as a result of the temperature gradient.

### 1.6.3 Gas humidity rate

The collection of particles in a flue gas in a wet scrubber could be improved if the particles are grown into larger ones by a preconditioning technique such as heterogeneous condensation of water vapor with the particles acting as nuclei [21, 148–151]. The grown particles can then be efficiently collected by an inertial mechanism or a mist separator. Heterogeneous condensation of water vapor is most suitable for gas streams with significant

humidity content. Steam is injected in the gas inlet or above the scrubbing liquid inlet to saturate the wet scrubbers with water vapor which leads the latter to condense on the fine particles and to grow their volume. Several authors have investigated this effect on the removal of fine particles in a scrubber. The influence of humidity on the removal of a fine particle by a wet scrubber was studied by Yang et al. [117]. The authors found that an increase in the gas inlet steam led to an increase in the amount of condensable water on the particle surface. This resulted in the improvement of the collection efficiency from 50 to 85%. Huang et al. [152] attained a significantly enhanced collection efficiency of particles with diameters less than 150 nm by mixing saturated steam at 100°C with a normal temperature waste stream permitting submicron particles to grow into micron sizes. At a liquid-to-gas ratio of 2.5 l.m<sup>-3</sup>, the removal efficiency of particles less than 100 nm by the venturi scrubber was greater than 90%. Fan et al. [153] conducted experimental studies on the removal of coal-fired fine particles (PM<sub>2.5</sub>) by a condensation scrubber. The authors added steam to the gas inlet. This resulted in the improvement of the removal of fine particles as the amount of condensable water vapor increased leading to the condensation growth of particles.

### 1.6.4 Liquid flowrate

The liquid flow rate is another very important operating parameter in a wet scrubber. Lehner et al. [154] investigated the aerosol (PM<sub>3.0</sub>) collection efficiency of a venturi scrubber working in self-priming mode (i.e., operating without an external pump). The authors found that, as the liquid flowrate increased from 1.5 to 3.0 L.m<sup>-3</sup> the collection efficiency for the entire particle range also increased. Lehner et al. [154] attributed this to the increase in the interfacial surface for particle collection at higher liquid flow rates. Meikap et al. [144] reported that at a constant gas flow rate of  $3.0 \times 10^{-3} \text{ Nm}^3 \cdot \text{s}^{-1}$  in a multi-stage bubble column scrubber, the fly-ash (2 - 15µm) collection efficiency increases as the liquid flow rate is increased. Meikap et al. [144] argued that this was due to an increase in the dispersed phase hold-up and interfacial contact area. Meikap et al. [144] conclusion was supported by the investigation made by Calvert et al. [112]. Likewise, as the liquid flowrate increases, the number of collectors also increases leading to a better droplet-particle collision. A similar conclusion was reached by Wu et al. [22] when they developed a mathematical model to investigate the dust removal efficiency of wet flue gas desulfurization systems. The overall spray scrubber collection efficiency increased as the liquid flowrate increased from 1.32 m<sup>3</sup>.h<sup>-1</sup> to 2.26 m<sup>3</sup>.h<sup>-1</sup>. Wu et al. [22] determined that more intense moving droplets increased the

chances of particle capture. Vasudevan et al. [125] conducted lab-scale studies using a spray scrubber to treat the flue gas stream from a fixed bed gasifier. Vasudevan et al. [125] reported that, as the spray liquid flow rate increased from 25 ml.min<sup>-1</sup> to 30 ml.min<sup>-1</sup>, collection efficiency improved from 50.3% to 60%. Vasudevan et al. [125] attributed this to an increase in the number of droplets due to higher liquid flowrate.

### 1.6.5 Droplet diameter

The droplet diameter plays an important role in the collection of particles by a wet scrubber. Danzomo et al. 2012 [155] developed a model for the collection efficiency of particles in a counter-current scrubber at different droplet sizes of 500 µm, 1000 µm, 1500 µm and 2000 µm. For 5 µm and 10 µm particle sizes, the collection efficiencies were found to be 89.7% and 98.2% at 500 µm droplet diameter and for a liquid-to-gas ratio of 0.7 l.m<sup>-3</sup>. As the droplet diameter increased to 2000 µm, the collection efficiency at 5 µm and 10 µm decreased to 43.9% and 58.8% respectively. Simin et al. [91] investigated the scrubbing of urea duct particles in a spray scrubber using CFD simulations. As the droplet diameter increased from 200 µm to 1000 µm, the collection efficiency at particle size 40 µm decreased. Simin et al. [91] concluded that the droplet diameter is negatively correlated to the collection efficiency thus, the surface area for particle collection increases with decreasing droplet diameter. Rafidi et al. [156] developed a model to predict the removal of particles in a spray scrubber and compared the results with experiments from a full-scale spray scrubber in a coal-fired power plant. Rafidi et al. [156] reported that the collection efficiency increased as the droplets became smaller. The authors argued that smaller droplets have higher velocities, thus increasing relative velocities between the droplets and the particles, resulting in a higher Stokes number and hence higher collection efficiency by impaction. Claudia et al. [116] developed a mathematical model to evaluate particle capture efficiency in a wet electrostatic scrubber. The authors found that the model predicted a decrease in the capture efficiency for particle sizes 100 nm and 1 µm with an increase in droplet sizes. As droplet sizes increases, both the collisional efficiency and the droplet–particle contact probability are increased and an improvement of removal efficiency is obtained. Larger particles (5 µm) did not witness an increase in the capture efficiency even when the droplet diameters were smaller. Claudia et al. [116] concluded that the effect of a lower collisional efficiency competed with the increase of droplet–particle contact probability leading to lower capture efficiency.

### 1.6.6 Particle diameter

The diameter of the particle in a flue gas is arguably the most important parameter in determining its collection by a wet scrubber [91, 125]. Lee et al. [145] evaluated the performance of a turbulent wet scrubber to effectively remove dust particles arising from a coal-powered thermal power plant. Lee et al. [145] disclosed that an increase in the fly ash particle diameter from 0.65  $\mu\text{m}$  to 5.0  $\mu\text{m}$  led to an increase in the removal efficiency from 43% to 100%. A similar tendency was observed in a venturi scrubber by Mi et al. [94], where the overall removal efficiency improved from 92.7% to 95.1% as the particle size increased from 10  $\mu\text{m}$  to 45  $\mu\text{m}$ . In a study involving a sieve-tray spray scrubber by Wu et al. [22], the dust collection efficiency improved from 14.8% to 99% as the particle size increased from 1  $\mu\text{m}$  to 20  $\mu\text{m}$ . In a spray scrubber, Keshavarz et al. [157] achieved a significant increase in the particle collection efficiency from 60% at a particle size of 0.5  $\mu\text{m}$  to almost 90% at a particle size of 4.5  $\mu\text{m}$ . A laboratory experiment to measure the collection efficiency of aerosol particles by water drops was studied by Pranesha and Kamra [158]. The authors reported that the collection efficiency increased with an increase in particle size. Pranesha and Kamra [158] also suggested that with an increase in particle diameter, the collection efficiency may attain an upper limit which may be less than one. Simin et al. [91] observed a similar tendency at a particle size of 10  $\mu\text{m}$  with a maximum collection efficiency of 97% in spray scrubber. Another point to consider is that several authors [14, 124, 131, 132, 156, 158–160] have reported a tendency of the particle collection efficiency to increase with particle diameter, then dip in the intermediate region around 0.1  $\mu\text{m}$  to 0.6  $\mu\text{m}$  and then increase till it reaches 100% as the particle diameter increases. As particle diameter increase, the collection due to the impaction mechanism improves leading to the overall performance of the scrubber. Pilat et al. [132] confirmed this when they calculated the particle collection efficiencies of single droplets considering impaction, diffusion, diffusiophoresis and thermophoresis. The particle collection efficiency improved (30% to 88%) with increasing particle size (0.25  $\mu\text{m}$  to 4  $\mu\text{m}$ ) predominantly due to the inertial impaction mechanism.

## 1.7 Overview of experimental and theoretical studies about particle removal by wet Scrubber

Table 4 Summary of studies on particle removal in wet scrubber

Scrubber type	Authors	Numerical studies	Experimental studies (Lab- vs. Large-scale)	Particle size( $\mu\text{m}$ )	Droplet size ( $\mu\text{m}$ )	Gas temperature (K)	Ratio liquid/gas (-)	Air/gas flow rate ( $\text{m}^3/\text{h}$ )	Liquid flow rate ( $\text{m}^3/\text{h}$ )	Fractional/Overall efficiency (-)
	Mohan et al. (2008)	-	Lab	2 - 200	80 - 200	343 - 353	N.I.	15.79 - 28.58	0.03 - 0.12	Eff = 94.23%
	Tomb et al. (1972)	-	Lab	0.68 - 10	225 - 950	N.I.	N.I.	300	0.100 - 0.750	$E_{ff}(dp=0.68 \mu\text{m})=15\%$ $E_{ff}(dp=2.5 \mu\text{m})=32\%$ $E_{ff}(dp>3.5 \mu\text{m})=35\%$
	Kim et al. (2001)	Numerical approach considering Impaction, Diffusion & Interception	-	0.1 - 8	100	N.I.	0.025 - 0.05	N.I.	N.I.	$E_{ff}(dp=0.1 \mu\text{m})=9-20\%$ $E_{ff}(MPPS=1 \mu\text{m})=1.8-4\%$ $E_{ff}(dp>6 \mu\text{m})=100\%$
	Danzomo et al. (2012)	A new analytical approach considering Impaction	-	5,10 (PM10)	500 - 2000	N.I.	0.7 - 2.7	$10.4 \times 10^4$	209.736	$E_{ff}(dp=5 \mu\text{m})=43.80-99.98\%$ $E_{ff}(dp=10 \mu\text{m})=58.72-100\%$
	Muller et al. (2001)	-	Lab	0 - 400	N.I.	N.I.	N.I.	795	0.8-1.1	Eff = 96-99.9 %
	Vasudevan et al. (1985)	Analytical approach considering heat transfer, mass transfer, condensation, nucleation, temperature and flow fields, and phoretic phenomena	Lab	0.1 - 12.3	90	653	$15 \times 10^{-4}$	0.78	$12 \times 10^{-4}$	Eff = 26.70%
70					653	$19 \times 10^{-4}$	0.78	$15 \times 10^{-4}$	Eff = 50.3%	
60					653	$20 \times 10^{-4}$	0.78	$18 \times 10^{-4}$	Eff = 60%	
90					523	$15 \times 10^{-4}$	0.78	$18 \times 10^{-4}$	Eff = 36.7%	
70					523	$19 \times 10^{-4}$	0.78	$15 \times 10^{-4}$	Eff = 61.5%	
60					523	$20 \times 10^{-4}$	0.78	$18 \times 10^{-4}$	Eff = 70.5%	
60					523	$50 \times 10^{-4}$	0.324	$18 \times 10^{-4}$	Eff = 82 %	
	Biswas et al. (2008)	-	Lab	2 - 200	80 - 200	343 - 353	15.9 - $108.1 \times 10^{-4}$	11.1 - 20.1	$30 - 120 \times 10^{-3}$	(hydrodynamic study)
	Centner et al. (1989)	Analytical models considering inertial impaction, turbulent diffusion and coalescence induced by turbulence	Lab	N.I.	25	293	N.I.	1000 - 2000	0.075 - 0.3	For $Q_{liquid} = 0.150 \text{ m}^3/\text{h}$ $E_{ff}(dp = 0.5 \mu\text{m}) = 20-62 \%$

## Chapter I State of the art

	Lim et al. (2006)	Numerical approach considering Impaction, Interception and Brownian diffusion	-	PM10	100 - 2000	N.I.	N.I.	300.6	0.0468 - 0.2052	$E_{ff}(dp=0.5 \mu m) = 40\%$ $E_{ff}(dp=2 \mu m)=90\%$ $E_{ff}(dp>4 \mu m)=95-99.9\%$
	Bianchini et al. (2016, 2018)	An existing mathematical model considering interception	Lab	PM2.5	100	323 - 328	N.I.	36	0.1 - 1	Eff >99.9% Eff = 28.25%
	Hu et al. (2021)	-	Lab	0.268 - 125	N.I.	289.2-289.6	N.I.	12024	1.35	Eff = 95.59% to 96.81%
VWS	Bianchini et al. (2016)	-	Lab	PM2.5	40	323 - 328	N.I.	31	0.3	Eff = 60.36% (PM2.5)
VWS+BCWS					N.I.				0.3	Eff = 89.75% (PM2.5)
IWS	Zheng et al. (2018)	Analytical approach considering impaction, interception diffusiophoresis thermophoresis and diffusion	Lab	0.1 - 10	N.I.	323 - 363	N.I.	180	5	Eff = 24 - 85%
CWS	Elisa Achilles and Guerra (2020)	-	Lab	PM2.5	77.1 - 271.5	N.I.	0.10 - 0.43	N.I.	N.I.	$E_{ff} = 98.44\%$
	Krames and Büttner (1994)	-	Lab	PM10	5 - 100	293	0.05 - 0.25	500 - 2500	1200	Eff = 99.2%
CPWS	Zhang et al. (2020)	-	Lab	PM100	N.I.	N.I.	N.I.	216 - 837	0.54	Eff = 99.85%
SPWS	S. H. Huang et al. (2020)	A dimension-reduction method Numerical approach	-	1.5, 2.28, and 2.9	N.I.	N.I.	N.I.	N.I.	N.I.	25% > Eff < 80%
CDS	Bertinat (1980)	Numerical calculations	-	0.2	100	N.I.	0.001	N.I.	N.I.	$\geq 99.9\%$
OWS	Cho et al. (2020)	-	Lab	PM5	N.I.	N.I.	N.I.	192 - 270	N.I.	99.7% for $PM \geq 2.5 \mu m$ , 89.4% for $1.0 < PM \leq 2.5 \mu m$ , 62.1% for $0.5 < PM < 1.0$ , and 36.5% for $PM \leq 0.5 \mu m$
EWS	Pilat et al. (1974)	Numerical approach considering diffusion, impaction and electrostatic forces	Lab	0.05 - 5	50	293	590	N.I.	N.I.	Exp.: Uncharged conditions: 68.8% Charged conditions: 93.6% Theo.: Uncharged conditions: 17.4%

## Chapter I State of the art

										Charged conditions: near 100%
	Zhao and Zheng (2008)	Monte Carlo method for population balance considering impaction, interception, diffusion & electrostatic attraction	-	0.08-20	1000	433	$200 \times 10^{-4}$	61072.56	N.I.	Uncharged particle and droplet: 5% Charged particles: 25% Charged droplets: 70% Particles and droplets were oppositely charged: > 99%
	Carotenuto et al. (2010)	Innovative mathematical model considering impaction, diffusiophoresis thermophoresis interception, diffusion & electrostatic attraction	-	0.1 – 5.0	100 - 500	298	N.I.	1700	0.5	Eff > 99.5%
	Ha et al. (2010)	-	Lab	0.3-0.9	192	N.I.	N.I.	1.2	0.048	Eff = 97%
	Su et al. (2020)	-	Lab	PM10	249.5	N.I.	0.017 – 0.125	180	N.I.	Maximum Eff. increase of 40% & 60%
	Di Natale et al. (2015)	-	Lab	0.01 - 0.45	290	Atmospheric temperature	0.88 & 1.15	0.170 – 0.222	0.195	Uncharged particles and droplets: very small removal efficiency Charged droplets: 35% Particles and droplets were oppositely charged: 91%
	Bandyopadhyay and Biswas (2007)	-	Lab	9.82	102.3	$305 \pm 1$	$30 \times 10^{-4}$	22.3	0.066	Eff = almost 100 %
	Ru et al. (2017)	Empirical models considering impaction, interception, diffusion & electrostatic attraction	Lab	PM10 and PM 2.5	Mean diameter 150	$295.8 \pm 1.5$	N.I.	N.I.	0.18	Exp.: 88% (PM2.5) & 94% (PM10) Theo.: good agreement with the experimental results
U-TS	Zhou et al. (2017)	Empirical models considering impaction, interception &	Lab	2 5	2000	323 - 333	1.5 – 2.5	103.2 – 348.3	N.I.	Exp. Eff = 29.8%, Theo. Eff = 28.6% Exp. Eff = 88.5%, Theo. Eff = 87.2%

## Chapter I State of the art

		diffusion		10						Exp. Eff = 97.3%, Theo. Eff = 97.3 %
TWS	Lee et al. (2013)	-	Lab	0.65 - 20	N.I.	N.I.	N.I.	307.8 - 457.2	N.I.	0.5 < dp ≤ 1 μm: Eff increases from 52 to 97.5% dp ≥ 2: Eff = 100%
								457	N.I.	0.5 < dp ≤ 1 μm: Eff increases from 67 to 98.5% dp ≥ 2: Eff = 100%
VWS	Ali et al. (2013)	Mathematical model considering impaction	Lab	1	N.I.	N.I.	N.I.	N.I.	0.3 - 1	Eff = 99.5%
	Mi and Yu (2012)	-	Lab	40	N.I.	N.I.	5×10 <sup>-4</sup>	4000	2	Eff = 95.1%
				10						Eff = 92.7%
	Tsai et al. (2005)	-	Lab	0.05 - 0.478	N.I.	523 ± 293	1.17	10.8	N.I.	Eff = 80 - 96%
							1.50			
							1.80			
	Bal et al. (2019)	-	Lab	2.8 - 50	N.I.	303 - 305	N.I.	2.09 - 4.18	N.I.	Eff = 99.91%
	Ahmed et al. (2018)	Eulerian-Lagrangian approach considering inertial impaction	-	1.0	N.I.	N.I.	2 & 2.5	N.I.	N.I.	Eff = 97 - 98%
Kim and Park (2020)	New approach based on one-dimensional mass, momentum and energy equations considering impaction	-	0.47 - 1.5	N.I.	atmospheric temperature	0.00144 & 0.00173	N.I.	N.I.	Eff = 79 - 99%	
Attaullah et al. (2020)	Calvert and Mohebbi approach considering inertial impaction	-	PM1	20 - 80	N.I.	0.5 to 2	N.I.	N.I.	>65% Eff < 100%	
Huang et al. (2007)	Empirical approach based on Calvert's theory (Impaction)	Lab	0.05 - 0.478	N.I.	298	1.5	12	N.I.	Theo. Eff > 75%	
						2.0	15		Exp. Eff = 21 - 90%	
						2.5	18			
HAS	Cui et al. (2017)	Fourth-order Runge- Kutta approach considering impaction, diffusiophoresis thermophoresis & diffusion	Lab	0.01 - 10	600	288	N.I.	2.59	2.16	Eff. PM <sub>10</sub> = 100% Eff. PM <sub>5</sub> = 100% Eff. PM <sub>2.5</sub> = 83%
WFGDS	Wu et al. (2019)	A novel droplets swarm model + adaptation of impaction model	Lab	1 - 50	N.I.	N.I.	N.I.	79 - 129	1.5	Theo: Eff = 88.37 - 88.9% Exp: Eff = 88.9 -

										91.7%
Huang et al. (2020)	A dimension-reduction method/Numerical approach	-	PM10	2000	343.15	N.I.	10000	132		Eff = 10 -100%
Rafidi et al. (2018)	Euler–Lagrange CFD approach considering inertial impaction & Brownian diffusion	Lab	2 - 3.5	1100 - 2100	300 - 360	3.1 – 9.1	N.I.	N.I.		Theo.: Eff = 47 – 76% Exp.: Eff = 45 – 86%
Zhang et al. (2021)	-	Large	PM1, PM1-2.5, PM2.5-10	N.I.	322 - 332	N.I.	1500–3000	4.5–10		Eff = 45.2–28.3%
Yang et al. (2010)	-	Lab	0.023 – 9.314	N.I.	313 - 393	15	99.5	1.05		E <sub>ff</sub> =40-85%
Chen et al. (2018)	-	Large	0.1 - 100	N.I.	298	10	1.5293.10 <sup>7</sup> - 2.2939.10 <sup>7</sup>	N.I.		(OST), Eff = 77.2%
										(TST), Eff = 84.3%
										(FST), Eff = 87.2%

Where N.I.: No information, SWS: spray wet scrubbers, VWS: venturi wet scrubber, BCWS: bubble column wet scrubber, EWS: Electrostatic wet scrubber, TWS: turbulent wet scrubber, WFGDSS: wet flue gas desulfurization scrubber, OST: Open scrubbing tower, U-TS: U-type scrubber, TST: tray scrubbing tower, FST: Flow pattern control device scrubbing tower, HAS: heat absorbing scrubber, IWS: Innovative wet scrubber, CDS: Charged-Droplet scrubber, CWS: Cyclone wet scrubber, CPWS: composite wet scrubber, SPWS: sieve plate wet scrubber, OWS: orifice wet scrubber

Table 4 presents a summary of experimental and numerical studies on the collection of particles in a wet scrubber. The tables shows that they are indeed several studies on the collection of particles by a wet scrubber, but no study was found specifically dedicated to removal of nanoparticles by a spray scrubber under waste incineration.

## 1.8 Conclusions of the chapter

In this chapter, a literature review was carried out on nanomaterials and wet scrubbing technology.

The conclusion for the nanomaterial section includes:

1. Several definitions of nanomaterials exist with the EU commission definition emphasizing the source, the US Environmental Protection Agency highlighting the chemical novelty of the material while the ISO stresses the size range of the material.
2. There are no international guidelines on the safe disposal of nanomaterials at end-of-life as such nanowaste currently follows conventional waste management pathways.
3. In waste incineration, several studies have reported that after combustion, the majority of the nanomaterials end up in the bottom ash in their nano-sized form. But, a fraction of the nanomaterials were also found in the fly ash.

The conclusion for the wet scrubbing section includes:

4. A wet scrubber does participate in the collection of PM even though it is principally designed to treat acid gases
5. There exist a variety of scrubbers such as tray, venturi and spray scrubbers that are employed in various industrial applications such as asphalt production waste incineration and cement production plants
6. The collection of particles larger than 5.0  $\mu\text{m}$  in a wet scrubber is governed by the impaction mechanism while 0.1  $\mu\text{m}$  is captured by Brownian diffusion. A particle may still be collected by interception mechanism if it comes within one particle radius of a droplet. Other mechanisms involved in a scrubber include gravity, phoretic and electrostatic forces.
7. Generally, the gas flowrate, the liquid flowrate, the gas humidity rate and the particle diameter are positively correlated to the particle collection efficiency of a scrubber. Conversely, the droplet diameter is inversely correlated to the scrubber performance.

## **Chapter 2: Materials and methods**

## **2.1 Introduction**

This chapter presents the materials and methods used in this thesis. The experimental setup is described in this section. The setup was designed to be representative of a full-scale spray scrubber present in the flue-gas cleaning line of a hazardous waste incineration plant in terms of the height-to-diameter ratio, liquid-to-gas ratio, gas inlet, and outlet temperatures, gas humidity, gas residence time, gas flow regime, droplet diameter and particle concentration. The aerosol investigated is also described, as well as the apparatus used for aerosol generation and counting. This section also describes the droplet collectors used and the method employed to evaluate the collected particles in the discharge water. Lastly, the general experimental methodology – Box–Behnken design is also reported.

## **2.2 Description of the experimental setup**

### **2.2.1 Incineration plant – Full-scale spray scrubber**

The full-scale spray scrubber is part of a configuration of four spray scrubbers operating in series present in the flue-gas treatment line of the Salaise II hazardous waste incineration plant (WIP). The plant is operated by the company Séché Environnement/Trédi. The hazardous WIP (Figure 12) is typically fed with waste containing halogens and sulfur compounds. To treat and perform an energy valorization of the waste, the WIP is composed of a rotary kiln for the combustion and post-combustion steps capable of attaining high temperature (1100<sup>0</sup>C), while the energy recovery step consists of a boiler. The fumes treatment step is based on an electrostatic precipitator and four spray scrubbers for particle capture and gaseous compounds reaction and separation. The first scrubber is operated in a co-current mode while the other three scrubbers are counter-current spray scrubbers. The full-scale scrubber considered in the present thesis is the second spray scrubber operating in counter-current mode (Figure 12).

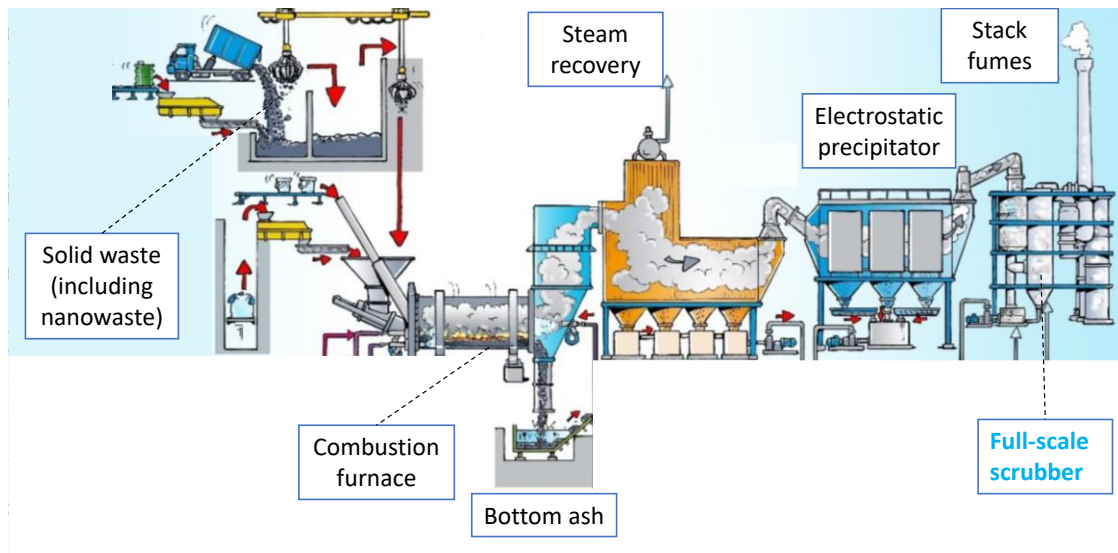


Figure 12 Full-scale Industrial unit TREDI Salaise-2 © Groupe Séché Environnement

The full-scale spray scrubber considered for pilot-scale investigation has a height of 15 m and a diameter of 2.7 m. Water is used as the collection liquid and is supplied by 30 spray nozzles at 4 levels located inside the scrubber. The typical liquid-to-gas ratio encountered ranges from 2 – 12 L.m<sup>-3</sup>. Further parameters of the full-scale scrubber are shown in Table 5.

### 2.2.2 Pilot-scale spray scrubber

The pilot scrubber was designed to allow as much as possible a scale similitude regarding gas phase residence time compared with the full-sale scrubber considered in the flue gas treatment line of the Salaise II plant. When scaling down the full-scale scrubber to the pilot-scale scrubber, it was important to consider both the geometric and the dynamic similarities. To achieve this, a *similitude of the gas residence time* was selected. The geometric similarities criteria between the full-scale scrubber and the pilot-scale scrubber were accounted for in the form of dimensioning the length, width, and height of the pilot-scale scrubber. The dynamic similarities (i.e., Hydrodynamic and thermal) were accounted for in the form of the gas velocity, the Reynolds number, and the temperature gradient. For that purpose, the following design and operating parameters are kept constant between the full-scale and the pilot-scale scrubbers:

- (i) The design parameters-
  - the ratio between the height (h) and the diameter (d) of the column h/d
  - the same droplet diameter at the outlet of the spraying nozzle
- (ii) The same flow properties-

- the turbulent flow regime
  - the ratio of the liquid flow rate ( $Q_L$ ) to the gas flow rate ( $Q_G$ )  $Q_L/Q_G$
- (iii) The same thermodynamic parameters-
- The same inlet (200°C) and outlet (70°C) temperatures
  - The same humidity conditions i.e., a mixing ratio of 15% (g of water/g of air) at the inlet i.e., approximately 1% relative humidity or 90 g/m<sup>3</sup> absolute humidity
- (iv) The same particle concentrations and distributions at the inlet of the scrubber i.e., at the outlet of the electrostatic precipitator

The full-scale data were obtained from the NANOWET project report [65] in which the mass characterization of particles in the flue gases of the incineration plant operated by Séché Environnement (Salaise II) was conducted in normal operations of the plant. The full-scale and the pilot-scale scrubbers design and operating parameters are presented in

*Table 5 Full-scale and pilot-scale spray scrubbers parameters at nominal conditions*

Parameters	Specifications Trédi (Salaise II, outlet ESP)	Pilot-scale scrubber
Height of scrubber, h	15 m	1.9 m
Diameter of scrubber, d	2.7 m	0.3 m
h to d ratio	5.55	6.3
Number of nozzles	30 spray nozzles (3 nozzles/5m)	20 nozzles 4 stages
Gas nature	Flue-gas	Room air
Gas flowrate, $Q_G$	50 to 60,000 Nm <sup>3</sup> .h <sup>-1</sup>	45 Nm <sup>3</sup> .h <sup>-1</sup>
Relative humidity	Inlet 1% (200°C)	1%
Gas temperature	T inlet = 200 - 240°C T outlet = 55 - 75°C	T inlet = 200°C T outlet = 70°C
Gas velocity, $U_g$	3 m.s <sup>-1</sup>	0.2 m.s <sup>-1</sup>
Reynolds number, Re	>30000	~3000
Gas residence time	5 s	5 s
Liquid to Gas ratio	2 - 12 l.m <sup>-3</sup>	~5 l.m <sup>-3</sup>
Droplet diameter, D	70 μm (ratio G/L: 0.2Nm <sup>3</sup> /l)	70 μm at 10 bar

Droplet residence time, $T_D$	No information	1 s
Droplet velocity	No information	13.8 m.s <sup>-1</sup>
Particle concentration (after ESP)	$dN/d\log dp \sim 10^6$ (part.cm <sup>-3</sup> ) $dp$ modal=0.3 $\mu$ m	-

Table 5 indicates a significant difference in gas velocity between the full-scale scrubber (3 m.s<sup>-1</sup>) and the pilot-scale scrubber (0.2 m.s<sup>-1</sup>). While the gas velocity mainly impacts the gas residence time i.e., the particle residence time, which has been maintained at a constant value (5 s) for both the full-scale and pilot-scale, higher gas velocities such as those in the full-scale scrubber may also have secondary impacts on the flow patterns, liquid-to-gas ratio, droplet size, and droplet velocity which in turn could affect the performance of the scrubber.

It should be noted that the complex matrix of pollutants encountered in the WIP flue gas treatment lines at the inlet of the scrubber was drastically simplified at the lab scale. A controlled particle size distribution and number concentration of carbon nanoparticles were injected, as particulate matter, into the gas flow feeding the pilot. Figure 13 shows the schematic of the experimental test setup.

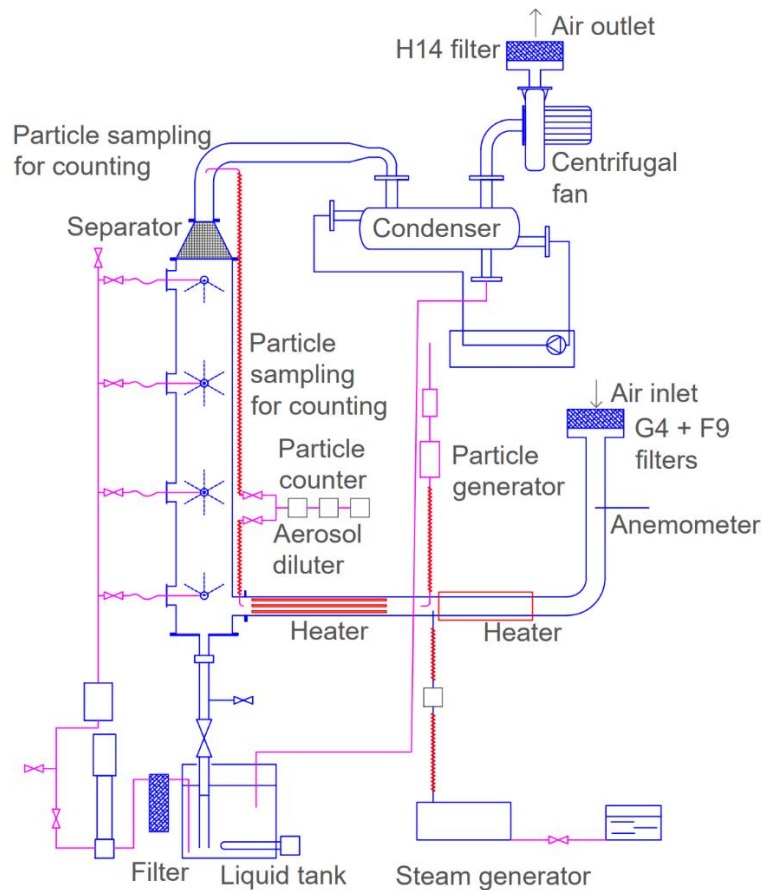


*Figure 13 Scheme of the experimental setup*

To operate the setup (Figure 13), the laboratory ambient air is supplied to the test bench by a centrifugal fan located downstream of the scrubber. The ambient air is filtered by passing through a G4 and an F9 filters to remove PM from the airflow before entering the pilot. To be representative of thermodynamic conditions encountered at the inlet of the full-scale scrubber, the airflow is heated in two steps: first heated to 70°C by a heating resistor placed in the flow and the second heating step is performed by an injection of steam whose mass flows depends on the air flowrate. The airflow is further heated to 200°C by a second heating resistor positioned on the surface of the air duct. At this point, carbon nanoparticles generated by the DNP 2000 (Palas) particle spark generator are injected. Water serves as the liquid collector and the water temperature was set to 60°C to attain the target gas outlet temperature of 70°C. A photograph of the pilot scrubber and its associated apparatus is shown in Figure 14.



Centrifugal fan    Water pump    Spray scrubber    Water tank    Dilution system    Particle generator (DNP 2000 – Palas)    Particle counter (SMPS)    Heating system

*Figure 14 Photograph of the experimental setup*

Single orifice spray nozzles with external diameters of 0.45 mm located at four different levels inside the scrubber supplied the water to the setup (Figure 15).



Level 1(bottom)

Level 2

Level 3

Level 4 (top)

*Figure 15 Image of nozzles at four different spray headers*

While the liquid flowrate and droplet diameter are theoretically independent, in practice they are partially correlated given the spraying technology (spray nozzles) employed. To account for this, the number and the location of the nozzles were adjusted accordingly. Given that this step could introduce secondary effects, three different experimental conditions were investigated to determine the influence of nozzle configuration modification on the collection efficiency. Particle counting was conducted upstream and downstream of the scrubber by the

SMPS (Grimm) to quantify the particle collection efficiency of the scrubber. Gas dilutions were also performed before particle counting to lower the high humidity and/or temperature of the gas so that stable and repeatable particle size measurements were obtained as the effects of condensation and nucleation were minimized.

**2.2.3 Collection efficiency measurement**

The nanoparticle collection efficiency of the scrubber is determined by measuring the concentration and particle size distribution of the upstream and downstream sampling points. A measurement lasted for a total of 40 minutes consisting of 5 scans of upstream measurement and another 5 scans of downstream measurement. The fractional collection efficiency, i.e., the collection efficiency of the scrubber for a specific particle diameter, is calculated according to the following expression:

$$Eff_{dpi} = \frac{C_{up,dpi} - C_{down,dpi}}{C_{up,dpi}} \tag{9}$$

Where dpi = characteristic diameter of the ith particle size range (in nm).

To establish repeatable and reproducible experimental results, the experimental campaigns for each operating condition were conducted four times over two days as presented in Figure 16. Tests A and B were conducted on the same day with a 30 minutes modification and re-establishment of the operating conditions before Test B is performed. Similarly, Tests C and D were conducted 24 hours later.

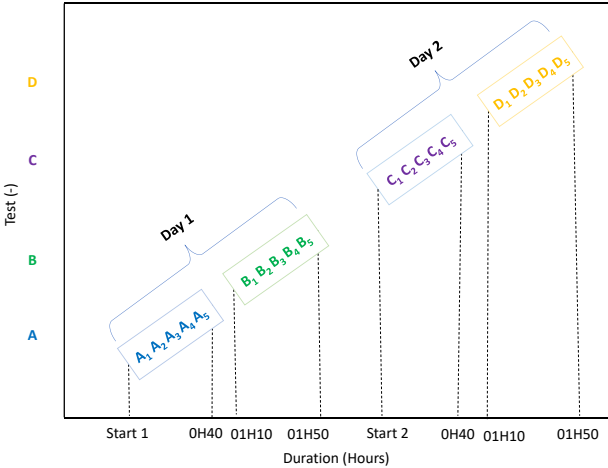


Figure 16 Breakdown of the experimental test procedure (not drawn to scale)

## 2.2.4 Measurement of uncertainty

The uncertainty due to conducting the same measurement four times may be more significant than the uncertainty in a single experimental measurement if the results obtained from repeating the measurement are not consistent and reproducible or if there is a high degree of variation in the results. This variability can be caused by factors such as errors in the equipment (SMPS and DNP particle generator), human errors, or variables that were not able to be controlled during the experiment. The uncertainty in the 20 sampling measurements (A<sub>1</sub> to D<sub>5</sub>) shown in Figure 16 was calculated using the standard error (SE) which in turn was calculated from the standard deviation (SD). SD was calculated with the assumption that the measurement errors follow a normal distribution. The standard deviation is a measure of the spread of the data and is calculated using the formula:

$$SD = \sqrt{\frac{(\sum(X_i - \bar{X})^2)}{N}} \quad (10)$$

Where  $X_i$  is each measurement,  $\bar{X}$  is the mean of the measurements and N is the total number of measurements.

The standard error (SE) is shown on the collection efficiency curves as an error bar calculated for each particle size collection efficiency as follows:

$$SE = \bar{X} \pm SD \quad (11)$$

## 2.3 Aerosol Investigated

The incineration of waste-containing nanoproducts could lead to the release of nanomaterials from the bulk material. Likewise, depending on factors such as the precursor, combustion temperature and oxygen concentration, nano-sized particles could be released in the gas phase during waste incineration. To represent the particle size distribution (PSD) present in the flue gas downstream of the electrostatic precipitator, carbon nanoparticles are generated by a nanoparticle spark generator (DNP 2000 PALAS) by generating a jump *spark* between two graphite electrodes under high voltage.

A scanning electron microscope (SEM) observation (Figure 17) of the carbon nanoparticles collected on a sampling filter positioned downstream to the DNP spark generator at room temperature shows that the generated carbon nanoparticles coagulated to form agglomerates.

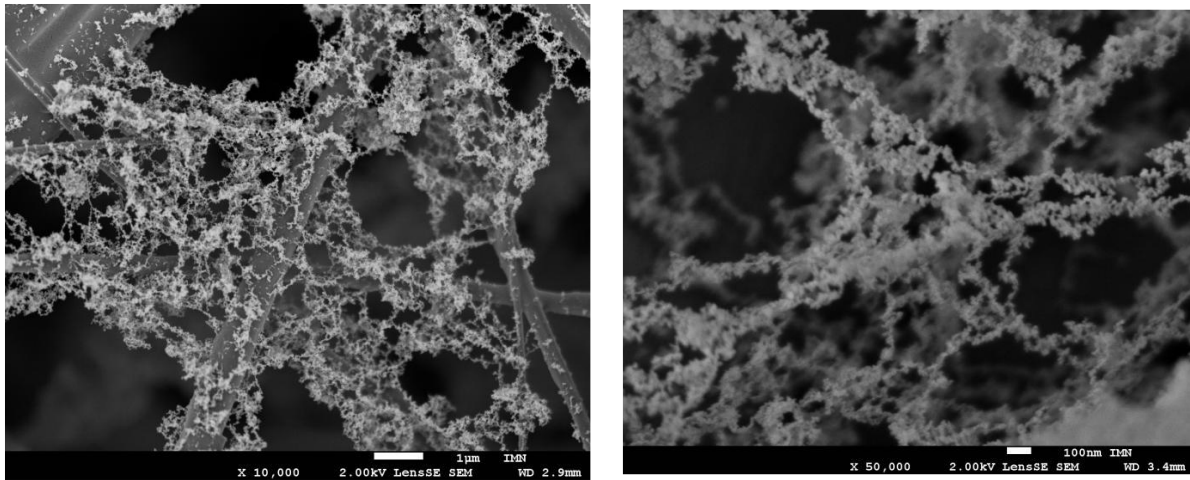


*Figure 17 SEM observation of carbon nanoparticle agglomerates generated by the DNP 2000 generator (Palas)*

### **2.3.1 Carbon particle generator and measurement equipment**

#### **2.3.1.1 Defined Nano Particle (DNP) 2000 PALAS spark generator**

As stated earlier, the generation of carbon nanoparticles in this work was done by using the DNP 2000 (Palas) spark generator. The DNP 2000 generates nano-scale carbon particles by spark discharge produced from two opposing cylindrical graphite electrodes (Figure 18). The generated particles are transported by a stream of nitrogen gas at a volume flow of  $4.5 \text{ l.min}^{-1}$  acting as a carrier gas. Given the high number concentration of the primary nano-sized particles ( $>10^7 \text{ particles.cm}^{-3}$ ), the particles coagulate to form agglomerates. Particle agglomeration is minimized by utilizing an exact dilution of the generated particles with clean compressed air at  $40 \text{ l.min}^{-1}$  volume flow. The consumption of electrodes is automatically compensated by the adjustment of the electrodes. The size distribution of the generated carbon particles depends on the spark frequency ( $13 - 200 \text{ s}^{-1}$ ) and the dilution air flow rate. During the experiments, the spark frequency was adjusted to the highest by setting the storm current button of the high-voltage supply to 999V. To maintain the reproducible and constant operation of the generated, the generator flow channel was periodically cleaned of deposited particles by using cotton buds dipped in liquid ethanol. Occasionally, consumed electrodes were replaced by new ones.

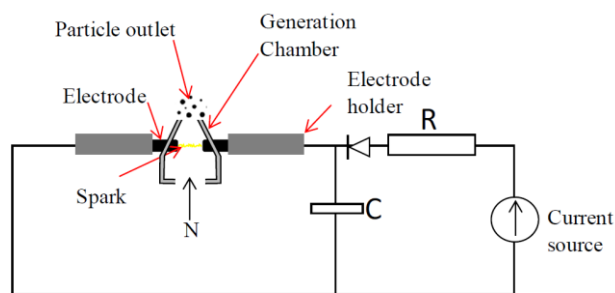


*Figure 18 Principle of the spark generator*

### **2.3.1.2 Particle counter and mobility particle sizer SMPS, Grimm**

The most commonly used particle sizing instrument, the Scanning Mobility Particle Sizer (SMPS Grimm) was used in this work to quantify the number and size distribution of carbon particles generated by the DNP 2000 (Palas). The SMPS consists of a Differential Mobility Analyzer (DMA) and a Condensation Particle Counter (CPC). The SMPS operates on the principle of electrostatic classification of charged particles and sizes particles based on their mobility equivalent diameter for particle number concentration from 10 to 1000 nm in 23, 43, or 64 size channels for particle concentration in a range of 0 -  $10^7$  particles.cm<sup>-3</sup> and sampling flow of 0.3 l.min<sup>-1</sup>. The operation of the SMPS consists of initially neutralizing sampled particles with a bipolar charger. The particle air flow then enters the DMA column into a space between the wall and a central electrode. Monodisperse particles in a narrow range of electrical mobility exit the DMA and subsequently enter the condensation particle counter (CPC), where the particles grow into large sizes due to exposure to butanol vapor. This permit the particles to be detected by a laser light scattering device. The particle size in mobility diameter is determined by combining this information with knowledge of the charging probability. Coupled with the particle counting capability of the CPC, size distributions are obtained. The measurement of a size distribution requires the instrument to scan through a range of voltages which is typically on a timescale of five minutes.

### **2.3.2 Dilution before counting/sampling**

As particle sampling is realized by sampling probes connected to heating lines that are introduced into the gas flow, upstream and downstream of the scrubber. It was vital to maintain isokinetic sampling. Isokinetic sampling is important when measuring the particle size distribution (PSD) as it ensures that the particles being measured are representative of the population in the sample and that the measurement is not biased by the flow conditions of the sample. According to the literature, for the sampling of submicronic and nano-sized particles,

the isokinetic sample error is insignificant [128]. Arouca et al. [189] reported that the isokinetic sampling conditions for nano-sized particles (12-130 nm) do not depend on the sampling velocity, the flowing duct flow rate, or on the diameter of the sampling nozzle. To that effect, no additional modification of the sampling probes was made for the various gas flowrates investigated. However, to avoid surpassing the maximum allowed operating particle concentration, temperature and humidity of the SMPS, a two-step dilution was implemented. The first dilutor was operated at 150°C while the second (a VKL diluter) was at room condition. In the VKL dilution system, dilution occurs by homogeneous mixing of a definite amount of clean air with a definite amount of aerosol (Figure 19). The ratio of the mixed amount of aerosol and clean air is predetermined and stable during dilution. The two dilutions gave a combine dilution factor of around 1: 100.

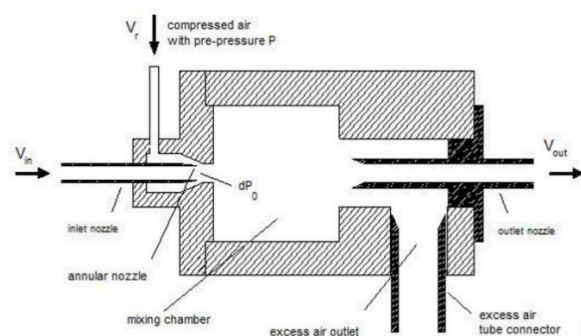


Figure 19 VKL 100 dilution system © Palas

### 2.3.3 Carbon particle size distribution and concentration

A measurement of the particle concentration distribution upstream of the pilot scrubber at nominal conditions was performed. Figure 20 represents the average PSD and the cumulative frequency distributions measured over 4 different sampling periods.

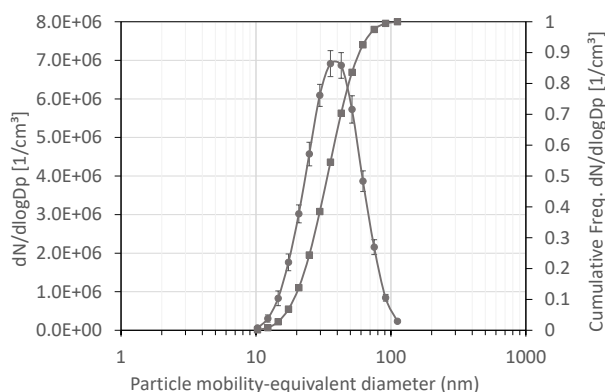


Figure 20 Particle size distribution of carbon nanoparticles upstream of setup at nominal conditions (average for N:4; standard deviation)

The concentrations of nanoparticles were respectively  $7.0 \cdot 10^6$  particles. $\text{cm}^{-3}$  with a particle mode between 35 and 42 nm.

## 2.4 Liquid collectors

### 2.4.1 Droplet characterization

Droplet diameter and velocity measurements were performed by the Lechler company, which is the manufacturer of the spray nozzles used in the study. The Phase Doppler Anemometry (PDA) measurements consisting of vertical and horizontal velocity measurements by four lasers were implemented. Two lasers for horizontal speed and two for vertical velocity. The tests were done with a single orifice hollow cone nozzle 220.185.1Y.AC (Figure 21) at room conditions.

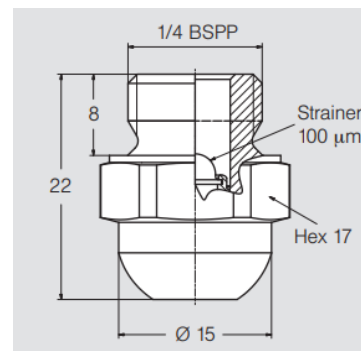


*Figure 21 single orifice hollow cone nozzle 220.185.1Y.AC nozzle*

The measurements were done at different distances (nozzle to laser) and different liquid pressures. A summary of the results is presented in Table 6. The PDA uses laser light scattering to measure the droplet size and velocity. In Table 6, the mean vertical and horizontal velocities for each test condition are presented. The droplet diameters (SMD/D32, DV10, DV50 and DV90) presented in Table 6 are statistical measures of the droplet size distribution. They represent different percentiles of the droplets in the spray and are used to describe the size distribution of droplets. The Sauter Mean Diameter (SMD) also called D32 represents the mean diameter with the same ratio of volume to the surface area as the droplet population. DV10 also known as the surface mean diameter represents the droplet size in volume that is exceeded by only 10% of the droplets, meaning 90% of the droplets are smaller than this size. DV50 (also known as the median droplet size) represents the droplet size in volume that is exceeded by 50% of the droplets, this means that half of the droplets are

smaller than this size and half are larger. DV90 represents the droplet size (in volume) that is exceeded by 90% of the droplets, meaning only 10% of the droplets are smaller than this size.

*Table 6 Summary of droplet characterization measurement*

Pressure (bar)	Volume flow (L.min- 1)	Distance (mm)	Droplet diameter				Mean velocity	
			SMD/D32 ( $\mu\text{m}$ )	DV10 ( $\mu\text{m}$ )	DV50 ( $\mu\text{m}$ )	DV90 ( $\mu\text{m}$ )	Vertical ( $\text{m.s}^{-1}$ )	Horizontal ( $\text{m.s}^{-1}$ )
3	0.1	20*	91.1	54.5	111.6	194.6	5.98	3.59
3	0.1	70	95.8	64.9	116.8	184.2	4.26	0.68
3	0.1	150	80.6	44.1	106.4	179	3.26	0.23
5	0.13	20*	83.9	54.5	101.2	173.8	8.13	5.86
5	0.13	70	78.3	49.3	96	153.1	5.14	1.04
5	0.13	150	69.3	38.9	96	158.3	4.23	0.25
10	0.18	20*	69.2	44.5	81.4	137.9	11.4	7.73
10	0.18	70	62.8	38	81.4	129.2	5.95	1.13
10	0.18	150	58	33.7	72.7	120.5	4.59	0.15
20	0.26	20*	62.9	40.2	74.9	127	16.19	10.89
20	0.26	70	54.2	31.5	70.6	114	7.61	1.43
20	0.26	150	49.4	29.3	59.7	105.3	5.31	0.5

\* Distance considered in the present study and SMD is Sauter Mean Diameter

However, when describing droplet size, a single number is often needed. In the present study, the Sauter mean diameter (D32) is used to represent the mean droplet size as it characterizes processes such as efficiency studies and mass transfer [190, 191]. In Table 6, for a given measurement distance (example 20 mm) a change in the spray pressure leads to the modifications of the liquid flowrate, droplet velocity and droplet diameters. As the spray pressure increases, the liquid flowrate and the droplet velocities increases. However, an increase in the spray pressure leads to a decrease in the droplet diameters (SMD/D32, DV10, DV50 and DV90).

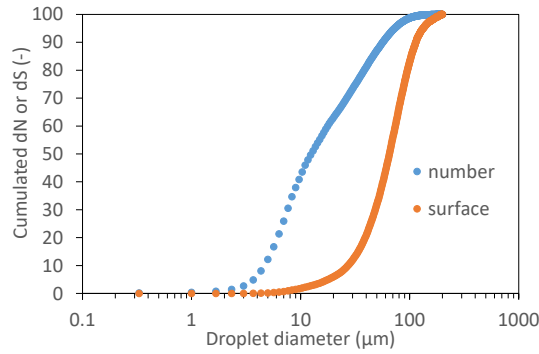


Figure 22 Cumulated droplet number/surface

To provide further information about the droplet size distribution, Figure 22 represents the cumulative frequency distribution plot (number) and the droplet surface area plot. The cumulative frequency distribution plot has a gradual slope indicating a wider droplet size distribution. The width of the curve shows a greater variation in droplet size. For the droplet surface area plot, the curve is a step curve indicating that the droplet size in terms of droplet surface is narrow.

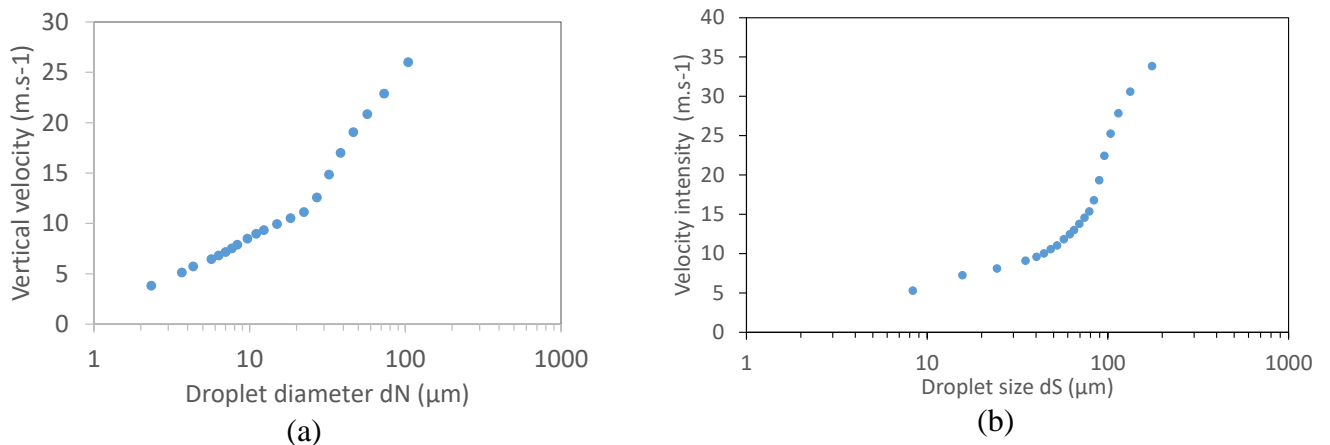


Figure 23 Droplet velocity intensity vs (a) Droplet size number distribution and (b) Droplet size surface distribution

Figure 23(a and b) present the droplet velocity intensity against the droplet size number distribution and droplet size surface distribution respectively. These plots permits identify the relationship between the droplet size and the droplet velocity. Both plots have a positive slope indicating that as droplet size increases, droplet velocity also increases. However, larger droplet sizes (above 30  $\mu\text{m}$  in number or 80  $\mu\text{m}$  in surface) have much steeper slopes as such higher velocities.

## 2.4.2 Range of droplet diameter

The range of droplet diameters used in this work is presented in Table 7. Table 7 also shows the liquid flowrate for one nozzle and the liquid pressure corresponding to each droplet diameter. One can see that a significant increase in water pressure (from 6 to 25 bars) does not significantly give a wider range of droplet diameter.

Pressure (bar)	Volume flow per nozzle (L.min <sup>-1</sup> )	SMD/D32 (μm)
25	0.30	60
10	0.18	70
6	0.14	80

*Table 7 Range of droplet parameters for a single spray nozzle*

The design droplet parameters were obtained from linear inter and extrapolations of the droplet characterization (Figure 24) studies earlier presented in Table 6. It should be noted that the characterization studies were conducted for a single spray nozzle in the direction of gravity at room conditions. Conducting a spray droplet characterization study in a room versus in an in-situ spray scrubber with a counter-current gas flow rate, gas temperature, and relative humidity can lead to significant differences in the results. Other factors that could lead to a variation in the results include the presence of other spray nozzles and the geometry of the scrubber. All this could result in significant droplet evaporation or condensation or coagulation that in turn modify the actual droplet size distribution and velocity.

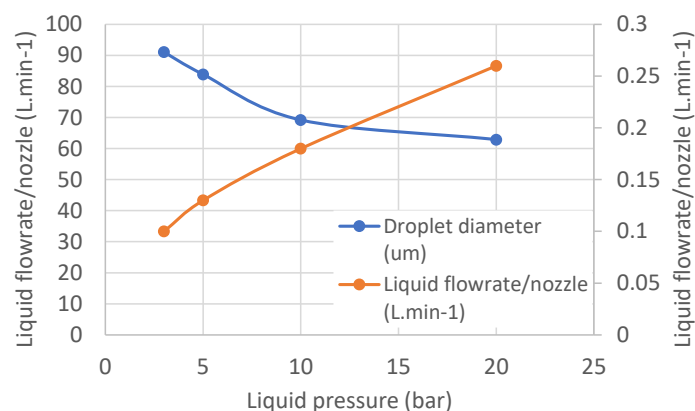


*Figure 24 Linear extrapolation of droplet parameters at 20 mm from the nozzle*

## 2.5 Methodology

### 2.5.1 Overall methodology

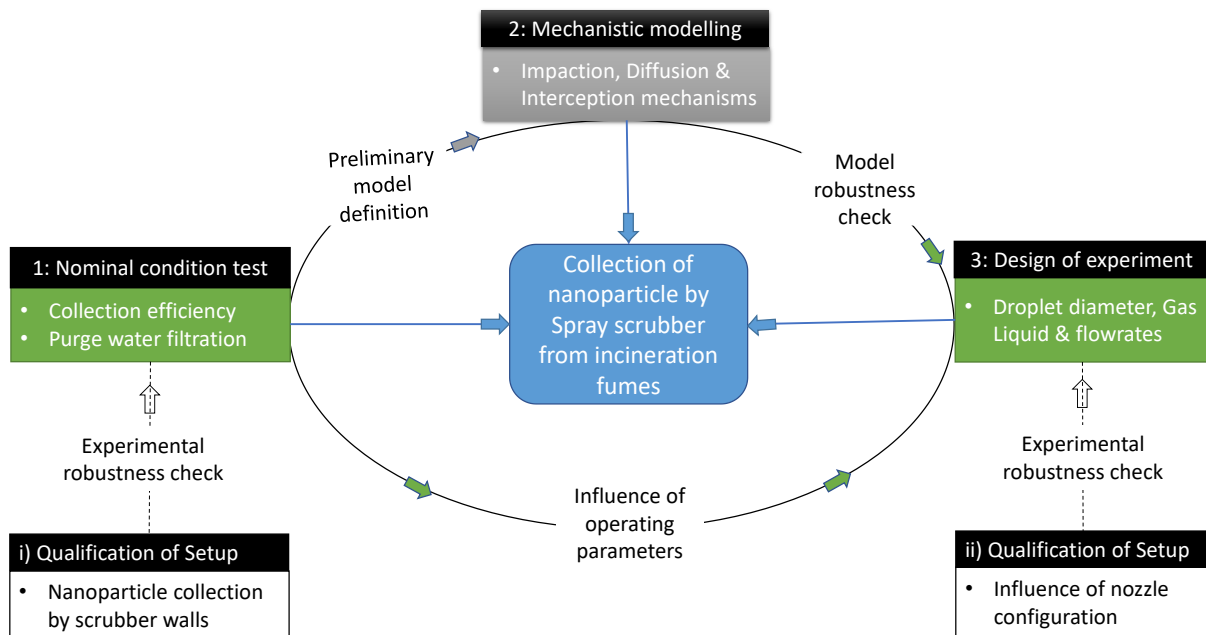


Figure 25 Overall research methodology

To evaluate the performance of the pilot-scale scrubber concerning the collection of NPs contained in incineration fumes, the research strategy presented in Figure 25 was employed. The strategy consists of initially conducting an experimental campaign at nominal conditions to quantify the collection efficiency of carbon nanoparticle NP by the pilot scrubber. Complementary purge water filtration measurements were carried out to measure the fraction of NPs that end up in the discharge water. Also at nominal conditions, experimental robustness checks were conducted to measure the collection of NP by the scrubber walls/surfaces, when there were no liquid collectors.

The results of the nominal condition campaigns were used to fit a mechanistic particle collection model based on impaction, Brownian diffusion and interception particle collection mechanisms. To investigate the influence of key operating parameters (droplet diameter, liquid and gas flow rates) on the performance of the pilot scrubber, the design of experiment methodology (DOE) was used. The results of the DOE permitted to verification of the mechanistic model robustness when the operating parameters were varied. Given the droplet spraying technology used, an experimental robustness check was performed to verify the influence of varying the nozzles configurations on the pilot scrubber collection efficiency.

## 2.5.2 Design of Experiment

The conventional method of studying the influence of several independent variables in a process on a response(s) involves changing one variable at a time while keeping other variables constant. This approach relies on “trial and error” and more importantly, ignores the interactions between the independent variables. In a new approach called the Design of Experiments (DOE), several independent variables are varied systematically and simultaneously to obtain a response or a group of responses. Aside from the advantage of time and cost savings, DOE can be used to screen the main variables from a list of several variables and can also be used to optimize the variables for desirable response(s). DOE can also give insight both about the main effects and interaction effects (i.e., the combined effect of multiple variables) on the response(s). DOE involves two stages: a screening stage to narrow the critical independent variables under assessment and a response surface methodology (RSM) to determine the responses' shape. A common type of RSM, the Box-Behnken design (BBD), is reported to be more efficient than other types of RSM such as central composite, Doehlert matrix, or three-level full factorial designs [192].

BBDs are not based on complete or fractional factorial designs but are rotatable or nearly rotatable second-order designs based on three-level incomplete factorial designs. In the case of three independent variables, for example, the design points are positioned in the middle of the sub-areas of the edges of the experimental domain, as shown in the graphical plot below (Figure 26).

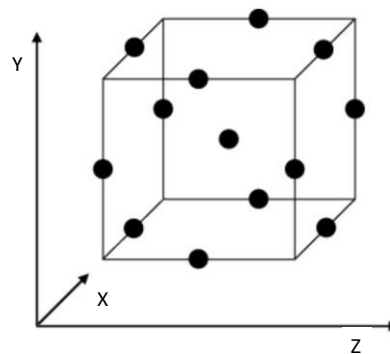


Figure 26 Graphical representation of three-factor Box–Behnken design

The predetermined number of experiments (N) required for the development of the BBD is given as:

$$N = 2k(k - 1) + C_o \quad (12)$$

Where k is the number of independent variables and  $C_o$  is the number of center points.

### 2.5.3 Operating conditions for experimental campaigns

In this work, the main variables were screened using semi-empirical particle collection models (mechanistic models) considering impaction, Brownian diffusion and interception mechanisms. This was achieved after the mechanistic model results were fitted to the initial DOE experimental runs at nominal conditions. Independent variables such as gas flowrate, gas temperature, liquid flowrate, droplet diameter and scrubber geometry (height and diameter) were originally considered. However, three main independent operating variables were identified: gas flowrate, liquid flowrate and droplet diameter. Eight responses (Table 9) were selected corresponding to the nanoparticle collection efficiencies at particle sizes 17, 20, 24, 29, 35, 42, 51 and 62 nm in mobility-equivalent diameters. The range of responses was selected to cover particle diameters in the Brownian diffusion region, the intermediate region, and the impaction-interception dominant region.

*Table 8 Box–Behnken design responses*

Responses (%)	Y <sub>1</sub>	Y <sub>2</sub>	Y <sub>3</sub>	Y <sub>4</sub>	Y <sub>5</sub>	Y <sub>6</sub>	Y <sub>7</sub>	Y <sub>8</sub>
Particle size (nm)	17	20	24	29	35	42	51	62

The responses were selected bearing in mind the measurement instability resulting from low particle concentration generated (by the Palas DNP-2000 generator) and counted (by the scanning mobility particle sizer) for particle sizes less than 14 nm or greater than 91 nm.

*Table 9 Box–Behnken design experimental variables*

Variables	Symbol	Level		
		-1	0	+1
Gas flowrate (Nm <sup>3</sup> .h <sup>-1</sup> )	A	35	45	55
Liquid flowrate (L.min <sup>-1</sup> )	B	1.6	3.2	4.8
Droplet sizes (μm)	C	60	70	80

The range of the three independent factors is shown in Table 9. The liquid flowrate is obtained by adjusting the number of spray nozzles while maintaining the liquid pressure as reported in Table 7. These values represent scaled-down values encountered at the inlet of a full-scale spray scrubber in the hazardous WIP operated by our industrial partner Séché Environnement. The range at three levels is coded as low (-1), medium (0) and high (+1).

**Level 0 is the nominal conditions encountered in the full-scale plant.** Levels -1 and +1 are acceptable lower and upper conditions encountered in the full-scale plant respectively. The most commonly used form of RSM, i.e., three-level, three-factorial Box-Behnken design (BBD) was employed for the DOE design. Seventeen experimental runs were conducted involving twelve factorial runs and five replica runs at central points, as depicted by the dots in the cube matrix in Figure 27. Replication was used to estimate the effects of natural process variations. The Design-Expert® software, V13 (Stat-Ease, Inc., Minneapolis, MN, USA) was used for the BBD model analysis.

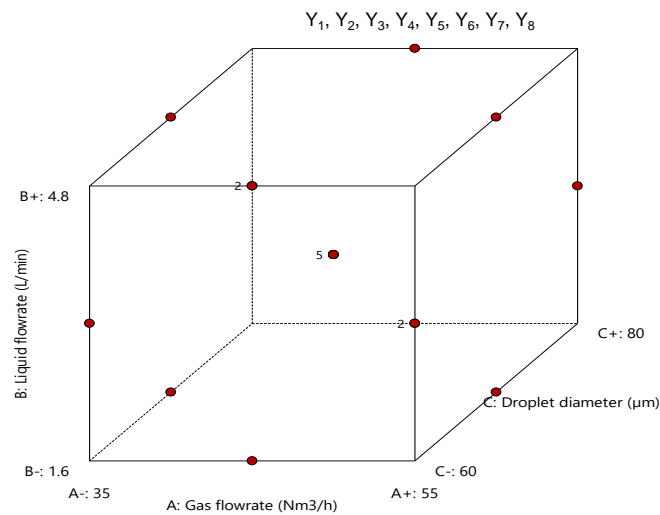


Figure 27 BBD cube matrix of 17 runs for 3 independent factors and 8 responses

### 2.5.4 Statistical analysis of BBD results

A regression analysis is carried out to determine if a relationship exists between the independent variables investigated and the selected responses. If a non-linear relationship exists, a second-order quadratic polynomial regression (13) is used to examine the relationship between the independent factors A, B, and C and the responses -  $Y_1, Y_2, Y_3, Y_4, Y_5, Y_6, Y_7,$  and  $Y_8$ .

$$Y = b_0 + b_1A + b_2B + b_3C + b_{11}A^2 + b_{22}B^2 + b_{33}C^2 + b_{12}AB + b_{13}AC + b_{23}BC \quad (13) \\ + \text{error} \quad )$$

Where Y is the predicted response,  $b_0$ , is a constant term,  $b_1, b_2,$  and  $b_3$  are the regression coefficients of linear terms,  $b_{11} b_{22} b_{33}$  are quadratic coefficients, and  $b_{12} b_{13} b_{23}$  are interaction terms [193].

A test for significance for the overall BBD model equations and the BBD model terms is made to validate the regression BBD models. Furthermore, additional checks such as

coefficient of determination ( $R^2$ ) and examination of the residuals are also made to test for the BBD model lack-of-fit.

## **2.6 Qualification of experimental setup**

Before investigating the performance of the pilot-scale scrubber concerning the collection of nanoparticles, it is pertinent to isolate the particle collection solely by the liquid collectors inside the scrubber, i.e., droplets and liquid wall films. This is done for two reasons; a) the influence of a scrubber wall on the performance of the scrubber is much more pronounced in the pilot-scale scrubber than in the full-scale scrubber due to a higher surface-to-volume ratio and b) liquid collections have a much more significant influence on the scrubber performance than the geometry of the scrubber [149]. In scaling the results of the present work to full-scale scrubbers, a study of the performance of the pilot-scale scrubber considering nanoparticle collection due only to droplet contact may also be relevant. Thus, the following subsection discusses the nanoparticle collection by the scrubber contact surfaces (both the walls of the scrubber and the nozzle apparatus). Subsequently, the nanoparticle collection due only to the liquid collectors (i.e., droplets and liquid wall films) will be deduced from this. Given the spraying technology employed in this work, a study of the likely secondary effect of the modification of the nozzle configuration is discussed in this section. Lastly, the quantification of the transfer of nanoparticles at nominal conditions from the gas phase to the liquid phase is made.

### **2.6.1 Particle removal efficiency of the pilot-scale scrubber with no liquid injection**

To investigate the nanoparticle removal efficiency by the scrubber when there is no liquid flow, i.e., the nanoparticle collection by the inlet surfaces of the scrubber (walls and nozzle apparatus), experimental campaigns were conducted at 3 different gas flowrates: 35, 45, and 55  $\text{Nm}^3\cdot\text{h}^{-1}$ . To maintain the same scrubber temperature ( $70^\circ\text{C}$ ) similar to when there is a liquid flow rate, the gas inlet temperature was set to  $70^\circ\text{C}$  as against the usual  $200^\circ\text{C}$ . While the nozzles were physically located over the 4 stages in the scrubber during these tests, no liquid flow was supplied. Figure 28 shows a plot of the nanoparticle collection efficiency of the scrubber with no liquid injection as a function of particle diameter at different gas flowrates. Significant fractional collection efficiency is observed for all particle diameters and all gas flow rates, indicating that nanoparticles are collected by the inlet surfaces of the scrubber.

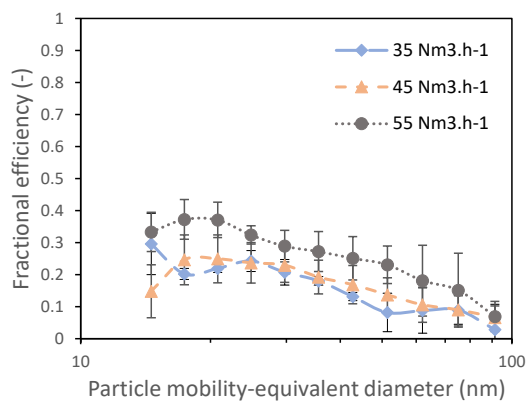


Figure 28 Nanoparticle collection efficiency by the scrubber with no liquid injection at varying gas flowrates at 70°C - 1% RH (average for N: 4; standard deviation)

The collection of particles by the scrubber walls and nozzles is similar for both gas flowrates of 35 and 45 Nm<sup>3</sup>.h<sup>-1</sup>. However, a slight increase in the particle collection efficiency due to particle collection of walls is observed at 55 Nm<sup>3</sup>.h<sup>-1</sup> gas flowrate. Moreover, the results indicate that the particle collection efficiency due to walls (no liquid injection) increases when decreasing the particle diameter, varying from 10 to 20% for a particle diameter of 80 and 20 nm respectively.

According to Nerisson et al. [194] the main mechanisms responsible for particle collection onto walls are:

- Sedimentation under the effect of gravity
- Impaction under the effect of centrifugal force
- Brownian and turbulent diffusion
- Thermal precipitation (thermophoresis) and electrical precipitation

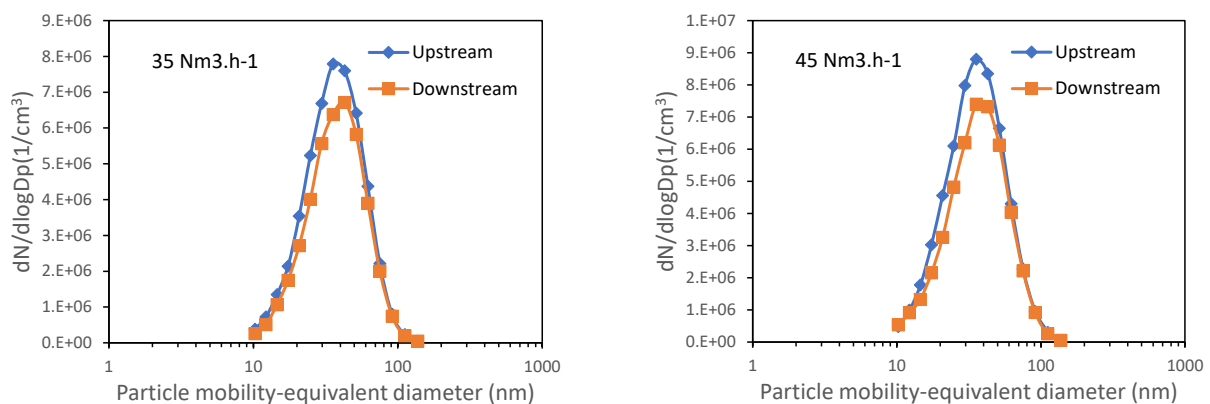
Thermal and electrical precipitation, which have the potential to influence the boundary layer of the gas flow, are considered to be insignificant in these experiments as no electrical forces were applied and the gas temperature was maintained constant throughout the scrubber. This was achieved by ensuring a constant gas temperature at the inlet and outlet, as well as using heat-insulated walls. Additionally, sedimentation, which is the combined effect of drag and gravity forces, is also considered to be negligible given the small size of the particles injected into the scrubber. Instead, the primary mechanism for particle deposition in the scrubber is found to be particle impaction under the effect of inertial forces. This collection mechanism is accentuated by an increase in both gas flow rate and particle diameter, and occurs outside of the boundary layer. When the scrubber is operated with liquid, particle deposition by turbulent

impaction can occur if the particles receive sufficient energy from the droplets to leave their fluid flow line and impact the walls.

The particle collection by Brownian diffusion occurs for low inertia particles having penetrated the viscous sub-layer next to the wall when submitted to turbulent diffusion forces in the flow buffer layer. The influence of the gas flowrate on the particle collection observed in Figure 28, could be explained by the increase of the turbulent diffusion of the low inertia particles for the higher gas flowrate and by the inertial impaction on the scrubber walls of the larger particles.

Indeed, Lancaster et al. [149] obtained similar results in a wet scrubber where they injected steam (but not liquid flow) in a saturated air at 20°C and flowrate of 45 ft.sec<sup>-1</sup> for the collection of particles with diameter 1.0 µm. The authors reported that up to 33% of dust particles was collected by wall deposition principally due to impaction mechanism.

In Figure 29, the PSD upstream and downstream of the scrubber operating with no liquid injection is presented. No significant particle aggregation phenomena in the scrubber are observed as there is no overall shift of the PSD from upstream to downstream. However, the presence of vapor can promote adhesion forces, leading to the phenomenon of condensation and aggregation of particles. In this case, the modal diameter of the particles tends to increase from the upstream to the downstream direction. This is likely due to the smallest particles undergoing condensation and aggregation to form larger particles, which can explain why the efficiency is higher for particles with a diameter of 20 nm compared to those with a diameter of 80 nm (Figure 28).



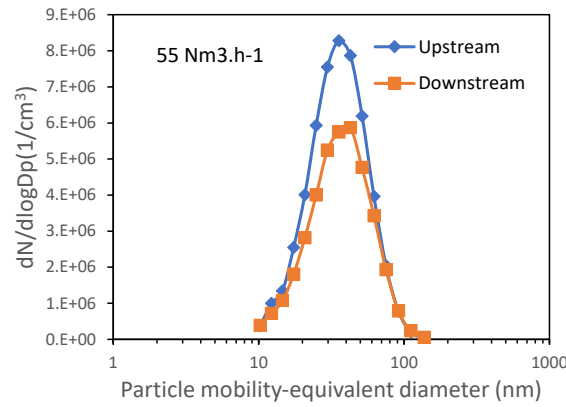


Figure 29 Particle size distribution upstream and downstream of the scrubber operating with no liquid injection at varying gas flowrates (average for  $N:4$ ; standard deviation)

Thus, the walls of the pilot-scale scrubber do participate in the collection of nanoparticles even when there are no liquid collectors. Note that these tests were performed at a constant temperature of  $70^{\circ}\text{C}$  at the inlet and outlet of the scrubber for technical reasons (preserving the integrity of the fibrous filter at the outlet of the pilot-scale scrubber), thus neglecting deposition by thermophoresis.

Table 10 Carbon nanoparticle relaxation time

dp (nm)	12	14	17	20	24.	29	35	42	51	62	75	91
$\tau_p^+$ ( $10^{-8}$ )	1.12	1.34	1.61	1.94	2.34	2.84	3.46	4.23	5.21	6.47	8.10	1.03

Where  $\tau_p^+$  is the dimensionless particle relation time and dp is particle diameter (nm)

Table 10 shows the dimensionless particle relation time ( $\tau_p^+$ ) as a function of particle diameter.  $\tau_p^+$  is estimated from the expression in the study of Nerisson et al.[194]. Particle relaxation time is the time required for a particle to adjust to the local gas flow velocity and is inversely proportional to the particle diameter. For particles with a short relaxation time, their motion is more closely aligned with the gas flow velocity, and they are more likely to be transported farther into the scrubber before being deposited. In the case of

Table 10, diffusion and diffusion-impaction mechanisms are more likely to be the dominant deposition mechanisms.

### 2.6.2 Influence of nozzle configurations on the particle collection efficiency

Spray nozzles located on nozzle heads at four (4) distinct locations in the scrubber supply the water droplets inside the pilot-scale scrubber. To conduct experimental tests at different liquid

flowrates corresponding to a constant droplet diameter, the number and location of the spray nozzles are varied accordingly. This could have secondary effects on the operating parameters investigated in this work. Thus, three different tests, described in Table 11, were performed to investigate the influence of nozzle location on the performance of the pilot-scale scrubber.

Table 11 Nozzle configurations for test A, B and C

Test A: Gas flowrate: 35 Nm <sup>3</sup> .h <sup>-1</sup> , liquid flowrate: 1.6 L.min <sup>-1</sup> & droplet diameter: 70 μm			
Spray stage	Number of nozzles		
	a <sub>1</sub> configuration	a <sub>2</sub> configuration	a <sub>3</sub> configuration
Stage 4	1	0	2
Stage 3	3	9	4
Stage 2	3	0	2
Stage 1 (bottom)	2	0	1
Total nozzles	9	9	9

Test B: Gas flowrate: 45 Nm <sup>3</sup> .h <sup>-1</sup> , liquid flowrate: 3.2 L.min <sup>-1</sup> & droplet diameter: 70 μm		
Spray stage	Number of nozzles	
	b <sub>1</sub> configuration	b <sub>2</sub> configuration
Stage 4	3	4
Stage 3	6	5
Stage 2	6	5
Stage 1 (bottom)	3	4
Total nozzles	18	18

Test C: Gas flowrate: 45 Nm <sup>3</sup> .h <sup>-1</sup> , liquid flowrate: 4.8 L.min <sup>-1</sup> & droplet diameter: 60 μm		
Spray stage	Number of nozzles	
	c <sub>1</sub> configuration	c <sub>2</sub> configuration
Stage 4	4	4
Stage 3	5	6
Stage 2	5	4
Stage 1 (bottom)	3	3
Total nozzles	17	17

The influence of the nozzle location on the collection of nanoparticles by the pilot-scale scrubber for the A, B, and C conditions (Table 11) is represented in Figure 30, Figure 31 and Figure 32 respectively. For the range of operating parameters tested, little (Figure 30) to no (Figure 31 and Figure 32) influence of changing the location of the spray nozzles is observed. This conclusion is in line with studies by Keshavarz et al. [157] where the authors compared mathematical models and experimental results on the performance of a spray scrubber in gaseous pollutants scrubbing and aerosol removing processes. Keshavarz et al. [157] reported that the nozzle locations have no significant effect on the performance of the overall efficiency of particles (PM<sub>5.0</sub>) by the scrubber.

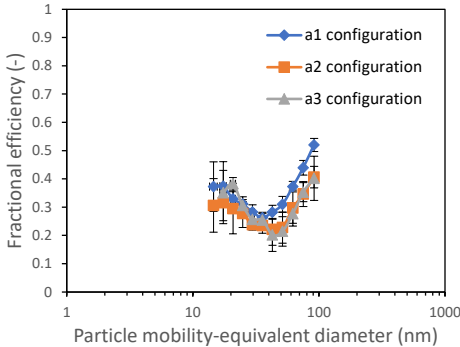


Figure 30 Collection efficiency at Test A conditions for varying nozzle configurations (average N=4; standard deviation)

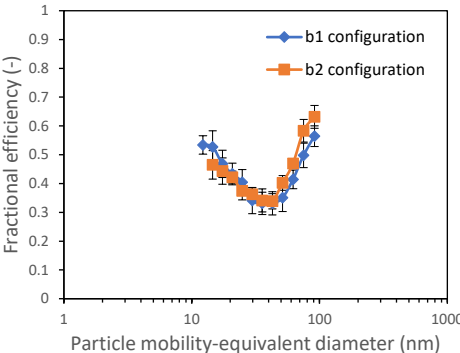
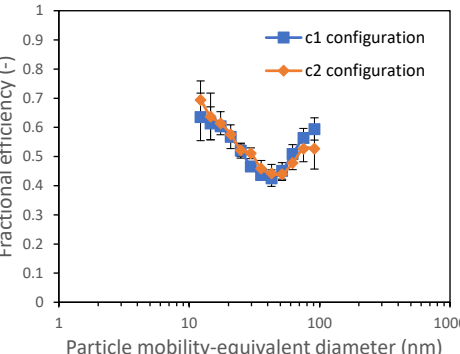


Figure 31 Collection efficiency at Test B conditions for varying nozzle configurations (average N=4; standard deviation)



*Figure 32 Collection efficiency at Test C conditions for varying nozzle configurations (average N=4; standard deviation)*

### 2.6.3 Quantification of transfer of nanoparticles to liquid-phase

To quantify the fraction of nanoparticles that is collected by the droplets and transferred to the discharged water at nominal conditions, a material balance analyzing the incoming and outgoing carbon nanoparticle flows was performed. The mass balance of the particles in the pilot setup is given as:

$$\phi_e = \phi_1 + \phi_2 + \epsilon \quad (14)$$

$\phi_e$ : inbound gas phase particle flux

$\phi_1$ : outbound gas phase particle flux

$\phi_2$ : particle flow transferred to the liquid phase

$\epsilon$ : wall/surface losses



*Figure 33 Particle/liquid vacuum filtration apparatus*

The particle mass fluxes in the gas phase are determined from the particle size distributions of the SMPS spectrometer considering a sphericity assumption on each class of particles. The carbon nanoparticle density is also considered. Membrane filtration was used to quantify the total mass or flux of particles transferred to the purged water by a vacuum pump (Figure 33). Cellulose acetate filters with a 47 mm diameter and a pore size of 0.02  $\mu\text{m}$  were used. The filtered liquid was recovered by bypassing the purge water recovered at the bottom of the pilot scrubber during nominal operating conditions for a duration of 30 min. A total of 30 L of purged water was filtered.

The measured nanoparticle flow transferred to the liquid phase ( $\phi_2$ ) on the filter was found to be:  $0.0654 \text{ g.h}^{-1}$ .

$$\phi_e = \sum_{i=1}^n Pc \cdot Volp \cdot \rho_p \cdot Q_G \quad (15)$$

Where  $Pc$  is particle concentration ( $\#.cm^{-3}$ ),  $Volp$  is volume of particle ( $m^3$ ),  $n$  is number of particle size,  $Q_G$  is gas flowrate ( $cm^3.h^{-1}$ ) and  $\rho_p$  is the particle density ( $1279 \text{ kg.m}^{-3}$ ).

Using the expression above, the mass of inbound gas phase particle flux ( $\phi_e$ ) was calculated to be  $0.17496 \text{ g.h}^{-1}$ . Figure 34 shows the mass balance of the carbon nanoparticles at nominal conditions.

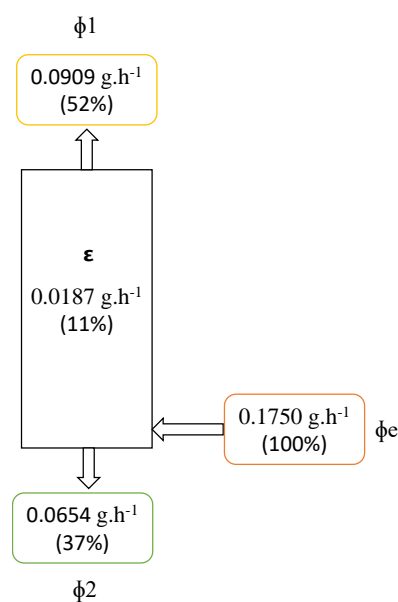


Figure 34 Mass balance of carbon nanoparticles at nominal conditions

37% of the mass of the carbon nanoparticles is transferred to the liquid phase while 11% is collected by the walls of the scrubber. The 11% wall collection represents a much lower value than the almost 30% collection previously discussed when there is no liquid flow present in the scrubber. This could be attributed to the continuous washing of the scrubber walls by the liquid film.

## 2.7 Conclusions of the chapter

This chapter presents the overall research methodology for the study of carbon nanoparticle collection by a pilot-scale scrubber operating under waste incineration conditions. The pilot scale scrubber was designed and operated to represent a full-scale spray scrubber present in the flue-gas cleaning line of a hazardous waste incineration plant in terms of the height-to-

diameter ratio, liquid-to-gas ratio, gas inlet and outlet temperatures, gas humidity, gas residence time, and gas flow regime, droplet diameter and particle concentration.

It was reported that the experimental setup was equipped with a DNP 2000 (Palas) particle generator (for the generation of the carbon nanoparticles), an SMPS (for the counting of the PSD of the generated nanoparticles) and a two-step dilution system to lower the flue gas particle concentration, gas temperature and humidity conditions. The particle size distribution, SEM observation and the particle concentration of the carbon nanoparticles investigated were also reported in this chapter. The liquid droplet diameter and velocity characterization measurements were likewise described. The characterization measurements of liquid droplet diameter and velocity highlighted the challenges associated with using spray nozzles. It was found that altering the liquid flow rate of the nozzle also led to changes in the droplet diameter.

To investigate the influence of the main operating parameters on the collection efficiency of carbon nanoparticles by the pilot-scale scrubber, a Design of experiment methodology - Box Behnken design was employed. The three independent operating parameters (variables) considered were the droplet diameter, gas and liquid flowrates.

Three test bench qualifications campaigns were conducted. The first involved quantifying the collection of nanoparticles by the scrubber walls at gas flowrates of 35, 45 and 55 Nm<sup>3</sup>.h<sup>-1</sup> in the absence of liquid flowrate. It was found that a significant quantity of nanoparticles (up to 30%) is collected by the walls of the scrubber. Given that spray nozzle were used in this thesis to supply the liquid, a second qualification test was carried out involving the investigation of the influence of the modification of nozzle configurations on the pilot scrubber collection efficiency at three distinct operating conditions. The influence of the nozzle configuration was found to be negligible. Lastly, a vacuum filtration measurement of the purged water to quantify the transfer of nanoparticles from the gas phase to the liquid phase at nominal conditions was conducted. It was found that 37% of the mass of the carbon nanoparticles was transferred to the liquid phase while 11% is collected by the walls of the scrubber.

# **Chapter 3: Optimization of nanoparticle collection by spray scrubber using Box-Behnken Design**

### **3.1 Introduction**

This section discusses the experimental results using the Box-Behnken design (BBD) methodology. Three operating factors; Gas flowrate (factor A), liquid flowrate (factor B) and droplet diameter (factor C) were investigated. The numerical values for these factors were presented in chapter 2 (Table 9). Eight responses were selected to cover the particle diameter in the Brownian diffusion region, the intermediate region and the impaction-interception regions (

Table 8). As detailed in chapter II, analysis of variance and fit statistics are first performed to verify the adequacy of the BBD models at a 95% confidence level. For the BBD models that were found to be statistically significant, the regression equations are used to predict the responses and the results are compared to the experimental data. Surface plots, representing the combined influence of two independent factors (while keeping the third constant) are then plotted. Using the Design Expert V13 software, the optimal operating conditions set that maximizes the fractional collection efficiencies (BBD responses) of the pilot-scale scrubber is determined and confirmatory experimental runs are conducted.

### **3.2 Box-Behnken Design (BBD) responses**

Carbon nanoparticles with sizes from 1 to 100 nm were initially intended to be investigated. However, the two extrema of particle size distribution (corresponding to particles lower than 14 nm and greater than 72 nm, see Figure 20) exhibit too low particle number per size range to allow stable fractional efficiency estimation. It was then decided to exclude particle sizes for which the SMPS counted less than 3,000 particles upstream of the scrubber. This threshold was selected to minimize the uncertainty associated with low particle number count by the SMPS. Thus, the range of the BBD responses in this study is between 17 nm to 62 nm particle diameters (Figure 35).

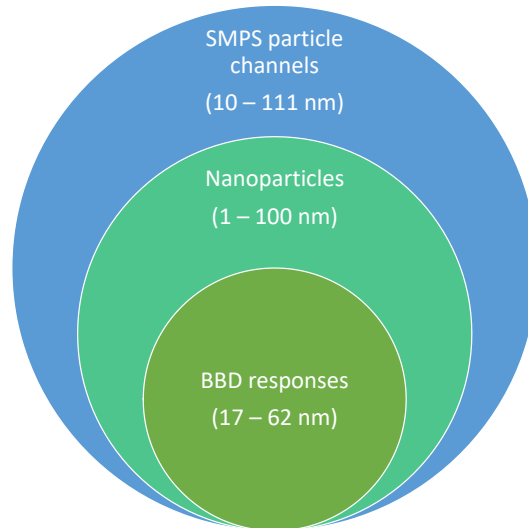


Figure 35 Range of BBD responses

Figure 36 presents the average fractional collection efficiency of the pilot-scale scrubber for the five (5) replicas of the central points (level 0). The shape of the collection efficiency curve is in accordance with earlier studies [14, 130]. Four (4) of the responses  $Y_1$ ,  $Y_2$ ,  $Y_3$  and  $Y_4$  corresponding to particle diameters 17, 20, 24 and 29 nm fall to the left part of the efficiency curve, i.e., the “diffusion-dominant” region. BBD responses  $Y_5$  and  $Y_6$  at particle diameters 35 and 42 nm respectively fall in the intermediate region. The intermediate region corresponds to the MPPS where neither diffusion nor impaction-interception mechanisms are dominant.

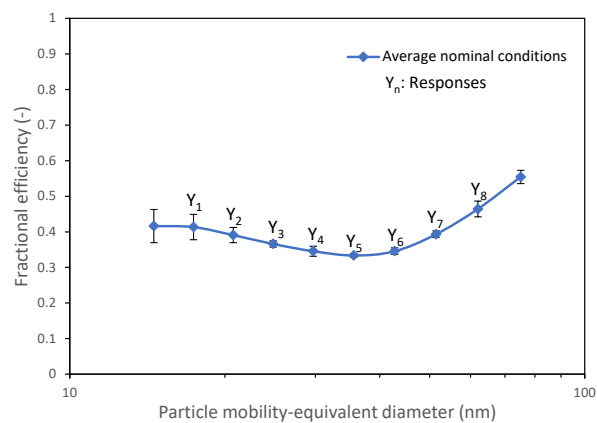


Figure 36 Depiction of chosen responses at average nominal conditions

Indeed, the results of the seventeen (17) BBD experimental runs (Table 19) show that nine have their MPPS at 35 nm while another six runs have their MPPS at 42 nm. As such in the present work, particle collection at both 35 and 42 nm ( $Y_5$  and  $Y_6$ ) is referred to as the intermediate region. Also, in Figure 36, responses  $Y_7$  and  $Y_8$  corresponding to the collection

at particle diameters 51 and 62 nm lie to the right part of the curve, i.e., the “impaction-interception dominant” region.

### 3.3 Box–Behnken statistical analysis

Design-Expert® software, V13 (Stat-Ease, Inc., Minneapolis, MN, USA) is used for the BBD model analysis for each of the responses. Analysis of variance (ANOVA) is used to test the full BBD model and individual terms in the BBD model for statistical significance, adequacy and correctness. Model reduction is carried out in the case of inadequate (non-significant) BBD models while BBD model transformation (i.e., square-root transformation or log transformation) is performed if the default model explaining the relationship between the factors and the responses is found to be unfitting. BBD model statistics considered include:

- the mean square variation, which is a measure of the sum of squares divided by the degrees of freedom (DF);
- F-value, which compares the source’s mean square to the residual mean square;
- p-value, which represents the probability that there are no factor effects on the responses;
- Fit-statistics (R-squared, Adjusted R-squared, Predicted R-squared and Adequate Precision)

R-squared represents the amount of variation around the mean explained by the BBD model. The Adjusted R-squared measures the amount of variation around the mean explained by the model, adjusted for the number of terms in the model. Predicted R-squared represents the amount of variation in the new predicted data explained by the BBD. Finally, Adequate Precision measures the signal-to-noise ratio. It compares the range of the predicted data at the design points to the average prediction error.

#### 3.3.1 Analysis of Variance (ANOVA)

To investigate the combined effect of the independent factors (A: Gas flowrate, B: Liquid flowrate and C: Droplet diameter) on the responses (

Table 8), experiments were performed for different combinations of the operating parameters and the results are shown in Table 19 that includes the experimental and predicted values for the different combination of factors of the experimental design. Before predicting response values using the BBD models, significant terms in the BBD models for each response were

found by analysis of variance (ANOVA) and significance was primarily decided by the F-statistic calculated from the data. The following subsections present the various statistical analysis. Responses  $Y_2$ ,  $Y_5$  and  $Y_8$  are discussed to represent particle diameters in the diffusion region, intermediate region and impaction-interception regions respectively.

### 3.3.1.1 ANOVA for response $Y_2$ @ 20 nm

Table 12 shows the summary of the ANOVA test for the BBD model  $Y_2$  (fractional collection efficiency of nanoparticle with size 20 nm). The Model F-value of 20.86 implies that the overall model is statistically significant as there is only a 0.03% (p-value) probability that an F-value this large could be attributed to background noise.

*Table 12 Full ANOVA data for  $Y_2$*

Source	Sum of Squares	df	Mean Square	F-value	p-value
Model	756.92	9	84.10	20.86	0.0003 significant
A-Gas flowrate	10.35	1	10.35	2.57	0.1531
B-Liquid flowrate	332.82	1	332.82	82.55	< 0.0001
C-Droplet diameter	265.65	1	265.65	65.89	< 0.0001
AB	2.25	1	2.25	0.5581	0.4794
AC	0.2025	1	0.2025	0.0502	0.8291
BC	0.1600	1	0.1600	0.0397	0.8478
A <sup>2</sup>	12.86	1	12.86	3.19	0.1173
B <sup>2</sup>	8.58	1	8.58	2.13	0.1880
C <sup>2</sup>	125.18	1	125.18	31.05	0.0008
Residual	28.22	7	4.03		
Lack of Fit	12.29	3	4.10	1.03	0.4691 not significant
Pure Error	15.93	4	3.98		
Cor Total	785.14	16			
Std. Dev.	2.01			R <sup>2</sup> 0.9641	
Mean	41.34			Adjusted R <sup>2</sup> 0.9178	
C.V. %	4.86			Predicted R <sup>2</sup> 0.7178	

Adeq Precision 16.9160

In

Table 12, the model terms (B and C) are significant. Factor A is found to be insignificant. All the factor interaction terms (AB, AC and BC) together with the quadratic form for the gas flowrate ( $A^2$ ) and liquid flowrate ( $B^2$ ) are statistically non-significant ( $p$ -value  $> 0.05$ ). Although the Lack of Fit is not significant relative to the pure error i.e., there is a 46.91% ( $p$ -value) chance that a Lack of Fit of 1.03 could occur due to noise, a model reduction is carried out to improve the overall BBD model  $Y_2$  and thus prevent overfitting the BBD model. This model reduction was achieved using the corrected version of the Akaike Information Criterion (AICc). The corrected version of the Akaike Information Criterion (AICc) is an adjustment to the AIC that accounts for the number of parameters in a model and the sample size. It is used to balance the fit of the model to the data (as measured by the likelihood) with the complexity of the model (as measured by the number of parameters). The AICc is a measure of the relative quality of a statistical model for a given set of data. It adjusts the AIC for small sample sizes, providing a more accurate estimate of the model's relative quality.

*Table 13 Reduced ANOVA data for  $Y_2$*

Source	Sum of Squares	df	Mean Square	F-value	p-value
Model	723.57	3	241.19	50.92	$< 0.0001$ significant
B-Liquid flowrate	332.82	1	332.82	70.27	$< 0.0001$
C-Droplet diameter	265.65	1	265.65	56.09	$< 0.0001$
$C^2$	125.09	1	125.09	26.41	0.0002
Residual	61.57	13	4.74		
Lack of Fit	45.65	9	5.07	1.27	0.4373 not significant
Pure Error	15.93	4	3.98		
Cor Total	785.14	16			
Std. Dev.	2.18	$R^2$	0.9216		
Mean	41.34	Adjusted $R^2$	0.9035		
C.V. %	5.27	Predicted $R^2$	0.8562		
		Adeq Precision	23.1369		

Table 13 presents the summary of the ANOVA test for  $Y_2$  when non-significant terms are excluded. An improvement in the model F-value is observed, from 20.86 to 50.92. The Fit-statistics also improved: the Predicted  $R^2$  of 0.8562 is reasonably close to the Adjusted  $R^2$  of 0.9035; i.e., the difference is less than 0.2; the signal-to-noise ratio (Adeq. Precision) is 23.1369 which is greater than the desired value of 4. Hence, the BBD model can be effectively applied to investigate the response  $Y_2$ .

### 3.3.1.2 ANOVA for response $Y_5$ @ 35 nm

Table 14 Full ANOVA data for  $Y_5$

Source	Sum of Squares	Df	Mean Square	F-value	p-value	
Model	212.19	9	23.58	12.33	0.0016	significant
A-Gas flowrate	6.48	1	6.48	3.39	0.1081	
B-Liquid flowrate	57.78	1	57.78	30.23	0.0009	
C-Droplet diameter	56.71	1	56.71	29.67	0.0010	
AB	7.56	1	7.56	3.96	0.0870	
AC	0.3025	1	0.3025	0.1583	0.7026	
BC	1.69	1	1.69	0.8842	0.3784	
A <sup>2</sup>	30.81	1	30.81	16.12	0.0051	
B <sup>2</sup>	9.10	1	9.10	4.76	0.0655	
C <sup>2</sup>	45.02	1	45.02	23.56	0.0018	
Residual	13.38	7	1.91			
Lack of Fit	12.25	3	4.08	14.43	0.0130	significant
Pure Error	1.13	4	0.2830			
Cor Total	225.56	16				
Std. Dev.	1.38		$R^2$	0.9407		
Mean	34.32		Adjusted $R^2$	0.8644		
CV %	4.03		Predicted $R^2$	0.1234		
			Adeq. Precision	15.9736		

Table 14 shows the summary of the ANOVA for the fractional collection efficiency at a particle diameter of 35 nm ( $Y_5$ ). The overall BBD model is statistically significant as represented by the p-value 0.0016 of the model. However, the interaction terms (AB, BC and AC) are non-significant (p-value >0.05). The Lack of Fit (F-value of 14.43) is significant. There is only a 1.30% (p-value) chance that a Lack of Fit F-value this large could occur due to noise. A significant lack of fit could adversely affect the BBD model fitting.



Table 15 Reduced model for response  $Y_5$

Source	Sum of Squares	Df	Mean Square	F-value	p-value	
Model	193.53	5	38.71	13.29	0.0002	significant
A-Gas flowrate	6.48	1	6.48	2.23	0.1639	
B-Liquid flowrate	57.78	1	57.78	19.84	0.0010	
C-Droplet diameter	56.71	1	56.71	19.47	0.0010	
A <sup>2</sup>	29.15	1	29.15	10.01	0.0090	
C <sup>2</sup>	47.31	1	47.31	16.25	0.0020	
Residual	32.03	11	2.91			
Lack of Fit	30.90	7	4.41	15.60	0.0093	significant
Pure Error	1.13	4	0.2830			
Cor Total	225.56	16				
Std. Dev.	1.71		R <sup>2</sup>	0.8580		
Mean	34.32		Adjusted R <sup>2</sup>	0.7934		
CV %	4.97		Predicted R <sup>2</sup>	0.5795		
			Adeq. Precision	14.7095		

In Table 14, the summary of the ANOVA for  $Y_5$  when non-significant terms are removed is presented. The model remains significant (F-value of 13.29). However, the large Lack of Fit remains significant. The Fit-statistics are improved, particularly the Predicted R<sup>2</sup> moving from 0.1234 to 0.5795. This implies that close to 60% of the variation in new data predicted by the reduced BBD model for  $Y_5$  can be explained by the model. The Adequacy Precision (14.7095) is higher than the desired value of 4. The model term A-Gas flowrate is reinstated even though it is non-significant (p-value > 0.05) to maintain hierarchy (i.e., A is retained as A<sup>2</sup> is significant). Thus, considering nothing else can be done to improve the fit of the model, the reduced BBD model for response  $Y_5$  could be used to navigate the design space but keeping in mind that the model may not be a very good predictor of the response in some specific areas of the design space.

### 3.3.1.3 ANOVA for response $Y_8$ @ 62 nm

Table 16 Full ANOVA data for  $Y_8$

Source	Sum of Squares	Df	Mean Square	F-value	p-value	
Model	192.75	9	21.42	4.91	0.0238	significant
A-Gas flowrate	38.28	1	38.28	8.78	0.0210	
B-Liquid flowrate	22.45	1	22.45	5.15	0.0576	
C-Droplet diameter	35.70	1	35.70	8.19	0.0243	
AB	11.90	1	11.90	2.73	0.1425	
AC	1.96	1	1.96	0.4494	0.5241	
BC	7.02	1	7.02	1.61	0.2450	
A <sup>2</sup>	69.40	1	69.40	15.91	0.0053	
B <sup>2</sup>	2.27	1	2.27	0.5215	0.4936	
C <sup>2</sup>	0.8909	1	0.8909	0.2043	0.6650	
Residual	30.53	7	4.36			
Lack of Fit	5.52	3	1.84	0.2944	0.8285	not significant
Pure Error	25.01	4	6.25			
Cor Total	223.28	16				
Std. Dev.	2.09		R <sup>2</sup>	0.8633		
Mean	43.95		Adjusted R <sup>2</sup>	0.6875		
CV %	4.75		Predicted R <sup>2</sup>	0.4293		
			Adeq. Precision	8.9278		

Table 16 shows the ANOVA for response  $Y_8$ . With a p-value (0.0238) that is less than 0.05, the model is statistically significant. The Lack of Fit is not significant i.e., there is an 82.85% chance that a Lack of Fit F-value this large could occur due to noise.

Table 17 shows the summary of the ANOVA when non-significant model terms (AB, AC, BC, and B<sup>2</sup>) are omitted.

*Table 17 Reduced model for response Y<sub>8</sub> @ 62 nm*

Source	Sum of Squares	Df	Mean Square	F-value	p-value	
Model	168.54	4	42.14	9.24	0.0012	significant
A-Gas flowrate	38.28	1	38.28	8.39	0.0134	
B-Liquid flowrate	22.45	1	22.45	4.92	0.0466	
C-Droplet diameter	35.70	1	35.70	7.83	0.0161	
A <sup>2</sup>	72.11	1	72.11	15.81	0.0018	72.11
Residual	54.74	12	4.56			
Lack of Fit	29.73	8	3.72	0.5945	0.7539	not significant
Pure Error	25.01	4	6.25			
Cor Total	223.28	16				
Std. Dev.	2.14		R <sup>2</sup>	0.7548		
Mean	43.95		Adjusted R <sup>2</sup>	0.6731		
CV %	4.86		Predicted R <sup>2</sup>	0.5311		
			Adeq. Precision	10.5446		

Here again, the overall model remains significant and the model Fit-statistics (predicted R<sup>2</sup> and Adequacy precision) slightly improved.

The full and reduced ANOVA for responses Y<sub>1</sub>, Y<sub>3</sub>, Y<sub>4</sub>, Y<sub>6</sub> and Y<sub>7</sub> are not detailed in this chapter and are shown in *Annex 3-4a*.

### 3.3.1.4 Summary of the ANOVA for reduced BBD models

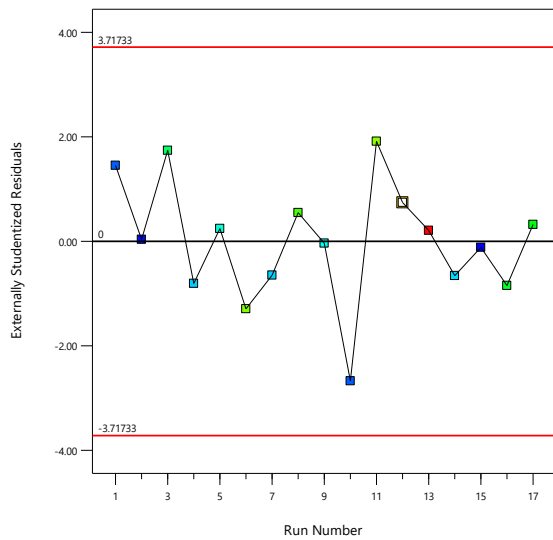
Table 18 presents the summary of the ANOVA at reduced model terms for all the responses. Model term reduction was performed for all the responses thus reducing the terms from nine (9) to the values shown as degrees of freedom. All the BBD models in Table 18 are statistically significant ( $p$ -value  $< 0.05$ ). In cases, the Adequacy Precision is much higher than the desired value of 4, the  $R^2$ , Adjusted  $R^2$  and the predicted  $R^2$  are higher than 0.5 and reasonably close to each other.

Table 18 Summary of ANOVA of reduced BBD models

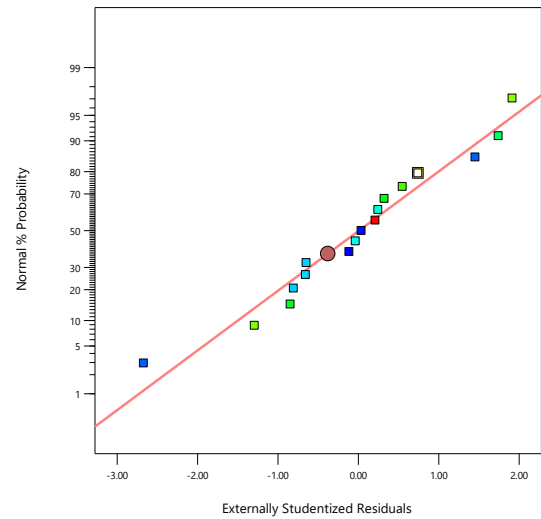
DOE Model	Sum of Squares	Degrees of freedom	Mean Square	F-value	p-value (Model)	Fit statistics			
						Adeq. Precision	$R^2$	Adjusted $R^2$	Predicted $R^2$
Y <sub>1</sub>	785.72	5	157.14	69.98	$< 0.0001$	29.2605	0.9695	0.9557	0.9451
Y <sub>2</sub>	723.57	3	241.19	50.92	$< 0.0001$	23.1369	0.9216	0.9035	0.8562
Y <sub>3</sub>	489.17	3	163.06	32.61	$< 0.0001$	18.5301	0.8827	0.8556	0.7673
Y <sub>4</sub>	280.06	3	93.35	21.94	$< 0.0001$	15.4178	0.8350	0.7970	0.7072
Y <sub>5</sub>	193.53	5	38.71	13.29	0.0002	14.7095	0.8580	0.7934	0.5795
Y <sub>6</sub>	141.98	5	28.40	12.20	0.0003	14.4141	0.8473	0.7778	0.5659
Y <sub>7</sub>	172.12	4	43.03	16.40	$< 0.0001$	13.3885	0.8454	0.7939	0.6372
Y <sub>8</sub>	168.54	4	42.14	9.24	0.0012	10.5446	0.7548	0.6731	0.5311

### 3.3.2 Examination of residuals

Model adequacy checking was performed to determine whether the model would adequately predict the results. Figure 37 (a), Figure 38(a) and Figure 39(a) present the externally studentized residuals vs Run number for responses Y<sub>2</sub>, Y<sub>5</sub> and Y<sub>8</sub> respectively (plots for responses Y<sub>1</sub>, Y<sub>3</sub>, Y<sub>4</sub>, Y<sub>6</sub> and Y<sub>7</sub> are shown in *Annex 3-4b*). These plots verify hidden variables that may have affected the responses while conducting the experiments. The scattered and randomized nature of the plots gives assurances against trends that may negatively impact the analysis. All the data points lay within the limits which shows a good fit of the BBD models. The color codes represent the collection efficiency from minimum in blue to the maximum in red.



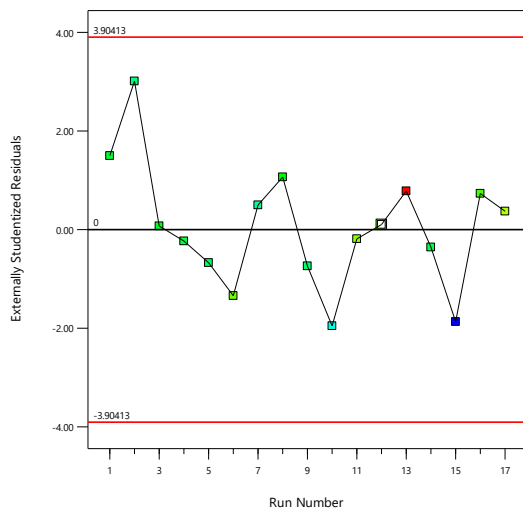
(a)  $Y_2$  @ 20 nm



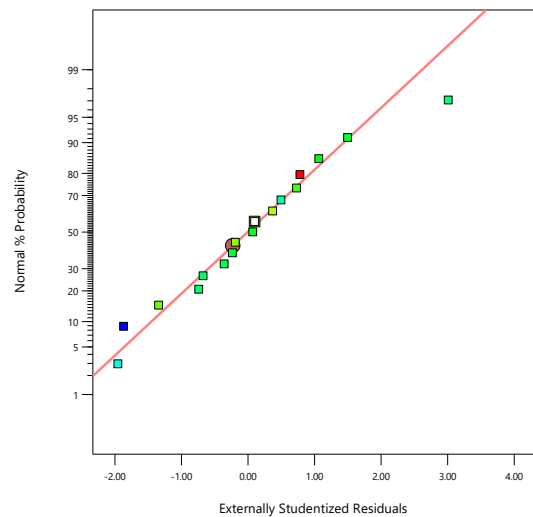
(b)  $Y_2$  @ 20 nm

Figure 37 Diagnostic plots for  $Y_2$

Figure 37(b), Figure 38(b) and Figure 39(b) show that the normal% probability plot of residuals for responses  $Y_1$ ,  $Y_5$  and  $Y_8$  respectively are normally distributed, as they follow a straight line and show no deviation of the variance. Similar behavior is observed in the plots for responses  $Y_2$ ,  $Y_3$ ,  $Y_4$ ,  $Y_6$  and  $Y_7$  (shown in *Annex 3-4b*).



(a)  $Y_5$  @ 35 nm



(b)  $Y_5$  @ 35 nm

Figure 38 Diagnostic plots for  $Y_5$

## Chapter III Optimization of nanoparticle collection by spray scrubber using Box-Behnken Design

Given that the normal% probability plots of the responses do not have a definite pattern such as an “S-shaped”, the default BBD second-order polynomial models for all the responses (Equations (16) to (23) are accepted and no transformation is performed.

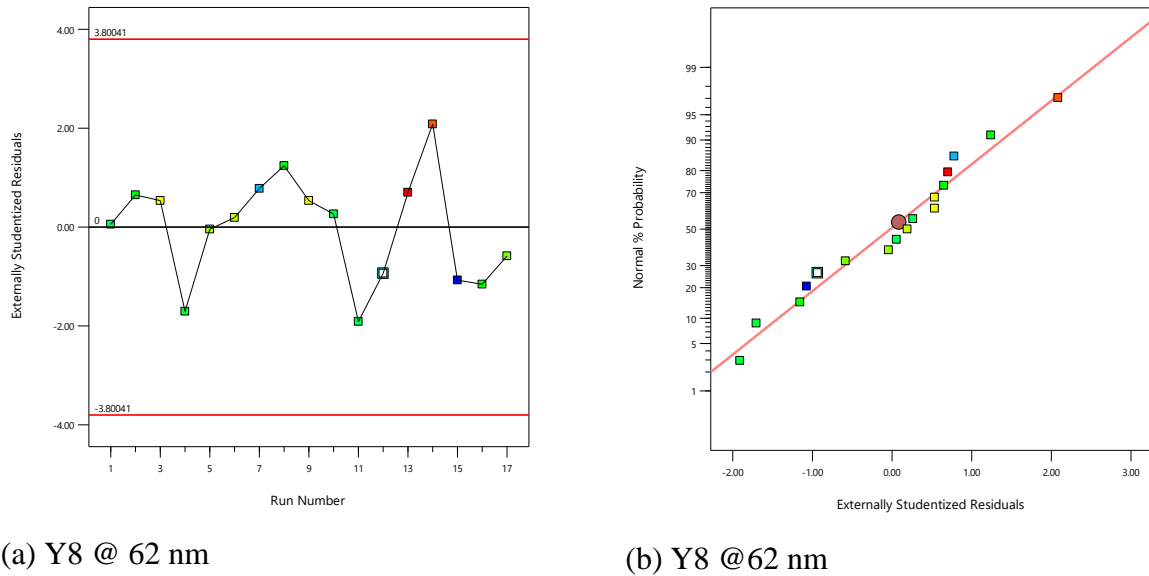


Figure 39 Diagnostic plots for  $Y_8$

### 3.4 Box–Behnken Design experimental results

The BBD models (Equations (16) to (23) consisting of regression equations of linear and second-order polynomials were fitted to the actual experimental data for the determination of predicted responses (i.e., collection efficiency) and are given as follows:

$$Y_1 = 2.95394 - 0.001862A - 0.011875B - 0.066337C + 0.008887B^2 + 0.000435C^2 \quad (16)$$

$$Y_2 = 3.32517 + 0.040313B - 0.081849C + 0.000543C^2 \quad (17)$$

$$Y_3 = 2.72667 + 0.034297B - 0.066065C + 0.000439C^2 \quad (18)$$

$$Y_4 = 2.46608 + 0.026484B - 0.060126C + 0.000409C^2 \quad (19)$$

$$Y_5 = 1.54003 + 0.024549A + 0.016797B - 0.049526C - 0.000263A^2 + 0.000335C^2 \quad (20)$$

$$Y_6 = 0.870773 + 0.026081A + 0.014453B - 0.032166C - 0.000271A^2 + 0.000216C^2 \quad (21)$$

$$Y_7 = -0.500122 + 0.0407A + 0.010469B - 0.001587C - 0.000423A^2 \quad (22)$$

$$Y_8 = -0.360767 + 0.039325A + 0.010469B - 0.002113C - 0.000413A^2 \quad (23)$$

$Y_1$  has model terms not present in other responses in the diffusion-dominant region. This could be due to uncertainty in counting particles as such a low diameter by the SMPS. The

### Chapter III Optimization of nanoparticle collection by spray scrubber using Box-Behnken Design

experimental and predicted values for the eight nanoparticle collection efficiencies ( $Y_1$  to  $Y_8$ ) at the design points and the three independent variables in the uncoded form are shown in Table 19. The predicted values are very close to the experimental data. This attests to the relevance of the proposed BBD models.

Table 19 Box–Behnken design matrix for the three independent factors and corresponding responses

Run	A: Gas flowrate (Nm <sup>3</sup> .h <sup>-1</sup> )	B: Liquid flowrate (L.min <sup>-1</sup> )	C: Droplet diameter (µm)	Y <sub>1</sub> (%)		Y <sub>2</sub> (%)		Y <sub>3</sub> (%)		Y <sub>4</sub> (%)		Y <sub>5</sub> (%)		Y <sub>6</sub> (%)		Y <sub>7</sub> (%)		Y <sub>8</sub> (%)	
				Actual	Predicted														
1	45	1.6	80	36.5 ± 8	35.1	34.4 ± 4	31.7	34.7±5	30.6	34±3	31.6	33.8 ± 3	32.1	33.2 ± 3	32.8	37.3 ± 3	36.5	42.2 ± 4	42.0
2	55	1.6	70	33.4 ± 5	34.3	32.4 ± 4	32.1	31.4±2	30.8	33.4±1	30.4	32.5 ± 4	29.6	33.6 ± 5	31.5	36.9 ± 2	36.4	43.4 ± 5	42.2
3	45	3.2	70	44.3 ± 5	41.1	42.1 ± 2	38.5	37.4±3	36.3	36.2±2	34.6	34.1 ± 4	34.1	33.9 ± 3	34.9	40.2 ± 3	39.7	47.0 ± 2	45.8
4	45	3.2	70	41.5 ± 5	41.1	37.1 ± 5	38.5	36.5±2	36.3	35.9±1	34.6%	33.6 ± 4	34.1	33.9 ± 4	34.9	37.8 ± 5	39.7	42.7 ± 3	45.8
5	45	3.2	70	38.8 ± 4	41.1	39.3 ± 3	38.5	35.1±4	36.3	33±4	34.6	32.9 ± 5	34.1	34.7 ± 4	34.9	39.2 ± 2	39.7	45.8 ± 4	45.8
6	55	3.2	60	49.4 ± 7	49.0	47.6 ± 5	49.8	42.9±4	45.3	40.8±3	41.6	36.6 ± 4	38.3	36.8 ± 4	37.9	40.2 ± 7	39.7	46.4 ± 5	46.0
7	35	3.2	80	41.3 ± 5	41.9	37.2 ± 4	38.1	36.4±6	36.1	35±2	35.8	31.8 ± 5	31.3	33.0 ± 2	30.7	34.1 ± 2	31.3	38.8 ± 4	37.4
8	35	4.8	70	51.7 ± 7	52.4	46.3 ± 5	45.0	41.8±5	41.8	37.1±5	38.8	34.5 ± 5	33.2	33.4 ± 5	32.8	35.2 ± 4	34.5	43.3 ± 3	41.2
9	45	3.2	70	39.8 ± 2	41.1	38.7 ± 4	38.5	37.3±5	36.3	34.9±3	34.6	32.8 ± 1	34.1	36.2 ± 2	34.9	39.2 ± 4	39.7	47.0 ± 3	45.8
10	55	3.2	80	37.0 ± 6	38.2	34.3 ± 4	38.1	30.8±5	36.1	32.9±1	35.8	30.7 ± 2	33.0	32.5 ± 3	34.1	36.1 ± 2	36.5	42.3 ± 5	41.7
11	45	4.8	80	49.8 ± 5	49.5	47.9 ± 3	44.6	43.2±4	41.6	41.5±3	40.1	37.1 ± 4	37.5	36.5 ± 2	37.4	37.7 ± 2	39.8	42.5 ± 4	45.4
12	35	3.2	60	52.8 ± 3	52.8	51.4 ± 4	49.8	47.5±2	45.3	41.2±1	41.6	36.6 ± 3	36.5	33.5 ± 6	34.6	32.7 ± 2	34.4	40.1 ± 3	41.6
13	45	4.8	60	60.4 ± 2	60.4	56.8 ± 4	56.3	52.1±3	50.8	46.6±1	45.8	43.7 ± 2	42.7	42.6 ± 3	41.3	45.1 ± 3	43.0	50.9 ± 3	49.6
14	45	3.2	70	42.4 ± 8	41.1	37.4 ± 7	38.5	36.7±6	36.3	32.9±4	34.6	33.4 ± 3	34.1	34.2 ± 2	34.9	40.2 ± 3	39.7	49.6 ± 2	45.8
15	35	1.6	70	38.0 ± 6	38.0	32.1 ± 3	32.1	29.9±4	30.8	27.2±4	30.4	25.6 ± 2	27.9	26.5 ± 5	28.2	29.2 ± 5	31.2	36.1 ± 3	37.9
16	55	4.8	70	49.1 ± 4	48.7	43.6 ± 3	45.0	41.9±2	41.8	41±2	38.8	35.9 ± 3	35.0	36.8 ± 4	36.2	38.7 ± 2	39.8	43.7 ± 3	45.5
17	45	1.6	60	45.5 ± 4	46.0	44.1 ± 6	43.4	39.1±6	39.8	37.7±1	37	37.8 ± 2	37.3	37.5 ± 5	36.6	39.9 ± 5	39.6	45.3 ± 3	46.3

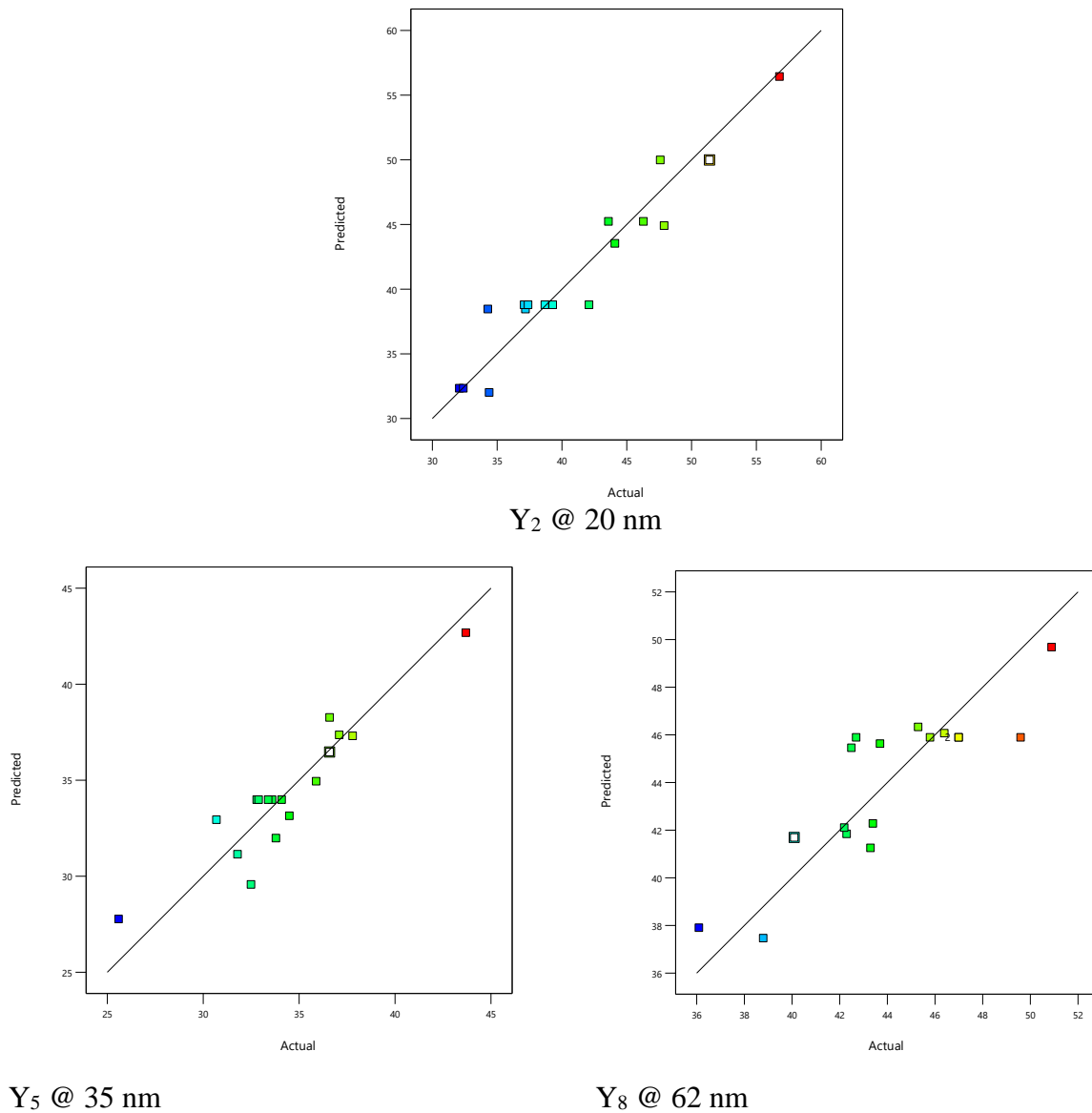


*Figure 40 Experimental (actual) particle removal efficiency versus predicted particle removal efficiency for Y<sub>2</sub>, Y<sub>5</sub> and Y<sub>8</sub>*

In Figure 40, parity diagrams are proposed to compare the BBD model response predictions with the actual experimental values. For the responses shown (see *Annex 3-4c* for other plots), the predicted nearly mirrors all the experimental data, again, validating the BBD models to make accurate predictions in the design space.

### 3.5 Interactions of independent parameters

This section presents 2D contours and 3D response surface plots as a function of two factors (keeping the third-factor constant). These plots are employed to understand both the main and interaction effects of the impact of factors A, B and C on the responses Y<sub>1</sub>, Y<sub>2</sub>, Y<sub>3</sub>, Y<sub>4</sub>, Y<sub>5</sub>, Y<sub>6</sub>,

$Y_7$  and  $Y_8$ . The factors A, B and C are studied at their extreme values (Level -1 and Level +1). Similar to ANOVA for the responses, a grouping of the responses is made. Response  $Y_2$  is selected to represent the diffusion-dominant region,  $Y_5$  for the intermediate region and  $Y_8$  for the impaction-interception mechanism region. To quantify the influence of a factor or the interaction between factors on the various responses, the following coded equations ((24)(31) have been generated using the Design Expert V13 software.

$$Y_1 = 41.10 - 1.86A + 7.2B - 5.44C + 2.28B^2 + 4.35C^2 \quad (24)$$

$$Y_2 = 38.78 + 6.45B - 5.76C + 5.43C^2 \quad (25)$$

$$Y_3 = 36.44 + 5.49B - 4.56C + 4.39C^2 \quad (26)$$

$$Y_4 = 34.62 + 4.24B - 2.86C + 4.09C^2 \quad (27)$$

$$Y_5 = 33.98 + 0.90A + 2.697B - 2.66C - 2.63A^2 + 3.35C^2 \quad (28)$$

$$Y_6 = 34.89 + 1.66A + 2.31B - 1.90C - 2.71A^2 + 2.16C^2 \quad (29)$$

$$Y_7 = 39.62 + 2.59A + 1.68B - 1.59C - 4.23A^2 \quad (30)$$

$$Y_8 = 45.89 + 2.19A + 1.68B - 2.11C - 4.13A^2 \quad (31)$$

Design-Expert software provides prediction equations in terms of actual units (Eqns (16 to (23) and coded units (24)(31). The coded equations ((24)(31) are useful in identifying the relative impact of the factors by comparing the factor coefficients. And would be used alongside the surface plots in the following sections. By default, the Design-Expert® software carries out regression calculations using the coded units. In this units, the low and high settings for each factor are set to -1 and +1, respectively. To obtain the actual equations, each term in the coded equations is substituted with its corresponding coding formula as shown below [195]:

$$\text{Coded equation} = \frac{(\text{Actual unit} - \text{Average Actual unit})}{(\text{Range between low and high Actual units}) / 2} \quad (32)$$

### 3.5.1 Responses $Y_2$ @ 20 nm

Figure 41(a1-b2) shows the interactive plots of the effect of the gas flowrate (**factor A**) and liquid flowrate (**factor B**) at constant droplet diameter (**factor C**) on the collection of nanoparticles at a diameter of 20 nm ( $Y_2$ ). **Factor A has no influence on  $Y_2$** . Indeed, from the coded equation (25) for  $Y_2$ , there is no contribution due to Factor A. Similarly, for responses  $Y_3$

and  $Y_4$ , there is no influence of factor A (*Annex 3-1a*). For response  $Y_1$ , a small and negative influence of factor is observed (*Annex 3-1a*).

Liquid flowrate (factor B) has a strong and positive influence on  $Y_2$ . As the liquid flowrate (factor B) increases from 1.6 to 4.8 L.min<sup>-1</sup>,  $Y_2$  increase from about 44% to 56.8% (at factor C: 60  $\mu\text{m}$  as shown in Figure 41a) or  $Y_2$  increased from 31.1% to about 44% (at factor C: 80  $\mu\text{m}$  shown in Figure 41b) due principally diffusion mechanism. An increase in the liquid flowrate (factor B) improves the droplet packing density which leads to a higher probability of particle capture. From Equation 25, factor B has the highest impact on  $Y_2$ . This is also the case for the other responses  $Y_1$ ,  $Y_3$  and  $Y_4$  (24(26(27)).

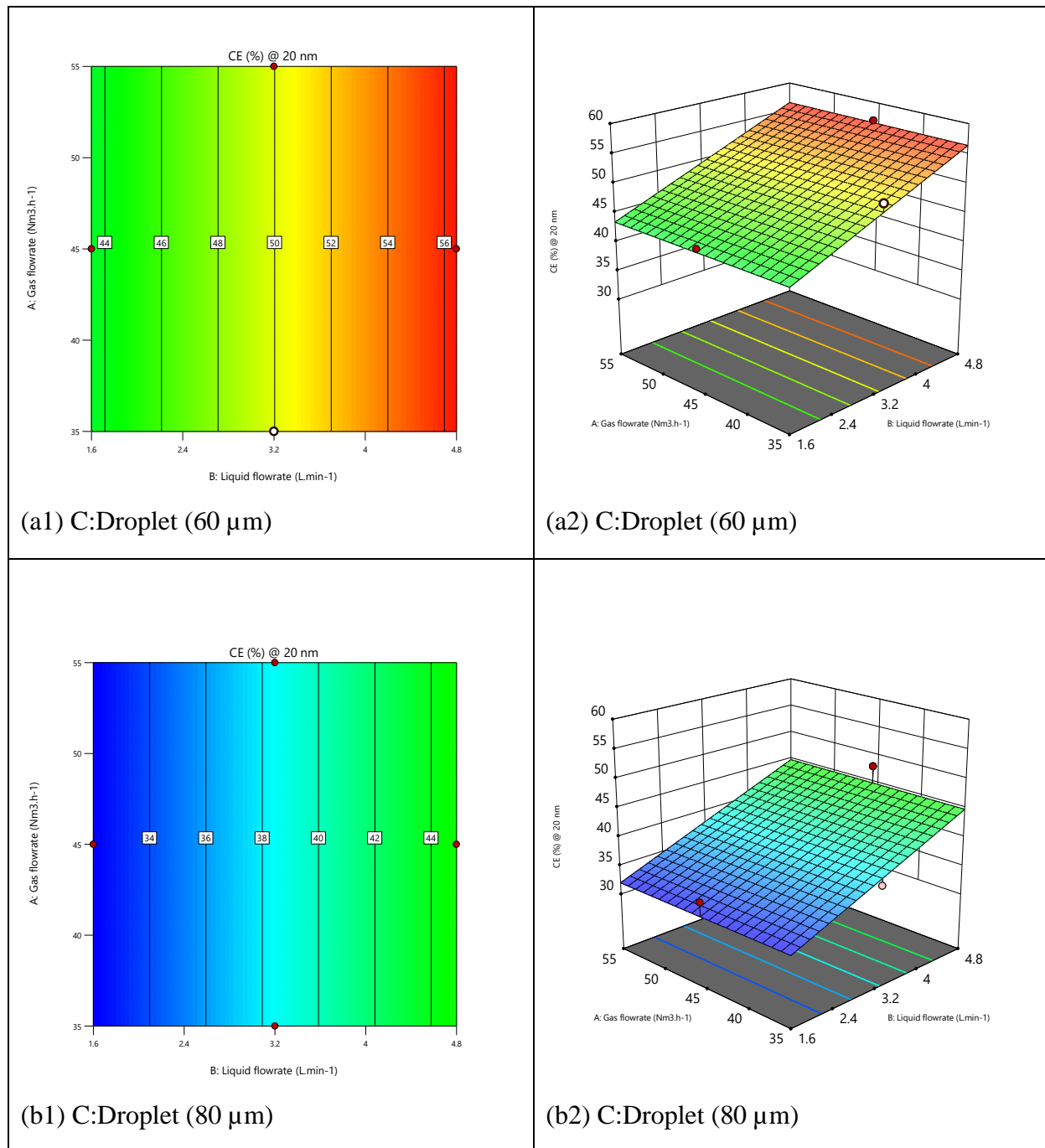
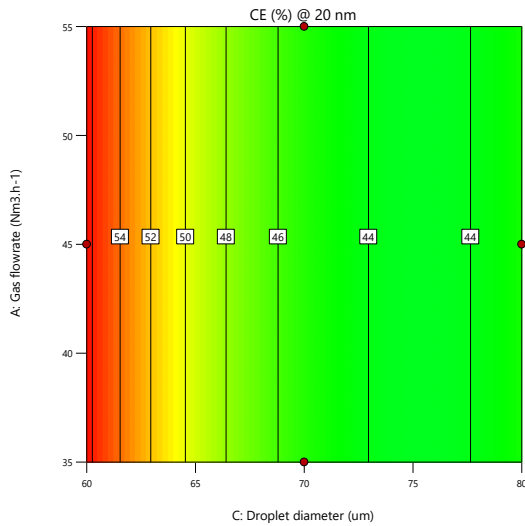


Figure 41 Counter and response surface plots showing the influence of factors A and B on  $Y_2$  at constant C (a: 60 and b: 80  $\mu\text{m}$ )

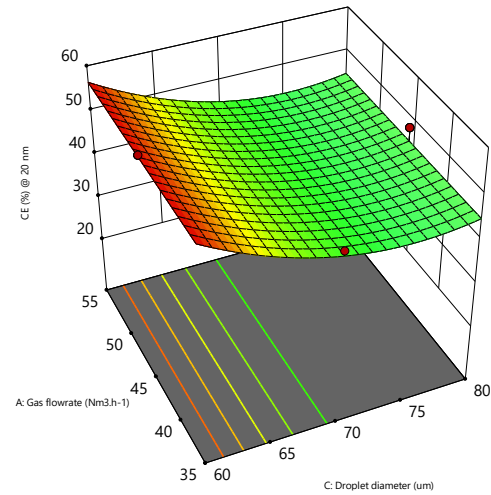
Figure 42(a1-b2) shows the surface plots for combined influence gas flowrate (factor A) and of the droplet diameter (Factor C) at constant liquid flowrate (factor B) on  $Y_2$ . As earlier stated, factor A has no impact on  $Y_2$ . As the droplet diameter (Factor C) decreases from 80 to about 70  $\mu\text{m}$  little effect is observed on  $Y_2$ . As the droplet diameter (Factor C) further decreases to 60  $\mu\text{m}$ ,  $Y_2$  improves from 44% to 56.8% (Figure 42(a1-a2)) or from 32% to 44%

### Chapter III Optimization of nanoparticle collection by spray scrubber using Box-Behnken Design

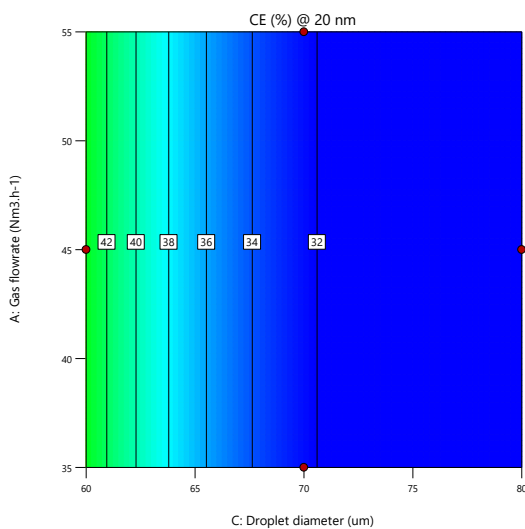
(Figure 42(b1-b2)). As the droplet diameter decreases, the droplet surface areas improve leading to higher collection efficiency. The Peclet number also increases with decreasing droplet diameter (Factor C), which leads to higher particle removal due to the diffusion mechanism. This same behavior is reported for  $Y_1$ ,  $Y_3$  and  $Y_4$  (*Annex 3-1b*). The coded equations factor C has a strong and negative influence on  $Y_2$ .



(a1) B: Liquid flowrate (4.8 L.min<sup>-1</sup>)

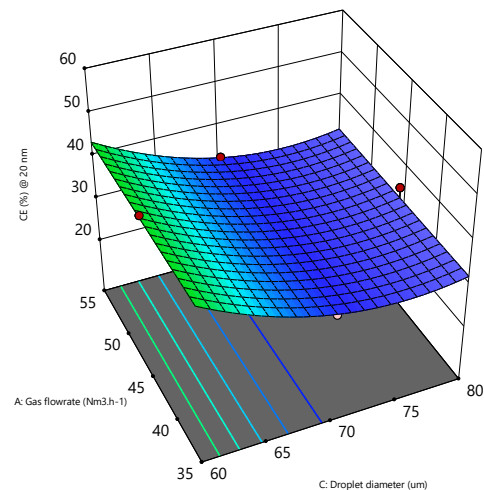


(a2) B: Liquid flowrate (4.8 L.min<sup>-1</sup>)



(b1)

B: Liquid flowrate (1.6 L.min<sup>-1</sup>)



(b2) B: Liquid flowrate (1.6 L.min<sup>-1</sup>)

Figure 42 Counter and response surface plots showing the influence of factors A and C on  $Y_2$  at constant B (a:4.8 and b:1.6 L.min<sup>-1</sup>)

Figure 43(a1-b2) shows the surface plots of the combined influence of the liquid flowrate (factor B) and the droplet diameter (factor C) on  $Y_2$  at constant gas flowrate (factor A). Irrespective of factor A (35 or 55 Nm<sup>3</sup>.h<sup>-1</sup>) the behavior of the plots remains the same (recall

### Chapter III Optimization of nanoparticle collection by spray scrubber using Box-Behnken Design

gas flow has no influence on  $Y_2$ ), minimum  $Y_2$  value (32.1%) occurs at the region of factor B: 1.6 - 1.8 L.min<sup>-1</sup> and droplet diameter (Factor C): 71 – 80 μm. However, the shape of the curve indicates that the minimum value of  $Y_2$  is closer to 70 μm. Likewise, the combined effect of factors B and C at 4.8 L.min<sup>-1</sup> and 60 μm gives the maximum value  $Y_2$  (56.8%). Factor B has the tendency on  $Y_1$ ,  $Y_3$  and  $Y_4$  (*Annex 3-1c*)

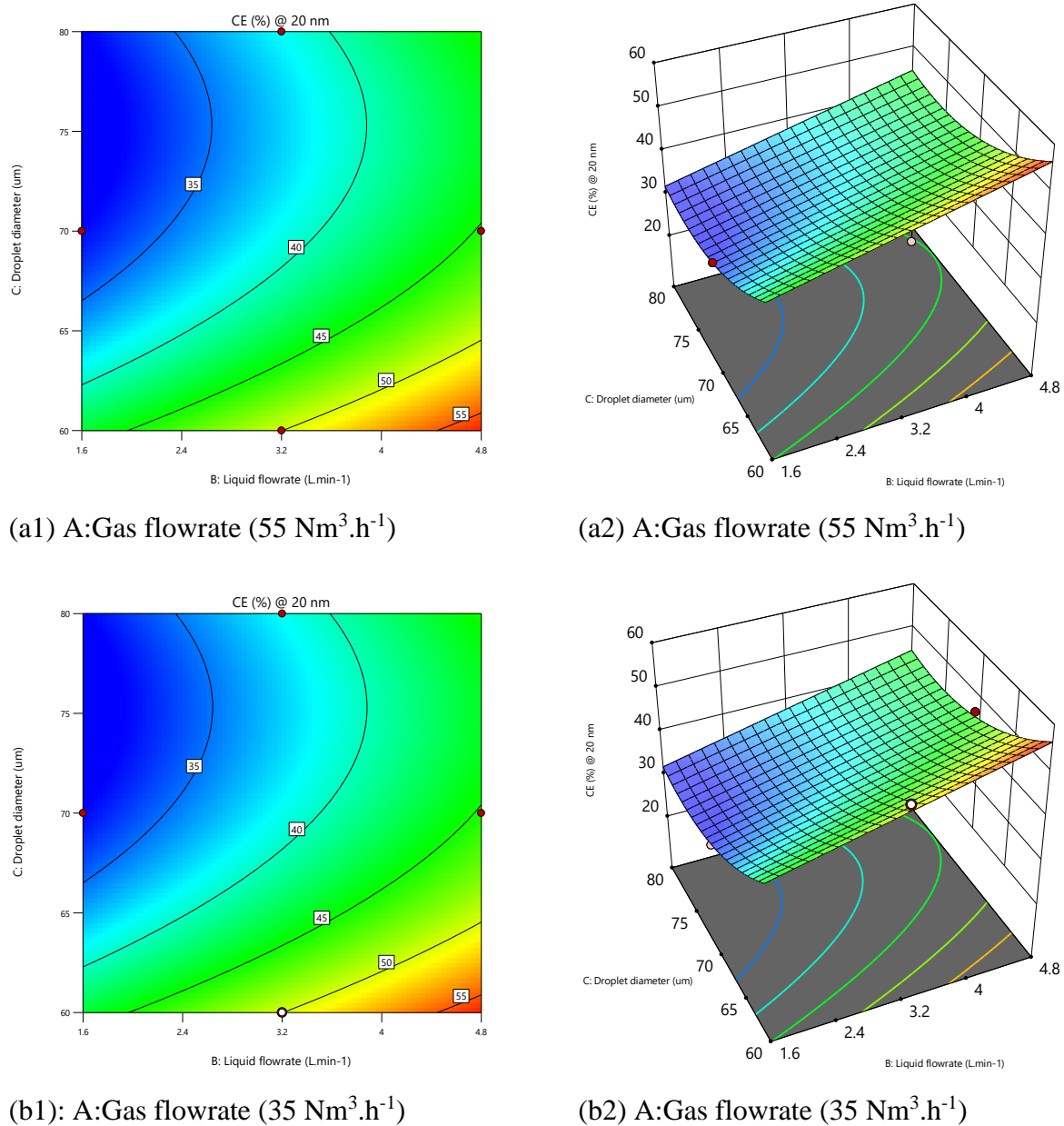
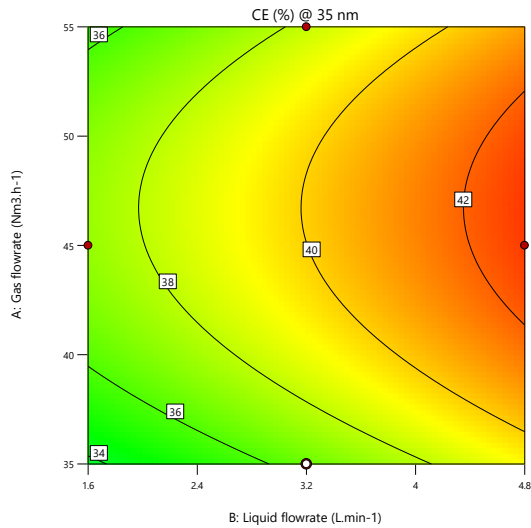


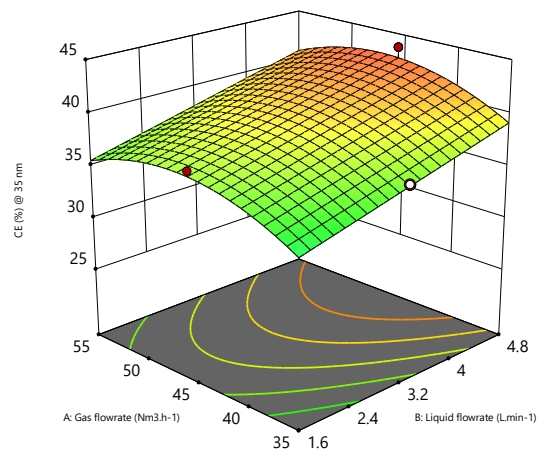
Figure 43 Counter and response surface plots showing the influence of factors B and C on  $Y_2$  at constant A (a: 55 and b: 35 Nm<sup>3</sup>.h<sup>-1</sup>)

### 3.5.2 Responses $Y_5$ @ 35 nm

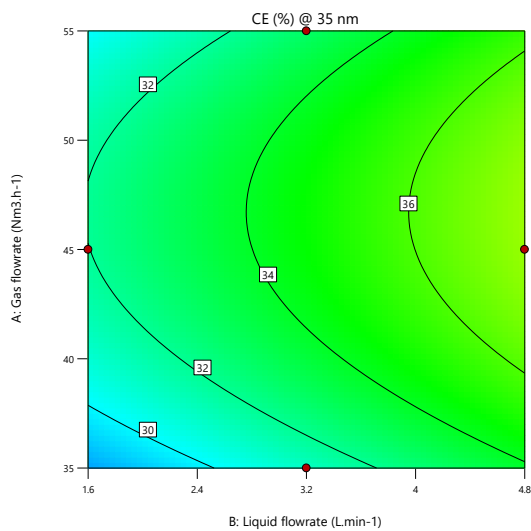
Figure 44 (a1-b2) shows the combined influence of gas (factor A) and liquid (factor B) flowrates on response  $Y_5$  (collection at particle size 35 nm) at constant droplet diameter (60 and 80  $\mu\text{m}$ ). As the liquid flowrate increase from 1.6 to 4.8  $\text{L}\cdot\text{min}^{-1}$ , response  $Y_5$  also increases given that the droplet number increases and hence the probability of particle collection by the various capture mechanisms improves. For gas flowrate (factor A), a lower gas flowrate ( $35 \text{ Nm}^3\cdot\text{h}^{-1}$ ) is not observed to favor  $Y_5$  due to the diffusion mechanism as reported for previous responses ( $Y_1$  to  $Y_4$ ).  $Y_5$  falls within the intermediate-region, as such none of the three primary particle collection mechanisms dominantly act on  $Y_5$ . As the gas flowrate (factor A) increases from  $35 \text{ Nm}^3\cdot\text{h}^{-1}$  to about  $48 \text{ Nm}^3\cdot\text{h}^{-1}$ ,  $Y_5$  improves due to the particle collection by the impaction mechanism. A small decrease in  $Y_5$  is observed as the gas flowrate approaches  $55 \text{ Nm}^3\cdot\text{h}^{-1}$ . A high gas flowrate could result in entrained droplets (particularly at the highest liquid flowrate) and hence limit particle capture. The maximum  $Y_5$  value (43.7%) occurs at the zone around the gas flowrate of  $48 \text{ Nm}^3\cdot\text{h}^{-1}$  and liquid flowrate of  $4.8 \text{ L}\cdot\text{min}^{-1}$ . A look at the coded equation for  $Y_5$  shows that the linear term of factor A is positively correlated to  $Y_5$  while the quadratic with a much higher coefficient is negatively correlated to  $Y_5$ . This same tendency is observed for  $Y_6$  (*Annex 3-2a*). Although factor plays a higher positive influence in the case of  $Y_6$ . Lastly, the maximum  $Y_6$  value occurs at the zone where factor A is  $\sim 48 \text{ Nm}^3\cdot\text{h}^{-1}$  and factor B  $4.8 \text{ L}\cdot\text{min}^{-1}$ .



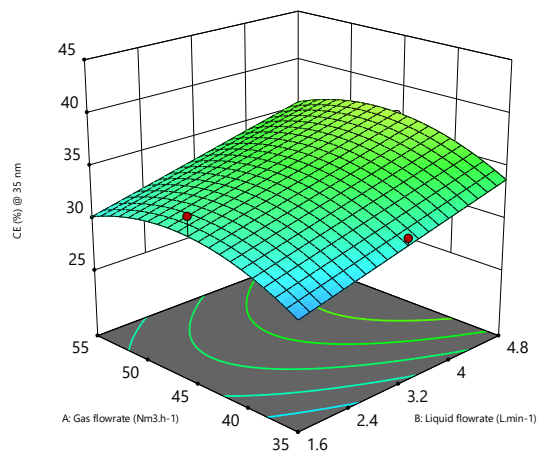
(a1) C: Droplet (60  $\mu\text{m}$ )



(a2) C: Droplet (60  $\mu\text{m}$ )



(b1) C: Droplet (80  $\mu\text{m}$ )



(b2) C: Droplet (80  $\mu\text{m}$ )

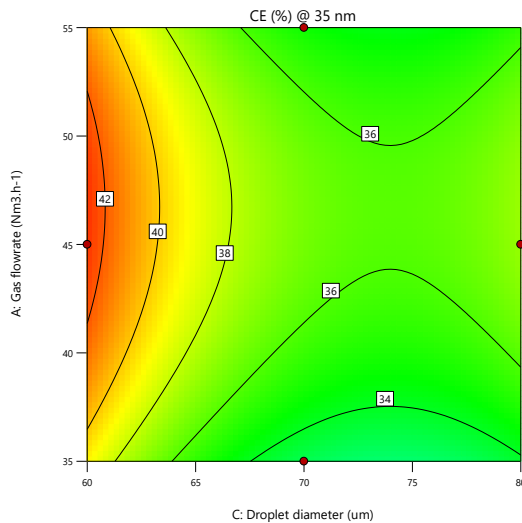
Figure 44 Counter and response surface plots showing the influence of factors A and B on  $Y_5$  at constant C (a: 60 and b: 80  $\mu\text{m}$ )

Figure 45 (a1-b2) presents the combined influence of gas flowrate (factor A) and droplet diameter (factor C) on  $Y_5$  at constant liquid flowrate (factor B). Figure 44 (a2, a1) presents a hyperbolic paraboloid curve (riding-saddle surface), indicating that both factors (A and C) have a significant opposite influence on  $Y_5$ . It can be observed a saddle point at  $A=46$  and  $C=74 \mu\text{m}$  whatever B is, indicating a local extremum (relative minimum along the C axis and relative maximum along the A axis) of  $Y_5$ . Although  $Y_5$  lies in the intermediate region, no dominant particle collection mechanism acts on  $Y_5$ , it is however close enough to the

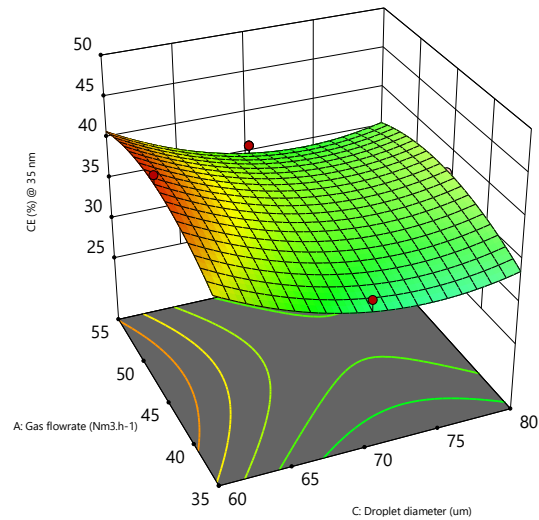
### Chapter III Optimization of nanoparticle collection by spray scrubber using Box-Behnken Design

diffusion-dominant region to be affected by the forces of Brownian diffusion. As droplet diameter (factor C) decreases from 80  $\mu\text{m}$  to 60  $\mu\text{m}$ ,  $Y_5$  also decreases, this is particularly the case where gas flowrate (factor A) is 35 and 55  $\text{Nm}^3.\text{h}^{-1}$ . At factor A of 46  $\text{Nm}^3.\text{h}^{-1}$ , this tendency is less pronounced. For low droplet diameter (factor C) values, close to 60  $\mu\text{m}$ ,  $Y_5$  values are higher due to lower Peclet number which in turn favors particle removal due to Brownian diffusion. Smaller droplets also increase  $Y_5$  by having a higher surface area to volume ratio leading to improved particle capture.

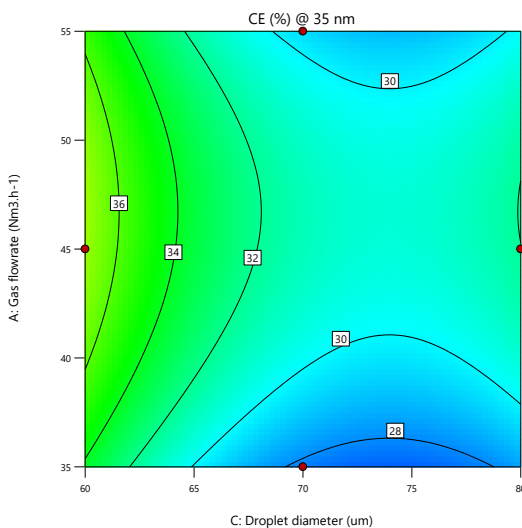
The maximum  $Y_5$  occurs in the region where factor A is 46  $\text{Nm}^3.\text{h}^{-1}$  and droplet diameter (factor C) is 60  $\mu\text{m}$ . A similar tendency is observed for  $Y_6$  (*Annex 3-2b*). However, for  $Y_6$  the minimum value (26.5%) occurred at the lowest value of factor B and factor C  $\sim 75 \mu\text{m}$ .



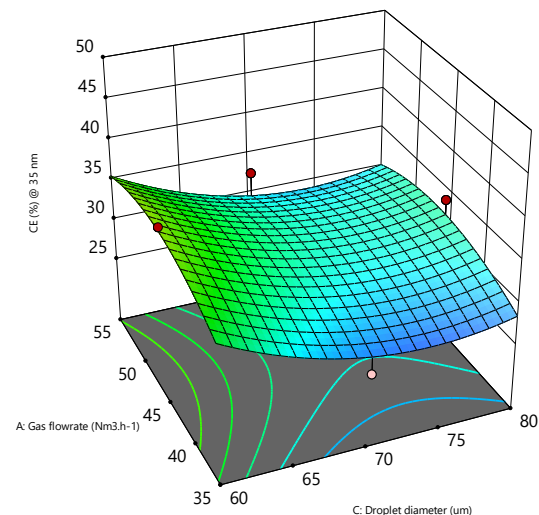
(a1) B: Liquid flowrate ( $4.8 \text{ L}.\text{min}^{-1}$ )



(a2) B: Liquid flowrate ( $4.8 \text{ L}.\text{min}^{-1}$ )



(b1) B: Liquid flowrate ( $1.6 \text{ L}.\text{min}^{-1}$ )

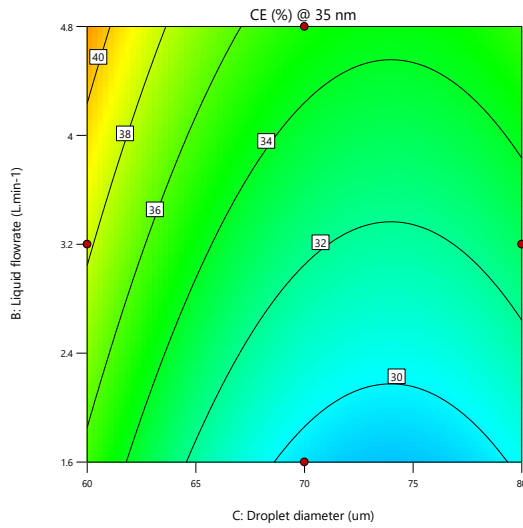


(b2) B: Liquid flowrate ( $1.6 \text{ L}.\text{min}^{-1}$ )

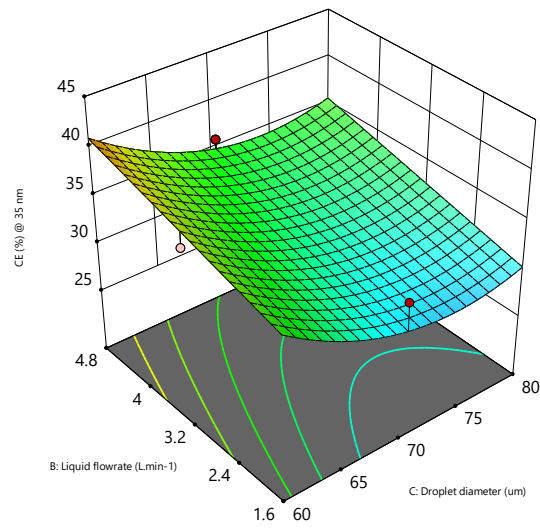
*Figure 45 Counter and response surface plots showing the influence of factors A and C on  $Y_5$  at constant B (a:4.8 and b:1.6 L.min<sup>-1</sup>)*

Figure 46(a1-b2) shows the interactive plots of the influence of liquid flowrate (factor B) and droplet diameter (factor C) on  $Y_5$  at constant gas flowrate (factor A). Both factors B and C have a significant influence on  $Y_5$  as seen in the slopes of the plots.

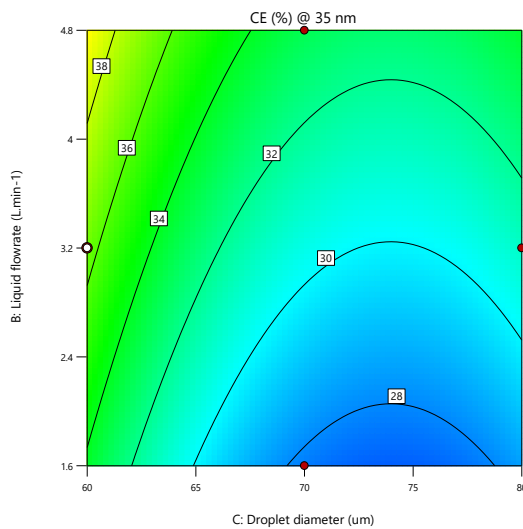
Liquid flowrate (factor B) is positively correlated to  $Y_5$ , in contrast to droplet diameter (factor C) which displayed a parabolic curve with a minimum value of  $Y_5$  close to the mid-point of factor C. As factor C decrease from 80  $\mu\text{m}$  to about 75  $\mu\text{m}$ ,  $Y_5$  values decrease.  $Y_5$  improves when factor C further decreases from 75  $\mu\text{m}$  to 60  $\mu\text{m}$ . Regardless of the value of factor C, the value of  $Y_5$  improves when factor B increases due to an improvement in the number of collectors.  $Y_5$  maximum value occurs in the zone where factor B and C are highest and smallest respectively.  $Y_5$  minimum value (25.6%) is the region where factor B is 1.6 L.min<sup>-1</sup> and factor C is about 75  $\mu\text{m}$ . This same tendency is observed for  $Y_6$  (**Annex 3-2c**). Both responses  $Y_5$  and  $Y_6$  have roughly similar coefficients of linear and quadratic terms.



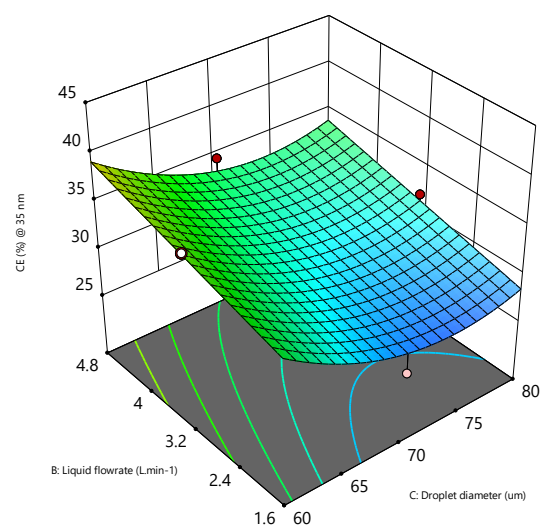
(a1) A: Gas flowrate ( $55 \text{ Nm}^3 \cdot \text{h}^{-1}$ )



(a2) A: Gas flowrate ( $55 \text{ Nm}^3 \cdot \text{h}^{-1}$ )



(b1) A: Gas flowrate ( $35 \text{ Nm}^3 \cdot \text{h}^{-1}$ )



(b2) A: Gas flowrate ( $35 \text{ Nm}^3 \cdot \text{h}^{-1}$ )

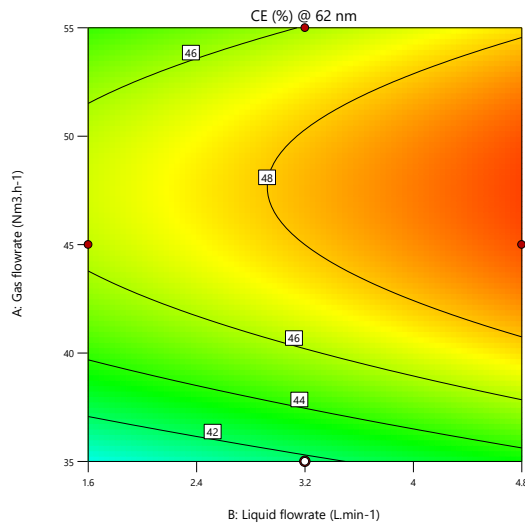
Figure 46 Counter and response surface plots showing the influence of factors B and C on  $Y_8$  at constant A (a:  $55 \text{ Nm}^3 \cdot \text{h}^{-1}$  and b:  $35 \text{ Nm}^3 \cdot \text{h}^{-1}$ )

### 3.5.3 Responses $Y_8$ @ 62 nm

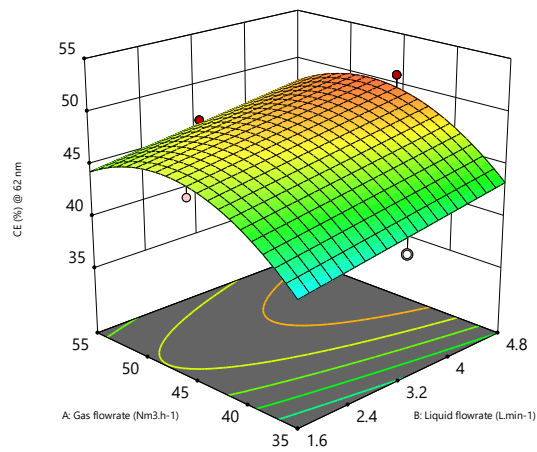
Figure 47(a1-b2) shows the combined influence of gas (factor A) and liquid (factor B) flowrates on response  $Y_8$  (collection at particle size 62 nm) at constant droplet diameter. The liquid flowrate has a positive correlation with  $Y_8$ . As liquid flowrate (factor B) increase from  $1.6$  to  $4.8 \text{ L} \cdot \text{min}^{-1}$ , response  $Y_8$  improves because the particle collection mainly due to the

### Chapter III Optimization of nanoparticle collection by spray scrubber using Box-Behnken Design

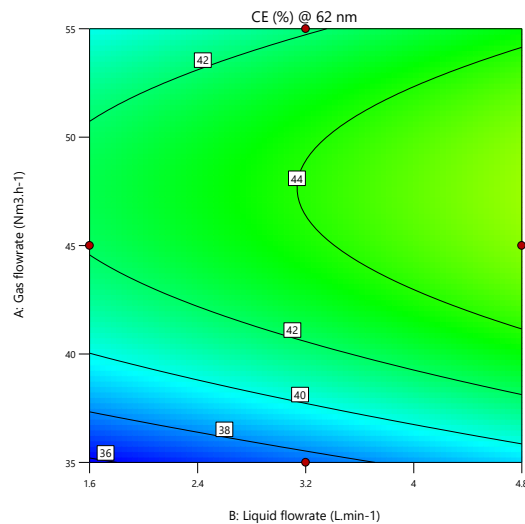
impaction mechanism increases when the droplet packing density increase. Gas flowrate (factor A) has a much higher influence on response  $Y_8$  than liquid flowrate (factor B).



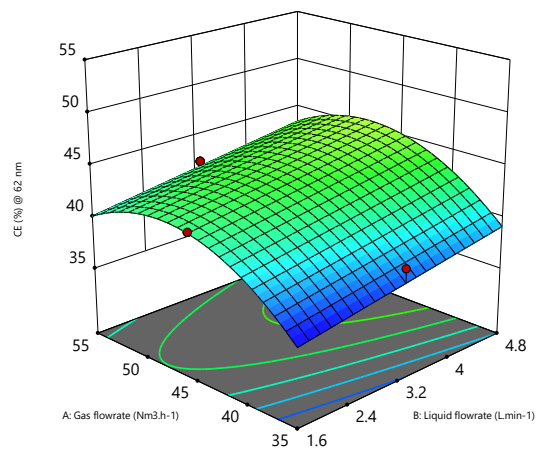
(a1) C: Droplet ( $60 \mu\text{m}$ )



(a2) C: Droplet ( $60 \mu\text{m}$ )



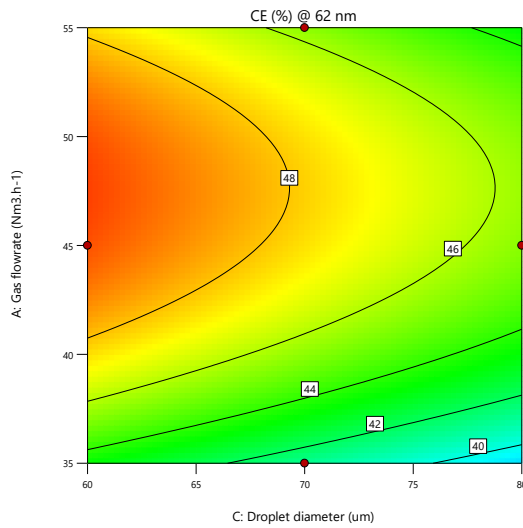
(b1) C: Droplet ( $80 \mu\text{m}$ )



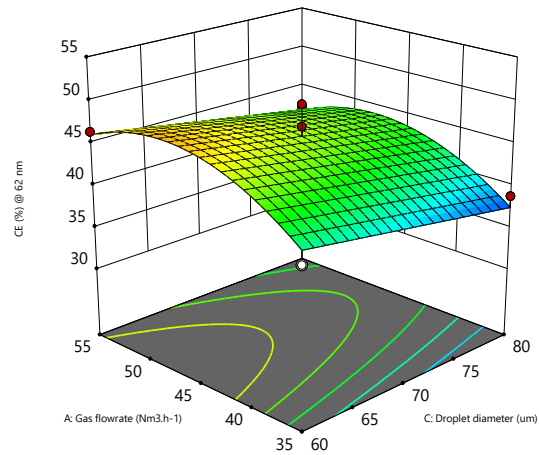
(b2) C: Droplet ( $80 \mu\text{m}$ )

Figure 47 Counter and response surface plots showing the influence of factors A and B on  $Y_8$  at constant C (a:  $60$  and b:  $80 \mu\text{m}$ )

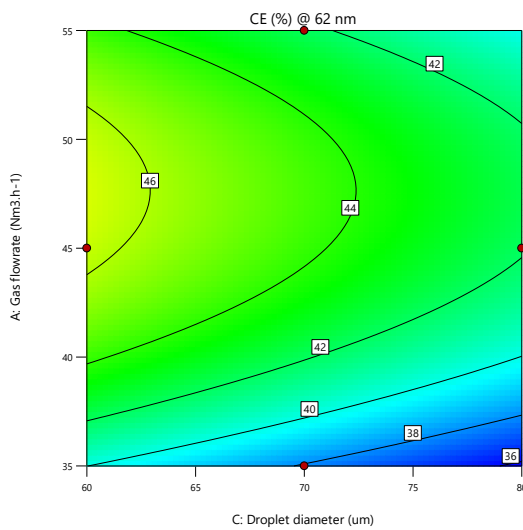
The maximum  $Y_8$  value (50.9%) occurs at the zone around the gas flowrate of  $48 \text{ Nm}^3.\text{h}^{-1}$  and liquid flowrate of  $4.8 \text{ L.min}^{-1}$ . This same tendency was observed for  $Y_7$  although the maximum  $Y_7$  value is lower (45.1%) than for  $Y_8$  (Annex 3-3a). Factor A has a much higher influence on both  $Y_7$  and  $Y_8$  than factor as shown in the coefficients of the coded equations.



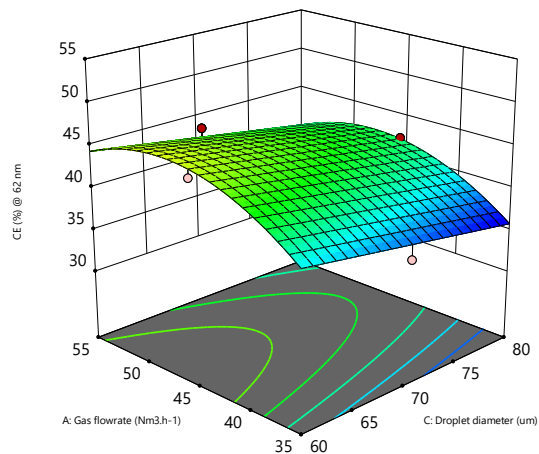
(a1) B: Liquid flowrate (4.8 L.min<sup>-1</sup>)



(a2) B: Liquid flowrate (4.8 L.min<sup>-1</sup>)



(b1) B: Liquid flowrate (1.6 L.min<sup>-1</sup>)



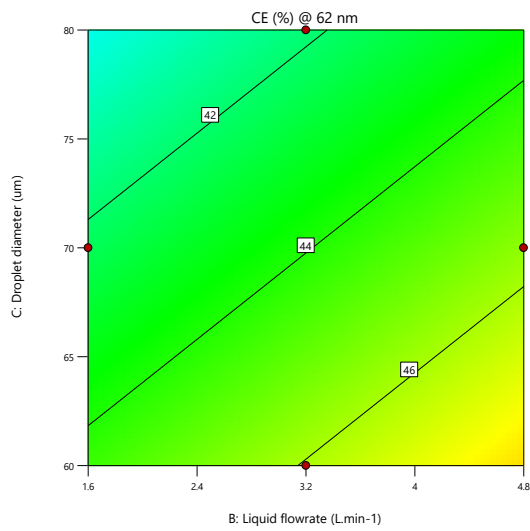
(b2) B: Liquid flowrate (1.6 L.min<sup>-1</sup>)

Figure 48 Counter and response surface plots showing the influence of factors A and C on  $Y_8$  at constant B (a:4.8 and b:1.6 L.min<sup>-1</sup>)

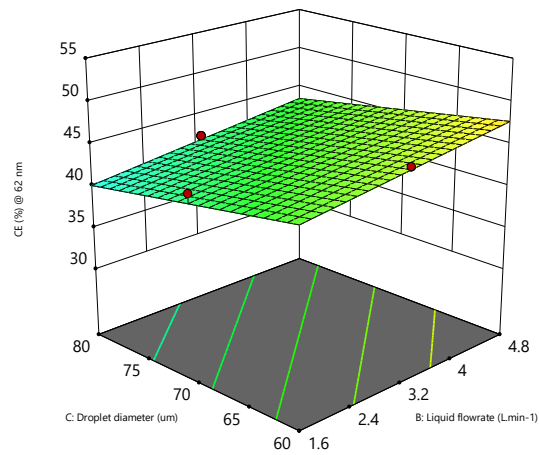
Figure 48(a1-b2) presents the interactive influence of gas flowrate (factor A) and droplet diameter (factor C) at constant liquid flowrate on the collection efficiency response  $Y_8$ . Factor A has a higher effect on  $Y_8$  as shown by the slopes of the 3D plots. A decreasing droplet diameter significantly increases  $Y_8$  as a decrease in the droplet diameter increases the Stokes number leading to particle collection due to the impaction mechanism. The combined interaction of gas flowrate (48 Nm<sup>3</sup>.h<sup>-1</sup>) and droplet diameter (60  $\mu$ m) gave a maximum  $Y_8$  value of 50.9%. Factors A and C have a similar influence on  $Y_7$  (*Annex 3-3b*) and are

Chapter III Optimization of nanoparticle collection by spray scrubber using Box-Behnken Design

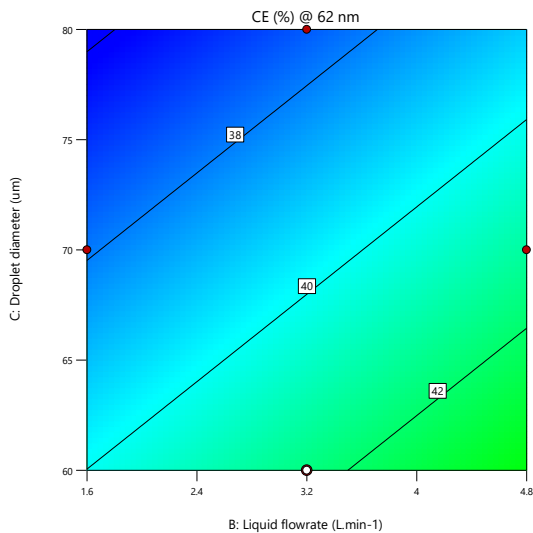
confirmed by the coded equations. For  $Y_7$ , the combined interaction of gas flowrate (48  $\text{Nm}^3.\text{h}^{-1}$ ) and droplet diameter (60  $\mu\text{m}$ ) gave a maximum  $Y_7$  value of 45.1%.



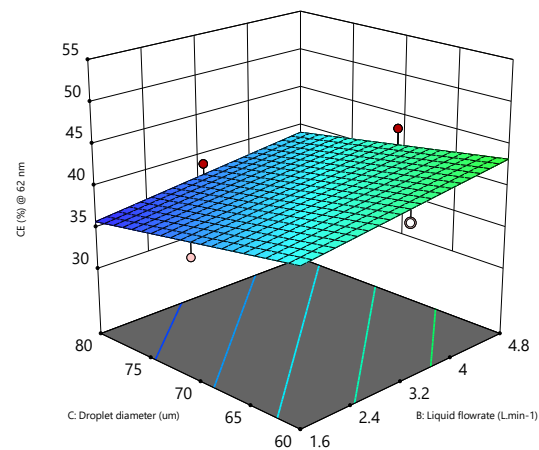
(a1) A: Gas flowrate ( $55 \text{ Nm}^3.\text{h}^{-1}$ )



(a2) A: Gas flowrate ( $55 \text{ Nm}^3.\text{h}^{-1}$ )



(b1) A: Gas flowrate ( $35 \text{ Nm}^3.\text{h}^{-1}$ )



(b2) A: Gas flowrate ( $35 \text{ Nm}^3.\text{h}^{-1}$ )

Figure 49 Counter and response surface plots showing the influence of factors B and C on  $Y_8$  at constant A (a:  $55$  and b:  $35 \text{ Nm}^3.\text{h}^{-1}$ )

Figure 49(a1-b2) presents the interactive effect of liquid flowrate (factor B) and droplet diameter (factor C) at constant gas flowrate on response  $Y_8$ . Both factors have nearly the same order of magnitude of impact on  $Y_8$ . Factor B is positively correlated to  $Y_8$  i.e., an increase in factor B leads to an increase in  $Y_8$ . Factor C is negatively correlated to  $Y_8$  i.e., a decreasing droplet diameter (60 to 80  $\mu\text{m}$ ). The minimum  $Y_8$  value (36.1%) occurs in the zone where factor B is the lowest ( $1.6 \text{ L.min}^{-1}$ ) and factor C is 80  $\mu\text{m}$ . The interactive effect of liquid

## Chapter III Optimization of nanoparticle collection by spray scrubber using Box-Behnken Design

flowrate (factor B) and droplet diameter (factor C) at constant gas flowrate on response  $Y_8$  is that of  $Y_7$  (*Annex 3-3c*). The minimum  $Y_7$  value (29.2%) occurs in the zone where factor B is the lowest ( $1.6 \text{ L}\cdot\text{min}^{-1}$ ) and factor C is  $80 \mu\text{m}$ .

### 3.6 Box–Behnken design model optimization

#### 3.6.1 Individual response surfaces and desirability approach

Figure 50 (a1) presents the predicted collection efficiencies at particle size 20 nm ( $Y_2$ ) at the actual factor coding. Maximum  $Y_2$  value (56.8%) occurs at A:  $35 \text{ Nm}^3\cdot\text{h}^{-1}$ , B:  $4.8 \text{ L}\cdot\text{min}^{-1}$  and C:  $60 \mu\text{m}$ .

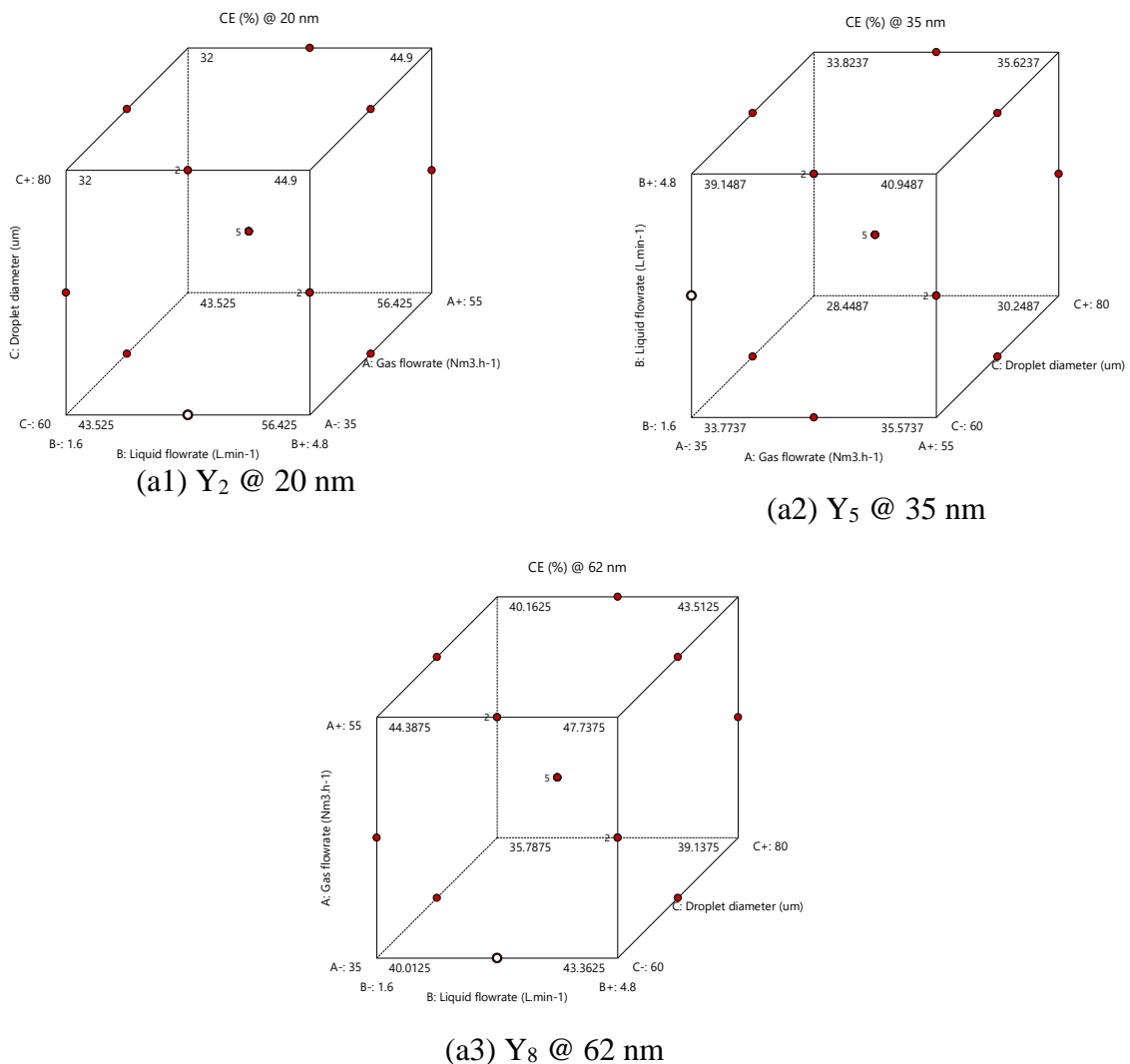


Figure 50 Individual response surfaces showing predicted collection efficiencies

For responses  $Y_5$  and  $Y_8$ , their maximum values (40.95% and 47.74%) occur at A:  $55 \text{ Nm}^3\cdot\text{h}^{-1}$ , B:  $4.8 \text{ L}\cdot\text{min}^{-1}$  and C:  $60 \mu\text{m}$ , which is different from the gas flowrate of max  $Y_2$ . Studying

the plots of the other responses (*Annex 3-4d*), the independent factors for which the optima are found for each response are not necessarily the same and a compromise solution may be required. Derringer and Suich [196] proposed a mathematical desirability function (F) to simultaneously optimize multiple responses. Using Derringer and Suich [196] approach, the predicted collection efficiencies values obtained from individual response surfaces (Figure 50) are transformed to a dimensionless scale  $d_i$ . The desirability function has a 0 to 1 range with  $f = 0$  being an unacceptable response value and  $f = 1$  being totally desirable. F is the estimated from the individual desirability values using a geometric mean function [192]. Design Expert V13 software uses the F function approach in determining the set of independent variables values that maximize F and by extension the responses.

### 3.6.2 Optimal operating factors and confirmatory experiment

Having established the statistical significance of the BBD model equations ((16 to (23), the Design Expert V13 software was used to predict the optimal conditions to achieve the maximum nanoparticle collection by the pilot-scale spray scrubber at the chosen particle diameters (Table 9). The three independent variables (A: Gas flowrate, B: liquid flowrate and C: droplet diameter) were fixed within the studied levels from low (-1) to high (+1), while the responses ( $Y_1, Y_2, Y_3, Y_4, Y_5, Y_6, Y_7$  and  $Y_8$ ) were each set to the maximum with the highest degree of importance (+5). The software proposed sixty-seven (67) optimal combinations with mathematical desirability ranging from 0.859 to 0.318. Confirmatory experimental campaigns were carried out in quadruplicates for validation at the optimal conditions corresponding to the highest desirability (0.859). The optimal conditions correspond close to the median value (Level 0) of factor A, factor B's maximum value (Level +1) and factor C's minimum value (Level -1), as shown in Table 20.

*Table 20 Optimal values for the collection of nanoparticles*

Parameter	Gas flowrate $\text{Nm}^3.\text{h}^{-1}$	Liquid flowrate $\text{L}.\text{min}^{-1}$	Droplet diameter $\mu\text{m}$	$Y_1$ (%)	$Y_2$ (%)	$Y_3$ (%)	$Y_4$ (%)	$Y_5$ (%)	$Y_6$ (%)	$Y_7$ (%)	$Y_8$ (%)
Predicted	46.1	4.8	60.0	60.1	56.4	50.9	45.8	42.7	41.4	43.1	49.9
Experiment	46.0	4.8	60.0	$62.6 \pm 1$	$58.7 \pm 2$	$55.7 \pm 2$	$52.2 \pm 1$	$48.3 \pm 2$	$45.7 \pm 2$	$45.9 \pm 1$	$48.7 \pm 1$

Table 20 shows that the predicted and the optimal results are in good agreement. In addition, these optimal results are higher than any of the 17 experimental runs presented in Table 19 (except for two  $Y_8$  values). Figure 51 shows parity plots of the distribution of experimental vs. predicted responses. Once again, close agreement between the experimental and the predicted values of the responses is observed. This shows that the Box-Behnken design methodology could be used effectively to optimize the collection of nanoparticles by a spray scrubber operating under waste incineration conditions.

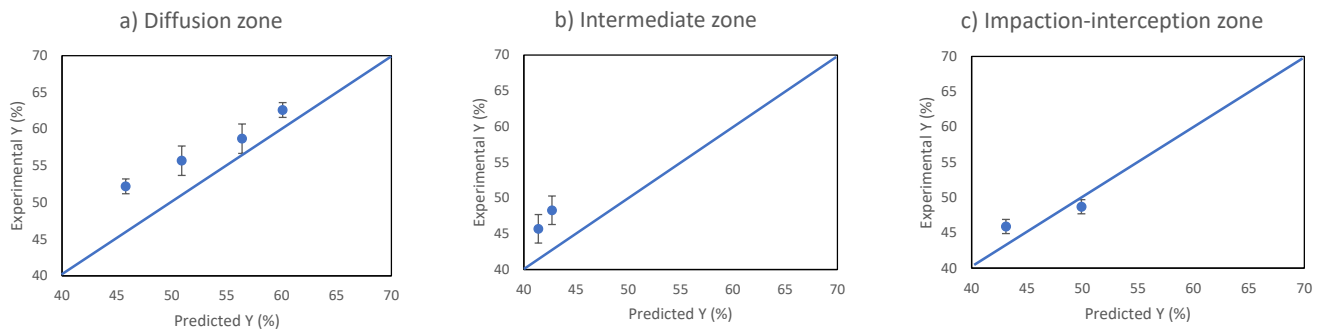


Figure 51 Parity plot showing the distribution of experimental vs. predicted responses

### 3.7 Conclusion of the chapter

In this chapter, the results of the experimental campaign using the Box-Behnken Design (BBD) methodology were presented. Regression BBD models for eight ( $Y_1$ ,  $Y_2$ ,  $Y_3$ ,  $Y_4$ ,  $Y_5$ ,  $Y_6$ ,  $Y_7$  and  $Y_8$ ) responses corresponding to nanoparticle collection efficiencies by the pilot-scale scrubber in the particle size range of 17, 20, 24, 29, 35, 42, 51 and 62 nm were presented. After verifying the statistical significance of the BBD models, predictions of responses were made and the results were found to be in good agreement with the experimental data. 2D and 3D plots, representing the combined influence of two independent factors (while keeping the third constant) were plotted to investigate the independent factors investigated (A: gas flowrate, B: liquid flowrate and C: droplet diameter). Responses in the diffusion region ( $Y_2$ ,  $Y_3$  and  $Y_4$ ) were found to be impacted by the factors similarly (except for  $Y_1$ ). Likewise,  $Y_5$  and  $Y_6$  were influenced by the factors in a like manner. This was also the case between responses  $Y_7$  and  $Y_8$ . Table 21 shows the summary of the influence of the studied factors based on the particle dominant or not mechanism.

*Table 21 Summary of the influence independent factors*

Influence of the parameter on the efficiency	Diffusion region	Intermediate region	Impaction region
A: Gas flowrate	No influence	Curvilinear relationship with maximum efficiency	Curvilinear relationship with maximum efficiency
B: Liquid flowrate	Positively correlated	Positively correlated	Positively correlated
C: Droplet diameter	Curvilinear relationship with minimum efficiency	Curvilinear relationship with minimum efficiency	Negatively correlated

For particles in the diffusion dominant region, there was no influence on the gas flowrate (except for  $Y_1$ ). The liquid flowrate was by far the most influencing factor and was found to be positively correlated to the responses in diffusion dominant region. A higher liquid flowrate improves the collection due to the diffusion mechanism as the droplet packing density increases. However, a non-linear relationship with minimum efficiency was observed between the droplet diameter and these responses. A smaller one has a larger surface-to-volume ratio for particle capture.

In the Intermediate region, the relationship between factor A and particle efficiency is also non-linear. Factor B demonstrates a positive correlation with collection efficiency. Factor C, on the other hand, exhibits a non-linear relationship with a minimum efficiency. For responses in the impaction region, a higher droplet flow increases the probability of particle capture. A decreasing droplet diameter also favors particle capture. An increase in the gas flowrate led to improvements in the collection efficiency however, a very high gas flowrate could lead to droplet entrainment. To determine the optimal operating conditions for the pilot-scale scrubber, the Design Expert V13 was used for the prediction. An optimal operating condition that maximizes the responses by the pilot-scale scrubber was proposed by using the Design Expert V13 at A:  $46 \text{ Nm}^3.\text{h}^{-1}$ , B:  $4.8 \text{ L.min}^{-1}$ , and C:  $60 \text{ }\mu\text{m}$ . Confirmatory experimental runs were conducted at the optimal conditions and the results (45.7 to 62.6% removal efficiency) were found to be in good agreement with the predicted data.

# **Chapter 4: Mechanistic modeling of particle collection efficiency**

## 4.1 Introduction

In this chapter, a particle collection model considering the individual contribution of inertial impaction, Brownian diffusion, interception and thermophoresis mechanisms is presented. Firstly, an estimation of key model parameters such as the droplet settling velocity, the droplet-particle relative velocity, the droplet packing density and the particle effective density is reported. A model fitting is then carried out to select a mechanistic model from the various authors reported in *chapter one* that “best-fit” the experimental results at *nominal conditions*. A sensitivity analysis is conducted to verify the influence of particle effective density, droplet packing density and droplet-particle relative velocity on the collection efficiency of the scrubber. The influence of the gas flowrate, liquid flowrate and droplet diameter is investigated using the selected final mechanistic model. Lastly, the mechanistic model is further tested for robustness by comparing its results to those of three DOE experimental runs (Run 6, Run 13 and Run 15).

## 4.2 Calculation of model parameters

The mathematical expressions for the individual particle collection mechanisms by various authors were presented in Table 1, Table 2 and Table 3. In these particle models, certain parameters such as the droplet settling velocity, the droplet-particle relative velocity, the droplet packing density and the particle effective density present challenges when calculating them. Indeed, even for the same operating conditions, different estimation approaches exist for which a wide range of values may be obtained. This section introduces the approach and assumptions considered in the estimation of these parameters in the present study.

### 4.2.1 Particle effective density ( $\rho_e$ )

The density of the carbon nanoparticles generated by the DNP 2000 spark generator may differ from the bulk density of carbon of  $2000 \text{ kg.m}^{-3}$  due to reasons such as the presence of voids in the internal structure of the nanoparticles and the non-spherical nature of the carbon nanoparticles. However, when estimating the carbon nanoparticle density, an assumption is made that they are spherical. This approach gives an "effective" or "apparent" density, not necessarily the true measure of the generated carbon nanoparticle density. Particle effective density cannot be measured directly [197]. It can be found if one of the following

combinations is known: mobility size – aerodynamic size, mobility size – particle mass, or aerodynamic size – particle mass [198, 199]. In this work, the aerodynamic and the electrical mobility diameters of the carbon nanoparticles at nominal operating conditions were measured separately by an electrical low-pressure impactor (ELPI, Dekati) and a Scanning Mobility Particle Spectrometers (SMPS, Grimm) respectively. The expression reported by DeCarlo et al. [198] below (Equation (33)) is then used to calculate carbon nanoparticle effective density.

$$\rho_e = \frac{C_c(d_a)d_a^2}{C_c(d_m)d_m^2} \rho_0 \quad (33)$$

Where  $C_c$  is the slip correction factor,  $\rho_0$  is the reference density ( $1000 \text{ kg.m}^{-3}$ ),  $\rho_e$  is the effective density,  $d_m$  is the electrical mobility diameter and  $d_a$  is the aerodynamic equivalent diameter.

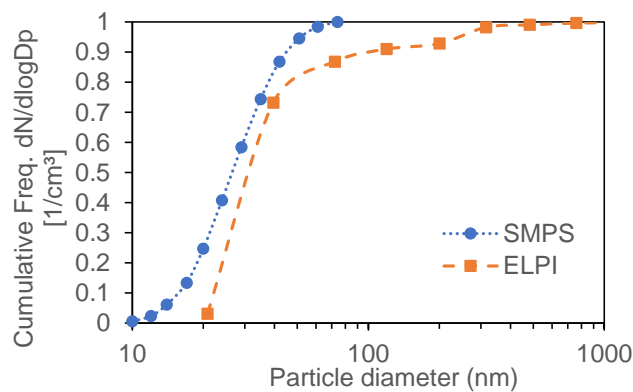


Figure 52 Cumulative particle size distribution of the carbon nanoparticles measured upstream of the scrubber with SMPS and ELPI particle counters (average for N:2; standard deviation)

The median diameter ( $D_{50}$ ) from the SMPS PSD was estimated as 26.61 nm and served as the electrical mobility diameter ( $d_m$ ) while the  $D_{50}$  from the ELPI PSD was determined as 33.38 nm and used as  $d_a$  (Figure 52). The particle effective density was calculated to be  $1279 \text{ kg.m}^{-3}$ . This value falls within the range of 1000 to 1800  $\text{Kg.m}^{-3}$  reported in the literature [200–202].

#### 4.2.2 Droplet settling velocity ( $V_t$ )

The terminal settling velocity of a droplet ( $V_t$ ) in a scrubber is defined as the maximum velocity that the droplet can attain as it falls through the gas stream. Hence, the droplet terminal velocity depends on several factors, including its size, spray ejection velocity and density, as well as the properties of the gas stream through which it is falling. Several forces

act on a droplet falling through a fluid. The force of gravity ( $F_G$ ) pulls the droplet downward and for a droplet acceleration equal to zero, it is balanced by an upward drag ( $F_D$ ) and buoyant forces ( $F_B$ ) of the gas resistance against the droplet (Figure 53). The effect of surface tension and viscous forces on the droplet is assumed to be negligible, as well as the effect of velocity and acceleration interactions between gas and particle around the vicinity of the particle.

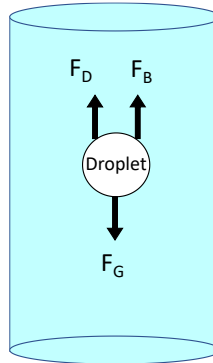


Figure 53 Principal forces acting on a droplet flowing in a fluid

The drag force is characterized by Stokes' law. Stokes' law is a mathematical expression that describes the drag force exerted on a small, spherical object moving through a fluid at low Reynolds number. The Reynolds number is a dimensionless number that compares the magnitude of the inertial forces to the viscous forces in a fluid flow. At low Reynolds numbers, the viscous forces dominate and the flow is said to be in the Stokes flow regime. In this regime, the drag force on a particle can be accurately described by Stokes' law. However, at high Reynolds numbers, the inertial forces become more significant and the flow is no longer in the Stokes flow regime. In this case, the drag force on a particle is not accurately described by Stokes' law. Instead, other drag models, such as the Newtonian drag model, may be more appropriate for predicting the drag force. Considering a droplet moving in a Stokes regime, the Stokes law expresses the drag force ( $F_D$ ), on a non-deforming spherical droplet of radius ( $R_D$ ) moving with a velocity ( $U_D$ ) in a gas with a viscosity ( $\mu$ ) as:

$$F_D = 6\pi\mu R_D U_D \quad (34)$$

The magnitude of the buoyancy force ( $F_B$ ) depends on the density of the gas ( $\rho_g$ ), the volume of the particle and the acceleration due to gravity ( $g$ ) and is expressed as:

$$F_B = \frac{4}{3}\pi R_D^3 \rho_g g \quad (35)$$

The gravity force acting on the droplet is given as:

$$F_G = \frac{4}{3}\pi R_D^3 \rho_D g \quad (36)$$

A droplet travels at constant velocity also known as terminal velocity when the net forces acting on the droplet is zero i.e.,  $F_G = F_D + F_B$ . Solving for  $U_D$  in the equations (20-22) above gives:

$$V_t = \frac{2gR_D^2(\rho_D - \rho_g)}{9\mu} \quad (37)$$

Davenport et al. [122] reported that the droplet terminal velocity depends on the droplet Reynold's number ( $Re_D$ ) and that equation (37) is appropriate when  $Re_D$  is less than one (Stokes regime). The Reynolds number is related to the drag force on a droplet because it determines the type of flow that occurs around the droplet, which in turn affects the magnitude of the drag force. At low Reynolds numbers, the drag force is relatively small, while at high Reynolds numbers, the drag force is much larger [122]. For  $Re_D$  above one ( $Re_D > 1$ ), Davenport et al. [122] proposed the following equations:

$$V_t = \left[ \frac{0.0721g(\rho_D - \rho_g)(2R_D)^{1.6}}{\mu^{0.6} \rho_g^{0.4}} \right]^{5/7} \quad 1 \leq Re_D \leq 500 \quad (38)$$

(Intermediate regime)

$$V_t = 1.74 \sqrt{\left[ \frac{2gR_D(\rho_D - \rho_g)}{\rho_g} \right]} \quad Re_D \geq 500 \quad (39)$$

(Newton regime)

In the present work, the range of droplet Reynold number was estimated from the following expression [108]:

$$Re_D = \frac{R_D U_D \rho_g}{\mu} \quad (40)$$

The value of the *calculated droplet Reynold* number ranges from **18 to 24**, hence, equation (38) is used to calculate the droplet settling velocity. However, calculating  $V_t$  at nominal conditions gives **0.21 m.s<sup>-1</sup>** using equation ((38) and **0.15 m.s<sup>-1</sup>** using equation (37).

#### 4.2.3 Relative velocity between droplets and particles (U)

Contrary to other particulate matter capture technologies such as a bag fabric filter or ESP where the collection medium is fixed (motionless), a spray scrubber involves mobile

collectors. The velocity of interest becomes the particle velocity in reference to the moving droplet velocity. Difficulties exist in estimating the relative velocity ( $U$ ) between particles and droplets in a scrubber given that both particles and droplets are in continuous motion and also could undergo deformation (droplet) or agglomeration (particles) as they travel in the gas stream. Kim et al. [14] calculated  $U$  as the velocity of the droplet relative to the scrubber. Other authors such as Wu et al. [22] estimated  $U$  by subtracting the mean particle velocity from the mean droplet velocity. Ardon-dryer et al. [124] estimate  $U$  as the droplet settling velocity ( $V_t$ ). Holmes et al. [203] proposed an arithmetic mean velocity representing all the zones of the scrubber with the following equation:

$$U = 0.5(2U_g + U_D) \quad (41)$$

Where  $U_g$  is the gas velocity and  $U_D$  is the droplet velocity at the spray jet.

In this work,  $U$  is estimated as the mean droplet velocity ( $U_D$ ) minus the particle velocity. The particle velocity is assumed to be the same as the moving gas velocity,  $U_g$ . Although inertial or diffusion phenomena occur in the vicinity of the droplet collectors, nano-sized and submicronic particles could be considered gas tracers. Average velocities of 15.9, 12.6 and 9.3  $\text{m}\cdot\text{s}^{-1}$  corresponding to the experimentally measured droplet velocities at 20 mm from the nozzle exist (Figure 54) for droplet diameters 60, 70 and 80  $\mu\text{m}$  respectively considered in the model as the droplet velocities. Although not used for the particle collection efficiency modeling, the droplet velocity at the exit of the nozzle was estimated considering the liquid flowrate and the measured external diameter (0.45 mm) of the nozzle as 25.2, 15.7 and 12.6  $\text{m}\cdot\text{s}^{-1}$  for droplet diameter 60, 70 and 80  $\mu\text{m}$  respectively.

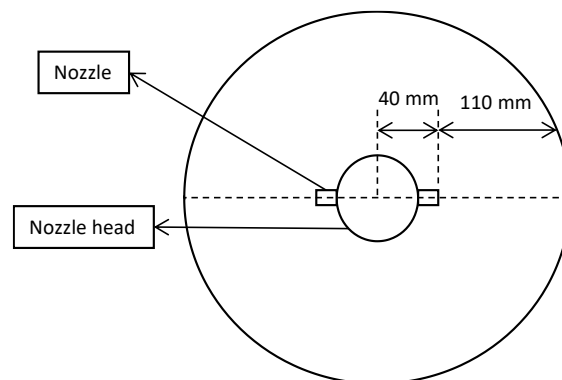


Figure 54 Cross-sectional view of the pilot-scale scrubber

To account for the possible range of relative velocity  $U$  encountered in the scrubber, a sensitivity calculation is plotted at *nominal operating conditions* from the equations  $U$  presented in Table 22 below.

*Table 22 Relative velocities for sensitivity analysis at nominal conditions*

$$U_1^* = U_D - (-U_g) \quad (42)$$

$$U_2 = 0.5(V_t + U_D) - (-U_g) \quad (43)$$

$$U_3 = V_t - (-U_g) \quad (44)$$

\* Relative velocity used in general collection efficiency modeling

The calculated values of  $U_1$ ,  $U_2$  and  $U_3$  for the sensitivity plots are **12.9, 6.6 and 0.4 m.s<sup>-1</sup>** respectively. Although a single value ( $D_{32}$ ) is used to represent the droplet velocity in each case for  $U_1$ ,  $U_2$  and  $U_3$ , it should be noted that the droplet velocity of a spray nozzle is a distribution and this could have a significant effect particularly at droplet-particle local interaction.

#### 4.2.4 Droplet packing density ( $\alpha$ )

Droplet packing density in a scrubber refers to the concentration of droplets within the scrubber. It is typically expressed as a volume ratio, with the total volume of the droplets being divided by the volume of the scrubber. Droplet packing density can be influenced by several factors, including the size of the droplets, the liquid flow rate, the flow rate of the gas through the scrubber and the geometry of the scrubber. In the present study, the total droplet volume is estimated from the volume of the liquid ( $Vol_D$ ) in the scrubber and is given as the product of the liquid flowrate ( $Q_L$ ) and the average residence time of a droplet ( $T_D$ ) in the scrubber:

$$Vol_D = Q_L T_D \quad (45)$$

$$T_D = \frac{h}{2} U_D \quad (46)$$

Where  $h$  is the height of the scrubber (m) and  $U_D$  is the droplet velocity (m.s<sup>-1</sup>) which is related to the droplet diameter. The average residence time of a droplet ( $T_D$ ) is estimated as the time it takes a droplet to travel from the mid-point of the scrubber with a velocity  $U_D$  to the bottom of the scrubber.

Droplet packing density plays an important role in the efficiency of contaminant removal as discussed in the previous chapter. To account for the possible range of the droplet packing density, a sensitivity plot is calculated considering varying values of  $T_D$  (Table 23).

*Table 23 Droplet residence times for droplet packing density sensitivity analysis*

$$T_{D1} = \frac{h}{2} U_D \quad (47)$$

$$T_{D2} = \frac{h}{2} 0.5(V_t + U_D) \quad (48)$$

$$T_{D3} = \frac{h}{2} V_t \quad (49)$$

### 4.3 Model selection

As discussed in *chapter one*, the overall collection efficiency is assumed to be the summation of the collection efficiencies obtained from the contributions due to the various removal mechanisms.

*Table 24 Summary of mechanistic model parameters*

Parameters	Values	Unit
Scrubber height, h	1.9	m
Scrubber diameter, d	0.3	m
Droplet diameter, D	60, 70, 80	$\mu\text{m}$
Gas temperature, T	343	K
Droplet velocity, $U_D$ (@ D = 60, 70 & 80 $\mu\text{m}$ resp.)	15.9, 12.6, 9.3	$\text{m}\cdot\text{s}^{-1}$
Liquid flowrate, $Q_L$	$2.65\cdot 10^{-5}$ , $5.33\cdot 10^{-5}$ , $8\cdot 10^{-5}$	$\text{m}^3\cdot\text{s}^{-1}$
Gas flowrate, $Q_G$	0.012, 0.015, 0.019	$\text{m}^3\cdot\text{s}^{-1}$
Gas velocity, $U_g$	0.17, 0.21, 0.26	$\text{m}\cdot\text{s}^{-1}$
Particle effective density, $\rho_e$	1000, 1279, 2000	$\text{kg}\cdot\text{m}^{-3}$
Density of air, $\rho_{air}$	0.909	$\text{kg}\cdot\text{m}^{-3}$

## Chapter IV Mechanistic modeling of particle collection efficiency

Gas viscosity, $\mu$	$1.83 \cdot 10^{-5}$	Pa·s
Gas molecules free mean path, $\lambda$	$6.73 \cdot 10^{-8}$	m
Solid volume fraction, $\alpha$	$1 \cdot 10^{-5}$ to $4 \cdot 10^{-5}$	-
Terminal settling velocity of droplets, $V_t$	0.18, 0.21, 0.25	$m \cdot s^{-1}$
Droplet Reynold's number	18 to 24	-

The mathematical expressions by several authors for the collection efficiencies due to impaction, Brownian diffusion and interception mechanisms were presented in Table 1, Table 2 and

Table 3 respectively. Table 24 gives a summary of the range of model parameters while the overall collection is given by Equation (6). Amongst the models, only those of Licht et al. [104], Kim et al. [14] and Lim et al. [20] were derived for wet scrubbers. Others are established theoretical models for atmospheric aerosol scavenging. Even for the models derived specifically for wet scrubbers, limited data is available on the operating conditions for which they were derived. Hence, in this work, a model “fitting” approach is chosen to validate the various theoretical models. The experimental results at nominal conditions (Figure 36) are used as the reference data. The fitting approach consists of three steps and is as follows:

- I. Selecting the “best-fit” models due to impaction and diffusion mechanisms to locate the particle diameter of minimum efficiency

Seven mathematical impaction collection models were initially considered (Table 1) of which two (Bae et al. [111] and Slinn et al. [27]) were determined to be unsuitable. The models proposed by Calvert et al. [112] and that of Walton and Woolcock [113] gave similar collection efficiencies and as such only the model by *Calvert et al.* [112] was selected. Similarly, the models by Licht et al. [104] and Kim et al. [14] also gave similar results and hence that of *Kim et al.* [14] was selected. The final impaction considered was that proposed by *Lim et al.* [20]. For Brownian diffusion, five models (Table 2) were originally considered of which two (Fan et al. [117] and Carotenuto et al. [116]) were found to be unsuitable. The remaining three models (Fuchs et al. [115], Bae et al. [111] and Jung and Lee [118]) gave similar collection efficiencies and as such the model reported by *Jung and Lee* [118] was selected. Figure 55 compares the mechanistic collection efficiency versus the experimental results at nominal conditions for the selected model combinations. It can be seen that the models are given by *Lim et al.* [20] (impaction) and *Jung and Lee* [118] (Brownian diffusion) are closer to the experimental data.

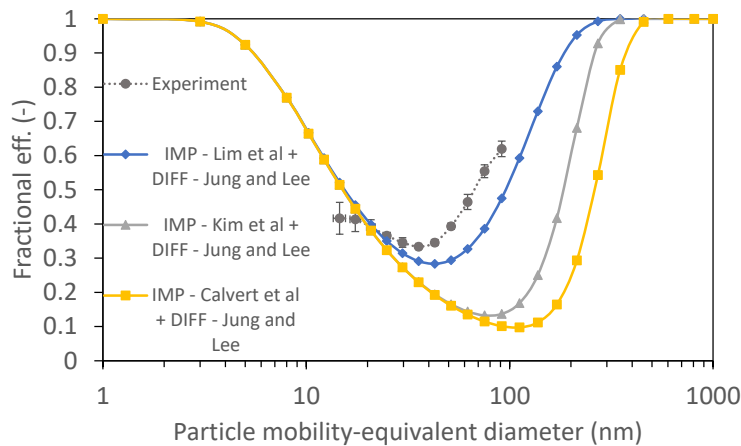


Figure 55 Comparison of overall collection efficiency considering selected impaction and diffusion models with experimental results at nominal conditions (average for N:4; standard deviation)

II. Selecting the “best-fit” models from step I and the addition of interception mechanisms

Having selected the best-fit models due to impaction and diffusion mechanisms, the particle collection due to the interception mechanism was then added to the overall collection efficiency model. Four (4) interception models were initially considered of which the results of the models by Fan et al. [117] and Fuchs et al. [115] were found to be the same. Thus, the model of *Fuchs et al.* [115] was selected. The last two interception mechanism models chosen were those of *Jung and Lee* [118] and *Bae et al.* [111].

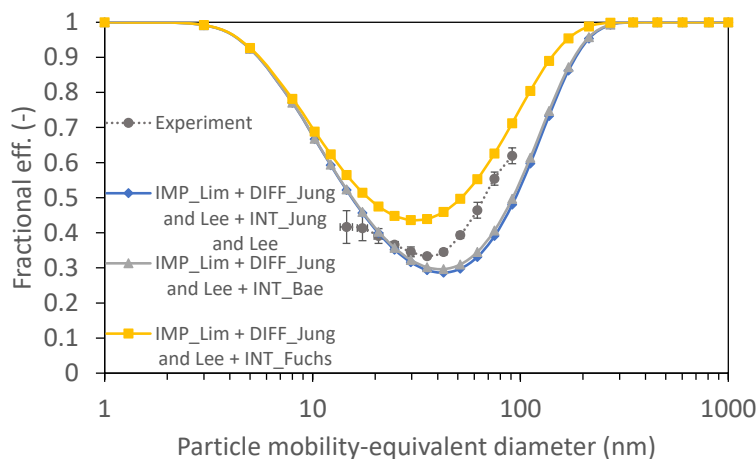


Figure 56 Comparison of overall collection efficiency considering selected impaction, diffusion and Interception models with experimental results at nominal conditions (average for N:4; standard deviation)

From Figure 56 above, the particle collection efficiency predicted by the models of Lim et al. [20] for the impaction mechanism, Jung and Lee [118] for Brownian diffusion and either Bae

et al. [111] or Jung and Lee [118] for interception mechanism is closer to the experimental result at nominal conditions.

III. Selecting the “best-fit” models from step II and adding of thermophoresis mechanism  
 The last step of the model fitting consists of adding the contribution due to the thermophoresis mechanism. The mathematical model for the effect of thermophoresis forces reported by *Davenport et al.* [114] (Equation (5) is employed. For the study conditions, the effect of thermophoresis was determined to be negligible and as such no observable difference is noticed with (Figure 70) or without (Figure 69) thermophoresis mechanism.

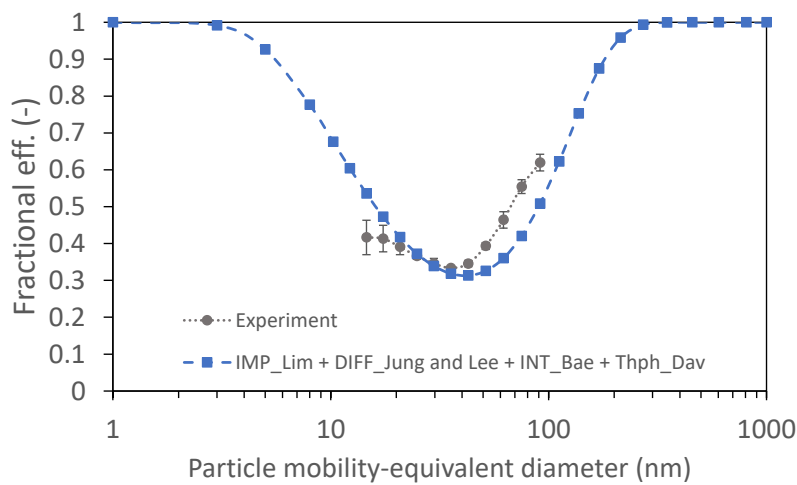


Figure 57 Comparison of overall collection efficiency considering selected impaction, diffusion, interception and thermophoresis models with experimental results at nominal conditions (average for N: 4; standard deviation)

Table 25: Final model composition

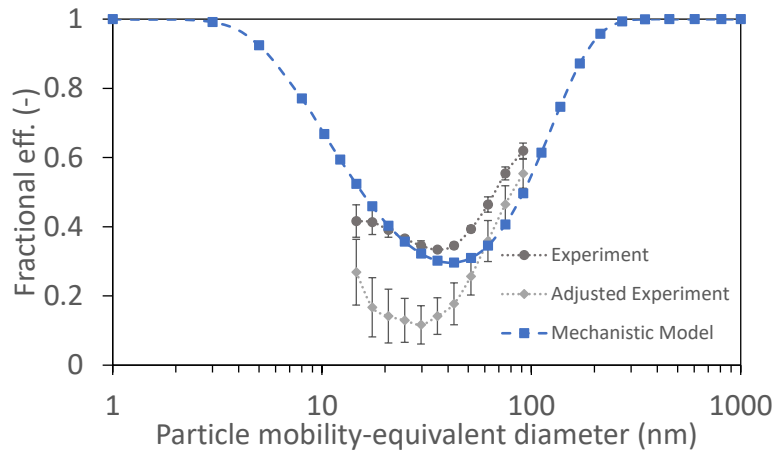
S/N	Impaction	Brownian diffusion	Interception	Thermophoresis
Model Author	Lim et al. [20]	Jung and Lee [118]	Bae et al. [111]	Davenport et al. [114]

Table 25 shows the composition of the “best-fit” model. This “best-fit” particle collection model is henceforth referred to as the mechanistic model and is employed for further investigations.

#### 4.4 Adjusted experimental data

In *chapter 2*, the experimental result of the nanoparticle collection by the walls of the scrubber (without liquid flow) was presented (Figure 28). In the present section, an

adjustment to the experimental results at nominal conditions is done by subtracting the collection efficiency by the walls of the scrubber from the collection efficiency when there is liquid flow in the scrubber (Figure 58). In doing this, an attempt is made to isolate the collection of nanoparticles solely by the liquid droplet collectors inside the scrubber.



*Figure 58 Comparison of experimental, adjusted experimental and mechanistic results at nominal conditions (average for N: 4; standard deviation)*

Figure 58 also compares the Adjusted experiment data to the mechanistic model results at nominal conditions. The adjusted experiment results give a much lower collection efficiency, especially for particles in the diffusion and intermediate regions. The adjusted experiment data represent rather the lowest possible nanoparticle collection efficiency extrema at the nominal conditions. The adjusted experiment results also show that the approach employed greatly simplifies the role of the scrubber in particle collection. The scrubber walls serve more roles than a surface for particle adhesion. The walls help guide the gas stream, the droplets and the captured particles. In doing this, the thermodynamic and hydrodynamic properties of the droplets and particles in the scrubber are affected by the walls in different ways such as the droplet evaporation rate, the droplet motion and the overall flow characteristics of the gas stream. This is particularly the case in the pilot-scale scrubber where the volume-to-surface area ratio is high (i.e., much higher than in the full-scale scrubber).

#### **4.5 Sensitivity analysis at nominal conditions**

In the following subsections, the nominal experimental data is compared to the mechanistic modeling results for the various particle density, droplet packing density and droplet-particle relative velocity obtained from the corresponding estimation approach.

#### 4.5.1 Particle effective density

Figure 59 represents the influence of the particle effective density on the collection of particles by the spray scrubber. As the particle density increases from 1000 to 2000  $\text{Kg.m}^{-3}$ , an improvement in the collection of larger particles ( $> 35 \text{ nm}$ ) is observed. Particles with a higher density will have more mass for a given size, which means they will have more inertia and be less affected by the gas stream and hence better collection due to impaction and interception mechanism. No influence of particle density is observed on smaller particles ( $< 35 \text{ nm}$ ). When the mechanistic model results at a particle density of 2000  $\text{Kg.m}^{-3}$  is compared to the experimental results at nominal conditions, the results are in close agreement.

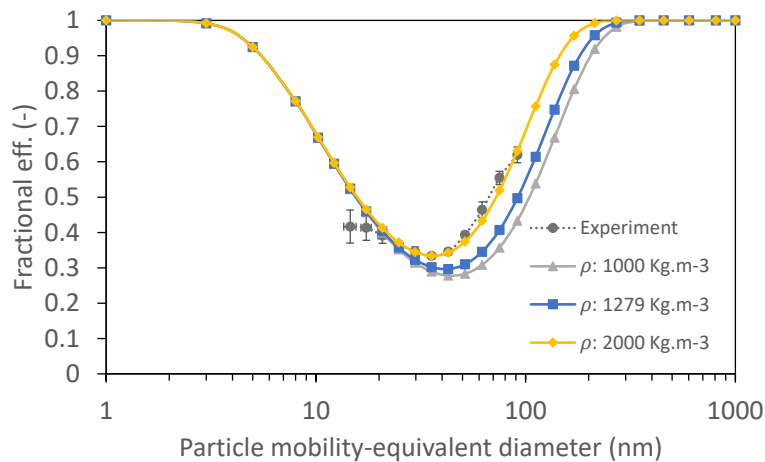


Figure 59 Comparison of mechanistic and experimental collection efficiencies at varying particle densities at nominal conditions (average for  $N: 4$ ; standard deviation)

#### 4.5.2 Droplet packing density

Figure 60 shows the sensitivity plot of the influence of the droplet packing density on the particle collection efficiency at nominal conditions. As discussed in the previous chapter, a higher droplet packing density will increase both the number of collectors and the collectors' surface area, hence the probability of particle capture. However, for the study conditions presented in Figure 60, as the packing density increase from 0.00003 to 0.002, no significant influence is observed on the particle removal efficiency for the entire particle diameter range.

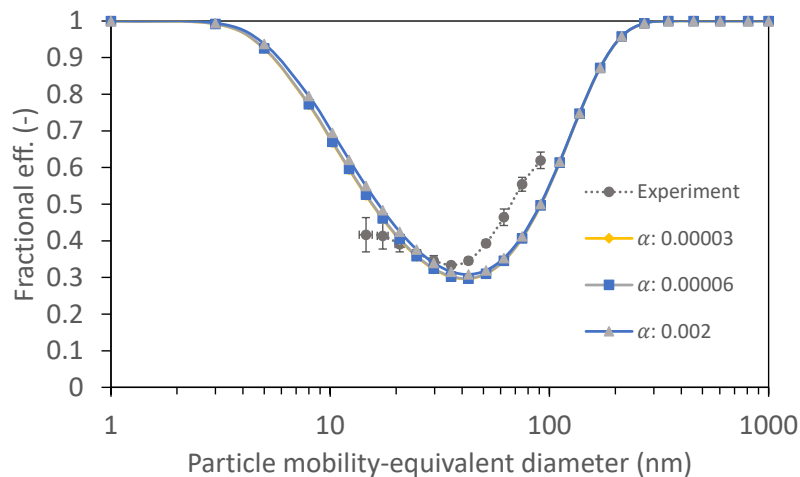


Figure 60 Comparison of mechanistic and experimental collection efficiencies at varying droplet packing density at nominal conditions (average for  $N: 4$ ; standard deviation)

### 4.5.3 Relative velocity

Figure 61 represents the sensitivity plot of the influence of the droplet-particle relative velocity at nominal conditions. The values of  $U_1$ ,  $U_2$  and  $U_3$  were calculated using the equations presented in Table 22. The collection efficiency at  $U_1$  closely agrees with experimental data. As the relative velocity decreases (from  $U_1$  to  $U_2$  and then to  $U_3$ ), the MPPS of the corresponding collection efficiency curve shifts to a larger particle diameter. Likewise, the collection of particles in the diffusion and intermediate region improves while that of larger particles slightly decreases. A possible explanation is that droplets may be more susceptible to Brownian diffusion at the lower relative velocity, which would cause them to more effectively collide and capture smaller particles, resulting in an increase in efficiency for smaller particles. Generally, low relative velocities such as  $0.43 \text{ m}\cdot\text{s}^{-1}$  ( $U_3$ ) are uncommon in a wet scrubber but are found in aerosol scavenging by raindrops. As such, the efficiency curves with  $U_1$  and  $U_2$  give a better fit to the experimental data.

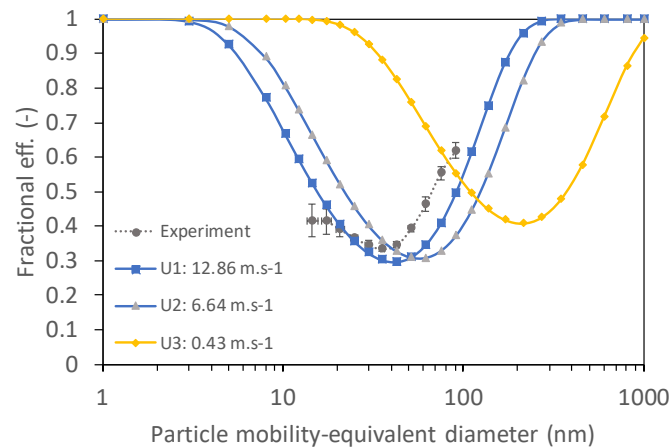


Figure 61 Comparison of mechanistic and experimental collection efficiency at varying droplet-particle relative velocity at nominal conditions (average for  $N: 4$ ; standard deviation)

#### 4.6 Mechanistic modeling of the influence of operating parameters

The following section discusses the influence of gas flowrate, liquid flowrate and droplet diameter on the collection of particles by the spray scrubber using the mechanistic model. The numerical range of the variables is within those of the Design of Experiment (DOE) previously presented. Given that spray nozzle was used for the experimental campaign and the mechanistic model was developed in reference to the experimental data (at nominal conditions), a change in the droplet diameter also results in a modification in the mechanistic model droplet velocity.

##### 4.6.1 Influence of Gas flowrate

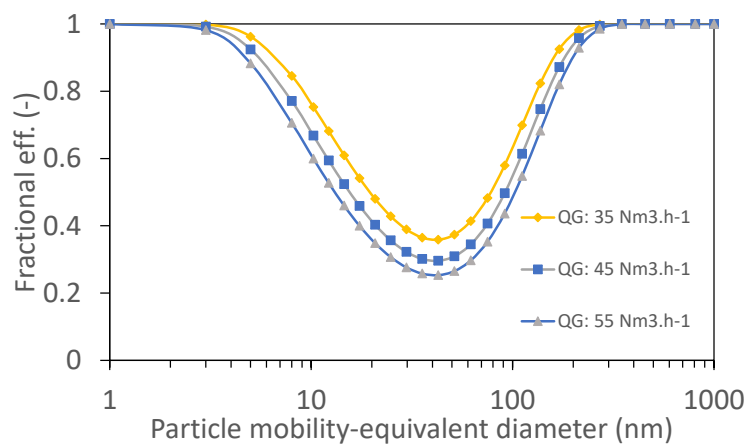


Figure 62 Mechanistic model results of the influence of gas flowrate on collection efficiency at a constant liquid flowrate of  $3.2 \text{ L.min}^{-1}$  and droplet diameter of  $70 \mu\text{m}$  (average for  $N: 4$ ; standard deviation)

For the range of gas flowrates investigated (Figure 62), an increase in the gas flow rate resulted in a decrease in the collection efficiency for the entire particle size range studied. A higher gas flowrate leads to a shorter particle residence time and thus, reduced collection efficiency. For the range of gas flowrates investigated, the corresponding gas velocities are much smaller than the droplet velocities. This assumption is fairly accurate as the mechanistic model considers the global view of the scrubber. At a more local level, certain regions in the scrubber may have droplet velocities very close to the gas velocities reported. Hence, a change in gas flowrate (i.e., gas velocity) has no noticeable effect on the droplet-particle relative velocity leading to no influence on the relative Reynolds number (Re). Therefore, no significant flow regime change occurred for the range of the gas and liquid flowrates studied.

#### 4.6.2 Influence of Liquid flowrate

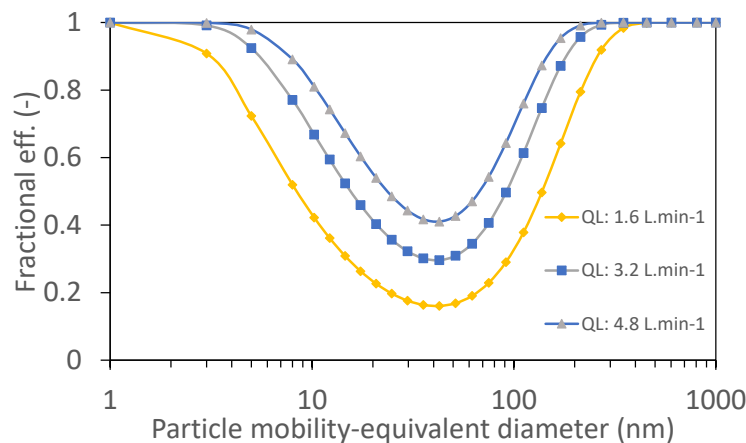


Figure 63 Mechanistic model results of the influence of liquid flowrate on collection efficiency at a constant gas flow rate of  $45 \text{ Nm}^3 \cdot \text{h}^{-1}$  and droplet diameter of  $70 \mu\text{m}$  (average for  $N: 4$ ; standard deviation)

As presented in the experimental results in **chapter 4**, the liquid flowrate has the most significant influence on the removal of nanoparticles by the scrubber. This is also the case with the mechanistic models (Figure 63). An increase in the liquid flowrate leads to an increased number of collectors and increase collection surfaces which in turn results in an improvement in the overall collection efficiency for the entire particle size range investigated.

#### 4.6.3 Influence of Droplet diameter and Droplet velocity

Before understanding the combined effect of droplet diameter and droplet velocity on the nanoparticle removal efficiency (as was the case in the experimental runs), the influence on only the droplet diameter is first of all investigated as shown in Figure 63a. As the droplet

diameter decreases, the overall collection efficiency improves (Figure 63a). This is because smaller droplets are likely to come into contact with and capture particles. This is due to the smaller droplets having a larger surface area relative to their volume, which increases the likelihood of collisions with particles. Another way that droplet diameter can affect particle collection is through the terminal velocity of the droplets. As stated previously, the droplet terminal velocity is the maximum velocity that a falling droplet will reach due to the balance of forces acting on it. Droplets with diameters of 60  $\mu\text{m}$  have a lower terminal velocity ( $0.17 \text{ m}\cdot\text{s}^{-1}$ ) than droplets at 80  $\mu\text{m}$  ( $0.25 \text{ m}\cdot\text{s}^{-1}$ ), which means they will be more likely to remain in the gas stream until they collide with and capture particles as they fall through the scrubber.

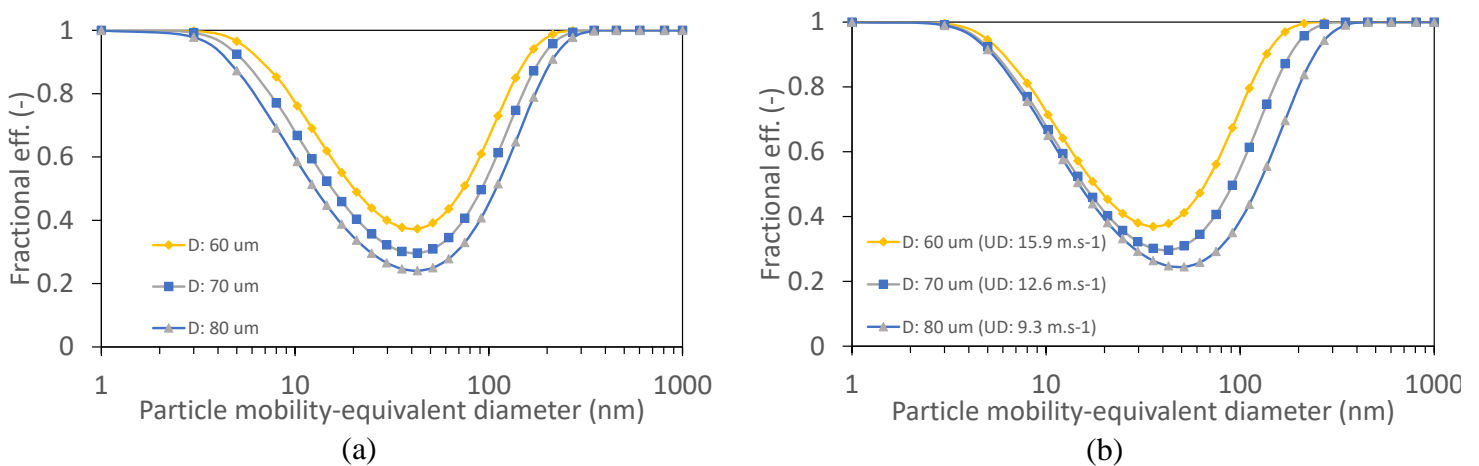


Figure 64 Mechanistic model results of the (a) droplet diameter and (b) combined influence of droplet diameter and velocity on collection efficiency at a constant gas flow rate of  $45 \text{ Nm}^3\cdot\text{h}^{-1}$  and liquid flowrate of  $3.2 \text{ L}\cdot\text{min}^{-1}$  (average for N: 4; standard deviation)

In Figure 64b, the droplet velocity is allowed change as the droplet diameter varies. This was the case in the experimental data given that nozzle technology was used to supply the spraying liquid. As the droplet diameter increased, the droplet velocity decreases leading to a shift in the collection efficiency MPPS to larger particle size (Similar to Figure 61). Likewise, a decrease in the droplet diameter led to an improvement in the particle collection efficiency. The combined influence of decreasing the droplet diameter and increasing the droplet velocity leads to higher collection, especially for larger particles.

#### 4.7 Mechanistic model robustness verification

The mechanistic model results were tested for robustness by comparing them to three different DOE experimental runs (Run 6, Run 13 and Run 15) that were previously presented in Table 16. The predicted values given by the Box- Behnken design (BBD) models are also

plotted. For the seventeen DOE experimental runs (Table 16), Run 15 gave the minimum collection efficiency curve, Run 13 had the maximum efficiency curve and Run 6 had a collection efficiency curve around the mid-point. Figure 65 compares the experimental, mechanistic and BBD model results at Run 15; gas flowrate (A) of  $35 \text{ Nm}^3 \cdot \text{h}^{-1}$ , liquid flowrate (B) of  $1.6 \text{ L} \cdot \text{min}^{-1}$  and droplet diameter (C) of  $70 \mu\text{m}$ . The experimental and BBD model results are in good agreement. However, there are discrepancies between the mechanistic model and the experimental data. Indeed, for the entire particle range, the *mechanistic model understates the experimental results* – particularly in the interception-impaction dominant region.

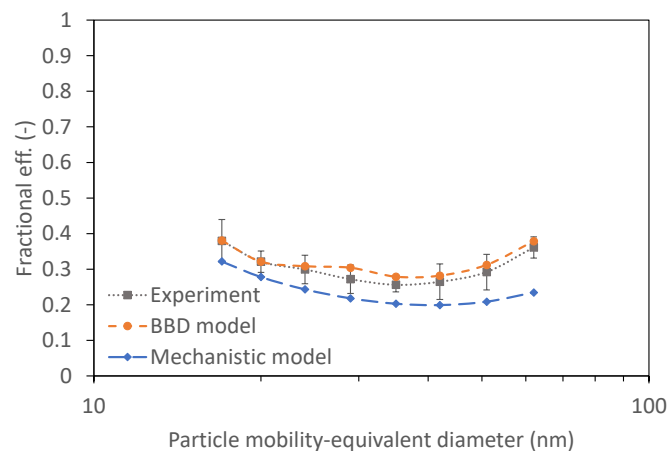
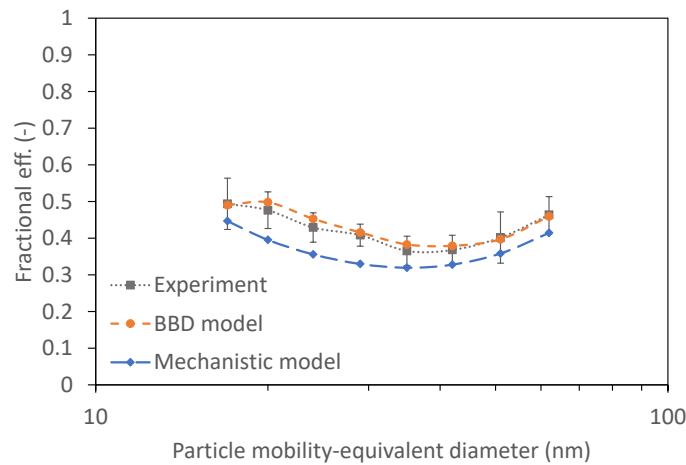


Figure 65 Comparison of experimental, BBD model and mechanistic model results at Run 15 – A:  $35 \text{ Nm}^3 \cdot \text{h}^{-1}$ , B:  $1.6 \text{ L} \cdot \text{min}^{-1}$  and C:  $70 \mu\text{m}$  (average for  $N: 4$ ; standard deviation)

Several factors could explain this behavior. The mechanistic model may not accurately represent the complex thermodynamic flow within the spray scrubber. Especially the effects of evolving particle properties (e.g., size or density) and the secondary influence of operating variables (e.g., effects of gas flowrate on droplet size). Given that the liquid flowrate has the most significant influence on the collection efficiency, it will appear that the mechanistic model results are understated at a low liquid flowrate.

Figure 66 compares the experimental, mechanistic and BBD model results at Run 6; gas flowrate (A) of  $55 \text{ Nm}^3 \cdot \text{h}^{-1}$ , liquid flowrate (B) of  $3.2 \text{ L} \cdot \text{min}^{-1}$  and droplet diameter (C) of  $60 \mu\text{m}$ . Here again, the experimental and BBD model results are in close agreement. However, there are differences between the mechanistic model and the experimental results but not as pronounced as in the previous Run 15. Indeed, Run 6 has a liquid flowrate ( $3.2 \text{ L} \cdot \text{min}^{-1}$ )

which is the same liquid flowrate as the nominal conditions that were used to fit the mechanistic model in the first place.



*Figure 66 Comparison of experimental, BBD model and mechanistic model results at Run 6 – A:  $55 \text{ Nm}^3.\text{h}^{-1}$ , B:  $3.2 \text{ L.min}^{-1}$  and C:  $60 \mu\text{m}$  (average for N: 4; standard deviation)*

In Figure 67, a comparison of the experimental, BBD model and mechanistic model results is made at Run 6; gas flowrate (A) of  $45 \text{ Nm}^3.\text{h}^{-1}$ , liquid flowrate (B) of  $4.8 \text{ L.min}^{-1}$  and droplet diameter (C) of  $60 \mu\text{m}$ . Once again, the experimental and BBD model data are in close agreement. However, differences exist between the mechanistic model and the experimental results. but not as pronounced as in the previous Run 13. At this liquid flowrate (4.8), the mechanistic model overstates the collection efficiency, especially for larger particle diameters.

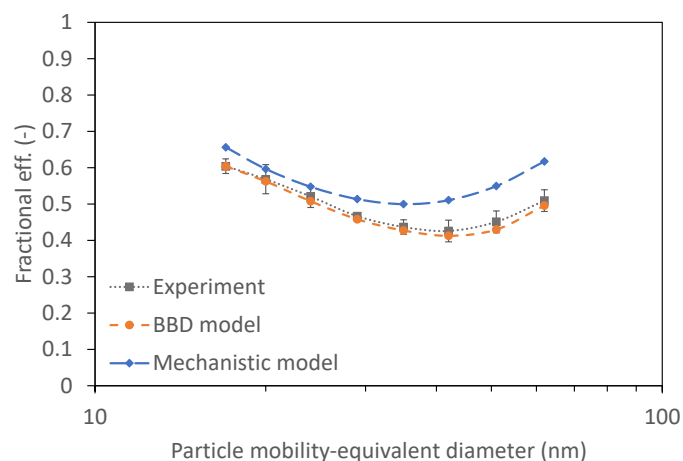


*Figure 67 Comparison of experimental, BBD model and mechanistic model results at Run 13 – A:  $45 \text{ Nm}^3.\text{h}^{-1}$ , B:  $4.8 \text{ L.min}^{-1}$  and C:  $60 \mu\text{m}$  (average for N: 4; standard deviation)*

## 4.8 Conclusion of the chapter

In this chapter, a mechanistic model for the collection of particles by a spray scrubber considering the individual contributions of inertial impaction, Brownian diffusion, interception and thermophoresis mechanisms was presented. Several authors proposed mathematical expressions for the individual mechanisms. The final chosen mechanistic model consists of the impaction mechanism by Lim et al. [20], Brownian diffusion by Jung and Lee [118], the Interception mechanism by Bae et al. [111] and Thermophoresis by Davenport et al. [114]. This configuration was found to be the “best fit” for the experimental data at nominal conditions.

A sensitivity analysis was conducted to verify the influence of key model parameters such as the particle density, droplet packing density and droplet-particle relative velocity on the particle collection efficiency of the scrubber. As the particle density increased from 1000 to 2000  $\text{Kg.m}^{-3}$ , the mechanistic model results improved and gave a better fit to the experimental data. Within the study conditions, no significant influence on the droplet packing density was observed. A decrease in the droplet-particle relative velocity led to a dislodgement of the collection efficiency MPPS to higher particle diameters.

The influence of the gas flowrate, liquid flowrate and droplet diameter was also investigated using the mechanistic model. And the results are consistent with those found in the literature. Lastly, the mechanistic model was tested for robustness by comparing its results to the actual and predicted (BBD model) results of three DOE experimental runs (Run 6, Run 13 and Run 15). In all three cases, the predicted BBD model results were in close agreement with the experimental data. However, the mechanistic model results were understated for Run 15, closely stated for Run 6 and overstated for Run 13.

## **General conclusions and perspectives**

The lack of regulations targeted at the safe disposal of engineered nanomaterials (ENM) at end-of-life implies that ENM are currently been treated via conventional waste management pathways. This leads to heightened concerns given that an increasing number of studies are associating the presence of ENM in the environment with potential health and environmental issues. It is therefore important to understand the fate of ENM in existing waste management facilities such as waste incineration plants. Spray scrubbers are flue gas cleaning technologies (FGCT) mainly employed in industrial applications such as waste incineration to treat acid gases but have also been reported to be used in various combinations with other FGCT units to limit the release of PM. However, scrubbers generally are reported to have a low collection efficiency for  $PM < 5.0 \mu m$ . In this Ph.D. dissertation, an evaluation of the performance of a pilot-scale spray scrubber for the collection of nanoparticles contained in incineration fumes has been made. The primary objectives of this thesis were:

- To carry out a literature review on the fate of ENM in conventional waste management facilities such as waste incineration plants with a focus on the removal of nanoparticles by scrubber technology present in these facilities
- To understand the physical phenomena involved in the capture of particles by a droplet in a scrubber and to quantify the parameters involved in the collection phenomena from various published works with the goal of developing a mechanistic model that would be validated with experimental data.
- To evaluate the performance of a pilot-scale spray scrubber on the removal of carbon nanoparticles present in an incineration fume representative of the average conditions (nominal conditions) typical of hazardous waste incineration plant scrubber
- To study the influence of key operating parameters such as the gas flowrate, liquid flowrate and droplet diameter on spray scrubber performance with regards to the collection of nanoparticles with the goal of finding an optimal operating condition
- To quantify the transfer of nanoparticles from the gas phase to the liquid phase at nominal conditions and also the collection of nanoparticles by the scrubber walls

To attain these objectives, a bibliographic review was first carried out as reported in **chapter I**. The review summarized the definition, types and production of nanomaterials based on published works. Over 27 definitions of nanomaterials were found in the literature. Nanomaterial definitions broadly consist of an emphasis on size, novelty and chemical composition. The global NM market primarily led by the carbon-based ENM is projected to

grow exponentially in the coming decades (i.e., with a compound annual growth rate of ~15%). This has led to concerns about the potential health and environmental impacts of ENM and an increased number of possible human exposure pathways. No national, regional, or global regulations on the safe disposal of nanomaterials at the end of their life were found in the literature. Thus, a focus was then placed on the fate of ENM in conventional waste management pathways such as in waste incineration plants. It was found that limited research (21 studies) has been conducted on the behavior of nanomaterials during waste incineration. These studies reported that several factors such as the chemical and physical nature of the nanomaterial, the combustion temperature, the residence time and the presence of other materials could affect the fate of ENM during waste incineration. For the specific ENM reported in these studies, ENM does survive the combustion temperature and the majority end up in the bottom ash. However, a fraction of the ENM was also transferred to the flue gas stream. Given the specificity of the studies and the complexity involved in waste incineration, care should be taken in generalizing these conclusions to all ENM or the same ENM but in different configurations of waste incineration. Yet, a significant knowledge gap exists on the fate of NM that join the flue gas after the combustion chamber. The second objective of **chapter I** was dedicated to examining wet scrubbing technology, including the operating principles, types, industrial applications, and various particle collection mechanisms involved in a scrubber. It was found that the particle collection mechanisms by a droplet include inertial impaction, Brownian motion, electrostatic attraction, interception, gravitational settling, condensation, centrifugal force and phoretic forces. Authors such as Lim et al. [20] and Kim et al. [14] argued that inertial impaction, Brownian motion, and interception are the dominant mechanisms in a wet scrubber. The Stokes, Peclet and interception numbers represented the dimensionless parameters that translate the inertial impaction, Brownian motion, and interception mechanisms respectively. Finally, this chapter reviewed the influence of gas flow rate, gas temperature, gas humidity rate, liquid flow rate, and droplet diameter on the particle collection efficiency of a wet scrubber. In general, the relationship between gas flow rate and particle removal efficiency in a wet scrubber is complex and may not be linear. Higher gas flowrate was reported to favor the collection of particles due to direct inertial impaction. However, a high gas flowrate results in a lower particle residence time and thus a lower overall particle removal efficiency.

An increase in the gas temperature could increase the overall droplet-particle interaction due to the evaporation of the droplet surfaces. However, higher gas temperatures can also lead to

increased evaporation of the liquid in the scrubber, which can reduce the number of droplets, hence the overall scrubber efficiency. In general, increasing the liquid flow rate can lead to improved particle removal efficiency, as it allows for more droplets to be present in the scrubber and increases the chances that particles will come into contact with and be collected by the droplet. Droplet diameter was found to be inversely correlated to the particle collection efficiency. It was presented that smaller droplets have a larger surface area to volume ratio, which allows them to come into contact with more particles. Additionally, smaller droplets are more susceptible to Brownian motion, which can cause them to collide with and collect particles.

**Chapter II** presented the materials and the overall research methodology employed in this thesis. The pilot-scale scrubber discussed in this work was designed and operated to represent a full-scale spray scrubber present in the flue-gas cleaning line of a hazardous waste incineration plant in terms of the height-to-diameter ratio, liquid-to-gas ratio, gas inlet and outlet temperatures, gas humidity, gas residence time, and gas flow regime, droplet diameter and particle concentration. The aerosols investigated in this thesis were carbon nanoparticles. The carbon nanoparticles with an estimated mean particle concentration of  $1.2 \cdot 10^6 \text{ \#} \cdot \text{cm}^{-3}$  were generated by a DNP 2000 (Palas) spark particle generator and counted with a Scanning Mobility Particle Spectrometer (SMPS). A two-step dilution (with a combined dilution factor of 100x) was performed to lower the flue gas particle concentration, gas temperature and humidity conditions before counting with the SMPS. The overall research methodology to evaluate the performance of the scrubber consisted of an initial experimental campaign at nominal conditions, followed by validation of the particle collection mechanistic model and also an investigation of the influence of the main operating parameters on the collection efficiency of carbon nanoparticles by the pilot-scale scrubber using a Design of experiment methodology - Box Behnken design. Three independent operating parameters (variables) were considered - the gas flow rate, the liquid flow rate and the droplet diameter. This resulted in seventeen (including five replica points) experimental runs for the Box Behnken design and analysis.

The liquid droplet diameter and velocity characterization measurements revealed the difficulties is using spray nozzles. Modifying the liquid flowrate of the spray nozzle could modify the droplet diameter also. To address this, a change in the liquid flow rate is accomplished by adjusting the overall number of spray nozzles in the scrubber. This could introduce possible secondary effects. Hence, preliminary qualification tests to investigate the

influence of the modification of nozzle configurations on the pilot-scale scrubber collection efficiency at three distinct operating conditions were conducted. ***No noticeable influence of modifying the configuration of the nozzle was observed.*** A second test bench qualification carried out consisted of quantifying the collection of nanoparticles by the pilot scrubber walls at three different gas flowrates. In this test, ***a significant mass (up to 30%) of the carbon nanoparticles was found to be collected by the walls of the scrubber.*** Lastly, a vacuum filtration measurement of the purged water collected at the bottom of the scrubber at nominal operating conditions was also performed to quantify the transfer of nanoparticles from the gas phase to the liquid phase. The results of the purge water vacuum filtration show that about ***37% of nanoparticles were transferred from the gas phase to the liquid phase*** at nominal operating conditions.

**Chapter III** presented the results of the experimental campaign using the Box-Behnken Design (BBD) methodology. Eight responses ( $Y_1$ ,  $Y_2$ ,  $Y_3$ ,  $Y_4$ ,  $Y_5$ ,  $Y_6$ ,  $Y_7$  and  $Y_8$ ) were selected, corresponding to collection efficiencies at particle diameters 17, 20, 24, 29, 35, 42, 51 and 62 nm respectively. The majority of the collection efficiency curves of the 17 experimental runs have their Greenfield gap (i.e., MPPS) at either  $Y_5$  or  $Y_6$ . We, therefore, referred to this region as the intermediate region while denoting the region around  $Y_1$ ,  $Y_2$ ,  $Y_3$  and  $Y_4$  as the diffusion-dominant region. The region around  $Y_7$  and  $Y_8$  was designated as the impaction-interception-dominant region. At nominal conditions (replica point), the pilot-scale scrubber has a collection efficiency of 35% to 62% for particle size 14 nm to 91 nm in mobility equivalent diameter. From the experimental data, Design Expert V13 was used to generate the BBD models. Before using the BBD models to predict the responses, significant terms in the BBD models for each response were found by analysis of variance (ANOVA) and significance was primarily decided by the F-statistic calculated from the data. For all the BBD models, model term(s) reduction was carried out to improve the overall model adequacy. However, no BBD model transformation was performed. For 17 experimental results, the predicted BBD model results were found to be in close agreement (i.e., within one standard deviation). 2D and 3D surface plots, representing the combined influence of two independent factors (while keeping the third constant) were plotted to investigate the independent factors investigated (A: gas flowrate, B: liquid flowrate and C: droplet diameter) on the collection efficiency. ***An optimal operating condition that maximizes the responses by the pilot-scale scrubber was proposed by the Design Expert V13 at A: 46 Nm<sup>3</sup>.h<sup>-1</sup>, B: 4.8 L.min<sup>-1</sup> and C: 60 μm. Confirmatory experimental runs were conducted at these optimal***

*conditions and the results (45.7% to 62.6% removal efficiency) were found to be in good agreement with the predicted data.*

**Chapter IV** presented a mechanistic model for the collection of particles by a spray scrubber considering the individual contributions of inertial impaction, Brownian diffusion, interception and thermophoresis mechanisms. Several authors proposed mathematical expressions for the individual mechanisms. *The final chosen mechanistic model consisted of the impaction mechanism by Lim et al. [20], Brownian diffusion by Jung and Lee [118], the Interception mechanism by Bae et al. [111] and Thermophoresis by Davenport et al. [114].* This configuration was found to be the “best fit” for the experimental data at nominal conditions.

A sensitivity analysis was conducted to verify the influence of key model parameters such as the particle density, droplet packing density and droplet-particle relative velocity on the particle collection efficiency of the scrubber. As the particle density increased from 1000 to 2000 kg.m<sup>-3</sup>, the mechanistic model results improved and gave a better fit to the experimental data. Within the study conditions, no significant influence on the droplet packing density was observed. A decrease in the droplet-particle relative velocity led to the dislodgement of the collection efficiency MPPS to higher particle diameters.

The influence of the gas flowrate, liquid flowrate and droplet diameter was also investigated using the mechanistic model. And the results are consistent with those found in the literature. Lastly, the mechanistic model was tested for robustness by comparing its results to the actual and predicted (BBD model) results of three DOE experimental runs (Run 6, Run 13 and Run 15). In all three cases, the predicted BBD model results were in close agreement with the experimental data. However, the mechanistic model results were understated for Run 15, closely stated for Run 6 and overstated for Run 13.

**The limitations to the present study are as follows:**

1. Limitations related to the scope-
  - ❖ Conclusions of this study may only be applicable to carbon-based nanoparticles and may not be generalized to other types of engineered nanoparticles.
  - ❖ The study was conducted at a pilot-scale, and therefore, care should be taken when extrapolating the results to a full-scale scrubber.
  - ❖ The study only investigated the impact three operating parameters ( gas flowrate, liquid flowrate and droplet diameter) on the collection efficiency. Other operating

parameters may play an important role on the collection efficiency depending on the spray scrubber configurations

- ❖ The isolated and careful characterization of the influence of wall/droplet interactions on nanoparticle capture by a water film has not been adequately explored
2. Limitations related to the complexity of the full-scale scrubber system:
    - ❖ The study did not consider the effect of other pollutants that may be present in the flue gas, which could impact the collection efficiency of nanoparticles.
    - ❖ The configuration of a full-scale scrubber may vary, and therefore, the results of the study may not be directly applicable to all scrubber configurations.
  3. Limitations related to the modeling approach:
    - ❖ The BBD model used in the study is best suited for optimization studies and may not provide physical/scientific insights into the processes occurring in the scrubber.
    - ❖ The global approach taken in the study ignores the local droplet-particle interactions, which could have a significant impact on the performance of a scrubber, especially given the complex thermodynamic conditions of a WIP scrubber.

The results of this thesis remain promising concerning bridging the existing knowledge gap of the fate of nanoparticles in a spray scrubber under waste incineration conditions. However, this thesis also opens up possible directions for future research. Thus, it would be interesting to:

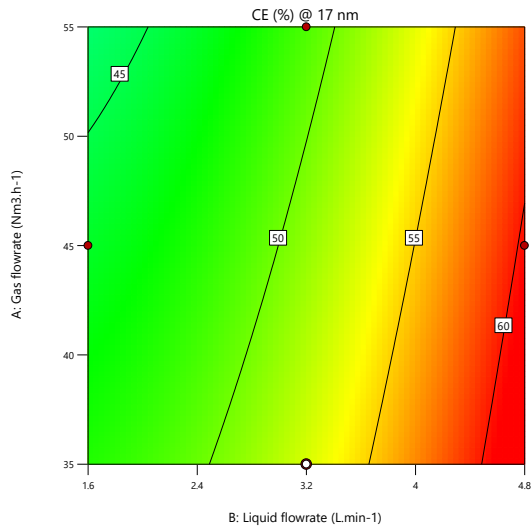
- Investigate a much wider range of parameters. Physical scaling down constraints necessitated us to have a range of parameters close to the nominal conditions. However, from the interactive plots in **chapter III**, the results indicate that we are not at the limits of these parameters and by extension not close to extrema in the full-scale scrubber. A much wider range of gas flow, liquid flow and droplet diameter could permit a better understanding of the influence of these variables on the removal efficiency
- Investigate the influence of other operating parameters such as the gas humidity, gas temperature, liquid types, liquid pH and liquid temperature on the collection of nanoparticles by spray scrubber. This will result in a comprehensive understanding of the complex droplet-particle capture phenomena involved in a scrubber

- Study the collection efficiency of organic and inorganic-based nanomaterials. This is particularly essential given that the hygroscopic characteristics of the carbon nanoparticles used in this thesis were not verified
- Investigate the collection of nanoparticles contained in real (actual) incineration fumes. The presence of other pollutants (acid gases) including larger PM could reveal new insights into the removal of nanoparticles by a spray scrubber under waste incineration conditions.
- Develop a computational fluid dynamics (CFD) numerical model to study the local flow interactions inside the scrubber. The thermodynamic interactions between the gas and droplets in the spray scrubber play a critical role in the ability of the scrubber to remove particles and these interactions are influenced by factors such as the temperature and flow rate of the gas, the properties of the water and gas, and the design of the scrubber

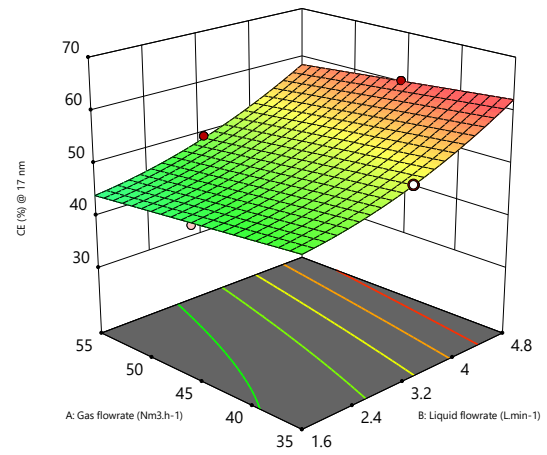
# Annexes

## Annex 3-1a: Counter and response surface plots showing the influence of factors A and B at constant C (a:60 and b:80 $\mu\text{m}$ )

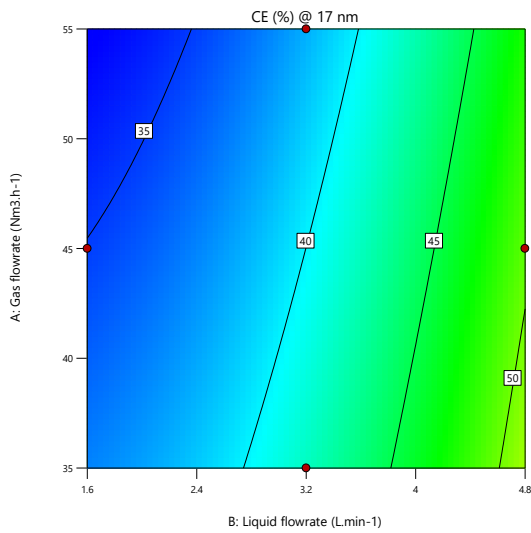
### Response $Y_1$ @ 17 nm



(a1) C:Droplet (60  $\mu\text{m}$ )

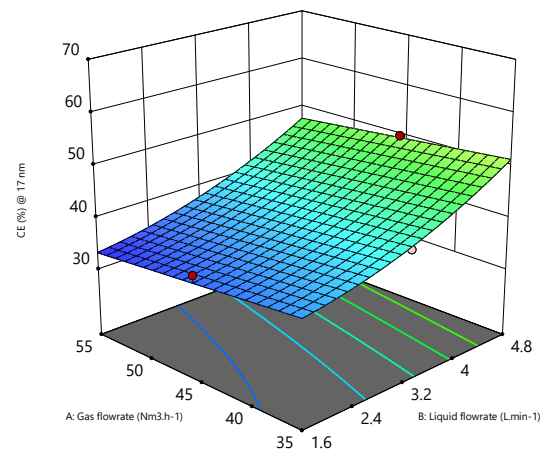


(a2) C:Droplet (60  $\mu\text{m}$ )



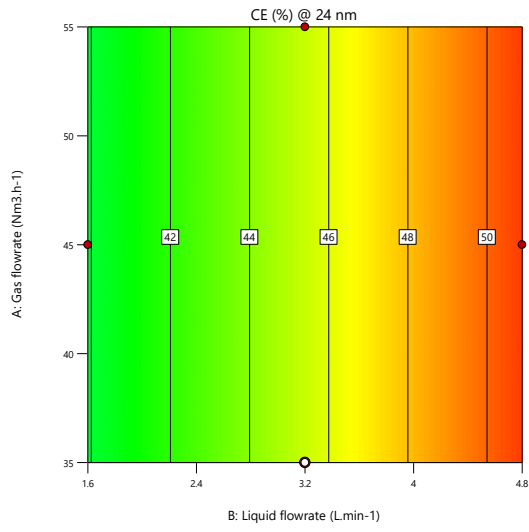
(b1)

C:Droplet (80  $\mu\text{m}$ )

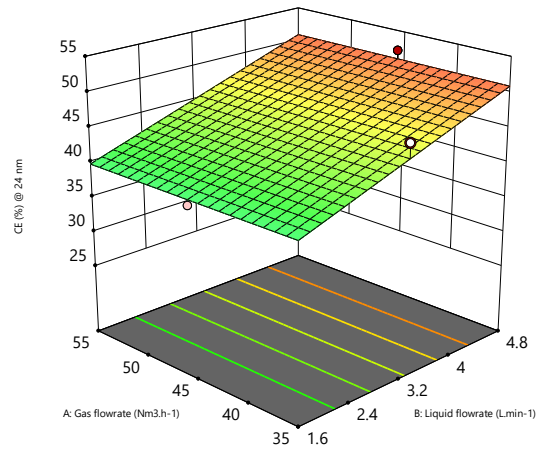


(b2) C:Droplet (80  $\mu\text{m}$ )

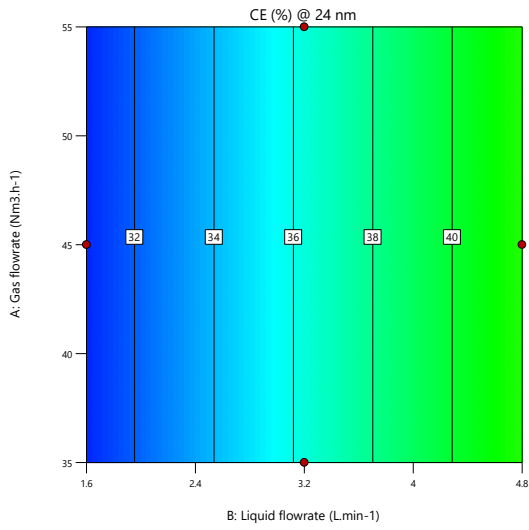
### Response $Y_3$ @ 24 nm



(a1) C:Droplet (60 μm)

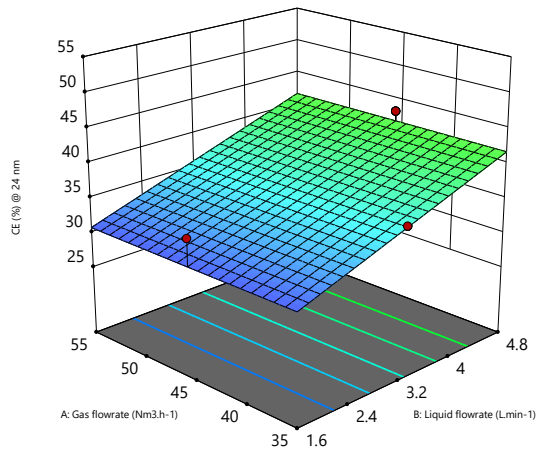


(a2) C:Droplet (60 μm)



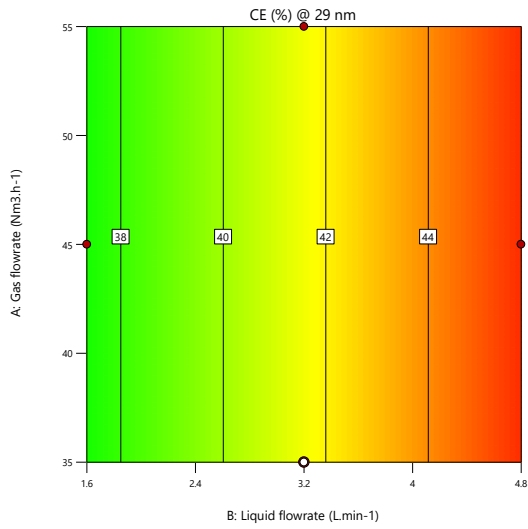
(b1)

C:Droplet (80 μm)

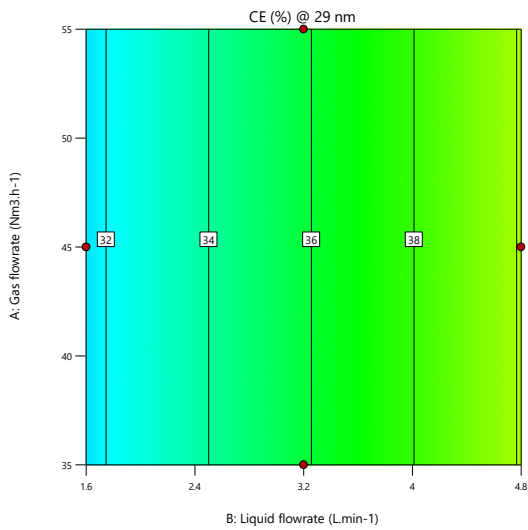


(b2) C:Droplet (80 μm)

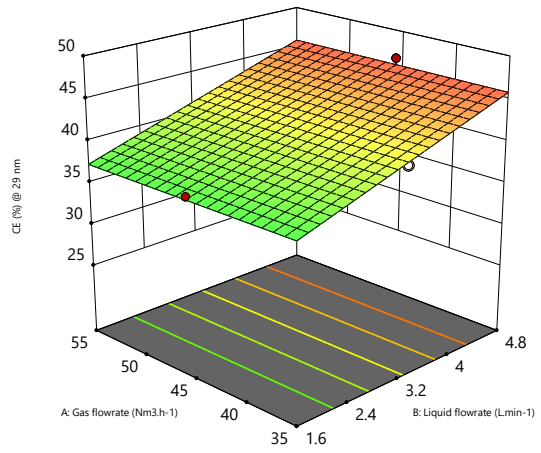
## Response $Y_4$ @ 29 nm



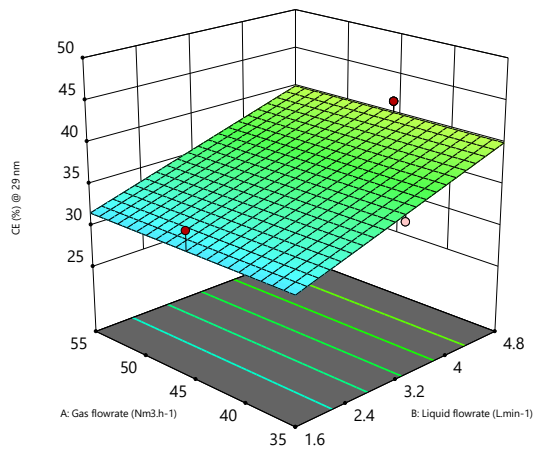
(a1) C:Droplet (60 μm)



(b1) C:Droplet (80 μm)



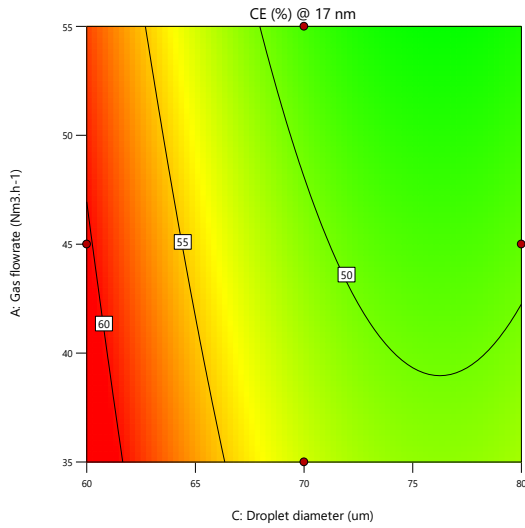
(a2) C:Droplet (60 μm)



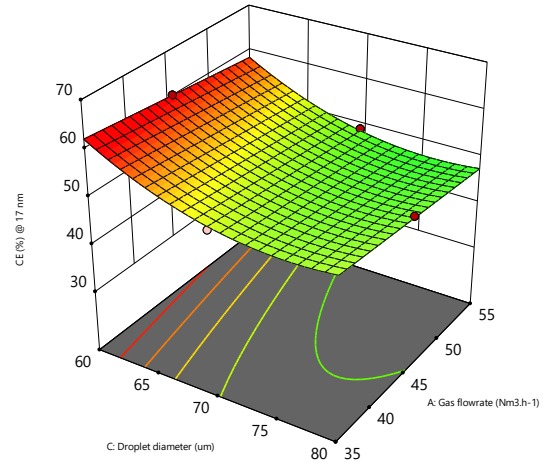
(b2) C:Droplet (80 μm)

**Annex 3-1b: Counter and response surface plots showing the influence of factors A and C at constant B (a:4.8 and b:1.6 L.min<sup>-1</sup>)**

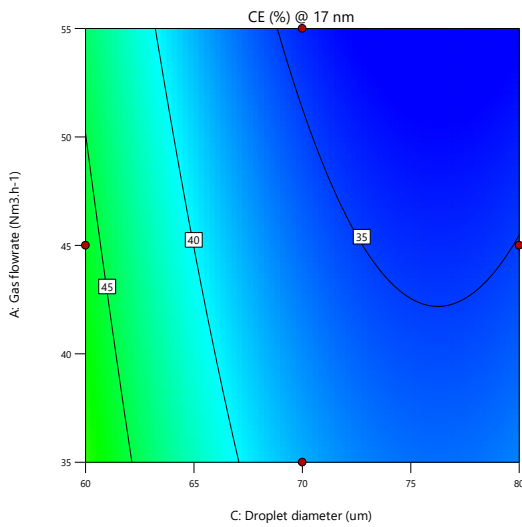
**Response Y<sub>1</sub> @ 17 nm**



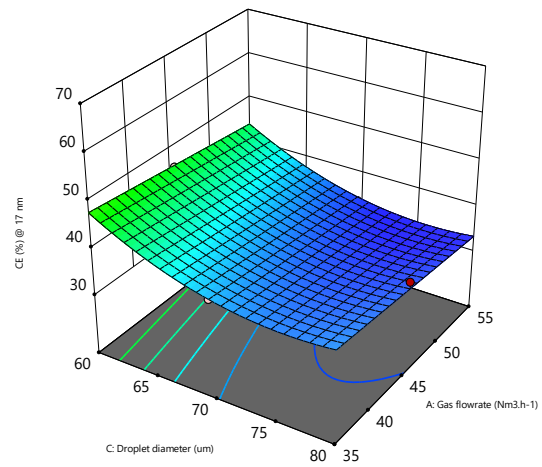
(a1) B: Liquid flowrate (4.8 L.min<sup>-1</sup>)



(a2) B: Liquid flowrate (4.8 L.min<sup>-1</sup>)

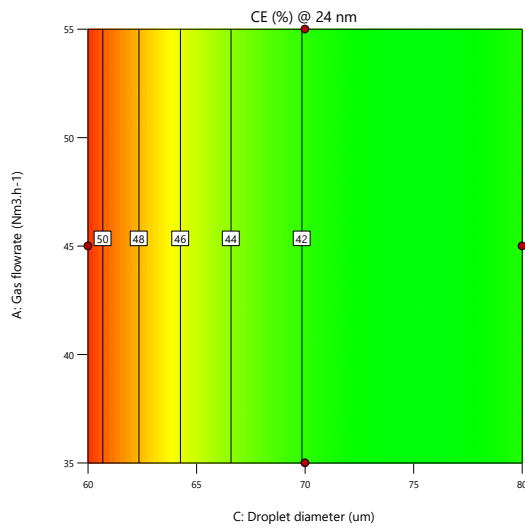


(b1) B: Liquid flowrate (1.6 L.min<sup>-1</sup>)

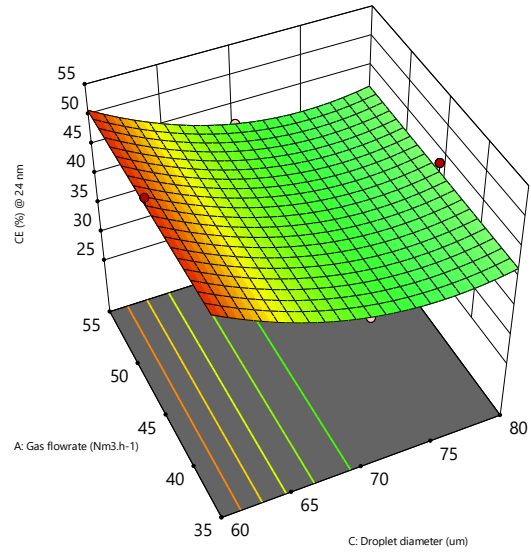


(b2) B: Liquid flowrate (1.6 L.min<sup>-1</sup>)

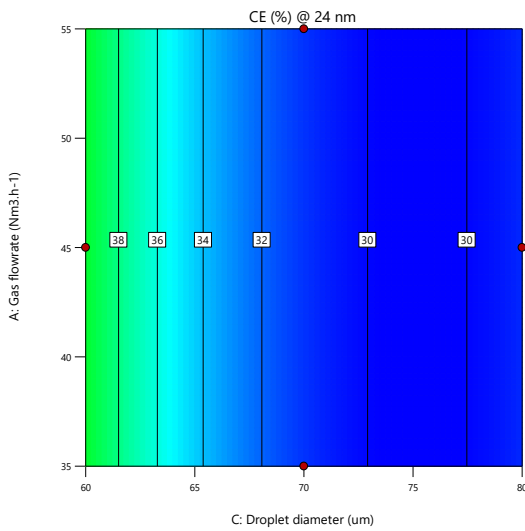
**Response  $Y_3$  @ 24 nm**



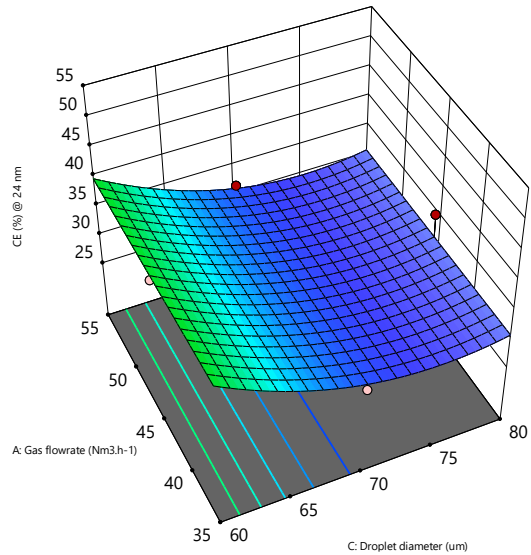
(a1) B: Liquid flowrate (4.8 L.min<sup>-1</sup>)



(a2) B: Liquid flowrate (4.8 L.min<sup>-1</sup>)

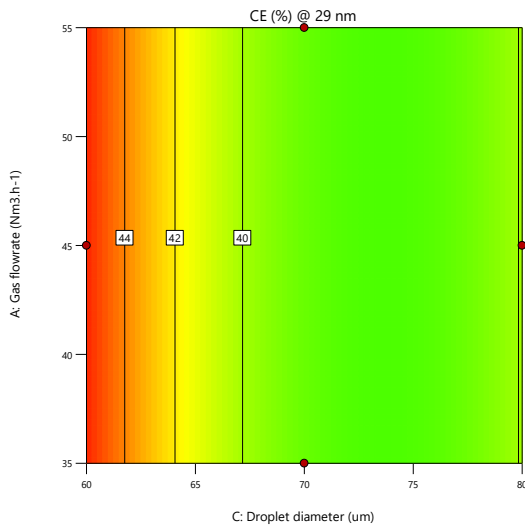


(b1) B: Liquid flowrate (1.6 L.min<sup>-1</sup>)

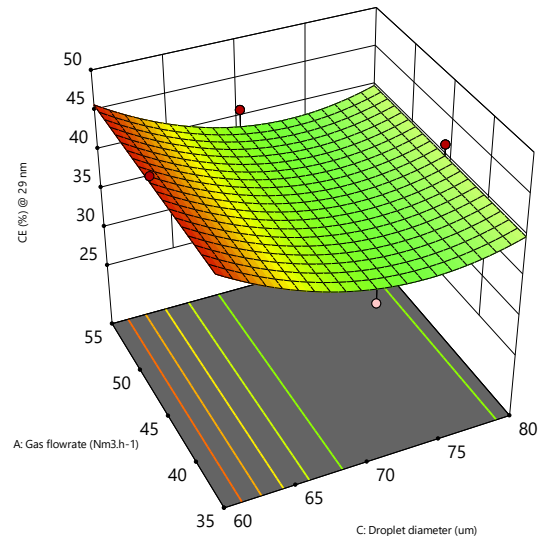


(b2) B: Liquid flowrate (1.6 L.min<sup>-1</sup>)

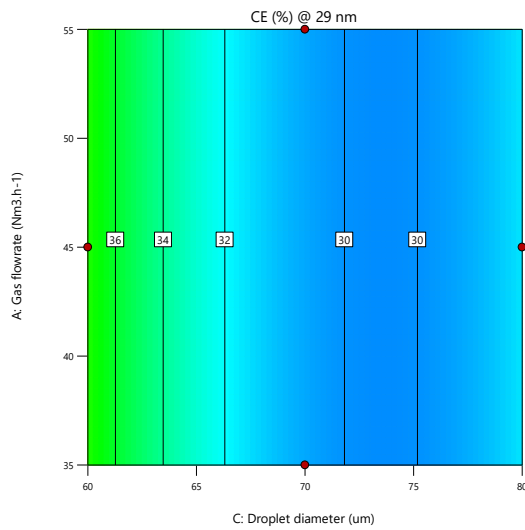
**Response Y<sub>4</sub> @ 29 nm**



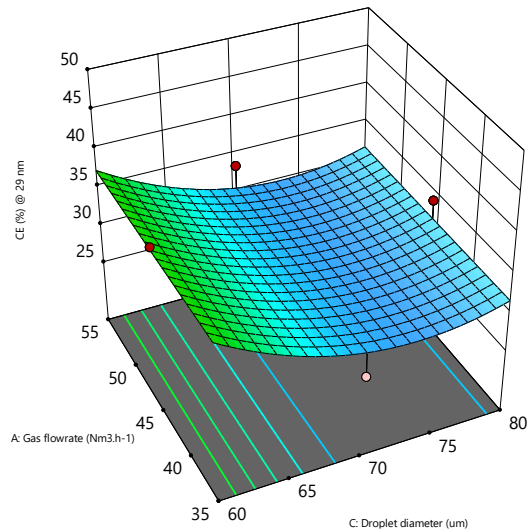
(a1) B: Liquid flowrate (4.8 L.min<sup>-1</sup>)



(a2) B: Liquid flowrate (4.8 L.min<sup>-1</sup>)



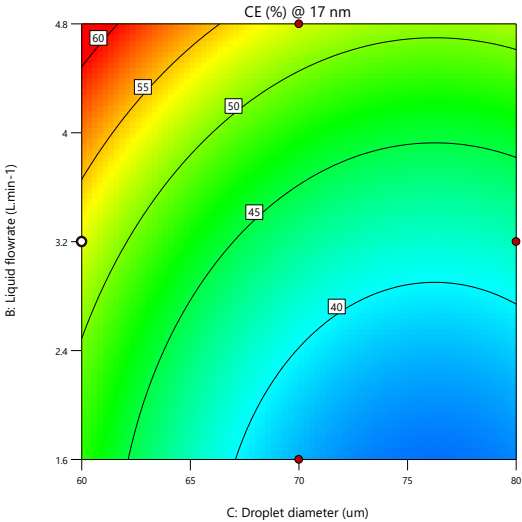
(b1) B: Liquid flowrate (1.6 L.min<sup>-1</sup>)



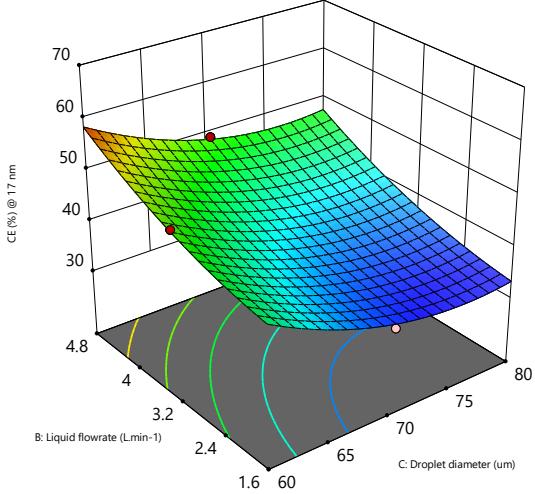
(b2) B: Liquid flowrate (1.6 L.min<sup>-1</sup>)

**Annex 3-1C: Counter and response surface plots showing the influence of factors B and C at constant A (a: 35 Nm<sup>3</sup>.h<sup>-1</sup> and b: 55 Nm<sup>3</sup>.h<sup>-1</sup>)**

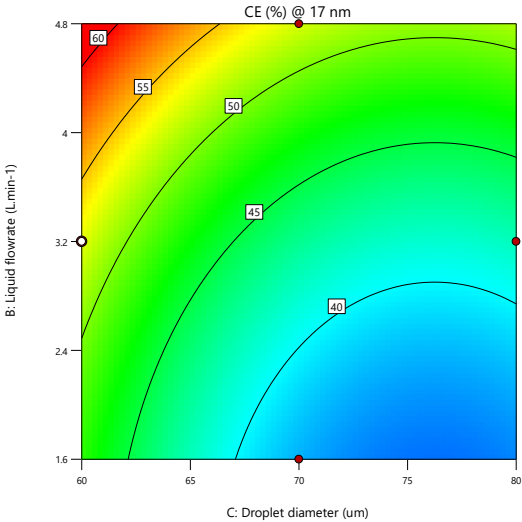
**Response Y<sub>1</sub> @ 17 nm**



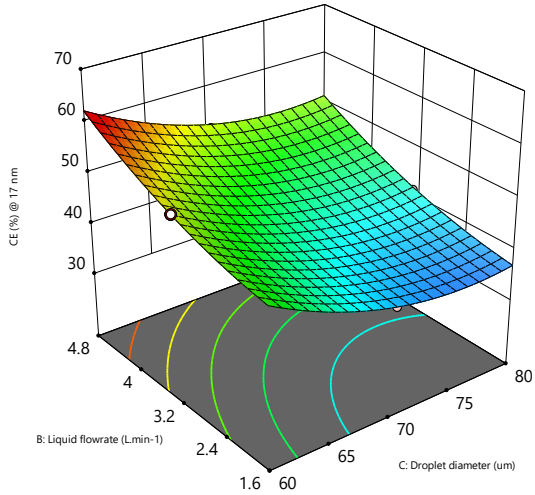
(a1) A: Gas flowrate (55 Nm<sup>3</sup>.h<sup>-1</sup>)



(a2) A: Gas flowrate (55 Nm<sup>3</sup>.h<sup>-1</sup>)

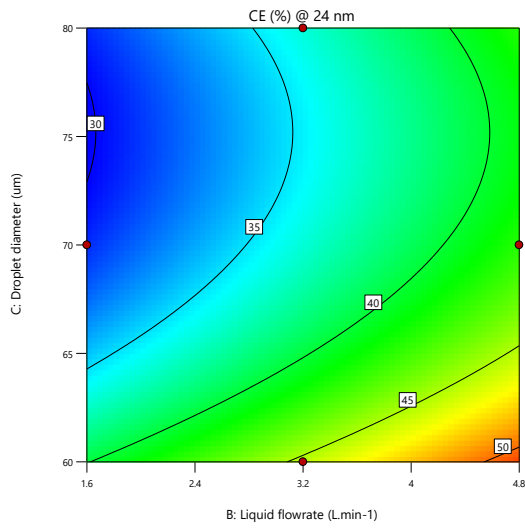


(b1): A: Gas flowrate (35 Nm<sup>3</sup>.h<sup>-1</sup>)

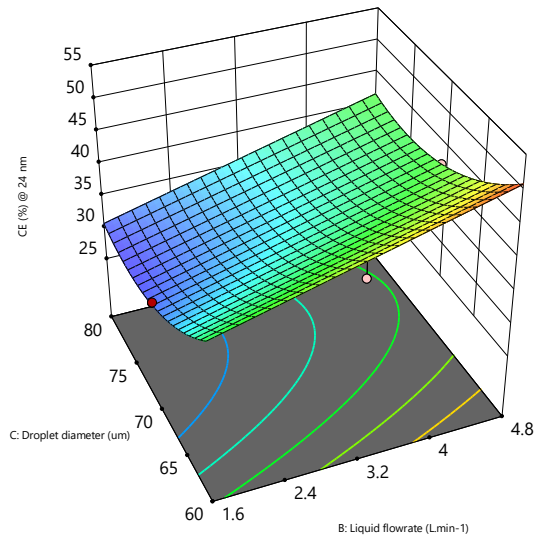


(b2) A: Gas flowrate (35 Nm<sup>3</sup>.h<sup>-1</sup>)

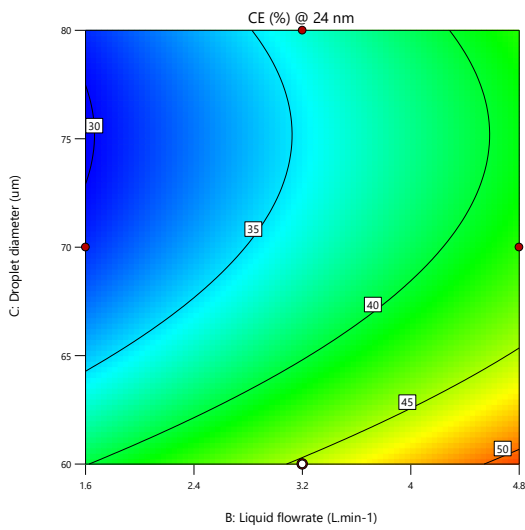
**Response  $Y_3$  @ 24 nm**



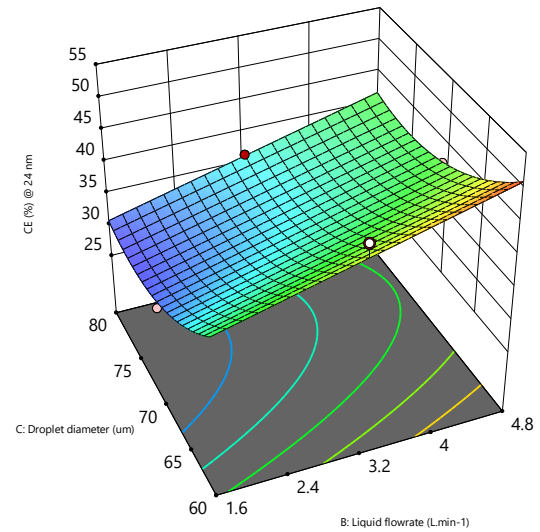
**(a1) A: Gas flowrate ( $55 \text{ Nm}^3 \cdot \text{h}^{-1}$ )**



**(a1) A: Gas flowrate ( $55 \text{ Nm}^3 \cdot \text{h}^{-1}$ )**

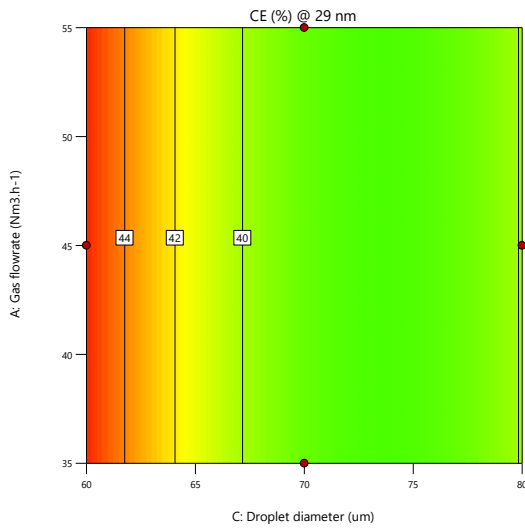


**(b1) A: Gas flowrate ( $35 \text{ Nm}^3 \cdot \text{h}^{-1}$ )**

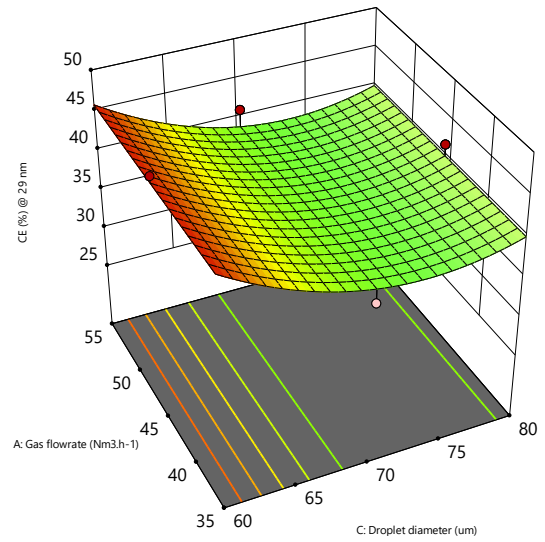


**(b2) A: Gas flowrate ( $35 \text{ Nm}^3 \cdot \text{h}^{-1}$ )**

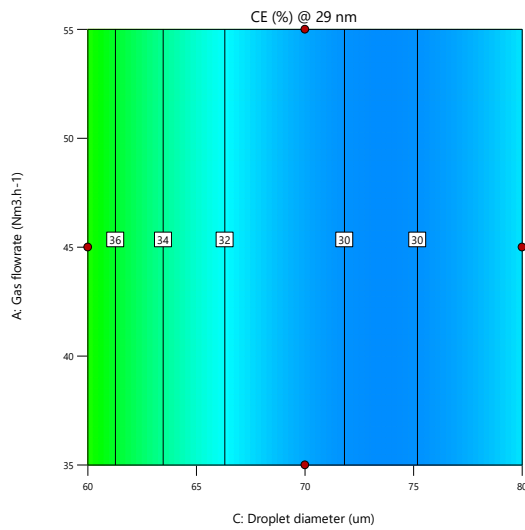
**Response Y<sub>4</sub> @ 29 nm**



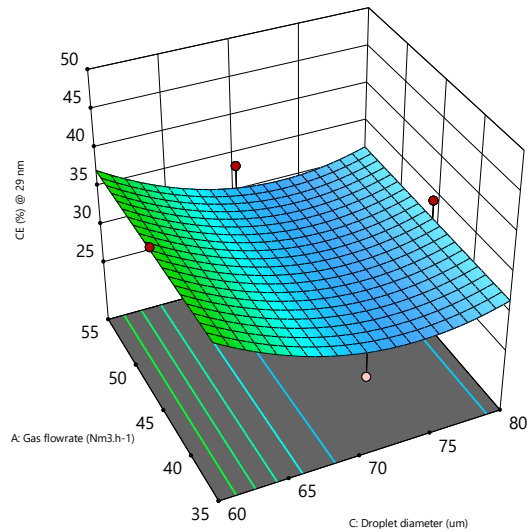
(a1) B: Liquid flowrate (4.8 L.min<sup>-1</sup>)



(a2) B: Liquid flowrate (4.8 L.min<sup>-1</sup>)



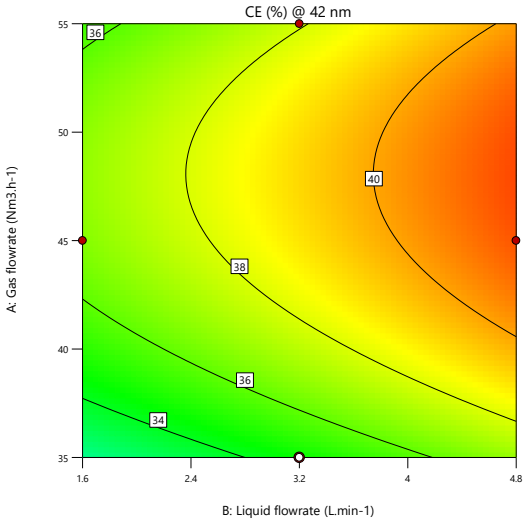
(b1) B: Liquid flowrate (1.6 L.min<sup>-1</sup>)



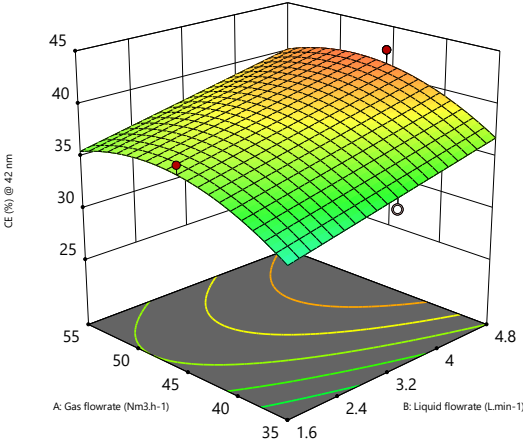
(b2) B: Liquid flowrate (1.6 L.min<sup>-1</sup>)

**Annex 3-2a: Counter and response surface plots showing the influence of factors A and B at constant C (a:60 and b:80 μm)**

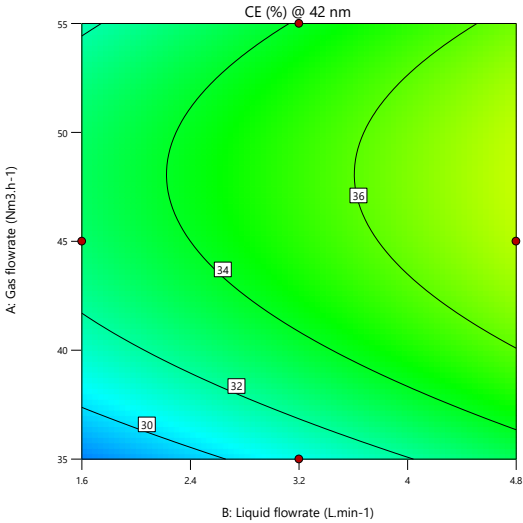
**Response Y<sub>6</sub> @ 42 nm**



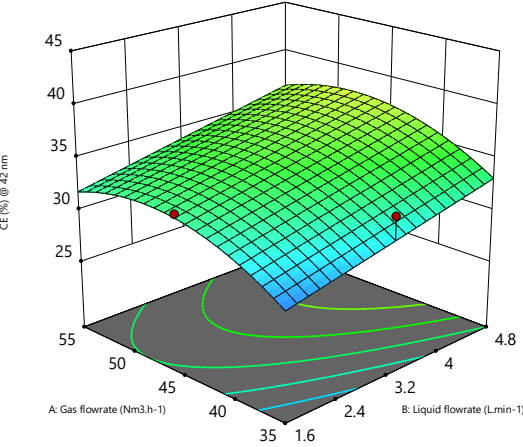
(a1) C: Droplet (60 μm)



(a2) C: Droplet (60 μm)



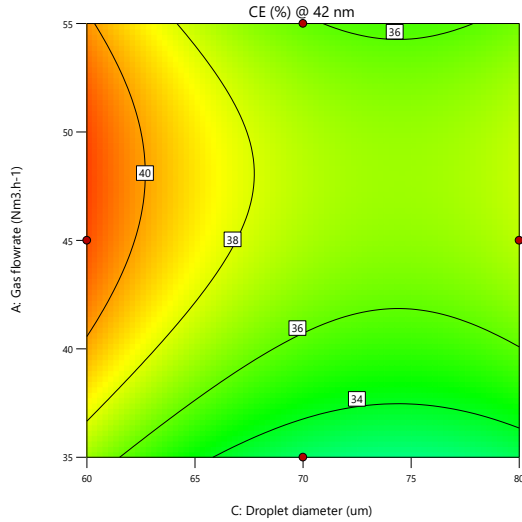
(b1) C: Droplet (80 μm)



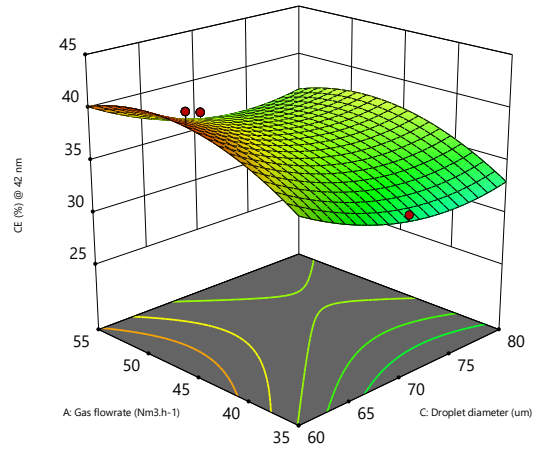
(b2) C: Droplet (80 μm)

**Annex 3-2b: Counter and response surface plots showing the influence of factors A and C at constant B (a:4.8 and b:1.6 L.min<sup>-1</sup>)**

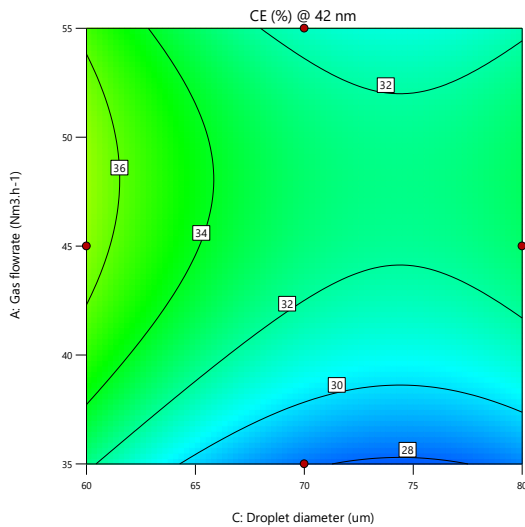
**Response Y<sub>6</sub> @ 42 nm**



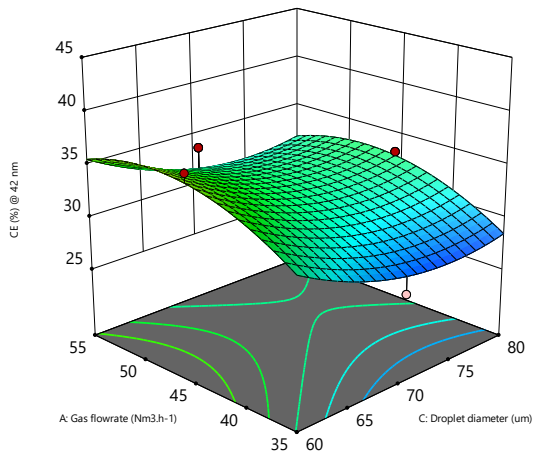
(a1) B: Liquid flowrate (4.8 L.min<sup>-1</sup>)



(a2) B: Liquid flowrate (4.8 L.min<sup>-1</sup>)



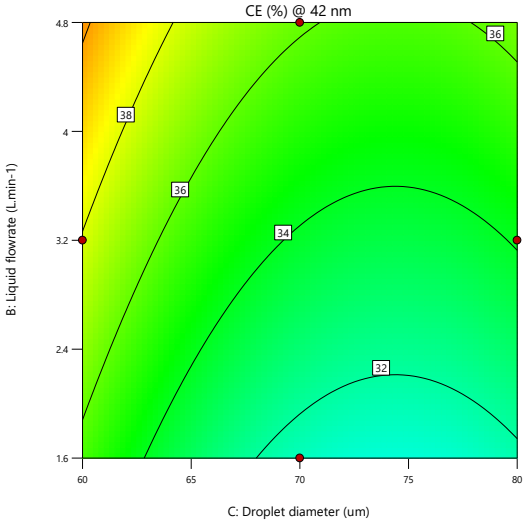
(b1) B: Liquid flowrate (1.6 L.min<sup>-1</sup>)



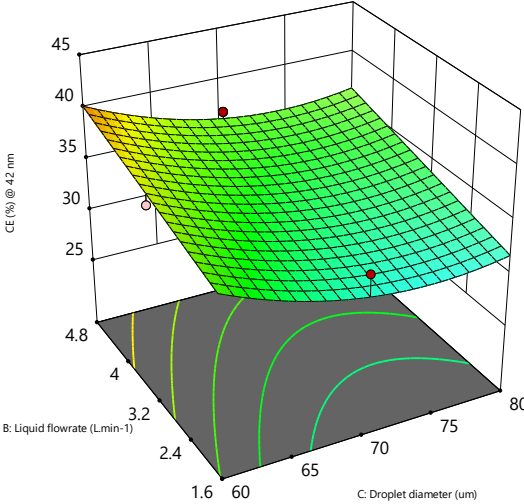
(b2) B: Liquid flowrate (1.6 L.min<sup>-1</sup>)

**Annex 3-2C: Counter and response surface plots showing the influence of factors B and C at constant A (a: 35 Nm<sup>3</sup>.h<sup>-1</sup> and b: 55 Nm<sup>3</sup>.h<sup>-1</sup>)**

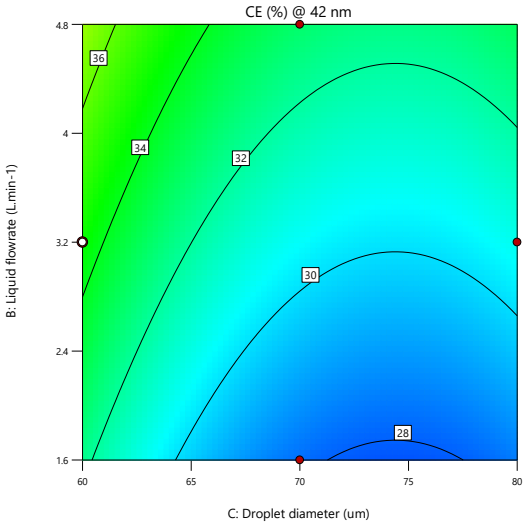
**Response Y<sub>6</sub> @ 42 nm**



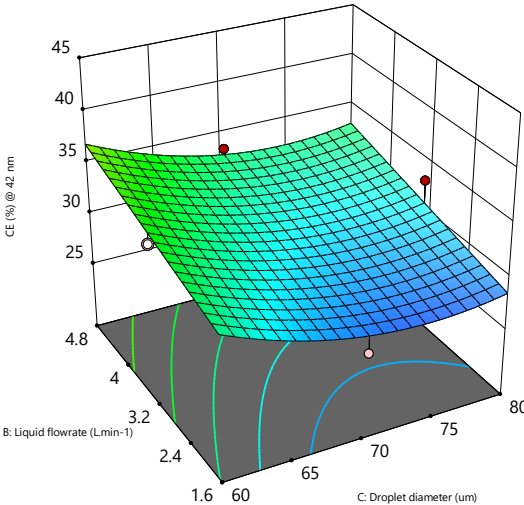
(a1) A: Gas flowrate (55 Nm<sup>3</sup>.h<sup>-1</sup>)



(a2) A: Gas flowrate (55 Nm<sup>3</sup>.h<sup>-1</sup>)



(b1) A: Gas flowrate (35 Nm<sup>3</sup>.h<sup>-1</sup>)

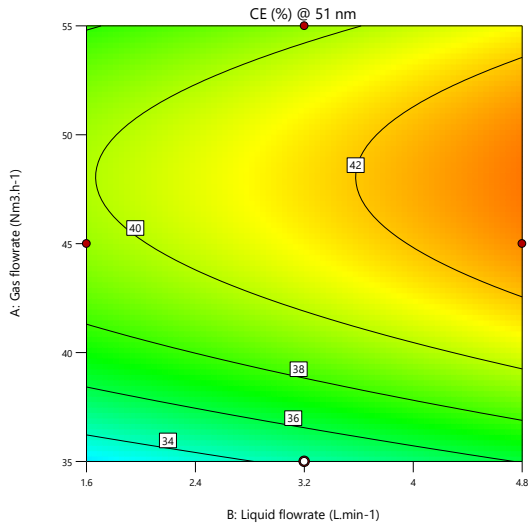


(b2)

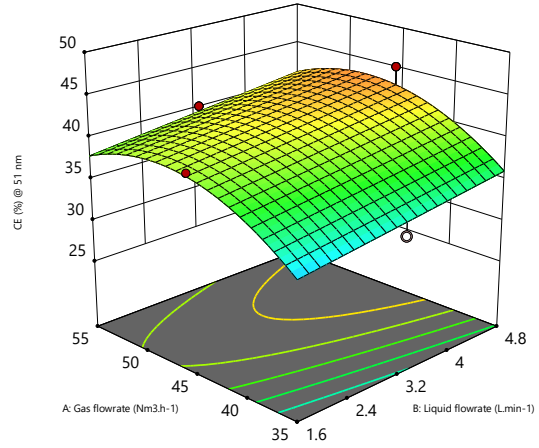
A: Gas flowrate (35 Nm<sup>3</sup>.h<sup>-1</sup>)

**Annex 3-3a: Counter and response surface plots showing the influence of factors A and B at constant C (a:60 and b:80  $\mu\text{m}$ )**

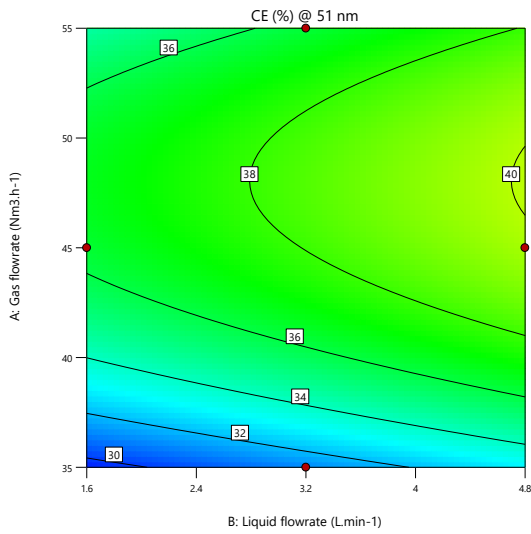
**Response  $Y_7$  @ 51 nm**



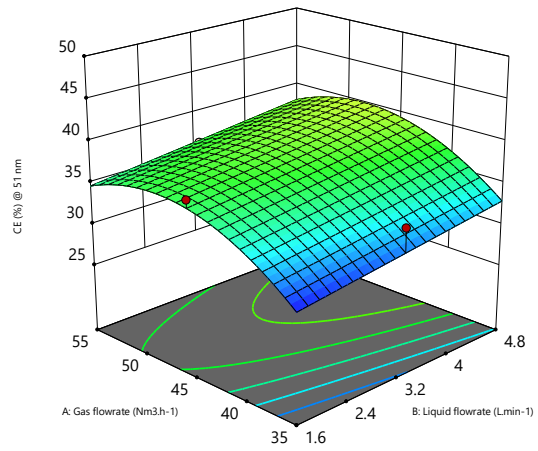
(a1) C: Droplet (60  $\mu\text{m}$ )



(a2) C: Droplet (60  $\mu\text{m}$ )



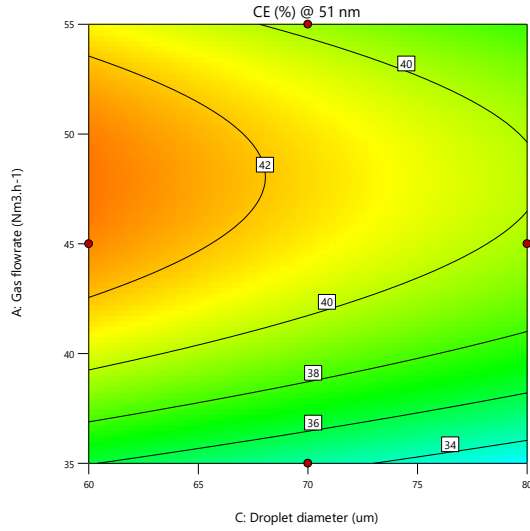
(b1) C: Droplet (80  $\mu\text{m}$ )



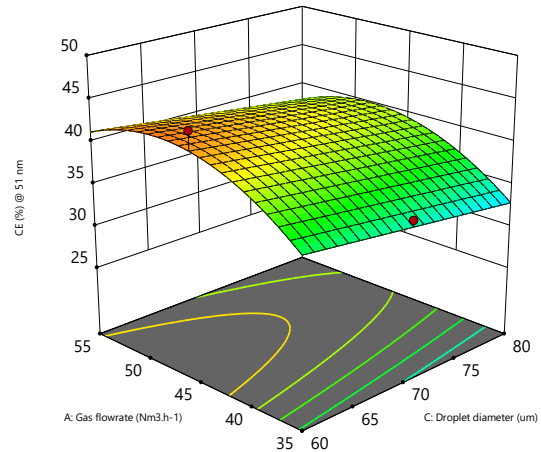
(b2) C: Droplet (80  $\mu\text{m}$ )

**Annex 3-3b: Counter and response surface plots showing the influence of factors A and C at constant B (a:4.8 and b:1.6 L.min<sup>-1</sup>)**

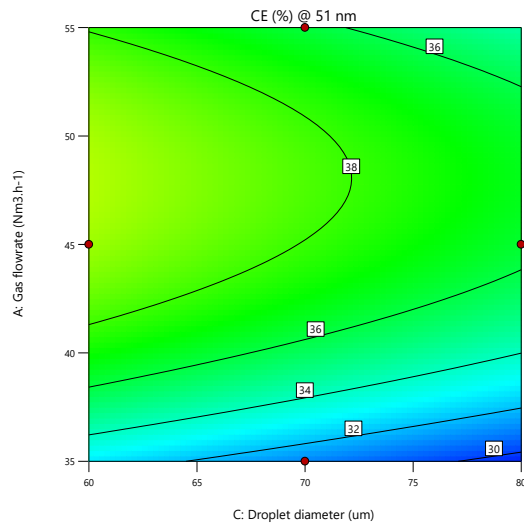
**Response Y<sub>7</sub> @ 51 nm**



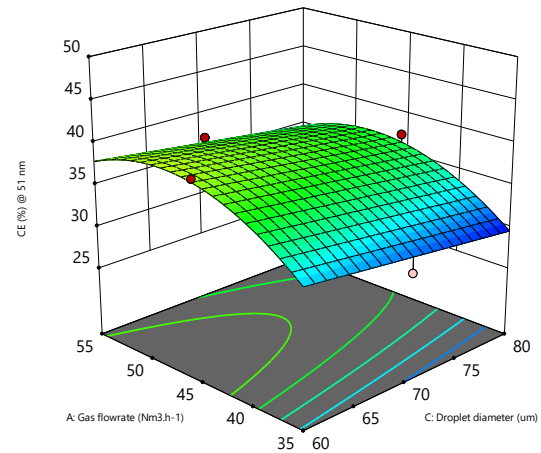
(a1) B: Liquid flowrate (4.8 L.min<sup>-1</sup>)



(a2) B: Liquid flowrate (4.8 L.min<sup>-1</sup>)



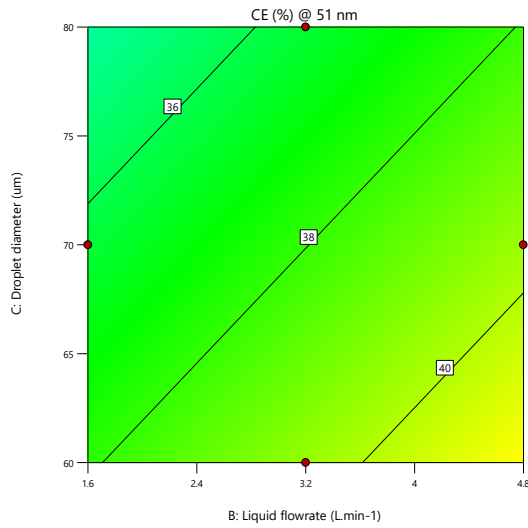
(b1) B: Liquid flowrate (1.6 L.min<sup>-1</sup>)



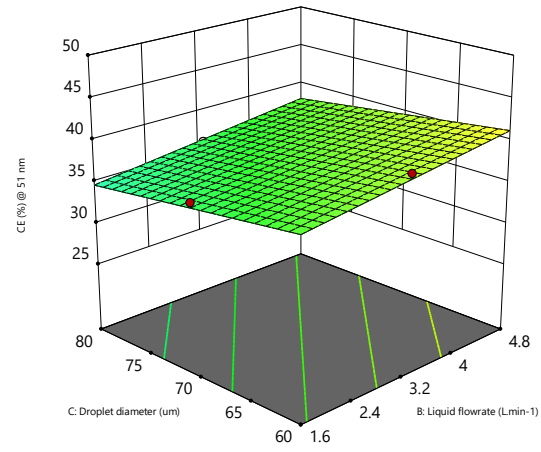
(b2) B: Liquid flowrate (1.6 L.min<sup>-1</sup>)

**Annex 3-3C: Counter and response surface plots showing the influence of factors B and C at constant A (a: 35 Nm<sup>3</sup>.h<sup>-1</sup> and b: 55 Nm<sup>3</sup>.h<sup>-1</sup>)**

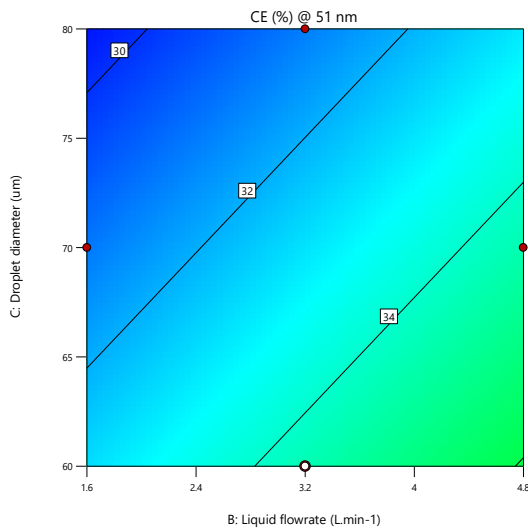
**Response Y<sub>7</sub> @ 51 nm**



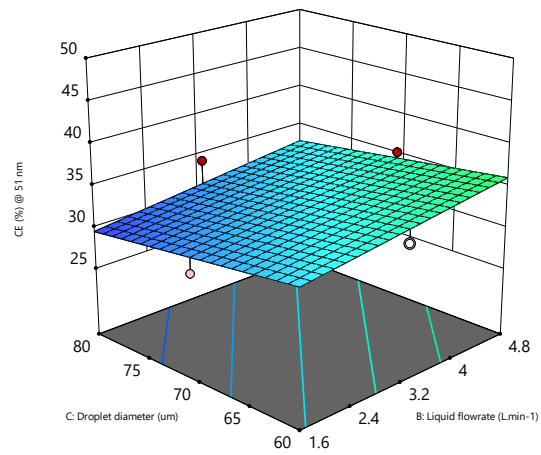
(a1) A: Gas flowrate (55 Nm<sup>3</sup>.h<sup>-1</sup>)



(a2) A: Gas flowrate (55 Nm<sup>3</sup>.h<sup>-1</sup>)



(b1) A: Gas flowrate (35 Nm<sup>3</sup>.h<sup>-1</sup>)



(b2) A: Gas flowrate (35 Nm<sup>3</sup>.h<sup>-1</sup>)

**Annex 3-4a: Full and Reduced ANOVA for responses Y<sub>1</sub> (@ 17 nm), Y<sub>3</sub> (@ 24 nm), Y<sub>4</sub> (@ 29 nm), Y<sub>6</sub> (@ 42 nm) and Y<sub>7</sub> (@ 51 nm)**

**Full Anova - Response Y<sub>1</sub> @ 17 nm**

<b>Source</b>	<b>Sum of Squares</b>	<b>df</b>	<b>Mean Square</b>	<b>F-value</b>	<b>p-value</b>
<b>Model</b>	789.17	9	87.69	28.88	0.0001 significant
A-Gas flowrate	27.75	1	27.75	9.14	0.0193
B-Liquid flowrate	414.72	1	414.72	136.58	< 0.0001
C-Droplet diameter	236.53	1	236.53	77.90	< 0.0001
AB	1.0000	1	1.0000	0.3293	0.5840
AC	0.2025	1	0.2025	0.0667	0.8036
BC	0.6400	1	0.6400	0.2108	0.6601
A <sup>2</sup>	1.61	1	1.61	0.5288	0.4907
B <sup>2</sup>	22.42	1	22.42	7.38	0.0299
C <sup>2</sup>	80.87	1	80.87	26.63	0.0013
<b>Residual</b>	21.25	7	3.04		
Lack of Fit	2.52	3	0.8408	0.1796	0.9051 not significant
Pure Error	18.73	4	4.68		
<b>Cor Total</b>	810.42	16			
<b>Std. Dev.</b>	1.74			<b>R<sup>2</sup> 0,9738</b>	
<b>Mean</b>	44.22			<b>Adjusted R<sup>2</sup> 0,9401</b>	
<b>C.V. %</b>	3.94			<b>Predicted R<sup>2</sup> 0,9141</b>	
				<b>Adeq Precision 20,6518</b>	

Reduced Anova - Response Y<sub>1</sub> @ 17 nm

Source	Sum of Squares	df	Mean Square	F-value	p-value
<b>Model</b>	785.72	5	157.14	69.98	< 0.0001 significant
A-Gas flowrate	27.75	1	27.75	12.36	0.0048
B-Liquid flowrate	414.72	1	414.72	184.67	< 0.0001
C-Droplet diameter	236.53	1	236.53	105.33	< 0.0001
B <sup>2</sup>	21.85	1	21.85	9.73	0.0098
C <sup>2</sup>	79.89	1	79.89	35.58	< 0.0001
<b>Residual</b>	24.70	11	2.25		
Lack of Fit	5.97	7	0.8529	0.1821	0.9746 not significant
Pure Error	18.73	4	4.68		
<b>Cor Total</b>	810.42	16			
<b>Std. Dev.</b>	1.50	<b>R<sup>2</sup></b>	0.9695		
<b>Mean</b>	44.22	<b>Adjusted R<sup>2</sup></b>	0.9557		
<b>C.V. %</b>	3.39	<b>Predicted R<sup>2</sup></b>	0.9451		
		<b>Adeq Precision</b>	29.2605		

Full Anova - Response Y<sub>3</sub> @ 24 nm

Source	Sum of Squares	df	Mean Square	F-value	p-value
<b>Model</b>	521.02	9	57.89	12.22	0.0017 significant
A-Gas flowrate	9.24	1	9.24	1.95	0.2051
B-Liquid flowrate	240.90	1	240.90	50.86	0.0002
C-Droplet diameter	166.53	1	166.53	35.16	0.0006
AB	0.4900	1	0.4900	0.1034	0.7571
AC	0.2500	1	0.2500	0.0528	0.8249
BC	5.06	1	5.06	1.07	0.3356
A <sup>2</sup>	10.95	1	10.95	2.31	0.1722
B <sup>2</sup>	6.71	1	6.71	1.42	0.2727
C <sup>2</sup>	81.98	1	81.98	17.31	0.0042
<b>Residual</b>	33.16	7	4.74		
Lack of Fit	29.76	3	9.92	11.67	0.0190 significant
Pure Error	3.40	4	0.8500		
<b>Cor Total</b>	554.18	16			
<b>Std. Dev.</b>	2.18			<b>R<sup>2</sup></b> 0.9402	
<b>Mean</b>	38.51			<b>Adjusted R<sup>2</sup></b> 0.8632	
<b>C.V. %</b>	5.65			<b>Predicted R<sup>2</sup></b> 0.1313	
				<b>Adeq Precision</b> 14.0259	

Reduced Anova - Response Y<sub>3</sub> @ 24 nm

---

<b>Source</b>	<b>Sum of Squares</b>	<b>df</b>	<b>Mean Square</b>	<b>F-value</b>	<b>p-value</b>
<b>Model</b>	489.17	3	163.06	32.61	< 0.0001 significant
B-Liquid flowrate	240.90	1	240.90	48.17	< 0.0001
C-Droplet diameter	166.53	1	166.53	33.30	< 0.0001
C <sup>2</sup>	81.74	1	81.74	16.35	0.0014
<b>Residual</b>	65.01	13	5.00		
Lack of Fit	61.61	9	6.85	8.05	0.0299 significant
Pure Error	3.40	4	0.8500		
<b>Cor Total</b>	554.18	16			
<b>Std. Dev.</b>	2.24			<b>R<sup>2</sup> 0.8827</b>	
<b>Mean</b>	38.51			<b>Adjusted R<sup>2</sup> 0.8556</b>	
<b>C.V. %</b>	5.81			<b>Predicted R<sup>2</sup> 0.7673</b>	
				<b>Adeq Precision 18.5301</b>	

---

Full Anova - Response Y<sub>4</sub> @ 29 nm

Source	Sum of Squares	df	Mean Square	F-value	p-value
<b>Model</b>	302.09	9	33.57	7.06	0.0087 significant
A-Gas flowrate	7.22	1	7.22	1.52	0.2577
B-Liquid flowrate	143.65	1	143.65	30.20	0.0009
C-Droplet diameter	65.55	1	65.55	13.78	0.0075
AB	1.32	1	1.32	0.2780	0.6143
AC	0.7225	1	0.7225	0.1519	0.7083
BC	0.4900	1	0.4900	0.1030	0.7576
A <sup>2</sup>	5.96	1	5.96	1.25	0.2998
B <sup>2</sup>	6.95	1	6.95	1.46	0.2659
C <sup>2</sup>	70.26	1	70.26	14.77	0.0063
<b>Residual</b>	33.30	7	4.76		
Lack of Fit	23.51	3	7.84	3.20	0.1452 not significant
Pure Error	9.79	4	2.45		
<b>Cor Total</b>	335.38	16			
<b>Std. Dev.</b>	2.18			<b>R<sup>2</sup></b> 0.9007	
<b>Mean</b>	36.55			<b>Adjusted R<sup>2</sup></b> 0.7731	
<b>C.V. %</b>	5.97			<b>Predicted R<sup>2</sup></b> -0.1671	
				<b>Adeq Precision</b> 11.0525	

Reduced Anova - Response Y<sub>4</sub> @ 29 nm

---

<b>Source</b>	<b>Sum of Squares</b>	<b>df</b>	<b>Mean Square</b>	<b>F-value</b>	<b>p-value</b>
<b>Model</b>	280.06	3	93.35	21.94	< 0.0001 significant
B-Liquid flowrate	143.65	1	143.65	33.76	< 0.0001
C-Droplet diameter	65.55	1	65.55	15.40	0.0017
C <sup>2</sup>	70.86	1	70.86	16.65	0.0013
<b>Residual</b>	55.32	13	4.26		
Lack of Fit	45.53	9	5.06	2.07	0.2521 not significant
Pure Error	9.79	4	2.45		
<b>Cor Total</b>	335.38	16			
<b>Std. Dev.</b>	2.06			<b>R<sup>2</sup> 0.8350</b>	
<b>Mean</b>	36.55			<b>Adjusted R<sup>2</sup> 0.7970</b>	
<b>C.V. %</b>	5.64			<b>Predicted R<sup>2</sup> 0.7072</b>	
				<b>Adeq Precision 15.4178</b>	

---

Full Anova - Response Y<sub>6</sub> @ 42 nm

Source	Sum of Squares	df	Mean Square	F-value	p-value
<b>Model</b>	152.18	9	16.91	7.69	0.0068 significant
A-Gas flowrate	22.11	1	22.11	10.05	0.0157
B-Liquid flowrate	42.78	1	42.78	19.45	0.0031
C-Droplet diameter	28.88	1	28.88	13.13	0.0085
AB	3.42	1	3.42	1.56	0.2524
AC	3.61	1	3.61	1.64	0.2410
BC	0.8100	1	0.8100	0.3682	0.5632
A <sup>2</sup>	31.90	1	31.90	14.50	0.0066
B <sup>2</sup>	2.35	1	2.35	1.07	0.3355
C <sup>2</sup>	18.97	1	18.97	8.62	0.0218
<b>Residual</b>	15.40	7	2.20		
Lack of Fit	11.69	3	3.90	4.20	0.0995 not significant
Pure Error	3.71	4	0.9270		
<b>Cor Total</b>	167.58	16			
<b>Std. Dev.</b>	1.48			<b>R<sup>2</sup></b> 0.9081	
<b>Mean</b>	34.64			<b>Adjusted R<sup>2</sup></b> 0.7899	
<b>C.V. %</b>	4.28			<b>Predicted R<sup>2</sup></b> -0.1509	
				<b>Adeq Precision</b> 12.6911	

Reduced Anova - Response Y<sub>6</sub> @ 42 nm

<b>Source</b>	<b>Sum of Squares</b>	<b>df</b>	<b>Mean Square</b>	<b>F-value</b>	<b>p-value</b>
<b>Model</b>	141.98	5	28.40	12.20	0.0003 significant
A-Gas flowrate	22.11	1	22.11	9.50	0.0104
B-Liquid flowrate	42.78	1	42.78	18.39	0.0013
C-Droplet diameter	28.88	1	28.88	12.41	0.0048
A <sup>2</sup>	31.08	1	31.08	13.36	0.0038
C <sup>2</sup>	19.73	1	19.73	8.48	0.0141
<b>Residual</b>	25.60	11	2.33		
Lack of Fit	21.89	7	3.13	3.37	0.1286 not significant
Pure Error	3.71	4	0.9270		
<b>Cor Total</b>	167.58	16			
<b>Std. Dev.</b>	1.53		<b>R<sup>2</sup> 0.8473</b>		
<b>Mean</b>	34.64		<b>Adjusted R<sup>2</sup> 0.7778</b>		
<b>C.V. %</b>	4.40		<b>Predicted R<sup>2</sup> 0.5659</b>		
			<b>Adeq Precision 14.4141</b>		

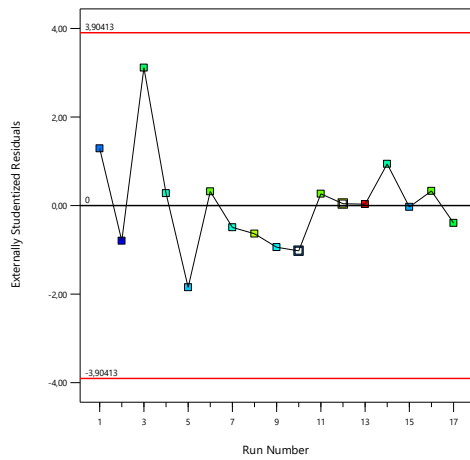
Full Anova - Response Y<sub>7</sub> @ 51 nm

Source	Sum of Squares	df	Mean Square	F-value	p-value
<b>Model</b>	192.08	9	21.34	12.97	0.0014 significant
A-Gas flowrate	53.56	1	53.56	32.56	0.0007
B-Liquid flowrate	22.45	1	22.45	13.64	0.0077
C-Droplet diameter	20.16	1	20.16	12.26	0.0100
AB	4.41	1	4.41	2.68	0.1456
AC	7.56	1	7.56	4.60	0.0692
BC	5.76	1	5.76	3.50	0.1035
A <sup>2</sup>	76.86	1	76.86	46.72	0.0002
B <sup>2</sup>	0.0095	1	0.0095	0.0058	0.9416
C <sup>2</sup>	2.23	1	2.23	1.35	0.2826
<b>Residual</b>	11.52	7	1.65		
Lack of Fit	7.63	3	2.54	2.62	0.1879 not significant
Pure Error	3.89	4	0.9720		
<b>Cor Total</b>	203.60	16			
<b>Std. Dev.</b>	1.28			<b>R<sup>2</sup></b> 0.9434	
<b>Mean</b>	37.63			<b>Adjusted R<sup>2</sup></b> 0.8707	
<b>C.V. %</b>	3.41			<b>Predicted R<sup>2</sup></b> 0.3707	
				<b>Adeq Precision</b> 15.0196	

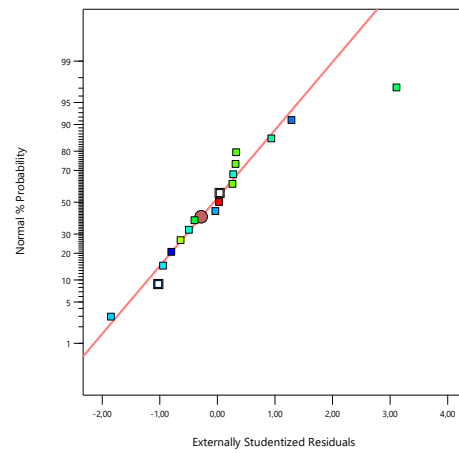
Reduced Anova - Response Y<sub>7</sub> @ 51 nm

<b>Source</b>	<b>Sum of Squares</b>	<b>df</b>	<b>Mean Square</b>	<b>F-value</b>	<b>p-value</b>
<b>Model</b>	172.12	4	43.03	16.40	< 0.0001 significant
A-Gas flowrate	53.56	1	53.56	20.42	0.0007
B-Liquid flowrate	22.45	1	22.45	8.56	0.0127
C-Droplet diameter	20.16	1	20.16	7.69	0.0169
A <sup>2</sup>	75.95	1	75.95	28.96	0.0002
<b>Residual</b>	31.48	12	2.62		
Lack of Fit	27.59	8	3.45	3.55	0.1183 not significant
Pure Error	3.89	4	0.9720		
<b>Cor Total</b>	203.60	16			
<b>Std. Dev.</b>	1.62			<b>R<sup>2</sup> 0.8454</b>	
<b>Mean</b>	37.63			<b>Adjusted R<sup>2</sup> 0.7939</b>	
<b>C.V. %</b>	4.30			<b>Predicted R<sup>2</sup> 0.6372</b>	
				<b>Adeq Precision 13.3885</b>	

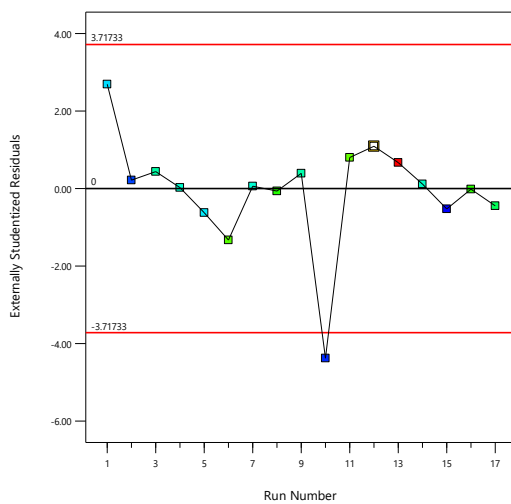
**Annex 3-4b: Diagnostic plots for responses  $Y_1$  (@ 17 nm),  $Y_3$  (@ 24 nm),  $Y_4$  (@ 29 nm),  $Y_6$  (@ 42 nm) and  $Y_7$  (@ 51 nm)**



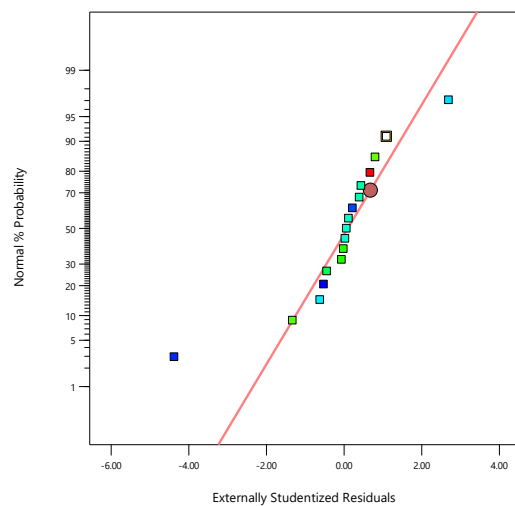
a)  $Y_1$  @ 17 nm



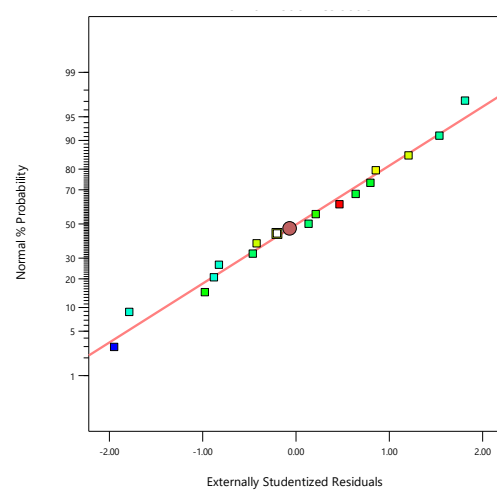
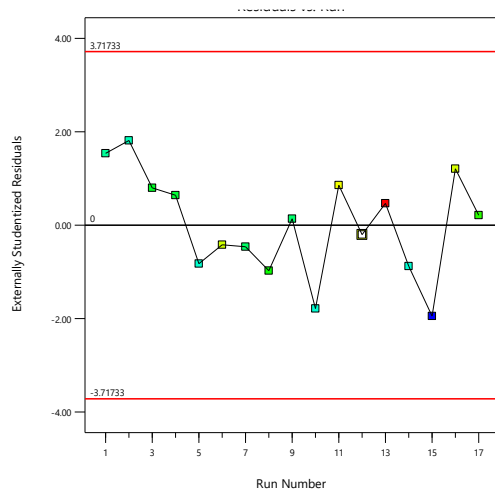
b)  $Y_1$  @ 17 nm



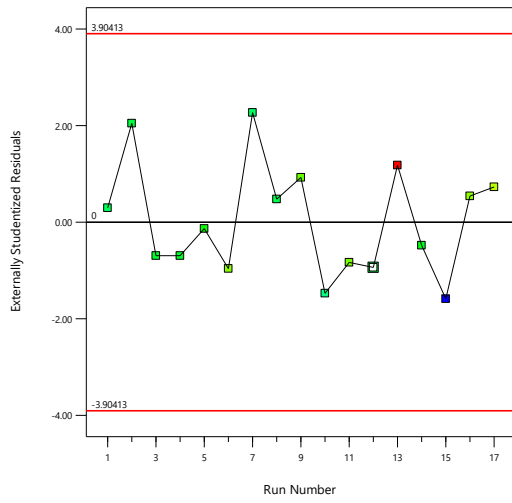
a)  $Y_3$  @ 24 nm



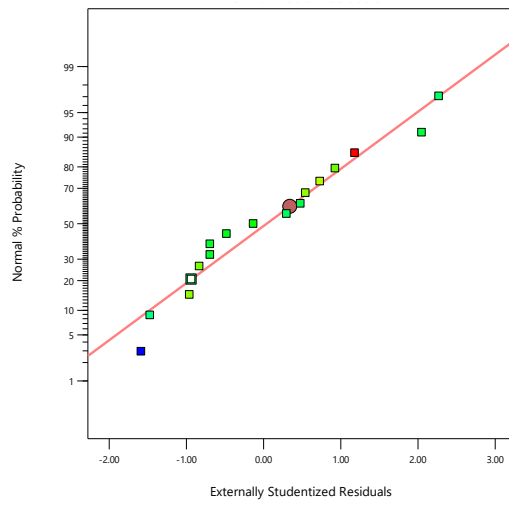
b)  $Y_3$  @ 24 nm



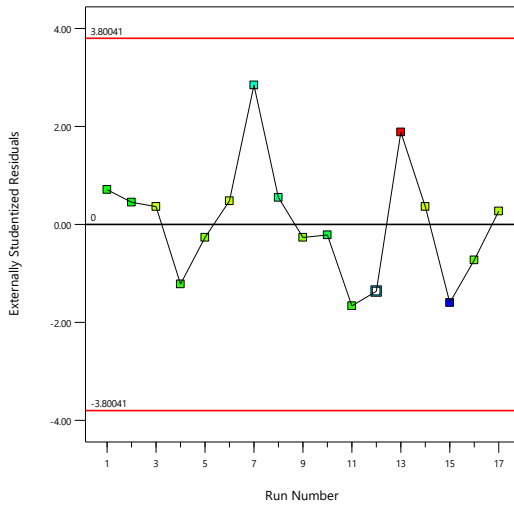
a) Y<sub>4</sub> @ 29 nm



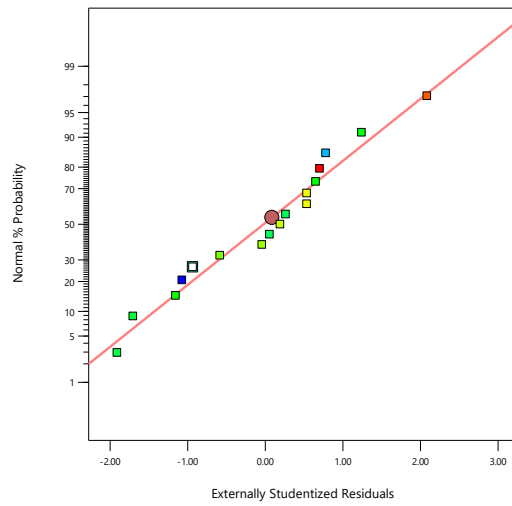
b) Y<sub>4</sub> @ 29 nm



a) Y<sub>6</sub> @ 42 nm



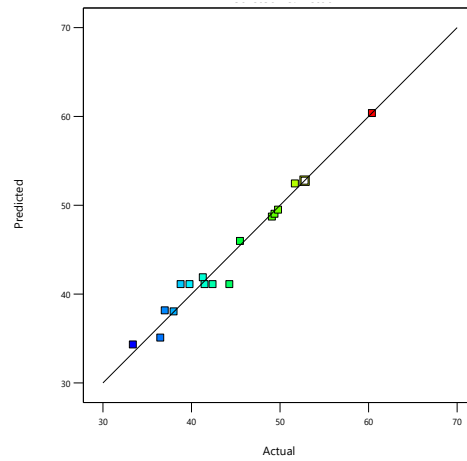
b) Y<sub>6</sub> @ 42 nm



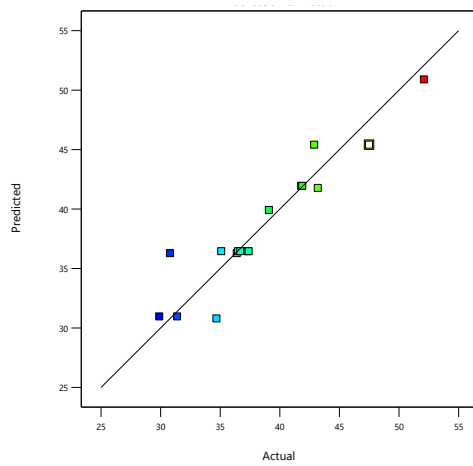
a) Y<sub>7</sub> @ 51 nm

b) Y<sub>7</sub> @ 51 nm

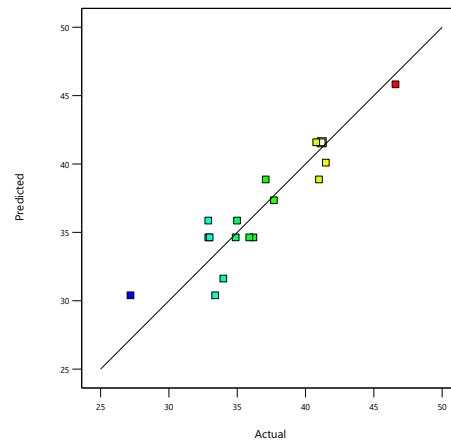
**Annex 3-4c: Experimental (Actual) particle removal efficiency versus Predicted particle removal efficiency for responses  $Y_1$  (@ 17 nm),  $Y_3$  (@ 24 nm),  $Y_4$  (@ 29 nm),  $Y_6$  (@ 42 nm) and  $Y_7$  (@ 51 nm)**



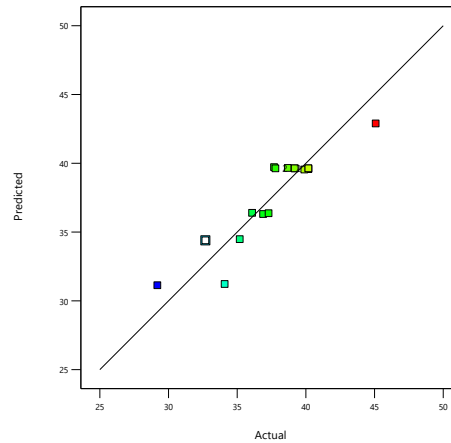
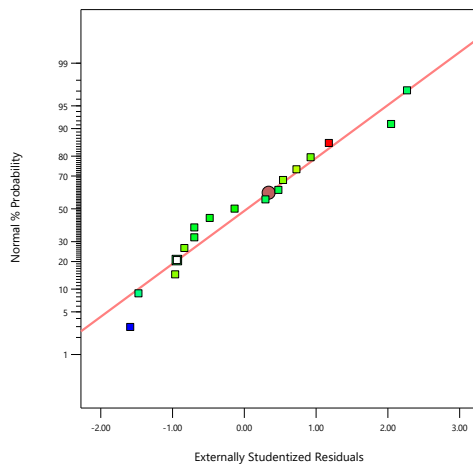
$Y_1$  @ 17 nm



$Y_3$  @ 24 nm



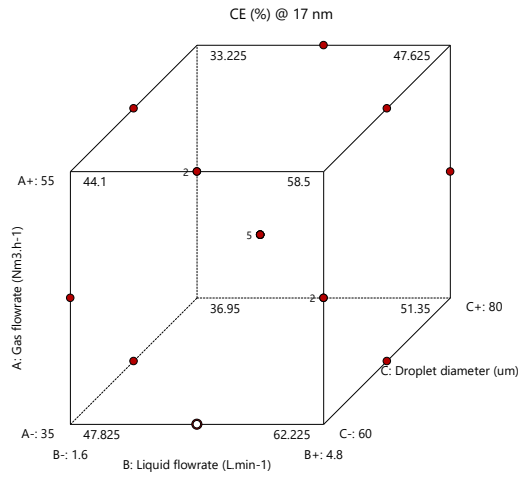
$Y_4$  @ 29 nm



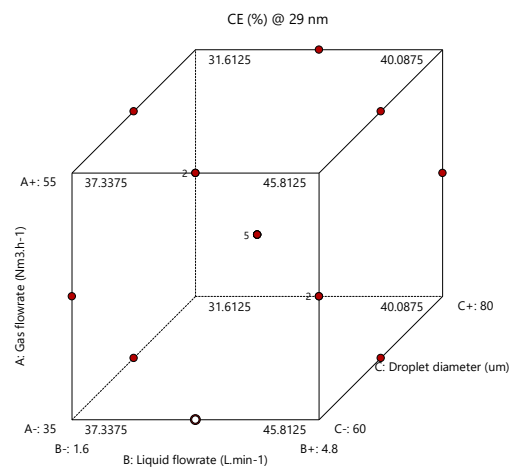
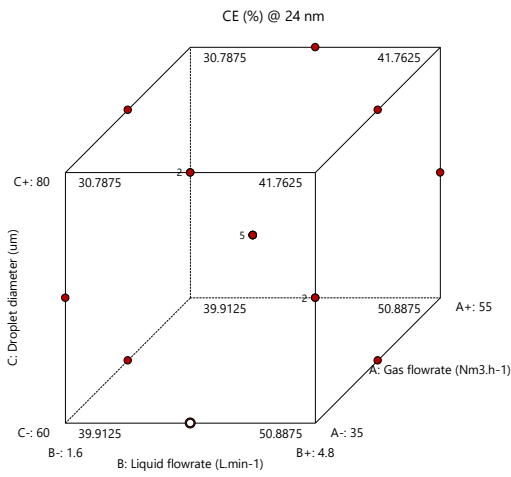
Y<sub>6</sub> @ 42 nm

Y<sub>7</sub> @ 51 nm

**Annex 3-4d: Individual response surfaces showing predicted collection efficiencies for responses Y<sub>1</sub> (@ 17 nm), Y<sub>3</sub> (@ 24 nm), Y<sub>4</sub> (@ 29 nm), Y<sub>6</sub> (@ 42 nm) and Y<sub>7</sub> (@ 51 nm)**

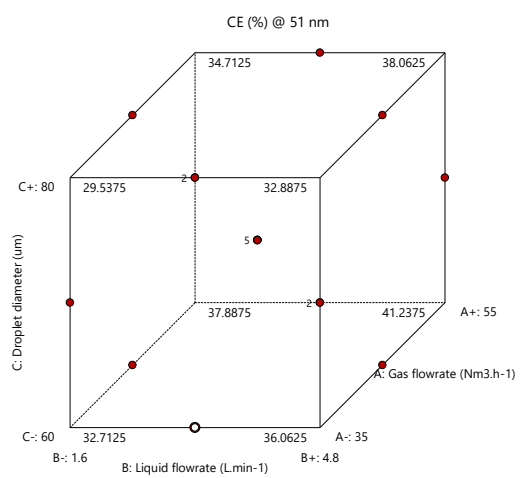
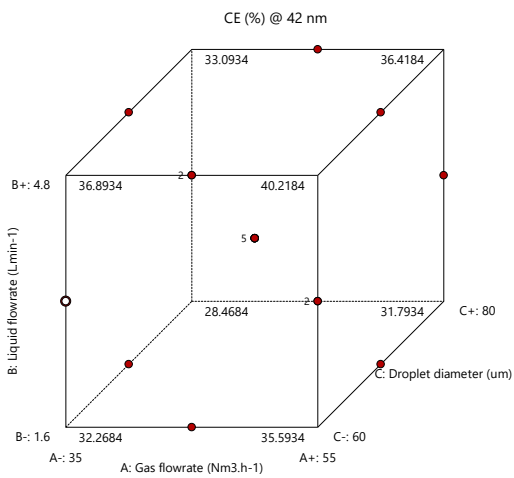


Y<sub>1</sub> @ 17 nm



Y<sub>3</sub> @ 24 nm

Y<sub>4</sub> @ 29 nm



Y<sub>6</sub> @ 42 nm

Y<sub>7</sub> @ 51 nm

# References

1. Wennersten, R., Fidler, J., Spitsyna, A.: Nanotechnology: A New Technological Revolution in the 21st Century. In: Handbook of Performability Engineering. pp. 943–952. Springer London, London (2008)
2. Nanomaterials Market Size, Share | Industry Forecast 2014-2022, <https://www.alliedmarketresearch.com/nano-materials-market>
3. Keller, A.A., Lazareva, A.: Predicted Releases of Engineered Nanomaterials: From Global to Regional to Local. *Environ. Sci. Technol. Lett.* 1, 65–70 (2014). <https://doi.org/10.1021/ez400106t>
4. Nemmar, A., Hoet, P.H.M., Vanquickenborne, B., Dinsdale, D., Thomeer, M., Hoylaerts, M.F., Vanbilloen, H., Mortelmans, L., Nemery, B.: Passage of Inhaled Particles Into the Blood Circulation in Humans. *Circulation.* 105, 411–414 (2002). <https://doi.org/10.1161/hc0402.104118>
5. Maher, B.A., Ahmed, I.A.M., Karloukovski, V., MacLaren, D.A., Foulds, P.G., Allsop, D., Mann, D.M.A., Torres-Jardón, R., Calderon-Garciduenas, L.: Magnetite pollution nanoparticles in the human brain. *Proc. Natl. Acad. Sci. U. S. A.* 113, 10797–10801 (2016). <https://doi.org/10.1073/pnas.1605941113>
6. Nowack, B., Bucheli, T.D.: Occurrence, behavior and effects of nanoparticles in the environment. *Environ. Pollut.* 150, 5–22 (2007). <https://doi.org/10.1016/j.envpol.2007.06.006>
7. Thomas, S., Al Mutairi, E., De, S.: Impact of Nanomaterials on Health and Environment. *Arab. J. Sci. Eng.* 38, 457–477 (2013). <https://doi.org/10.1007/s13369-012-0324-0>
8. Campos, A., López, I.: Current Status and Perspectives in Nanowaste Management. In: Handbook of Environmental Materials Management. pp. 2287–2314. Springer International Publishing (2019)
9. Allan, J., Belz, S., Hoeverler, A., Hugas, M., Okuda, H., Patri, A., Rauscher, H., Silva, P., Slikker, W., Sokull-Kluettgen, B., Tong, W., Anklam, E.: Regulatory landscape of nanotechnology and nanoplastics from a global perspective. *Regul. Toxicol. Pharmacol.* 122, 104885 (2021). <https://doi.org/https://doi.org/10.1016/j.yrtph.2021.104885>
10. Walser, T., Limbach, L.K., Brogioli, R., Erismann, E., Flamigni, L., Hattendorf, B., Juchli, M., Krumeich, F., Ludwig, C., Prikopsky, K., Rossier, M., Saner, D., Sigg, A., Hellweg, S., Günther, D., Stark, W.J.: Persistence of engineered nanoparticles in a municipal solid-waste incineration plant. *Nat. Nanotechnol.* 7, 520–524 (2012). <https://doi.org/10.1038/nnano.2012.64>
11. Vejerano, E.P., Leon, E.C., Holder, A.L., Marr, L.C.: Characterization of particle emissions and fate of nanomaterials during incineration. *Environ. Sci. Nano.* 1, 133–143 (2014). <https://doi.org/10.1039/c3en00080j>
12. Baran, P., Quicker, P.: Fate and behavior of nanoparticles in waste incineration. *Osterr. Wasser- und Abfallwirtschaft.* 69, 51–65 (2016). <https://doi.org/10.1007/s00506-016-0362-z>
13. Part, F., Berge, N., Baran, P., Stringfellow, A., Sun, W., Bartelt-Hunt, S., Mitrano, D., Li, L., Hennebert, P., Quicker, P., Bolyard, S.C., Huber-Humer, M.: A review of the fate of engineered nanomaterials in municipal solid waste streams. *Waste Manag.* 75, 427–449 (2018). <https://doi.org/https://doi.org/10.1016/j.wasman.2018.02.012>

14. Kim, H.T., Jung, C.H., Oh, S.N., Lee, K.W.: Particle removal efficiency of gravitational wet scrubber considering diffusion, interception, and impaction. *Environ. Eng. Sci.* 18, 125–136 (2001). <https://doi.org/10.1089/10928750151132357>
15. Commission, E., Centre, J.R., Pinasseau, A., Zenger, B., Roth, J., Canova, M., Roudier, S.: Best available techniques (BAT) reference document for waste treatment : Industrial Emissions Directive 2010/75/EU (integrated pollution prevention and control). Publications Office of the European Union (2018)
16. Chen, T.M., Tsai, C.J., Yan, S.Y., Li, S.N.: An efficient wet electrostatic precipitator for removing nanoparticles, submicron and micron-sized particles. *Sep. Purif. Technol.* 136, 27–35 (2014). <https://doi.org/10.1016/j.seppur.2014.08.032>
17. Dunuweera, S.P., Rajapakse, R.M.G.: Cement Types, Composition, Uses and Advantages of Nanocement, Environmental Impact on Cement Production, and Possible Solutions. *Adv. Mater. Sci. Eng.* 2018, 4158682 (2018). <https://doi.org/10.1155/2018/4158682>
18. Tsai, C.-J., Lin, C.-H., Wang, Y.-M., Hunag, C.-H., Li, S.-N., Wu, Z.-X., Wang, F.-C.: An efficient venturi scrubber system to remove submicron particles in exhaust gas. *J. Air Waste Manag. Assoc.* 55, 319–325 (2005). <https://doi.org/10.1080/10473289.2005.10464622>
19. Jung, C.H., Park, H.S., Kim, Y.P.: Analytic solution to estimate overall collection efficiency and the size distribution change of polydispersed aerosol for cyclone separator. *Sep. Purif. Technol.* 68, 428–432 (2009). <https://doi.org/10.1016/j.seppur.2009.05.023>
20. Lim, K.S., Lee, S.H., Park, H.S.: Prediction for particle removal efficiency of a reverse jet scrubber. *J. Aerosol Sci.* 37, 1826–1839 (2006). <https://doi.org/10.1016/j.jaerosci.2006.06.010>
21. Yang, L., Bao, J., Yan, J., Liu, J., Song, S., Fan, F.: Removal of fine particles in wet flue gas desulfurization system by heterogeneous condensation. *Chem. Eng. J.* 156, 25–32 (2010). <https://doi.org/10.1016/j.cej.2009.09.026>
22. Wu, Q., Gu, M., Du, Y., Zeng, H.: Synergistic removal of dust using the wet flue gas desulfurization systems. *R. Soc. Open Sci.* 6, 181696 (2019). <https://doi.org/10.1098/rsos.181696>
23. Taheri, M., Haines, G.F.: Optimization of Factors Affecting Scrubber Performance. *J. Air Pollut. Control Assoc.* 19, 427–431 (1969). <https://doi.org/10.1080/00022470.1969.10466508>
24. Ravi, G., Gupta, S.K., Viswanathan, S., Ray, M.B.: Optimization of Venturi Scrubbers Using Genetic Algorithm. *Ind. Eng. Chem. Res.* 41, 2988–3002 (2002). <https://doi.org/10.1021/ie010531b>
25. Viswanathan, S., Ananthanarayanan, N., Azzopardi, B.: Venturi Scrubber Modelling and Optimization. *Can. J. Chem. Eng.* 83, 194–203 (2008). <https://doi.org/10.1002/cjce.5450830206>
26. Mukherjee, S., Verma, A., Biswas, S., Bal, M., Meikap, B.: Removal of Cement Dust Particulates via Fully Submerged Self-Primed Venturi Scrubber. *CLEAN - Soil Air Water.* 49, (2021). <https://doi.org/10.1002/clen.202000241>
27. Slinn, W.G.N.: Precipitation scavenging
28. Mostafa, S.A., EL-Deeb, M.M., Farghali, A.A., Faried, A.S.: Evaluation of the nano silica and nano waste materials on the corrosion protection of high strength steel embedded in ultra-high performance concrete. *Sci. Rep.* 11, 1–16 (2021). <https://doi.org/10.1038/s41598-021-82322-0>
29. Saner, M., Stoklosa, A.: Commercial, Societal and Administrative Benefits from the

- Analysis and Clarification of Definitions: The Case of Nanomaterials. *Creat. Innov. Manag.* 22, 26–36 (2013). <https://doi.org/10.1111/CAIM.12014>
30. Nanotechnologies-Terminology and definitions for nano-objects-Nanoparticle, nanofibre and nanoplate. (2008)
  31. Epa, U., of the Science Advisor, O.: *Nanotechnology White Paper*. (2007)
  32. EU COMMISSION. (2022). <https://doi.org/10.2788/36237>
  33. Courty, M.A., Allue, E., Henry, A.: Forming mechanisms of vitrified charcoals in archaeological firing-assemblages. *J. Archaeol. Sci. Reports.* 30, 102215 (2020). <https://doi.org/10.1016/J.JASREP.2020.102215>
  34. Griffin, S., Masood, M.I., Nasim, M.J., Sarfraz, M., Ebokaiwe, A.P., Schäfer, K.H., Keck, C.M., Jacob, C.: Natural Nanoparticles: A Particular Matter Inspired by Nature. *Antioxidants* 2018, Vol. 7, Page 3. 7, 3 (2017). <https://doi.org/10.3390/ANTIOX7010003>
  35. Hochella, M.F., Mogk, D.W., Ranville, J., Allen, I.C., Luther, G.W., Marr, L.C., McGrail, B.P., Murayama, M., Qafoku, N.P., Rosso, K.M., Sahai, N., Schroeder, P.A., Vikesland, P., Westerhoff, P., Yang, Y.: Natural, incidental, and engineered nanomaterials and their impacts on the Earth system. *Science* (80-. ). 363, (2019). [https://doi.org/10.1126/SCIENCE.AAU8299/ASSET/713F7638-CAC2-4D54-8D14-FDFC821E2E4B/ASSETS/GRAPHIC/363\\_AAU8299\\_FA.JPEG](https://doi.org/10.1126/SCIENCE.AAU8299/ASSET/713F7638-CAC2-4D54-8D14-FDFC821E2E4B/ASSETS/GRAPHIC/363_AAU8299_FA.JPEG)
  36. Gokhale, S.: Effects of Engineered Nanomaterials Released into the Atmosphere. *J. Hazardous, Toxic, Radioact. Waste.* 20, (2016). [https://doi.org/10.1061/\(ASCE\)HZ.2153-5515.0000301](https://doi.org/10.1061/(ASCE)HZ.2153-5515.0000301)
  37. Chenthamara, D., Subramaniam, S., Ramakrishnan, S.G., Krishnaswamy, S., Essa, M.M., Lin, F.H., Qoronfleh, M.W.: Therapeutic efficacy of nanoparticles and routes of administration. *Biomater. Res.* 23, (2019). <https://doi.org/10.1186/S40824-019-0166-X>
  38. Majhi, K.C., Yadav, M.: Synthesis of inorganic nanomaterials using carbohydrates. *Green Sustain. Process Chem. Environ. Eng. Sci. Green Inorg. Synth.* 109–135 (2021). <https://doi.org/10.1016/B978-0-12-821887-7.00003-3>
  39. Carbon Nano Materials Market Size, Share and Forecast, 2031, <https://www.alliedmarketresearch.com/carbon-nano-materials-market>
  40. Calderón-Garcidueñas, L., González-Maciel, A., Mukherjee, P.S., Reynoso-Robles, R., Pérez-Guillé, B., Gayosso-Chávez, C., Torres-Jardón, R., Cross, J. V., Ahmed, I.A.M., Karloukovski, V. V., Maher, B.A.: Combustion- and friction-derived magnetic air pollution nanoparticles in human hearts. *Environ. Res.* 176, 108567 (2019). <https://doi.org/10.1016/j.envres.2019.108567>
  41. Buzea, C., Pacheco, I.I., Robbie, K.: Nanomaterials and nanoparticles: Sources and toxicity. *Biointerphases.* 2, MR17 (2007). <https://doi.org/10.1116/1.2815690>
  42. Smita, S., Gupta, S.K., Bartonova, A., Dusinska, M., Gutleb, A.C., Rahman, Q.: Nanoparticles in the environment: Assessment using the causal diagram approach, [/pmc/articles/PMC3388445/](https://pubmed.ncbi.nlm.nih.gov/23388445/), (2012)
  43. Biswas, P., Wu, & C.-Y.: Nanoparticles and the Environment. <http://dx.doi.org/10.1080/10473289.2005.10464656>. 55, 708–746 (2012). <https://doi.org/10.1080/10473289.2005.10464656>
  44. Krysanov, E.Y., Pavlov, D.S., Demidova, T.B., Dgebuadze, Y.Y.: Effect of nanoparticles on aquatic organisms. *Biol. Bull.* 2010 374. 37, 406–412 (2010). <https://doi.org/10.1134/S1062359010040114>
  45. Lovern, S.B., Strickler, J.R., Klaper, R.: Behavioral and physiological changes in *Daphnia magna* when exposed to nanoparticle suspensions (titanium dioxide, nano-C60, and C60HxC70Hx). *Environ. Sci. Technol.* 41, 4465 (2007).

- <https://doi.org/10.1021/ES062146P>
46. Roberts, A.P., Mount, A.S., Seda, B., Souther, J., Qiao, R., Lin, S., Pu, C.K., Rao, A.M., Klaine, S.J.: In vivo biomodification of lipid-coated carbon nanotubes by *Daphnia magna*. *Environ. Sci. Technol.* 41, 3028–3029 (2007). <https://doi.org/10.1021/ES062572A>
  47. Giese, B., Klaessig, F., Park, B., Kaegi, R., Steinfeldt, M., Wigger, H., Von Gleich, A., Gottschalk, F.: Risks, Release and Concentrations of Engineered Nanomaterial in the Environment. *Sci. Reports* 2018 8. 8, 1–18 (2018). <https://doi.org/10.1038/s41598-018-19275-4>
  48. Manžuch, Z., Akelytė, R., Camboni, M., Carlander, D., Perez, R., Kriščiūnaitė, G.G.: Study on the Product Lifecycles, Waste Recycling and the Circular Economy for Nanomaterials. (2021). <https://doi.org/10.2823/708711>
  49. ON, E., M, K.: Analytical approach to the waste management of nanomaterials in developing countries. *Front. Drug, Chem. Clin. Res.* 2, (2019). <https://doi.org/10.15761/FDCCR.1000117>
  50. Suzuki, S., Part, F., Matsufuji, Y., Huber-Humer, M.: Modeling the fate and end-of-life phase of engineered nanomaterials in the Japanese construction sector. *Waste Manag.* 72, 389–398 (2018). <https://doi.org/10.1016/J.WASMAN.2017.11.037>
  51. Gottschalk, F., Nowack, B.: The release of engineered nanomaterials to the environment. *J. Environ. Monit.* 13, 1145–1155 (2011). <https://doi.org/10.1039/C0EM00547A>
  52. Mueller, N.C., Buha, J., Wang, J., Ulrich, A., Nowack, B.: Modeling the flows of engineered nanomaterials during waste handling. *Environ. Sci. Process. Impacts.* 15, 251–259 (2012). <https://doi.org/10.1039/C2EM30761H>
  53. Mazari, S.A., Ali, E., Abro, R., Khan, F.S.A., Ahmed, I., Ahmed, M., Nizamuddin, S., Siddiqui, T.H., Hossain, N., Mubarak, N.M., Shah, A.: Nanomaterials: Applications, waste-handling, environmental toxicities, and future challenges - A review. *J. Environ. Chem. Eng.* 9, 105028 (2021). <https://doi.org/10.1016/j.jece.2021.105028>
  54. Stloukal, P., Pekařová, S., Kalendova, A., Mattausch, H., Laske, S., Holzer, C., Chitu, L., Bodner, S., Maier, G., Slouf, M., Koutny, M.: Kinetics and mechanism of the biodegradation of PLA/clay nanocomposites during thermophilic phase of composting process. *Waste Manag.* 42, 31–40 (2015). <https://doi.org/10.1016/J.WASMAN.2015.04.006>
  55. Shaik, S., Franchetti, M.J.: Recycling and Sustainability of Nanocomposites. *Appl. Nanocomposites.* 236–259 (2022). <https://doi.org/10.1201/9781003247074-11>
  56. Maiti, S., Ray, D., Mitra, D., Misra, M.: Study of compostable behavior of jute nano fiber reinforced biocopolyester composites in aerobic compost environment. *J. Appl. Polym. Sci.* 123, 2952–2958 (2012). <https://doi.org/10.1002/APP.34918>
  57. Balaguer, M.P., Aliaga, C., Fito, C., Hortal, M.: Compostability assessment of nano-reinforced poly(lactic acid) films. *Waste Manag.* 48, 143–155 (2016). <https://doi.org/10.1016/J.WASMAN.2015.10.030>
  58. Caballero-Guzman, A., Sun, T., Nowack, B.: Flows of engineered nanomaterials through the recycling process in Switzerland. *Waste Manag.* 36, 33–43 (2015). <https://doi.org/10.1016/J.WASMAN.2014.11.006>
  59. Förster, H., Thajudeen, T., Funk, C., Peukert, W.: Separation of nanoparticles: Filtration and scavenging from waste incineration plants. *Waste Manag.* 52, 346–352 (2016). <https://doi.org/10.1016/J.WASMAN.2016.03.050>
  60. Walser, T., Gottschalk, F.: Stochastic fate analysis of engineered nanoparticles in incineration plants. *J. Clean. Prod.* 80, 241–251 (2014).

- <https://doi.org/10.1016/J.JCLEPRO.2014.05.085>
61. Oischinger, J., Meiller, M., Daschner, R., Hornung, A., Warnecke, R.: Fate of nano titanium dioxide during combustion of engineered nanomaterial-containing waste in a municipal solid waste incineration plant. *Waste Manag. Res.* 37, 1033–1042 (2019). <https://doi.org/10.1177/0734242X19862603>
  62. Lang, I.-M., Hauser, M., Baumann, W., Mätzing, H., Paur, H.-R., Seifert, H.: Untersuchungen zur Freisetzung von synthetischen Nanopartikeln bei der Abfallverbrennung. (2015)
  63. Börner, R., Meiller, M., Oischinger, J., Daschner, R.: Untersuchung möglicher Umweltauswirkungen bei der Entsorgung nanomaterialhaltiger Abfälle in Abfallbehandlungsanlagen. (2016)
  64. Wielinski, J., Voegelin, A., Grobéty, B., Müller, C.R., Morgenroth, E., Kaegi, R.: Transformation of TiO<sub>2</sub> (nano)particles during sewage sludge incineration. *J. Hazard. Mater.* 411, 124932 (2021). <https://doi.org/10.1016/J.JHAZMAT.2020.124932>
  65. C. Dutouquet, L. Meunier, O. Aguerre-Chariol, A. Joubert, R. Boudhan, S. Durécu, L. Le Coq, O.L.B.: Caractérisation de l'émission particulaire de nanodéchets halogénés lors d'une incinération dans un four de laboratoire à 1100°C. *Congrès Français sur les Aérosols.* (2019). <https://doi.org/10.25576/ASFERA-CFA2019-16675>
  66. Dutouquet, C., Aguerre-Chariol, O., Meunier, L., Joubert, A., Durécu, S., Marlair, G., Le Coq, L., Le Bihan, O.: Lab-scale characterization of emissions from incineration of halogen- and sulfur-containing nanowastes by use of a tubular furnace. *Int. J. Environ. Sci. Technol.* 2021 193. 19, 1139–1152 (2021). <https://doi.org/10.1007/S13762-021-03227-Z>
  67. Longuet, C., Chivas-Joly, C., Leclerc, L., Sarry, G., Lopez-Cuesta, J.M., Pourchez, J.: Incineration of nanomaterials: physical and chemical transformations and biological consequences of emissions. *Environnement, Risques & Santé.* 19, 51–64 (2020). <https://doi.org/10.1684/ERS.2020.1413>
  68. Singh, D., Wohlleben, W., De La Torre Roche, R., White, J.C., Demokritou, P.: Thermal decomposition/incineration of nano-enabled coatings and effects of nanofiller/matrix properties and operational conditions on byproduct release dynamics: Potential environmental health implications. *NanoImpact.* 13, 44–55 (2019). <https://doi.org/10.1016/J.IMPACT.2018.12.003>
  69. Bouillard, J.X., R'Mili, B., Moranviller, D., Vignes, A., Le Bihan, O., Ustache, A., Bomfim, J.A.S.S., Frejafon, E., Fleury, D., R'Mili, B., Moranviller, D., Vignes, A., Le Bihan, O., Ustache, A., Bomfim, J.A.S.S., Frejafon, E., Fleury, D.: Nanosafety by design: risks from nanocomposite/nanowaste combustion. *J. Nanoparticle Res.* 15, 1519 (2013). <https://doi.org/10.1007/s11051-013-1519-3>
  70. Ounoughene, G., Chivas-Joly, C., Longuet, C., Le Bihan, O., Lopez-Cuesta, J.M., Le Coq, L.: Evaluation of nanosilica emission in polydimethylsiloxane composite during incineration. *J. Hazard. Mater.* 371, 415–422 (2019). <https://doi.org/10.1016/j.jhazmat.2019.03.026>
  71. Janhäll, S., Petersson, M., Davidsson, K., Öman, T., Sommertune, J., Kåredal, M., Messing, M.E., Rissler, J.: Release of carbon nanotubes during combustion of polymer nanocomposites in a pilot-scale facility for waste incineration. *NanoImpact.* 24, 100357 (2021). <https://doi.org/10.1016/J.IMPACT.2021.100357>
  72. Massari, A., Beggio, M., Hreglich, S., Marin, R., Zuin, S.: Behavior of TiO<sub>2</sub> nanoparticles during incineration of solid paint waste: A lab-scale test. *Waste Manag.* 34, 1897–1907 (2014). <https://doi.org/10.1016/j.wasman.2014.05.015>
  73. Baumann, W., Teuscher, N., Hauser, M., Gehrmann, J., Paur, H.R., Stapf, D.:

- Behaviour of engineered nanoparticles in a lab-scale flame and combustion chamber. In: *Energy Procedia*. pp. 705–712. Elsevier Ltd (2017)
74. Gogos, A., Wielinski, J., Voegelin, A., Emerich, H., Kaegi, R.: Transformation of cerium dioxide nanoparticles during sewage sludge incineration. *Environ. Sci. Nano*. 6, 1765–1776 (2019). <https://doi.org/10.1039/C9EN00281B>
  75. Josua Wielinski, J., Victor Lowry, G.: Investigations into the fate of engineered transition metal nano particles during sewage sludge incineration. (2021). <https://doi.org/10.3929/ETHZ-B-000473625>
  76. Mueller, N., Buha, J., Wang, J., ... A.U.-... S.P.&, 2013, U.: Modeling the flows of engineered nanomaterials during waste handling. *pubs.rsc.org*. (2013)
  77. Froggett, S.J., Clancy, S.F., Boverhof, D.R., Canady, R.A.: A review and perspective of existing research on the release of nanomaterials from solid nanocomposites. Part. *Fibre Toxicol*. 11, 1–28 (2014). <https://doi.org/10.1186/1743-8977-11-17/FIGURES/4>
  78. Ounoughene, G., Lebihan, O., Debray, B., Chivas-Joly, C., Longuet, C., Joubert, A., Lopez-Cuesta, J.M., Le Coq, L.: Thermal disposal of waste containing nanomaterials: First investigations on a methodology for risk management. In: *Journal of Physics: Conference Series*. p. 12024. Institute of Physics Publishing (2017)
  79. Vejerano, E.P., Holder, A.L., Marr, L.C.: Emissions of polycyclic aromatic hydrocarbons, polychlorinated dibenzo-p-dioxins, and dibenzofurans from incineration of nanomaterials. *Environ. Sci. Technol*. 47, 4866–4874 (2013). <https://doi.org/10.1021/es304895z>
  80. Fujimori, T., Toda, A., Mukai, K., Takaoka, M.: Incineration of carbon nanomaterials with sodium chloride as a potential source of PCDD/Fs and PCBs. *J. Hazard. Mater*. 382, 121030 (2020). <https://doi.org/10.1016/J.JHAZMAT.2019.121030>
  81. Maguhn, J., Karg, E., Kettrup, A., Zimmermann, R.: On-line analysis of the size distribution of fine and ultrafine aerosol particles in flue and stack gas of a municipal waste incineration plant: effects of dynamic process control measures and emission reduction devices. *Environ. Sci. Technol*. 37, 4761–4770 (2003). <https://doi.org/10.1021/es020227p>
  82. Lin, S.-L., Tang, W., Wu, J.-L., Lee, Y.-Y., Wang, C.-L., Chen, W.-H.: Particulate PCDD/F size distribution and potential deposition in respiratory system from a hazardous waste thermal treatment process. *Environ. Res*. 214, 113806 (2022). <https://doi.org/https://doi.org/10.1016/j.envres.2022.113806>
  83. Buonanno, G., Scungio, M., Stabile, L., Tirler, W.: Ultrafine particle emission from incinerators: The role of the fabric filter. *J. Air Waste Manage. Assoc*. 62, 103–111 (2012). <https://doi.org/10.1080/10473289.2011.636501>
  84. Cernuschi, S., Giugliano, M., Ozgen, S., Consonni, S.: Number concentration and chemical composition of ultrafine and nanoparticles from WTE (waste to energy) plants. *Sci. Total Environ*. 420, 319–326 (2012). <https://doi.org/10.1016/j.scitotenv.2012.01.024>
  85. ZEUTHEN, J.H., PEDERSEN, A.J., HANSEN, J., FRANDBSEN, F.J., LIVBJERG, H., RIBER, C., ASTRUP, T.: COMBUSTION AEROSOLS FROM MUNICIPAL WASTE INCINERATION—EFFECT OF FUEL FEEDSTOCK AND PLANT OPERATION. *Combust. Sci. Technol*. 179, 2171–2198 (2007). <https://doi.org/10.1080/00102200701386180>
  86. Eckert & Ralph, J.S., Strigle, F.F.: Performance of Wet Scrubbers on Liquid and Solid Particulate Matter. *J. Air Pollut. Control Assoc*. 24, 961–966 (1974). <https://doi.org/10.1080/00022470.1974.10469998>
  87. Mussatti, D., Hemmer, P., Pechan, E.H.: Section 6 Particulate Matter Controls Chapter

- 2 Wet Scrubbers for Particulate Matter.
88. Buchanan, L.M., Harstad, J.B., Phillips, J.C., Lafferty, E., Dahlgren, C.M., Decker, H.M.: Simple Liquid Scrubber for Large-Volume Air Sampling. *Appl. Microbiol.* 23, 1140–1144 (1972). <https://doi.org/10.1128/AM.23.6.1140-1144.1972>
  89. Bhargava, D. akshey: Wet Scrubbers – Design of Spray Tower to Control Air Pollutants. *Int. J. Environ. Plan. Dev.* Vol. 2:, (2016)
  90. Bao, J., Yang, L., Yan, J., Xiong, G., Lu, B., Xin, C.: Experimental study of fine particles removal in the desulfurated scrubbed flue gas. In: *Fuel*. pp. 73–79. Elsevier Ltd (2013)
  91. Wang, S., Wang, J., Song, C., Wen, J.: Numerical investigation on urea particle removal in a spray scrubber using particle capture theory. *Chem. Eng. Res. Des.* 145, 150–158 (2019). <https://doi.org/10.1016/J.CHERD.2019.03.011>
  92. Bhoi, P.R., Vallabhbai, S.: WET SCRUBBING OF BIOMASS PRODUCER GAS TARS USING VEGETABLE OIL. (2014)
  93. Schifftner, K.C.: Air pollution control equipment. (2009)
  94. Mi, T., Yu, X.M.: Dust removal and desulphurization in a novel venturi scrubber. *Chem. Eng. Process. Process Intensif.* 62, 159–167 (2012). <https://doi.org/10.1016/j.cep.2012.07.010>
  95. Pak, S.I., Chang, K.S.: Performance estimation of a Venturi scrubber using a computational model for capturing dust particles with liquid spray. *J. Hazard. Mater.* 138, 560–573 (2006). <https://doi.org/10.1016/J.JHAZMAT.2006.05.105>
  96. Calvert, S., Lundgren, D., Mehta, D.S.: Venturi Scrubber Performance. *J. Air Pollut. Control Assoc.* 22, 529–532 (1972). <https://doi.org/10.1080/00022470.1972.10469674>
  97. Ali, S., Waheed, K., Qureshi, K., Irfan, N., Ahmed, M., Siddique, W., Farooq, A.: Experimental investigation of aerosols removal efficiency through self-priming venturi scrubber. *Nucl. Eng. Technol.* (2020). <https://doi.org/10.1016/j.net.2020.03.019>
  98. Jones, W.P.: Development of the V enturi Scrubber. 12, 31 (2022)
  99. Arya, S., Sottile, J., Novak, T.: Development of a flooded-bed scrubber for removing coal dust at a longwall mining section. *Saf. Sci.* 110, 204–213 (2018). <https://doi.org/10.1016/J.SSCI.2018.08.003>
  100. Raj Mohan, B., Meikap, B.C.: Performance characteristics of the particulate removal in a novel spray-cum-bubble column scrubber. *Chem. Eng. Res. Des.* 87, 109–118 (2009). <https://doi.org/10.1016/J.CHERD.2008.05.011>
  101. Schifftner, K.C., Hesketh, H.D.: Wet scrubbers, second edition. *Wet Scrubbers, Second Ed.* 1–208 (2017). <https://doi.org/10.1201/9780203733899/WET-SCRUBBERS-KENNETH-SCHIFFTNER-HOWARD-HESKETH>
  102. Robert H. Perry, D.W.G.: Perry’s Chemical Engineers’ Handbook. McGraw-Hill, 1999 (1997)
  103. Raj Mohan, B., Jain, R.K., Meikap, B.C.: Comprehensive analysis for prediction of dust removal efficiency using twin-fluid atomization in a spray scrubber. *Sep. Purif. Technol.* 63, 269–277 (2008). <https://doi.org/10.1016/j.seppur.2008.05.006>
  104. Licht, W.: Air pollution control engineering: basic calculations for particulate collection. M. Dekker (1988)
  105. Kim, hyeok gyu, Kim, H.-J., Lee, M.-H., Kim, J.-H.: Experimental Study on the Enhancement of Particle Removal Efficiency in Spray Tower Scrubber Using Electrospray. *Asian J. Atmos. Environ.* 8, 89–95 (2014). <https://doi.org/10.5572/ajae.2014.8.2.089>
  106. Park, S.H., Jung, C.H., Jung, K.R., Lee, B.K., Lee, K.W.: Wet scrubbing of polydisperse aerosols by freely falling droplets. *J. Aerosol Sci.* 36, 1444–1458 (2005).

- <https://doi.org/10.1016/J.JAEROSCI.2005.03.012>
107. Joshi, J.B., Nandakumar, K., Patwardhan, A.W., Nayak, A.K., Pareek, V., Gumulya, M., Wu, C., Minocha, N., Pal, E., Kumar, M., Bhusare, V., Tiwari, S., Lote, D., Mali, C., Kulkarni, A., Tamhankar, S.: Computational fluid dynamics. *Adv. Comput. Fluid Dyn. Nucl. React. Des. Saf. Assess.* 21–238 (2019). <https://doi.org/10.1016/B978-0-08-102337-2.00002-X>
  108. Chate, D.M., Kamra, A.K.: Collection efficiencies of large water drops collecting aerosol particles of various densities. *Atmos. Environ.* 31, 1631–1635 (1997). [https://doi.org/10.1016/S1352-2310\(96\)00338-X](https://doi.org/10.1016/S1352-2310(96)00338-X)
  109. Wang, A., Song, Q., Yao, Q.: Study on inertial capture of particles by a droplet in a wide Reynolds number range. *J. Aerosol Sci.* 93, 1–15 (2016). <https://doi.org/10.1016/J.JAEROSCI.2015.11.010>
  110. Nagare, B., Marcolli, C., Stetzer, O., Lohmann, U.: Estimating collision efficiencies from contact freezing experiments. *Atmos. Chem. Phys. Discuss.* 15, 12167–12212 (2015). <https://doi.org/10.5194/acpd-15-12167-2015>
  111. Bae, S.Y., Jung, C.H., Kim, Y.P.: Relative contributions of individual phoretic effect in the below-cloud scavenging process. *J. Aerosol Sci.* 40, 621–632 (2009). <https://doi.org/10.1016/j.jaerosci.2009.03.003>
  112. Calvert, S.: Venturi and other atomizing scrubbers efficiency and pressure drop. *AIChE J.* 16, 392–396 (1970). <https://doi.org/10.1002/AIC.690160315>
  113. WALTON, W.H., WOOLCOCK, A.: The suppression of airborne dust by water spray. *Int. J. Air Pollut.* 3, 129–153 (1960)
  114. Davenport, H.M., Peters, L.K.: Field studies of atmospheric particulate concentration changes during precipitation. *Atmos. Environ.* 12, 997–1008 (1978). [https://doi.org/10.1016/0004-6981\(78\)90344-X](https://doi.org/10.1016/0004-6981(78)90344-X)
  115. Fuchs, N.: *The Mechanics of Aerosols*. Pergamon Press, Oxford (1964)
  116. Carotenuto, C., Di Natale, F., Lancia, A.: Wet electrostatic scrubbers for the abatement of submicronic particulate. *Chem. Eng. J.* 165, 35–45 (2010). <https://doi.org/10.1016/j.cej.2010.08.049>
  117. Fan, F., Yang, L., Yuan, Z., Hu, X.: Removal and condensation growth of inhalable particles in spray scrubber. *Huagong Xuebao/CIESC J.* 61, 2708–2713 (2010)
  118. Jung, C.H., Lee, K.W.: Filtration of Fine Particles by Multiple Liquid Droplet and Gas Bubble Systems. *Aerosol Sci. Technol.* 29, 389–401 (1998). <https://doi.org/10.1080/02786829808965578>
  119. Colbeck, I. (Ian): *Aerosol Science : Technology and Applications*. (2013)
  120. Bae, S.Y., Jung, C.H., Kim, Y.P.: Derivation and verification of an aerosol dynamics expression for the below-cloud scavenging process using the moment method. *J. Aerosol Sci.* 41, 266–280 (2010). <https://doi.org/10.1016/J.JAEROSCI.2009.11.006>
  121. Sparks, L.E., Pilat, M.J.: Effect of diffusiophoresis on particle collection by wet scrubbers. *Atmos. Environ.* 4, 651–660 (1970). [https://doi.org/10.1016/0004-6981\(70\)90038-7](https://doi.org/10.1016/0004-6981(70)90038-7)
  122. Pilat, M.J., Prem, A.: Calculated particle collection efficiencies of single droplets including inertial impaction, brownian diffusion, diffusiophoresis and thermophoresis. *Atmos. Environ.* 10, 13–19 (1976). [https://doi.org/10.1016/0004-6981\(76\)90253-5](https://doi.org/10.1016/0004-6981(76)90253-5)
  123. Pilat, M.J., Prem, A.: Effect of diffusiophoresis and thermophoresis on the overall particle collection efficiency of spray droplet scrubbers. *J. Air Pollut. Control Assoc.* 27, 982–988 (1977). <https://doi.org/10.1080/00022470.1977.10470521>
  124. Ardon-Dryer, K., Huang, Y.-W., Cziczo, D.J.: Laboratory studies of collection efficiency of sub-micrometer aerosol particles by cloud droplets on a single-droplet

- basis. *Atmos. Chem. Phys.* 15, 9159–9171 (2015). <https://doi.org/10.5194/acp-15-9159-2015>
125. Vasudevan, T. V., Gokhale, A.J., Mahalingam, R.: Phoretic phenomena in tar vapor-particulate mixture separation from fuel gas streams. *Can. J. Chem. Eng.* 63, 903–910 (1985). <https://doi.org/10.1002/cjce.5450630606>
  126. Schmitt, L.W. and K.H.: Thermophoresis and Diffusiophoresis of Aerosol,” *Aerosol Science*, Academic Press, London. *Sci. Res. Publ.* 163–194 (1966)
  127. Hsu, C.-J.: Diffusional mass transfer, A. H. P. Skelland, Wiley, New York (1974). 510 pages. \$24.95. *AIChE J.* 21, 621–621 (1975). <https://doi.org/10.1002/AIC.690210337>
  128. *Aerosol Measurement: Principles, Techniques, and Applications*. Second Edition Edited by Paul A. Baron (National Institute for Occupational Safety and Health) and Klaus Willeke (University of Cincinnati). Wiley-Interscience: New York. 2001. xxiv + 1132 pp. \$195.00. ISBN: 0-471-35636-0. *J. Am. Chem. Soc.* 124, 5251–5251 (2002). <https://doi.org/10.1021/ja015375e>
  129. Wang, L.K., Pereira, N.C.: *Air and noise pollution control*. Humana Press (1979)
  130. D’Addio, L., Di Natale, F., Carotenuto, C., Balachandran, W., Lancia, A.: A lab-scale system to study submicron particles removal in wet electrostatic scrubbers. *Chem. Eng. Sci.* 97, 176–185 (2013). <https://doi.org/10.1016/j.ces.2013.04.006>
  131. Zhao, H., Zheng, C.G.: Modeling of Gravitational Wet Scrubbers with Electrostatic Enhancement. *Chem. Eng. Technol.* 31, 1824–1837 (2008). <https://doi.org/10.1002/ceat.200800360>
  132. Pilat, M.J., Jaasund, S.A., Sparks, L.E.: Collection of aerosol particles by electrostatic droplet spray scrubbers. *Environ. Sci. Technol.* 8, 360–362 (1974). <https://doi.org/10.1021/es60089a006>
  133. Jaworek, A., Krupa, A., Sobczyk, A.T., Marchewicz, A., Szudyga, M., Antes, T., Balachandran, W., Di Natale, F., Carotenuto, C.: Submicron particles removal by charged sprays. *Fundamentals. J. Electrostat.* 71, 345–350 (2013). <https://doi.org/10.1016/j.elstat.2012.11.028>
  134. Dana, M.T., Hales, J.M.: Statistical aspects of the washout of polydisperse aerosols. *Atmos. Environ.* 10, 45–50 (1976). [https://doi.org/10.1016/0004-6981\(76\)90258-4](https://doi.org/10.1016/0004-6981(76)90258-4)
  135. Ramarao, B. V., Tien, C., Mohan, S.: Calculation of single fiber efficiencies for interception and impaction with superposed brownian motion. *J. Aerosol Sci.* 25, 295–313 (1994). [https://doi.org/10.1016/0021-8502\(94\)90081-7](https://doi.org/10.1016/0021-8502(94)90081-7)
  136. Strauss, W.: *Industrial gas cleaning; the principles and practice of the control of gaseous and particulate emissions*. 621 (1975)
  137. Ali, H., Plaza, F., Mann, A.: Numerical prediction of dust capture efficiency of a centrifugal wet scrubber. *AIChE J.* 64, 1001–1012 (2018). <https://doi.org/10.1002/AIC.15979>
  138. Viswanathan, S.: Modeling of Venturi Scrubber Performance. *Ind. Eng. Chem. Res.* 36, 4308–4317 (1997). <https://doi.org/10.1021/IE970235S/ASSET/IMAGES/LARGE/IE970235SF00007.JPG>
  139. Pemberton, C.S.: SCAVENGING ACTION OF RAIN ON NONWETTABLE PARTICULATE MATTER SUSPENDED IN THE ATMOSPHERE. *Intern. J. Air Pollution*. Vol: 3, (1960)
  140. Adah, E., Joubert, A., Boudhan, R., Henry, M., Durécu, S., Le Coq, L.: Spray Scrubber for Nanoparticle Removal from Incineration Fumes from the Incineration of Waste Containing Nanomaterials: Theoretical and Experimental Investigations. *Aerosol Sci. Technol.* 1–23 (2021). <https://doi.org/10.1080/02786826.2021.1974332>

141. Mohan, B.R., Biswas, S., Meikap, B.C.: Performance characteristics of the particulates scrubbing in a counter-current spray-column. *Sep. Purif. Technol.* 61, 96–102 (2008). <https://doi.org/10.1016/j.seppur.2007.09.018>
142. Ali, M., Yan, C., Sun, Z., Gu, H., Mehboob, K.: Dust particle removal efficiency of a venturi scrubber. *Ann. Nucl. Energy.* 54, 178–183 (2013). <https://doi.org/10.1016/j.anucene.2012.11.005>
143. Mayinger, F., Lehner, M.: Operating results and aerosol deposition of a venturi scrubber in self-priming operation. *Chem. Eng. Process. Process Intensif.* 34, 283–288 (1995). [https://doi.org/10.1016/0255-2701\(94\)04015-X](https://doi.org/10.1016/0255-2701(94)04015-X)
144. Meikap, B.C., Biswas, M.N.: Fly-ash removal efficiency in a modified multi-stage bubble column scrubber. *Sep. Purif. Technol.* 36, 177–190 (2004). [https://doi.org/10.1016/S1383-5866\(03\)00213-2](https://doi.org/10.1016/S1383-5866(03)00213-2)
145. Lee, B.-K., Mohan, B.R., Byeon, S.-H., Lim, K.-S., Hong, E.-P.: Evaluating the performance of a turbulent wet scrubber for scrubbing particulate matter. *J. Air Waste Manage. Assoc.* 63, 499–506 (2013). <https://doi.org/10.1080/10962247.2012.738626>
146. Darbandi, T., Risberg, M., Westerlund, L.: CFD modeling of the forces in the wet scrubber acting on particulate matter released from biomass combustion. *Therm. Sci. Eng. Prog.* 25, (2021). <https://doi.org/10.1016/J.TSEP.2021.100997>
147. Zhao, W., Fu, Y., Chen, Y., Sun, J., Tang, Q., Jiang, B., Kong, H., Xu, F., Ji, Q.: Effective fenton catalyst from controllable framework doping of Fe in porous silica spheres. *Microporous Mesoporous Mater.* 312, (2021). <https://doi.org/10.1016/j.micromeso.2020.110704>
148. Schauer, P.J.: Removal of Submicron Aerosol Particles from Moving Gas Stream. *Ind. Eng. Chem.* 43, 1532–1538 (1951). <https://doi.org/10.1021/ie50499a022>
149. Lancaster, B.W., Strauss, W.: A Study of Steam Injection into Wet Scrubbers. *Ind. Eng. Chem. Fundam.* 10, 362–369 (1971)
150. Yoshida, T., Kousaka, Y., Okuyama, K.: Growth of Aerosol Particles by Condensation. *Ind. Eng. Chem. Fundam.* 15, 37–41 (1976). <https://doi.org/10.1021/i160057a007>
151. Bao, J., Yang, L., Yan, J., Xiong, G., Shen, X.: Experimental Investigation on Improving the Removal Effect of WFGD System on Fine Particles by Heterogeneous Condensation. *Clean. Combust. Sustain. World.* 667–675 (2013). [https://doi.org/10.1007/978-3-642-30445-3\\_92](https://doi.org/10.1007/978-3-642-30445-3_92)
152. Huang, C.-H., Tsai, C.-J., Wang, Y.-M.: Control Efficiency of Submicron Particles by an Efficient Venturi Scrubber System. *J. Environ. Eng.* 133, 454–461 (2007). [https://doi.org/10.1061/\(ASCE\)0733-9372\(2007\)133:4\(454\)](https://doi.org/10.1061/(ASCE)0733-9372(2007)133:4(454))
153. Fan, F., Yang, L., Yan, J., Bao, J., Shen, X.: Experimental investigation on removal of coal-fired fine particles by a condensation scrubber. *Chem. Eng. Process. Process Intensif.* 48, 1353–1360 (2009). <https://doi.org/10.1016/J.CEP.2009.06.011>
154. Lehner, M.: Aerosol Separation Efficiency of a Venturi Scrubber Working in Self-Priming Mode. *Aerosol Sci. Technol.* 28, 389–402 (1998). <https://doi.org/10.1080/02786829808965533>
155. Danzomo, B.A., Salami, M.J.E., Jabirin, S., Khan, M.R., Nor, I.M.: PERFORMANCE EVALUATION OF WET SCRUBBER SYSTEM FOR INDUSTRIAL AIR POLLUTION CONTROL, (2012)
156. Rafidi, N., Brogaard, F., Chen, L., Håkansson, R., Tabikh, A.: CFD and experimental studies on capture of fine particles by liquid droplets in open spray towers. *Sustain. Environ. Res.* 28, 382–388 (2018). <https://doi.org/10.1016/j.serj.2018.08.003>
157. Keshavarz, P., Bozorgi, Y., Fathikalajahi, J., Taheri, M.: Prediction of the spray scrubbers' performance in the gaseous and particulate scrubbing processes. *Chem. Eng.*

- J. 140, 22–31 (2008). <https://doi.org/10.1016/j.cej.2007.08.034>
158. Pranasha, T.S., Kamra, A.K.: Scavenging of aerosol particles by large water drops 1. Neutral case. *J. Geophys. Res. Atmos.* 101, 23373–23380 (1996). <https://doi.org/10.1029/96jd01311>
  159. Greenfield, S.: Rain scavenging of radioactive particulate matter from the atmosphere. *J. Meteorol.* 14, 115–125 (1957). [https://doi.org/10.1175/1520-0469\(1957\)014<0115:RSORPM>2.0.CO;2](https://doi.org/10.1175/1520-0469(1957)014<0115:RSORPM>2.0.CO;2)
  160. LEE, J.: BLACK CARBON AND ELEMENTAL CARBON CONCENTRATIONS OF SPARK-GENERATED CARBON PARTICLES. 25, 1–37 (2008)
  161. Tomb, T.F., Emmerling, J.E., Kellner, R.H.: Collection of Airborne Coal Dust by Water Spray in a Horizontal Duct. *Am. Ind. Hyg. Assoc. J.* 33, 715–721 (1972). <https://doi.org/10.1080/0002889728506736>
  162. Muller, N., Benadda, B., Otterbein, M.: Mass transfer in a “droplets column” in presence of solid particles. *Chem. Eng. Process.* 40, 167–174 (2001). [https://doi.org/10.1016/S0255-2701\(00\)00136-7](https://doi.org/10.1016/S0255-2701(00)00136-7)
  163. Biswas, S., Rajmohan, B., Meikap, B.C.: Hydrodynamics characterization of a counter-current spray column for particulate scrubbing from flue gases. *Asia-Pacific J. Chem. Eng.* 3, 544–549 (2008). <https://doi.org/10.1002/apj.177>
  164. Centner, P., Büttner, H., Ebert, F.: Investigation of a wet dust scrubber with a pneumatic nozzle: Dust collection based on turbulent diffusion. *Chem. Eng. Technol. - CET.* 12, 439–444 (1989). <https://doi.org/10.1002/ceat.270120163>
  165. Bianchini, A., Pellegrini, M., Rossi, J., Saccani, C.: Theoretical model and preliminary design of an innovative wet scrubber for the separation of fine particulate matter produced by biomass combustion in small size boilers. *Biomass and Bioenergy.* 116, 60–71 (2018). <https://doi.org/10.1016/j.biombioe.2018.05.011>
  166. Bianchini, A., Cento, F., Golferà, L., Pellegrini, M., Saccani, C.: Performance analysis of different scrubber systems for removal of particulate emissions from a small size biomass boiler. *Biomass and Bioenergy.* 92, 31–39 (2016). <https://doi.org/10.1016/j.biombioe.2016.06.005>
  167. Hu, S., Gao, Y., Feng, • Guorui, Hu, F., Liu, C., Li, J.: Experimental study of the dust-removal performance of a wet scrubber. *Int. J. Coal Sci. Technol.* 8, (2021). <https://doi.org/10.1007/s40789-021-00410-y>
  168. Zheng, Z., Zhu, J., Xia, S., Zeng, Q.: An efficient wet scrubber to remove micron and submicron particles from exhaust gas. *J. Chem. Eng. Japan.* 51, 839–847 (2018). <https://doi.org/10.1252/jcej.17we167>
  169. Elisa Achilles, A.E., Guerra, V.G.: Performance of a cyclone scrubber in removal of fine particulate matter. *Chem. Ind. Chem. Eng. Q.* 26, 31–40 (2020). <https://doi.org/10.2298/CICEQ181220022A>
  170. Krames, J., Büttner, H.: The cyclone scrubber – a high efficiency wet separator. *Chem. Eng. Technol.* 17, 73–80 (1994). <https://doi.org/10.1002/ceat.270170202>
  171. Zhang, B., Hu, C., He, J., Sui, C., Chen, W.: IOP Conference Series: Earth and Environmental Science Performance evaluation of a three-stage composite wet scrubber for removing particulate matter Performance evaluation of a three-stage composite wet scrubber for removing particulate matter. (2020). <https://doi.org/10.1088/1755-1315/615/1/012117>
  172. Huang, S.H., Kang, J.L., Wong, D.S.H., Jang, S.S., Lin, C.A.: Particle-Scavenging prediction in sieve plate scrubber via dimension reduction in computational fluid dynamics. *Chem. Eng. Res. Des.* 160, 540–550 (2020). <https://doi.org/10.1016/j.cherd.2020.06.024>

173. Bertinat, M.P.: Charged-droplet scrubbing for controlling sub-micron particle emissions. *J. Electrostat.* 9, 137–158 (1980). [https://doi.org/10.1016/0304-3886\(80\)90046-7](https://doi.org/10.1016/0304-3886(80)90046-7)
174. Cho, K.S., Lee, Y.Y., Jang, S. nae, Yun, J., Kwon, J., Park, H.J., Seo, Y.: Removal of particulate matter from pork belly grilling gas using an orifice wet scrubber. *J. Environ. Sci. Heal. - Part A Toxic/Hazardous Subst. Environ. Eng.* 55, 1125–1130 (2020). <https://doi.org/10.1080/10934529.2020.1773712>
175. Ha, T.H., Nishida, O., Fujita, H., Wataru, H.: Enhancement of diesel particulate matter collection in an electrostatic water-spraying scrubber. *J. Mar. Sci. Technol.* 15, 271–279 (2010). <https://doi.org/10.1007/s00773-010-0086-x>
176. Su, L., Zhang, Y., Du, Q., Dai, X., Gao, J., Dong, P., Wang, H.: An experimental study on the removal of submicron fly ash and black carbon in a gravitational wet scrubber with electrostatic enhancement. *RSC Adv.* 10, 5905–5912 (2020). <https://doi.org/10.1039/c9ra10046f>
177. Di Natale, F., Carotenuto, C., D’Addio, L., Jaworek, A., Krupa, A., Szudyga, M., Lancia, A.: Capture of fine and ultrafine particles in a wet electrostatic scrubber. *J. Environ. Chem. Eng.* 3, 349–356 (2015). <https://doi.org/10.1016/j.jece.2014.11.007>
178. Bandyopadhyay, A., Biswas, M.N.: Fly ash scrubbing in a novel dual flow scrubber. *Waste Manag.* 27, 1845–1859 (2007). <https://doi.org/10.1016/j.wasman.2006.10.013>
179. Ru, Y., Zhao, L., Hadlocon, L.J.S., Zhu, H., Ramdon, S.K.: Laboratory evaluation of electrostatic spray wet scrubber to control particulate matter emissions from poultry facilities. *Environ. Technol. (United Kingdom)*. 38, 23–33 (2017). <https://doi.org/10.1080/09593330.2016.1184319>
180. Zhou, J., Zhou, S., Zhu, Y.: Experiment and Prediction Studies of Marine Exhaust Gas SO<sub>2</sub> and Particle Removal Based on NaOH Solution with a U-Type Scrubber. *Ind. Eng. Chem. Res.* 56, 12376–12384 (2017). <https://doi.org/10.1021/acs.iecr.7b02397>
181. Bal, M., Siddiqi, H., Mukherjee, S., Meikap, B.C.: Design of self priming venturi scrubber for the simultaneous abatement of HCl gas and particulate matter from the flue gas. *Chem. Eng. Res. Des.* 150, 311–319 (2019). <https://doi.org/10.1016/j.cherd.2019.08.005>
182. Ahmed, S., Mohsin, H., Qureshi, K., Shah, A., Siddique, W., Waheed, K., Irfan, N., Ahmad, M., Farooq, A.: Investigation of dust particle removal efficiency of self-priming venturi scrubber using computational fluid dynamics. *Nucl. Eng. Technol.* 50, 665–672 (2018). <https://doi.org/10.1016/j.net.2018.01.016>
183. Kim, J.S., Park, J.W.: A method of estimating aerosol particle removal rates using one-dimensional two-fluid equations for venturi scrubbers in filtered containment venting. *Ann. Nucl. Energy.* 145, 107543 (2020). <https://doi.org/10.1016/j.anucene.2020.107543>
184. Attaullah, Niazi, M.B.K., Ahsan, M., Ali, M.: Computational fluid dynamics simulation for the prediction of the venturi scrubber performance using finite volume method. *Int. J. Comput. Sci. Math.* 11, 338–346 (2020). <https://doi.org/10.1504/IJCSM.2020.107601>
185. Cui, H., Li, N., Peng, J., Cheng, J., Zhang, N., Wu, Z.: Modeling the particle scavenging and thermal efficiencies of a heat absorbing scrubber. *Build. Environ.* 111, 218–227 (2017). <https://doi.org/10.1016/j.buildenv.2016.11.006>
186. Huang, Y., Zheng, C., Li, Q., Zhang, J., Guo, Y., Zhang, Y., Gao, X.: Numerical simulation of the simultaneous removal of particulate matter in a wet flue gas desulfurization system. *Environ. Sci. Pollut. Res.* 27, 1598–1607 (2020). <https://doi.org/10.1007/s11356-019-06773-9>

187. Zhang, H., Dong, Y., Lai, Y., Zhang, X.: Synergistic removal of particles, SO<sub>2</sub>, and NO<sub>2</sub> in desulfurized flue gas during condensation. (2021). <https://doi.org/10.1007/s11356-020-12192-y>
188. Chen, Z., You, C., Liu, H., Wang, H.: The synergetic particles collection in three different wet flue gas desulfurization towers: A pilot-scale experimental investigation. *Fuel Process. Technol.* 179, 344–350 (2018). <https://doi.org/10.1016/j.fuproc.2018.07.025>
189. Arouca, F.O., Feitosa, N.R., Coury, J.R.: Effect of sampling in the evaluation of particle size distribution in nanoaerosols. *Powder Technol.* 200, 52–59 (2010). <https://doi.org/https://doi.org/10.1016/j.powtec.2010.02.007>
190. Chin, J.S., Lefebvre, A.H.: Some comments on the characterization of drop-size distribution in sprays. *icla.* 2, IVA/1/1-IVA/1/12 (1986)
191. Inthavong, K., Yang, W., Fung, M.C., Tu, J.Y.: External and Near-Nozzle Spray Characteristics of a Continuous Spray Atomized from a Nasal Spray Device. *Aerosol Sci. Technol.* 46, 165–177 (2012). <https://doi.org/10.1080/02786826.2011.617793>
192. Ferreira, S.L.C., Bruns, R.E., Ferreira, H.S., Matos, G.D., David, J.M., Brandão, G.C., da Silva, E.G.P., Portugal, L.A., dos Reis, P.S., Souza, A.S., dos Santos, W.N.L.: Box-Behnken design: An alternative for the optimization of analytical methods. *Anal. Chim. Acta.* 597, 179–186 (2007). <https://doi.org/10.1016/j.aca.2007.07.011>
193. Box, G.E.P., Behnken, D.W.: Some New Three Level Designs for the Study of Quantitative Variables. *Technometrics.* 2, 455–475 (1960). <https://doi.org/10.1080/00401706.1960.10489912>
194. Nerisson, P.: Modélisation du transfert des aérosols dans un local ventilé, <https://oatao.univ-toulouse.fr/7767/>, (2009)
195. Mugendiran, V., Gnanavelbabu, A., Ramadoss, R.: Parameter optimization for surface roughness and wall thickness on AA5052 Aluminium alloy by incremental forming using response surface methodology. *Procedia Eng.* 97, 1991–2000 (2014). <https://doi.org/10.1016/j.proeng.2014.12.442>
196. Derringer, G., Suich, R.: Simultaneous Optimization of Several Response Variables. <https://doi.org/10.1080/00224065.1980.11980968>. 12, 214–219 (2018). <https://doi.org/10.1080/00224065.1980.11980968>
197. Ristimäki, J., Virtanen, A., Marjamäki, M., Rostedt, A., Keskinen, J.: On-line measurement of size distribution and effective density of submicron aerosol particles. *J. Aerosol Sci.* 33, 1541–1557 (2002). [https://doi.org/10.1016/S0021-8502\(02\)00106-4](https://doi.org/10.1016/S0021-8502(02)00106-4)
198. DeCarlo, P.F., Slowik, J.G., Worsnop, D.R., Davidovits, P., Jimenez, J.L.: Particle morphology and density characterization by combined mobility and aerodynamic diameter measurements. Part 1: Theory. *Aerosol Sci. Technol.* 38, 1185–1205 (2004). <https://doi.org/10.1080/027868290903907>
199. Bau, S., Bémer, D., Grippari, F., Appert-Collin, J.C., Thomas, D.: Determining the effective density of airborne nanoparticles using multiple charging correction in a tandem DMA/ELPI setup. *J. Nanoparticle Res.* 16, 2629 (2014). <https://doi.org/10.1007/S11051-014-2629-2>
200. Liu, H., Pan, X., Wu, Y., Wang, D., Tian, Y., Liu, X., Lei, L., Sun, Y., Fu, P., Wang, Z.: Effective densities of soot particles and their relationships with the mixing state at an urban site in the Beijing megacity in the winter of 2018. *Atmos. Chem. Phys.* 19, 14791–14804 (2019). <https://doi.org/10.5194/acp-19-14791-2019>
201. Rissler, J., Messing, M.E., Malik, A.I., Nilsson, P.T., Nordin, E.Z., Bohgard, M., Sanati, M., Pagels, J.H.: Aerosol Science and Technology Effective Density Characterization of Soot Agglomerates from Various Sources and Comparison to

- Aggregation Theory Effective Density Characterization of Soot Agglomerates from Various Sources and Comparison to Aggregation Theory. *Aerosol Sci. Technol.* 47, 792–805 (2013). <https://doi.org/10.1080/02786826.2013.791381>
202. Kim, S.H., Mulholland, G.W., Zachariah, M.R.: Density measurement of size selected multiwalled carbon nanotubes by mobility-mass characterization. *Carbon N. Y.* 47, 1297–1302 (2009). <https://doi.org/https://doi.org/10.1016/j.carbon.2009.01.011>
203. Holmes, T., DeGarmo, J., States, C.M.-C.E.P.; (Unite., 1983, U.: Reversejet scrubber for control of fine particulates. *Chem. Eng. Prog.* (1983)

## **Titre : Évaluation des performances d'un épurateur à pulvérisation pour l'élimination des nanoparticules contenues dans les fumées d'incinération**

**Mots clés :** Incinération, épurateur par pulvérisation, nanoparticules, efficacité de la collecte, conception de Box- Behnken

Resume: L'augmentation des produits industriels et de consommation contenant des nanomatériaux manufacturés (ENM) conduit, à leur fin de vie, à une plus grande quantité d'ENM dans les flux de déchets. À l'échelle mondiale, plus de 300 000 tonnes de ENM se retrouvent annuellement dans les centres de stockage des déchets, mais également rejetés dans le sol, l'eau et l'air. Des recherches récentes ont montré que les nanomatériaux manufacturés peuvent survivre au processus de combustion dans le four d'incinération des déchets et se retrouver dans les gaz de combustion. Cependant, on connaît mal l'efficacité de capture des ENM au sein des technologies d'épuration des fumées d'incinération. Les laveurs humides qui sont principalement conçus pour traiter les polluants acides, peuvent également contribuer à réduire les rejets de particules (PM). Cependant, aucune étude n'a été réalisée

pour évaluer l'efficacité d'un épurateur à pulvérisation vis-à-vis de la collecte de nanoparticules dans des conditions d'incinération de déchets. La présente thèse vise à évaluer les performances d'un laveur pilote de laboratoire vis-à-vis de la collecte de nanoparticules contenues dans les fumées d'incinération dans des conditions opératoires et de similitude d'échelle représentatives d'un laveur à pulvérisation d'une usine d'incinération de déchets dangereux en termes de rapport hauteur/diamètre, de rapport liquide/gaz, de températures d'entrée/sortie du gaz, d'humidité du gaz, de temps de résidence du gaz, et de régime d'écoulement du gaz, de diamètre des gouttelettes et de concentrations des particules. L'influence de trois facteurs opérationnels - débit de gaz, débit de liquide et diamètre des gouttelettes - sur l'efficacité de collecte de nanoparticules de carbone du laveur pilote a été étudiée à l'aide de la méthodologie du plan d'expérience - Box-Behnken.

## **Title: Evaluation of the Performance of a Spray Scrubber for the Removal of Nanoparticles Contained in Incineration Fumes**

**Keywords:** Incineration, Spray scrubber, Nanoparticle, Collection efficiency, Box-Behnken design

**Abstract:** As the use of engineered nanomaterials (ENM) in industrial and consumer products increases, a larger amount of ENM will likely end up in waste streams at the end of their life and potentially be released into the environment. Globally, it is estimated that more than 300,000 metric tons of ENM are released into landfills, soil, water, and air each year. Recent research has shown that engineered nanomaterials can survive the combustion process in waste incineration and end up in flue gas. However, little is known about the capture efficiency of ENMs within incineration flue gas cleaning technologies. Wet scrubbers, which are primarily designed to treat acidic pollutants, can also help reduce particulate matter (PM) emissions.

However, no studies have been conducted to evaluate the effectiveness of a spray scrubber in collecting nanoparticles under waste incineration conditions. The present thesis aims to evaluate the performance of a pilot-scale scrubber concerning nanoparticle collection contained in an incineration flue gas representing the conditions of a hazardous waste incineration plant spray scrubber in terms of height-to-diameter ratio, liquid-to-gas ratio, gas inlet/outlet temperatures, gas humidity, gas residence time, and gas flow regime, droplet diameter and particle concentrations. Also, the influence of three independent operating factors - gas flowrate, liquid flowrate and droplet diameter on the collection of carbon nanoparticles by a pilot-scale scrubber was investigated using the Design of Experiment - Box- Behnken design methodology.